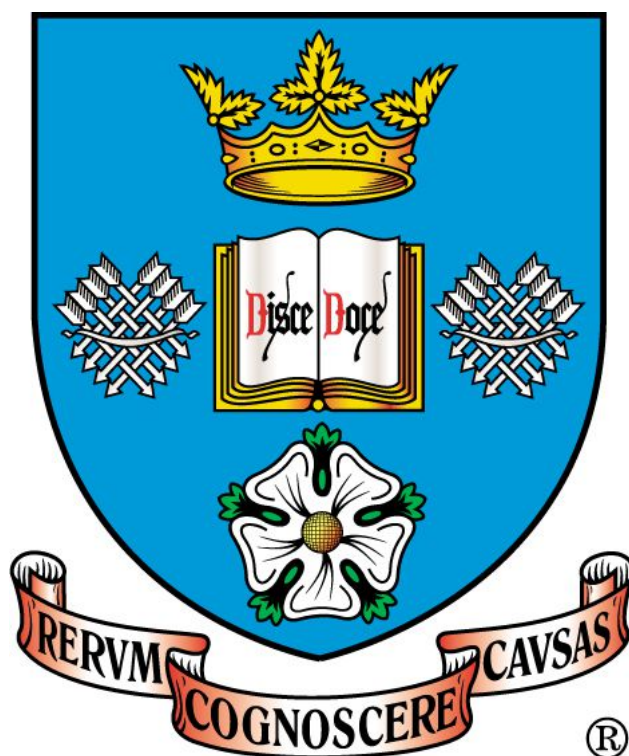


Anchored Photo-Electro-Catalysts for CO₂ Reduction Based on Transition Metal Complexes



Simon C. Parker

Doctorate of Philosophy

Department of Chemistry, University of Sheffield

Supervisors: Professor Julia Weinstein (University of
Sheffield) and Professor Robin Perutz (University of York)

December 2015

Abstract

The overarching goal of this thesis was to design, synthesise and characterise an electrocatalyst that can be anchored to a light-harvesting semiconductor resulting in a photo-electro-catalytic system capable of CO₂ reduction. These electrocatalysts are transition metal-containing complexes and a wide array of synthesis has been performed with several different metals having been tried and tested. These include a palladium pincer complex, a dinuclear copper complex, ruthenium diimine complexes and rhenium diimine complexes.

Work on the palladium and copper catalysts was stopped due to the precursor phosphine ligands oxidising very easily. This prevented modification of the ligands to incorporate anchoring groups. Work on the ruthenium complexes was completed with synthetic routes established that allow for a high degree of customisability when designing and synthesising these types of complexes, but these complexes failed to reduce CO₂ to CO or another reduction product.

Synthesis of rhenium catalysts was carried out and completed successfully. Electrochemical and gas chromatography experiments and analysis were performed. The conclusion was that the complex, Re(CO)₃Cl(bpy(CH₂PO₃H₂)₂) reduced CO₂ to CO when a potential of -2.3 V was applied, with 6 ± 0.6% of the gas sampled having been converted to CO within 1 hour.

Different methods to anchor complexes to various semiconductors were examined; a simple method of mixing a solution of the complex in DMSO and then adding it to the desired semiconductor was established. The anchoring was confirmed by UV-Vis spectroscopy and XPS.

The overall conclusion was that good progress was made in achieving the aims of the thesis. However, more work is needed, primarily the testing of the catalyst in conjunction with the N-Ta₂O₅ semiconductor. If this were to be done then the aim of the thesis, to synthesise an electrocatalyst that can be anchored on to a semiconductor that is capable of absorbing sunlight in order to drive the process of CO₂ reduction, would be completed.

Acknowledgements

I would like to thank my project supervisor Professor Julia Weinstein for all of her help and support during the course of the project.

I would like to thank Professor Robin Perutz at the University of York for providing guidance during this project.

I would like to thank Dr Paul Scattergood and Dr Stuart Archer for the synthesis of the $\text{PtCl}_2(\text{dcbpy})$ and the $\text{bpy}(\text{CH}_2\text{PO}_3\text{Et}_2)_2$ compounds as well as general guidance in the laboratory.

I would like to thank Dr Igor Sazanovich, Dr Elizabeth Baggaley, Dr Milan Delor, Lewis Cletheroe, Steven Spall and Jonathan Shewring for being there in the office to provide guidance.

I would like to thank Dr Robert Mitchell for providing the Ta_2O_5 and synthesising the N- Ta_2O_5 semiconductor.

I would like to thank Professor Stephanie Haywood, Dr Jay D. Wadhawan, Dr Sergey I. Rybchenko, Dr Rolf Crook, Dr Richard Brydson and Dr Richard Douthwaite, the other members of the White Rose consortium for all of their input.

Finally, I would like to thank the White Rose consortium itself for providing the funding that made this research possible.

Publications

1. *Synthesis, Characterization, and DNA Binding Properties of Ruthenium(II) Complexes Containing the Redox Active Ligand Benzo[*i*]dipyrido[3,2-*a*:2',3'-*c*]phenazine-11,16-quinone*. S. P. Foxon, C. Green, M. G. Walker, A. Wragg, H. Adams, J. A. Weinstein, S. C. Parker, A. J. H. M. Meijer and J. A. Thomas, *Inorg. Chem.*, 2012, **51**, 463–471.
2. *$d \rightarrow f$ Energy Transfer in Ir(III)/Eu(III) Dyads: Use of a Naphthyl Spacer as a Spatial and Energetic “Stepping Stone”*. D. Sykes, S. C. Parker, I. V. Sazanovich, A. Stephenson, J. A. Weinstein, and M. D. Ward, *Inorg. Chem.*, 2013, **52**, 10500–10511.
3. *Sensitisation of Eu(III)- and Tb(III)-based luminescence by Ir(III) units in Ir/lanthanide dyads: evidence for parallel energy-transfer and electron-transfer based mechanisms*. D. Sykes, A. J. Cankut, N. M. Ali, A. Stephenson, S. J. P. Spall, S. C. Parker, J. A. Weinstein and M. D. Ward., *Dalton Trans.*, 2014, **43**, 6414–6428.
4. *Vibrational energy transfer dynamics in ruthenium polypyridine transition metal complexes*. M. Fedoseeva, M. Delor, S. C. Parker, I. V. Sazanovich, M. Towrie, A.W. Parker, and J. A. Weinstein, *Phys. Chem. Chem. Phys.*, 2015, **17**, 1688–1696.
5. *Photoinduced charge separation in platinumum(II) diimine acetylide complexes*. S. C. Parker, J. Best, I. V. Sazanovich, R. D. Bennett, O. V. Bouganov, N. M. Shavaleev, A. H. Shelton, S. A. Tikhomirov, M. Towrie, J. A. Weinstein, XXIII IUPAC Symposium on Photochemistry, 11 – 16 July 2010, Ferrara, Italy.
6. *CO₂ reduction utilising photo-electro-catalytic approach based on transition metal complex catalysts anchored to semiconductors*. S. C. Parker, J. A. Weinstein, R. N. Perutz, 4th EuCheMS Chemistry Congress, 26 – 30 August 2012, Prague, Czech Republic.
7. *Transition metal photocatalysts for heterogeneous H₂ production and CO₂ reduction*. S. C. Parker, S. Archer, M. Delor, M. Towie, I. V. Sazanovich, J. A. Weinstein, 245th American Chemical Society National Meeting and Exposition, 7 – 11 April 2013, New Orleans, USA.

Abbreviations

A.U.	Arbitrary unit
BNAH	1-benzyl-1,4-dihydronicotinamide
bpy	2,2'-bipyridine
^t Bu ₂ bpy	4,4'-di-tert-butyl-2,2'-bipyridine
CB	Conduction band
CE	Counter electrode
CS	Catalytic selectivity
CV	Cyclic voltammetry
D	Deuterium
d	Doublet
dcbpy	4,4'-dicarboxy-2,2'-bipyridine
DCM	Dichloromethane
dd	Doublet of doublets
ddd	Doublet of doublets of doublets
DMF	Dimethylformamide
DMSO	Dimethyl sulfoxide
DMSO-d ₆	Hexadeuterodimethyl sulfoxide
dt	Doublet of triplets
e ⁻	Electron
E	Electron energy
E°	Standard electrode potential
EDTAH ₂ ²⁻	Ethylenediaminetetraacetic acid
EI	Electron ionisation
ES	Electrospray
Fc/Fc ⁺	Ferrocene-ferrocenium couple
FE	Faradaic efficiency
FT	Fourier transformation
GC	Gas chromatography
HOMO	Highest occupied molecular orbital
I	Current
IR	Infrared

J	Coupling constant
Ln	Natural logarithm
LUMO	Lowest unoccupied molecular orbital
m	Multiplet
m/z	Mass-to-charge ratio
M ⁺	Molecular ion
MALDI	Matrix assisted laser desorption ionisation
Me ₂ bpy	4,4'-dimethyl-2,2'-bipyridine
MLCT	Metal to ligand charge transfer
MS	Mass spectrometry
NHE	Normal hydrogen electrode
NMR	Nuclear magnetic resonance
n-BuLi	n-Butyllithium
OER	One electron reduction
OTf	Triflate
PCHP	1,3-bis(diphenylphosphinomethyl) benzene
phen	Phenanthroline
r.t.	Room temperature
R	Resistance
RE	Reference electrode
R _s	Resistance of electrolyte
s	Singlet
S ₀	Singlet ground state
S ₁	1 st singlet excited state
S _n	N th singlet excited state
SCE	Saturated calomel electrode
SHE	Standard hydrogen electrode
t	Triplet
T ₁	1 st triplet state
TCD	Thermal conductivity detector
td	Triplet of doublets
TEA	Triethylamine

TEOA	Triethanolamine
THF	Tetrahydrofuran
TOF	Turnover frequency
ToF	Time of flight
TON	Turnover number
TMSBr	Trimethylsilyl bromide
UV-Vis	Ultraviolet-Visible
VB	Valence band
vs.	Versus
WE	Working Electrode
XPS	X-ray photoelectron spectroscopy

Greek letters

ε	Extinction coefficient
μ	Micro
ν	Frequency
π	Pi
σ	Sigma
τ	Lifetime
υ	Scan rate

Units

$^{\circ}\text{C}$	Degree Celsius
A	Ampere
Å	Angstrom
atm	Atmosphere
cm	Centimetre
cm^{-1}	Wavenumber
eV	Electron volt
g	Gram
Hz	Hertz

L	Litre
M	Molar
mA	Milliampere
mg	Milligram
MHz	Megahertz
mJ	Millijoule
mL	Millilitre
mm	Millimetre
mM	Millimolar
mmol	Millimole
mol	Mole
mV	Millivolt
mVs^{-1}	Millivolt per second
nm	Nanometre
ns	Nanosecond
ppm	Parts per million
ps	Picosecond
s	Second
TW	Terawatt
V	Volt

Table of Contents

1. Introduction.....	1
1.1. Current Energy and Chemical Feedstock Production.....	1
1.1.1. Possible Solutions to the Energy Crisis.....	2
1.2. Creating Chemical Feedstocks	3
1.2.1. Reducing CO ₂ – Thermodynamic Considerations	4
1.2.2. Reducing CO ₂ – Kinetic Considerations	5
1.3. Catalyst Requirements	6
1.4. Photochemistry and Photophysics	7
1.5. Electrochemistry	8
1.6. Gas Chromatography	10
1.7. Identifying Types of Systems.....	10
1.7.1. Type One Systems	10
1.7.2. Type Two Systems.....	12
1.8. Aims of the Thesis	14
1.9. Aims of the Wider Project.....	15
1.10. Method of Achieving the Aims of the Thesis	16
1.10.1. Metal Complexes Containing Phosphine Ligands	17
1.10.2. Metal Complexes Containing Bipyridine Ligands.....	19
1.10.3. Metal Complexes Anchored to Semiconductors.....	25
1.10.4. Metal Complexes Containing Macrocyclic Ligands.....	29
1.10.5. Summary.....	31
1.11. References	33
2. Materials and General Procedures	38
2.1. ¹ H NMR Spectroscopy.....	38

2.2. ^{19}F NMR Spectroscopy	38
2.3. ^{31}P NMR Spectroscopy	38
2.4. Mass Spectrometry	39
2.5. Elemental Analysis	39
2.6. UV-Vis Spectroscopy	39
2.7. Emission Spectroscopy	39
2.8. Time-Resolved Emission Spectroscopy	40
2.9. IR Spectroscopy.....	40
2.10. Transient Absorption Spectroscopy.....	40
2.11. Electrochemistry.....	41
2.12. Gas Chromatography	42
2.13. X-ray Photoelectron Spectroscopy (XPS).....	43
2.14. References	43
3. Metal Complexes Containing Phosphine Ligands as Potential Catalysts for CO_2 Reduction	44
3.1. Introduction.....	44
3.1.1. System Design	45
3.2. Synthesis and Characterisation of $[\text{Pd}(\text{PCP})(\text{CH}_3\text{CN})][\text{BF}_4]$	46
3.2.1. Synthetic Method.....	46
3.2.2. Synthesis of 1,3-bis(diphenylphosphinomethyl) benzene (PCHP ligand).....	47
3.2.3. Synthesis of $[\text{Pd}(\text{PCP})(\text{CH}_3\text{CN})][\text{BF}_4]$	48
3.3. Results and Discussion of $[\text{Pd}(\text{PCP})(\text{CH}_3\text{CN})][\text{BF}_4]$	48
3.3.1. Electrochemical Data for $[\text{Pd}(\text{PCP})(\text{CH}_3\text{CN})][\text{BF}_4]$	48
3.3.2. Summary	51
3.4. Synthesis and Characterisation of $[\text{Cu}_2(\mu\text{-Ph}_2\text{Pbpy})_2(\text{CH}_3\text{CN})_2][\text{PF}_6]_2$	51

3.4.1. Synthetic Method	51
3.4.2. Synthesis of 6-(diphenylphosphino)-2,2'-bipyridine (Method 1)	52
3.4.3. Synthesis of 6-(diphenylphosphino)-2,2'-bipyridine (Method 2)	53
3.4.4. Synthesis of $[\text{Cu}_2(\mu\text{-Ph}_2\text{Pbpy})_2(\text{CH}_3\text{CN})_2][\text{PF}_6]_2$	54
3.5. Results and Discussion of $[\text{Cu}_2(\mu\text{-Ph}_2\text{Pbpy})_2(\text{CH}_3\text{CN})_2][\text{PF}_6]_2$	55
3.5.1. Electrochemical Data for $[\text{Cu}_2(\mu\text{-Ph}_2\text{Pbpy})_2(\text{CH}_3\text{CN})_2][\text{PF}_6]_2$	55
3.5.2. Summary	56
3.6. Consideration of Random and Systematic Errors	56
3.7. References	57
4. Ruthenium Complexes Containing Bipyridine Ligands as Potential Catalysts for CO_2 Reduction	59
4.1. Introduction	59
4.1.1. System Design	60
4.2. Synthesis and Characterisation of Bis-dcbpy Ruthenium Dicarbonyl Complexes (Route 1)	62
4.2.1. Synthetic Method	62
4.2.2. Synthesis of $\text{Ru}(\text{dcbpy})_2\text{Cl}_2$	62
4.2.3. Synthesis of $\text{Ru}(\text{dcbpy})_2\text{CO}_2$ (Method 1)	63
4.2.4. Synthesis of $\text{Ru}(\text{dcbpy})_2(\text{SO}_3\text{CF}_3)_2$	64
4.2.5. Synthesis of $\text{Ru}(\text{dcbpy})_2\text{CO}_2$ (Method 2)	65
4.3. Synthesis and Characterisation of Bis-dcbpy Ruthenium Dicarbonyl Complexes (Route 2)	66
4.3.1. Synthetic Method	66
4.3.2. Synthesis of $[\text{Ru}(\text{CO})_2\text{Cl}_2]_n$	66
4.3.3. Synthesis of $\text{Ru}(\text{CO})_2\text{Cl}_2(\text{dcbpy})$	67
4.3.4. Synthesis of $\text{Ru}(\text{CO})_2(\text{dcbpy})(\text{SO}_3\text{CF}_3)_2$	68

4.4. Synthesis and Characterisation of ^t Bu ₂ bpy Ruthenium Dicarbonyl Complexes	69
.....
4.4.1. Synthetic Method	69
4.4.2. Synthesis of Ru(CO) ₂ Cl ₂ (^t Bu ₂ bpy)	70
4.4.3. Synthesis of Ru(CO) ₂ (^t Bu ₂ bpy)(SO ₃ CF ₃) ₂	71
4.4.4. Synthesis of Ru(CO) ₂ (^t Bu ₂ bpy)(dcbpy)	72
4.4.5. Synthesis of Ru(CO) ₂ (^t Bu ₂ bpy)(bpy)	72
4.5. Synthesis and Characterisation of Bpy Ruthenium Dicarbonyl Complexes	73
.....
4.5.1. Synthetic Method	73
4.5.2. Synthesis of Ru(CO) ₂ Cl ₂ (bpy)	74
4.5.3. Synthesis of Ru(CO) ₂ (bpy)(SO ₃ CF ₃) ₂	75
4.6. Synthesis and Characterisation of Me ₂ bpy Ruthenium Dicarbonyl Complexes	76
.....
4.6.1. Synthetic Method	76
4.6.2. Synthesis of Ru(CO) ₂ Cl ₂ (Me ₂ bpy)	77
4.6.3. Synthesis of Ru(CO) ₂ (Me ₂ bpy)(SO ₃ CF ₃) ₂	78
4.6.4. Synthesis of [Ru(CO) ₂ (Me ₂ bpy)(dcbpy)] ²⁺	79
4.7. Synthesis and Characterisation of Phosphonate Ruthenium Dicarbonyl Complexes	80
.....
4.7.1. Synthetic Method	80
4.7.2. Synthesis of (Et ₂ O ₃ P) ₂ bpy	81
4.7.3. Synthesis of Ru(CO) ₂ (Me ₂ bpy){bpy(CH ₂ PO ₃ Et ₂) ₂ }	82
4.7.4. Synthesis of Ru(CO) ₂ (Me ₂ bpy){bpy(CH ₂ PO ₃ H ₂) ₂ }	83
4.8. Results and Discussion of Phosphonate Ruthenium Dicarbonyl Complexes	83
.....
4.8.1. Photophysical Data for Ru(CO) ₂ (Me ₂ bpy){bpy(CH ₂ PO ₃ Et ₂) ₂ }	83
4.8.2. Electrochemical Data for Ru(CO) ₂ (Me ₂ bpy){bpy(CH ₂ PO ₃ Et ₂) ₂ }	86

4.8.3. Photophysical Data for $\text{Ru}(\text{CO})_2(\text{Me}_2\text{bpy})\{\text{bpy}(\text{CH}_2\text{PO}_3\text{H}_2)_2\}$	87
4.8.4. Electrochemical Data for $\text{Ru}(\text{CO})_2(\text{Me}_2\text{bpy})\{\text{bpy}(\text{CH}_2\text{PO}_3\text{H}_2)_2\}$	88
4.8.5. Summary	92
4.9. Consideration of Random and Systematic Errors	92
4.10. References	94
5. Rhenium Complexes Containing Bipyridine Ligands as Potential Catalysts for CO_2 Reduction	97
5.1. Introduction	97
5.1.1. System Design	98
5.2. Synthesis and Characterisation of $\text{Re}(\text{CO})_3\text{Cl}\{\text{bpy}(\text{CH}_2\text{PO}_3\text{Et}_2)_2\}$	100
5.2.1. Synthetic Method	100
5.2.2. Synthesis of $\text{Re}(\text{CO})_3\text{Cl}\{\text{bpy}(\text{CH}_2\text{PO}_3\text{Et}_2)_2\}$	101
5.3. Results and Discussion of $\text{Re}(\text{CO})_3\text{Cl}\{\text{bpy}(\text{CH}_2\text{PO}_3\text{Et}_2)_2\}$	102
5.3.1. Photophysical Data for $\text{Re}(\text{CO})_3\text{Cl}\{\text{bpy}(\text{CH}_2\text{PO}_3\text{Et}_2)_2\}$	102
5.3.2. Electrochemical Data for $\text{Re}(\text{CO})_3\text{Cl}\{\text{bpy}(\text{CH}_2\text{PO}_3\text{Et}_2)_2\}$	105
5.3.3. Summary	108
5.4. Synthesis and Characterisation of $\text{Re}(\text{CO})_3\text{Cl}\{\text{bpy}(\text{CH}_2\text{PO}_3\text{H}_2)_2\}$	109
5.4.1. Synthetic Method	109
5.4.2. Synthesis of $\text{Re}(\text{CO})_3\text{Cl}\{\text{bpy}(\text{CH}_2\text{PO}_3\text{H}_2)_2\}$	109
5.5. Results and Discussion of $\text{Re}(\text{CO})_3\text{Cl}\{\text{bpy}(\text{CH}_2\text{PO}_3\text{H}_2)_2\}$	110
5.5.1. Photophysical Data for $\text{Re}(\text{CO})_3\text{Cl}\{\text{bpy}(\text{CH}_2\text{PO}_3\text{H}_2)_2\}$	110
5.5.2. Electrochemical Data for $\text{Re}(\text{CO})_3\text{Cl}\{\text{bpy}(\text{CH}_2\text{PO}_3\text{H}_2)_2\}$	113
5.5.3. Summary	118
5.6. Results and Discussion of Rhenium Complex Analogues	118
5.6.1. Photophysical Data for Rhenium Complex Analogues	118

5.6.2. Electrochemical Data for Rhenium Analogues	119
5.6.3. Summary	127
5.7. Consideration of Random and Systematic Errors	127
5.8. References	129
6. Metal Complexes Anchored to Semiconductors	131
6.1. Introduction	131
6.1.1. System Design	132
6.1.2. Experimental Design	134
6.2. Anchoring $\text{Re}(\text{CO})_3\text{Cl}\{\text{bpy}(\text{CH}_2\text{PO}_3\text{H}_2)_2\}$ onto TiO_2	134
6.2.1. Preparation of $\text{Re}(\text{CO})_3\text{Cl}\{\text{bpy}(\text{CH}_2\text{PO}_3\text{H}_2)_2\}$ onto TiO_2	135
6.2.2. Results and Discussion of $\text{Re}(\text{CO})_3\text{Cl}\{\text{bpy}(\text{CH}_2\text{PO}_3\text{H}_2)_2\}$ onto TiO_2 ...	136
6.3. Anchoring Complexes onto N- Ta_2O_5	137
6.3.1. Preparation of N- Ta_2O_5	137
6.3.2. Preparation of Dcbpy onto N- Ta_2O_5	137
6.3.3. Results and Discussion of Dcbpy onto N- Ta_2O_5	137
6.3.4. Preparation of $\text{PtCl}_2(\text{dcbpy})$ onto N- Ta_2O_5	138
6.3.5. Results and Discussion of $\text{PtCl}_2(\text{dcbpy})$ onto N- Ta_2O_5	139
6.3.6. Preparation of $\text{Re}(\text{CO})_3\text{Cl}\{\text{bpy}(\text{CH}_2\text{PO}_3\text{H}_2)_2\}$ onto N- Ta_2O_5	141
6.4. X-ray Photoelectron Spectroscopy (XPS).....	142
6.4.1. Preparation of XPS Samples	142
6.4.2. Results and Discussion of XPS Samples.....	143
6.5. Summary	144
6.6. Consideration of Random and Systematic Errors	145
6.7. References	146
7. Collaborations and Publications	149

7.1. Introduction	149
7.2. Collaborations.....	149
7.2.1. Publication (i)	149
7.2.2. Publication (ii)	151
7.2.3. Publication (iii)	153
7.2.4. Publication (iv).....	154
7.3. Work Presented at Symposia.....	156
7.3.1. Publication (v).....	157
7.3.2. Publication (vi).....	157
7.3.3. Publication (vii)	157
7.4. References	158
8. Conclusions and Future Work	160
8.1. Conclusions	160
8.1.1. Chapter 3	160
8.1.2. Chapter 4	160
8.1.3. Chapter 5	161
8.1.4. Chapter 6	161
8.2. Thesis Summary	162
8.3. Future Work.....	165
8.4. References	166

1. Introduction

The overarching goal of the work contained in this thesis is to design, synthesise and characterise a series of suitable electrocatalysts for the purpose of CO₂ reduction. These electrocatalysts are transition metal-containing complexes, which would also be capable of anchoring to a light-harvesting semiconductor, ideally in the form of semiconductor electrodes. The most efficient electrocatalyst can then be anchored to the semiconductor resulting in a novel photo-electro-catalytic system capable of CO₂ reduction. The exact reduction product produced is not a primary concern at this stage, although, for the catalysts to be discussed here, the products are most likely to be either CO or formate. Both of these are highly valuable as chemical feedstocks and are of great importance to various sectors of industry.

1.1. Current Energy and Chemical Feedstock Production

Throughout history, humankind has benefited greatly from being able to convert sources of energy into useable forms. During the last century, scientific and technological development has moved at an accelerated pace in part due to the discovery of fossil fuels. These fuels have enabled people to develop transport, agriculture and many other aspects of society.

However fossil fuels are a finite resource and although the timeframe on which this will occur is still open to debate it means that they will one day run out.¹ This presents a major problem as not only do we get energy from fossil fuels, we also use petroleum (a fossil fuel) to make a large number of our everyday products e.g. chemical feedstocks. The situation is also made more complicated by the fact that the global energy demand is set to increase from 16.5 terawatt (TW) in 2007 to 24.7 TW in 2030² whilst the remaining reserves of fossil fuels continue to decrease.³

Another problem also exists with fossil fuels in that when they are burnt they produce CO₂. Numerous studies⁴⁻¹⁰ have shown that increasing levels of CO₂ in the atmosphere are having a detrimental effect on the global climate; rising temperatures, more extreme weather patterns.

It therefore becomes clear that in order for humans to continue their development significant changes are going to have to be made to the way in which energy and chemical feedstocks are produced, whilst trying to limit or perhaps even reduce any environmental damage. This will not be an easy challenge.

However, there are several options open to us, which with appropriate investment and scientific development may allow us to meet this challenge.

1.1.1. Possible Solutions to the Energy Crisis

One possible solution to the problem of increasing energy demand whilst decreasing dependence on fossil fuels is to use sources of renewable energy. These include, wind wave, solar and nuclear* (*not technically a renewable source but is generally regarded as an alternative energy source). These sources all have their own advantages and disadvantages but these will not be discussed here. The source with the most potential to fulfil our energy demands is also the one, which needs the most development i.e. solar energy. There is enough solar energy reaching the earth in one day that if it was all collected and stored it could power the planet for an entire year, based on current energy consumption levels.¹¹ However, it is not currently possible to utilise anywhere close to this. Additionally even if the field of photovoltaics was to advance to the point where solar energy could supply most or all of our energy needs there would still be the problem of needing chemical feedstocks for all of the different industrial processes.

Fortunately, the sun may also provide the solution to this problem. This would be in the form of using photo-electro-chemical processes to drive reactions in which chemical feedstocks could be created. A further advantage of this is that CO₂ is often used as a starting material and is then converted to useful compounds such as methanol, formaldehyde, formic acid and methane. Although the technology already exists to make these chemical compounds from CO₂¹² it requires energy to do so, energy which we currently get from burning fossil fuels.

Therefore the ideal situation would be that we are able to derive all of our energy needs from either solar and/or other renewable energy sources and that we can also produce chemical feedstocks whilst reducing the amount of CO₂ in the atmosphere thereby limiting any further environmental damage.

There are however significant challenges with these goals. We will now take a closer look at some of these; however, we will focus on trying to produce chemical feedstocks from CO₂.

1.2. Creating Chemical Feedstocks

As previously mentioned CO₂ is a by-product of fossil fuel combustion as is shown in equation (1.1)



In order to meet our goals several fundamental challenges in chemical catalysis, electrochemistry, photochemistry, semiconductor physics and engineering will have to be overcome. When trying to create chemical feedstocks it is often best to look at systems which already exist and for this we are able to draw inspiration from nature which has spent billions of years developing ways to harness sunlight and convert it into useful materials i.e. glucose (O₂ is useful from our perspective).¹³

Photosynthetic organisms are able to use the highly efficient process of photosynthesis in order to create organic molecules, which are then used for a variety of purposes. One of the areas photochemists are currently working in is the development of artificial photosynthetic systems.¹⁴ Artificial photosynthesis has great potential to transform the world we live in as it could be used for energy storage, the splitting of water and the creation of chemical feedstock. However, mimicking natural photosynthesis has so far seen only limited success. The problem lies in trying to develop components that are both efficient and can be incorporated into a working system, which so far has proved difficult.

Figure 1.1 provides an example of a generic system in which a photon interacts with the chromophore. The electron excitation creates a charge separated state which causes a cascade of electron transfer ultimately resulting in the splitting of water and the production of hydrogen gas.¹⁴

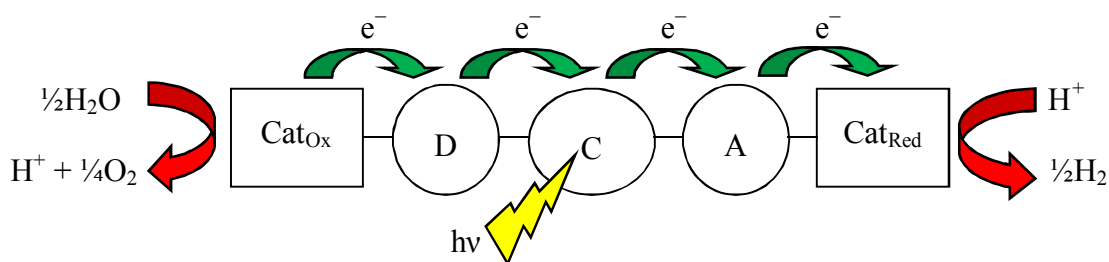


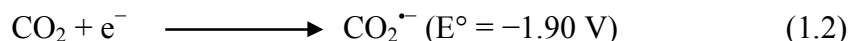
Figure 1.1: A representation of an artificial photosynthetic system showing the splitting of water upon interaction of light with the chromophore. D, C and A represent a donor, a chromophore and an acceptor respectively. Cat_{Ox} and Cat_{Red} are catalysts for oxidation and reduction respectively.¹⁴⁻¹⁶

In natural photosynthesis, a light harvesting antenna is present; this antenna does not carry out the charge separation itself but channels the collected energy towards a central region where charge separation does occur. This has the advantage of maximising the solar energy absorption. In order to design and synthesise artificial antennas significant effort is required. Nevertheless, artificial systems have been previously demonstrated.^{14, 17, 18}

The creation of chemical feedstocks is based on the reduction of CO₂, a process very similar to water splitting. Both rely on the energy and electrons, which are made available upon the absorption of light by the chromophore and antenna in photosynthetic organisms during the process of photosynthesis. The reduction of CO₂ can yield many different chemical compounds, which are of use to various sectors of industry as well as photosynthetic organisms.

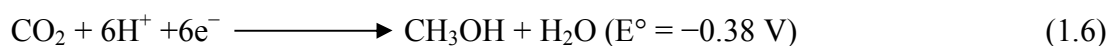
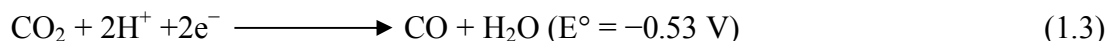
1.2.1. Reducing CO₂ – Thermodynamic Considerations

The energy required for the single electron reduction of CO₂ is given in equation (1.2)



This high-energy cost is due to the reorganizational energy needed to convert the linear CO₂ molecule into the bent CO₂^{•-} radical anion.

It is thermodynamically more favourable to perform instead multi-electron steps as shown in equations (1.3) – (1.7), all shown under standard conditions;



There are several different proton sources which can be utilised in the reaction, these include; water,¹⁹ PhCO₂H²⁰ and triethanolamine (TEOA), which is also capable of acting an electron donor.²¹

In current industrial processes, the chemical reduction of CO₂ follows one of two pathways.

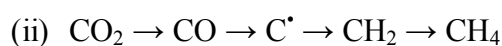


Figure 1.2: The two different pathways for CO₂ reduction currently used in industry.²²

1.2.2. Reducing CO₂ – Kinetic Considerations

From a kinetic viewpoint, it is reasonably difficult to convert CO₂ molecules, which are relatively simple, into more complex molecules such as methanol or formic acid. Current industrial processes such as the Fischer-Tropsch process rely on the fact that it is easier to convert CO₂ to CO and H₂O to H₂ than to make liquid fuels. An alternative method would be to try to find a series of individual catalysts that are each capable of assisting one of the sequential steps shown in figure 1.2. This would allow each of the catalysts to be fine-tuned separately before being brought together in an array. This approach would most likely be significantly easier than try to find a single catalyst that is capable to doing all of the steps. However, one potential downside to an array would be if one or more of the catalysts were more prone to decomposition than the others were. This would mean that some way to replace the decomposed catalyst easily

without stopping the array would need to be developed or the production cycle would be inefficient due to the continual stoppage time from replacing the catalyst(s).

1.3. Catalyst Requirements

Even if a suitable catalyst or a series of catalysts are found, other considerations need to be taken into account. The first consideration is the turnover number (TON) which is defined as; the number of moles of product formed per mole of catalyst.²³ This is an important number, which we want to be as high as possible if the catalyst is to be economically viable.

Another important number is the turnover frequency (TOF); number of turnovers per unit time.²³ This value relates to how quickly the product is able to form in the presence of the catalyst. It is possible to have a high TON but a low TOF; this would result in a large number of product molecules forming per catalyst molecule but it taking a long time for the product to be formed. Conversely, it is possible to have a low TON but a large TOF. This results in few product molecules per catalyst molecule but over a short timeframe. This scenario is usually the result of catalyst deactivation in which the catalytic system runs for a few cycles before breaking down, hence the low TON.

This highlights two problems; firstly catalyst deactivation which usually occurs because of side reactions in which the catalyst is converted to a non-catalytic species. Secondly as already mentioned decomposition of the catalyst can occur. An ideal catalyst would have a large TON and TOF and would not readily undergo deactivation or decomposition. However, as will be shown in later sections current CO₂ reduction catalysts are far from ideal.

Several other measures of whether a catalyst is suitable also exist; Faradaic efficiency (FE) and catalytic selectivity (CS), these are defined as equation 1.8 and 1.9.

$$FE = (\text{moles product} / \text{moles of electrons passed}) \times (\text{number of electrons needed for conversion})^{24} \quad (1.8)$$

$$\text{Catalytic selectivity (CS)} = \text{moles intended products} / (\text{moles H}_2 + \text{moles other products})^{24} \quad (1.9)$$

Both of these are helpful in trying to determine if an electrocatalyst is suitable, the FE shows how many of the electrons supplied go onto produce products whilst the CS shows what percentage of products are the desired products.

The final parameter to consider is the “over potentials”, this is defined as the difference between the potential that is applied and the potential we would expect from thermodynamic calculations.

1.4. Photochemistry and Photophysics

The following section gives basic background information on what photochemical processes are and how we can use photophysics in various experimental techniques to determine the photophysical properties of compounds.^{15, 25}

Photochemical processes are initiated when a component of a reaction mixture absorbs radiation e.g. UV-Vis light. There are two types of processes, primary and secondary. In a primary process, products are formed directly from the excited state of a reactant(s). In a secondary process, products are formed from intermediates, which are formed in the primary process. An area related to photochemistry is photophysics, with photophysical processes often competing with photochemical processes by deactivating the excited state. An example of a photochemical process is electron transfer to a different molecule, while an example of a photophysical process is fluorescence. Several other examples of photophysical processes are shown below in a modified Jablonski energy diagram.

Figure 1.3 conveys a large amount of information about exactly what can happen when a molecule is excited by the absorption of radiation. The initial absorption in which a transition from the ground state, S_0 , to an excited state, S_1 can be seen in green. This step is perhaps the most important as all the other possible transitions are dependent on it occurring. However, for this transition to occur, the radiation needs to have the correct energy to instigate the transition from S_0 to S_1 , (or S_n). The decay of the S_1 excited state straight back to the ground state S_0 is known as fluorescence and is the most common transition in which an excited state decays to the ground state. Nevertheless, an alternate route back to the ground state exists, via a triplet state. This route is normally forbidden due to spin selection rules. However it is still possible for

the process (known as phosphorescence) to occur, it is just kinetically unfavourable. This is because fluorescence operates on the $10^{-9} - 10^{-7}$ s timescale and phosphorescence on the $10^{-3} - 10^2$ s timescale. These differences in timescales can be used in various techniques to determine the photophysical properties of compounds such as the absorption spectrum, emission spectrum and the lifetime of the excited state. By using photochemical processes in conjunction with an electrocatalyst, CO_2 can be reduced to useful liquid fuels.

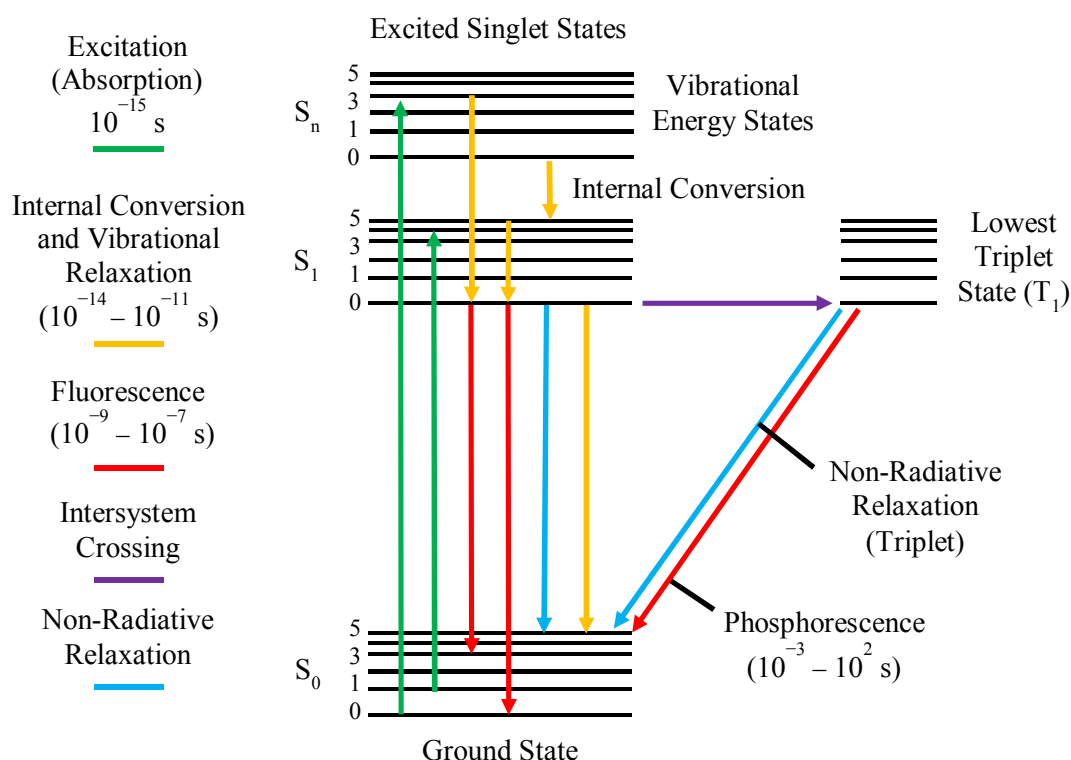


Figure 1.3: A modified Jablonski energy diagram showing the various possible transitions from the ground state to the excited state and then back to the ground state.

1.5. Electrochemistry

In order to determine the electrochemical properties of a system we use the technique of cyclic voltammetry (CV). Cyclic voltammetry uses three electrodes, a working electrode (WE), a counter electrode (CE) and a reference electrode (RE). The three electrodes are needed because $V = I \times R$, so if a voltage (potential difference, normally denoted as E and measured in volts) of E_1 is measured in a two electrode system where

a current (I_1) is flowing between the cathode and anode then what is actually measured is; $E = E_1 + I_1R_s$ (where R_s is the resistance of the electrolyte.) However if current flows between the (WE) and (CE) then the voltage is measured using the (RE) which does not allow current to flow through it.²⁶

There are several different types of electrode e.g. platinum wire and glassy carbon. Which ones are used depends on the composition of the system and where the potentials are expected to be. The standard hydrogen electrode (SHE) is the point of reference for all other electrode potentials and is given a value of 0.00 V. However, in practice, this reference is not practical and so the saturated calomel electrode (SCE) (Hg/Hg₂Cl₂, in saturated KCl solution) or the silver/silver chloride electrode (Ag/AgCl, in saturated KCl solution) is more commonly used.

An electrolyte solution is also needed to allow the current to flow between the electrodes. The electrolyte has to be soluble in common organic solvents but still be a charge carrier. Salts such as [Bu₄N]⁺[PF₆]⁻ and [Bu₄N]⁺[BF₄]⁻ are commercially available.

Once the system is set up correctly and attached to a potentiostat a voltage is then applied. The voltage then sweeps across a defined range until it reaches a predetermined point; the potential sweep is then reversed until it reaches the second predetermined point. The flow of current is recorded throughout the sweep and can then be plotted against voltage as shown in figure 1.4.

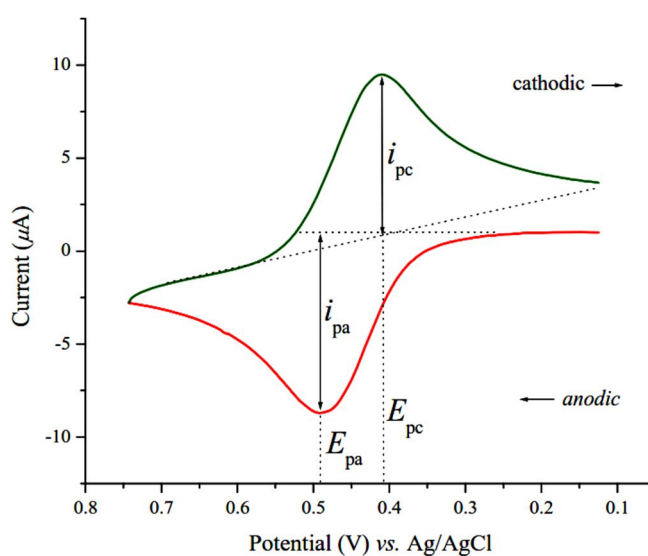


Figure 1.4: A standard cyclic voltammetry couple.²⁷

1.6. Gas Chromatography

Gas chromatography is an analytical technique that can separate and identify different components of a gaseous mixture. This is done by the use of a mobile and stationary phase. The mobile phase, also called the carrier gas is usually an inert gas such as hydrogen, nitrogen or argon. The stationary phase is usually a silica column. The gaseous sample is injected into the instrument where it is carried through the column by the carrier gas. Separation occurs because different gases will travel through the column at different rates due to their different retention on the silica. This usually takes place over a period of 15 minutes. As the gases exit the column, they come into contact with a detector. Several different types of detector are available, including, mass spectrometer, flame ionization and thermal conductivity. Our instrument uses thermal conductivity, by comparison of the reference gas with the gas being analysed. This generates a signal that is recorded along with the time of detection. By using the strength of the signal and the retention time, it is possible to identify the gases in the mixture and the amounts relative to each other, although this requires previous calibration with known concentrations of known gases.

1.7. Identifying Types of Systems

Before we consider the specific aims of this thesis and evaluate the relevant literature, we will first examine two of the different types of systems that exist, one of which will be the primary focus of this work. By identifying the various components of the systems and considering the thermodynamics of the processes involved we can help clarify the key differences between them. Our research will then focus exclusively on type two systems with no further mention of type one systems other than what is stated in the next section and briefly when discussing semiconductors in chapter 6.

1.7.1. Type One Systems

When categorising these systems it is easiest to do so by breaking them down into their individual components, a light absorbing unit and a chemical reduction unit. The first type of system identified has been known for many years in the literature.^{16, 28-33}

This consists of a light absorbing complex, often called the photosensitizer, and a semiconductor electrode that conducts the electrons to another electrode where the reduction takes place. This type of system is usually used for water splitting¹⁶ and requires either a sacrificial electron donor such as EDTAH₂²⁻ or a non-sacrificial donor such as I⁻/I₃⁻.

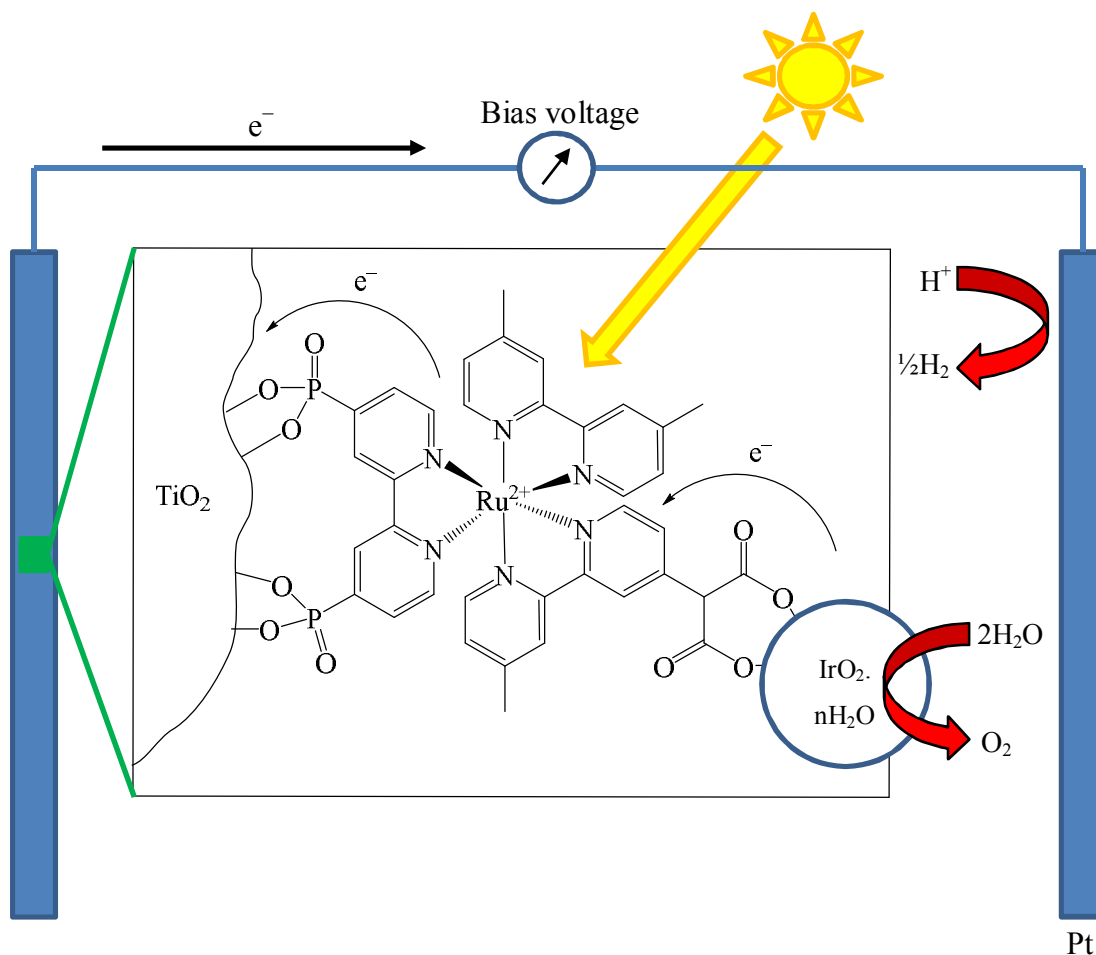


Figure 1.5: A schematic representation of a dye sensitized semiconductor electrode system in which the reduction of H⁺ to ½H₂ occurs by use of a platinum electrode.¹⁶

In Figure 1.5 a photon interacts with the photosensitizer, an anchor group containing [Ru(bpy)₃]²⁺ analogue, which results in the transfer of an electron to the semiconductor. The semiconductor then delivers the electron to a platinum electrode at which 2H⁺ is reduced to H₂. An anchored IrO₂·nH₂O is used to replenish the lost electron on the photosensitizer. This drives the other half of the water redox process converting H₂O to

2H^+ and $\frac{1}{2}\text{O}_2$. To help understand what drives these processes we can construct an energy level diagram for the system, Figure 1.6.

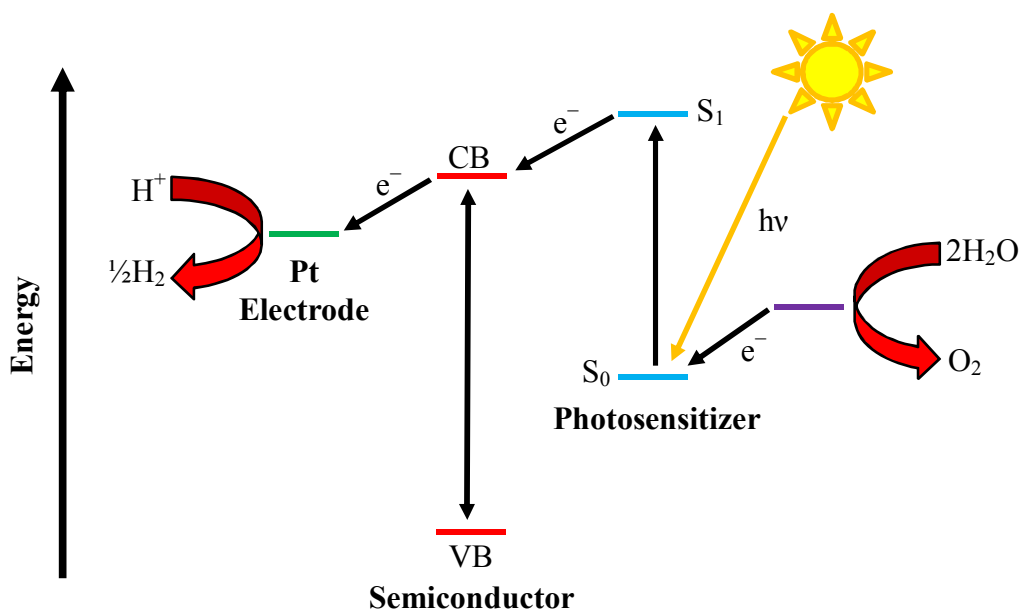


Figure 1.6: An energy level diagram of the processes involved during the splitting of water. Recombination pathways have not been shown to aid clarity.

In Figure 1.6 the photosensitizer absorbs a photon resulting in an excited state, S_1 , being produced. An electron transfer to the conduction band of the semiconductor then occurs due to it being lower in energy. A second electron transfer occurs because again the platinum electrode, or another reduction site, is in a lower energy state. It is through this series of progressively lower energy states that drives the electron transfers and subsequent reduction process. The oxidation process occurs because its energy level is above that of the photosensitizer ground state but below that of the excited state, the conduction band and the platinum electrode thus allowing the replenishment of the photosensitizer's electron, enabling the whole process to be repeated and deliver additional electrons to allow completion of the reduction process.

1.7.2. Type Two Systems

A second type of system exists in the literature,^{21, 34-39} in which the semiconductor acts as the light absorbing unit and the complex acts as the electrocatalyst where the

reduction takes place. This is in opposition to the previous type of system where the complex acts a photosensitizer, absorbing light whilst the semiconductor transfers the electrons to the reducing agent. Both of these types of systems rely on the absorption of light resulting in a transfer of electrons that then drive the redox processes. It is through the careful selection of both the complex and semiconductor that we are able to control the directionality of the electron transfer and thus drive the desired reduction process.

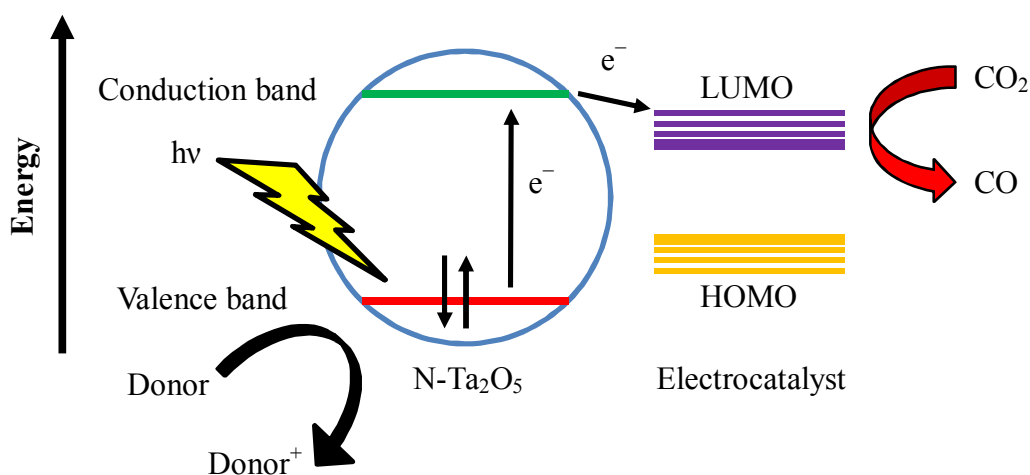


Figure 1.7: A schematic representation of the reduction of CO₂ to CO by use of a light absorbing nitrogen doped Ta₂O₅ semiconductor, which is coupled to an electrocatalyst.

This can be seen more clearly in Figure 1.7, in which a photon is absorbed by the nitrogen doped Ta₂O₅ semiconductor resulting in the creation of an electron-hole pair. The electron is then transferred from the conduction band to the LUMO of the electrocatalyst due to the LUMO being lower in energy. However, as seen earlier in this chapter the electrocatalyst needs two or more electrons in order to reduce CO₂ to a reduction product, in this example CO. This requires the use of a sacrificial donor to replenish the electron from the semiconductor allowing the generation of a new electron-hole pair and subsequent transfer of a second electron to complete the reduction process.

Having clarified the two main types of system that exist we can move onto the new research contained in this thesis and what sets it apart from that which has been done

previously. As already mentioned our work will focus entirely on the type two systems in order to achieve our goals.

The overarching goal being to design, synthesise and characterise a series of suitable electrocatalysts for the purpose of CO₂ reduction. These electrocatalysts are transition metal containing complexes that would also be capable of anchoring to a light harvesting semiconductor ideally in the form of semiconductor electrodes. The most efficient electrocatalyst can then be anchored to the semiconductor resulting in a novel photo-electro-catalytic system capable of CO₂ reduction. The exact reduction product produced is not a primary concern at this stage, although, for the catalysts to be discussed here, the products are most likely to be either CO or formate.

1.8. Aims of the Thesis

In order to fulfil our goal the work was broken down into several specific aims:

- (i) To evaluate the current literature regarding electrocatalysts for the purpose of CO₂ reduction and identify suitable candidates for modification with anchoring groups.
- (ii) To design, synthesise and characterise modified electrocatalysts for the purpose of CO₂ reduction. This modification will take the form of the addition of an anchoring group, either carboxylate or phosphonate, which will enable attachment to a semiconductor at a later stage. The first series of modified electrocatalysts are from known homogeneous catalysts based on either, copper phosphine or palladium phosphine complexes. The second series of modified electrocatalysts are derivatives from known homogeneous catalysts based on either ruthenium(II) diimine or rhenium(I) diimine complexes.
- (iii) To evaluate the capacity of the compounds synthesised during the fulfilment of aim (ii) to act as CO₂ reduction catalysts, whilst the anchoring group is in its protected form of a carboxylate ester or a phosphonate ester. This will be done through photophysical and electrochemical experiments.

- (iv) To deprotect the ester groups, resulting in either a $-C(O)OH$ or $-P(O)(OH)_2$ anchoring group on the complex. To evaluate the capacity of the compounds to act as CO_2 reduction catalysts then compare with the anchor-free derivatives, and the carboxylate vs. the phosphonate derivatives. This will be done through photophysical, electrochemical and gas chromatography experiments.
- (v) To elucidate the effect of the mode of attachment of the anchoring group to the diimine ligand, direct attachment vs. an attachment via a saturated $-CH_2-$ spacer group; the latter having been designed to alleviate the electron withdrawing effect of the anchors which has been perceived to hinder the catalytic activity.
- (vi) Identify the most efficient electrocatalyst from those evaluated. To then establish a method of anchoring the electrocatalyst to a semiconductor, either TiO_2 or Ta_2O_5 , and to determine if anchoring has been successful.

These aims when combined and fulfilled will allow the achievement of the goal of the work, which was to produce a photo-electro-catalytic system capable of CO_2 reduction. They will do this by resulting in the synthesis of a series of compounds for which we have tested and evaluated their catalytic capability for CO_2 reduction. Comparisons between anchor free complexes and anchor group containing complexes as well as carboxylate vs. phosphonate derivatives will have been made allowing for identification of the most efficient electrocatalyst synthesised. Once identified, this complex will be anchored onto the semiconductor for which a method of successful attachment will have been established.

1.9. Aims of the Wider Project

As stated in the previous section the work detailed in this thesis centres on the design and synthesis of molecular electrocatalysts that can be anchored onto a light harvesting semiconductor, for the purpose of creating a photo-electro-catalytic system capable of CO_2 reduction. This was part of a large interdisciplinary consortium “White Rose

CO₂Solar”, which included collaboration with the groups from the Universities of Hull, York, and Leeds.

The other groups in the consortium were engaged in the following tasks:

- (i) The synthesis of semiconductor materials for the absorption of sunlight (York).
- (ii) The modelling and measurement of the electronic band structure across the device (Hull).
- (iii) The characterisation and understanding of the electrocatalyst-semiconductor interface using scanning probe techniques (Leeds).

The overall goal of this research was to produce an integrated photo-electro-catalytic system capable of CO₂ reduction. The design of such a system may appear as shown below in Figure 1.8, in which the component that this thesis focuses on is highlighted.

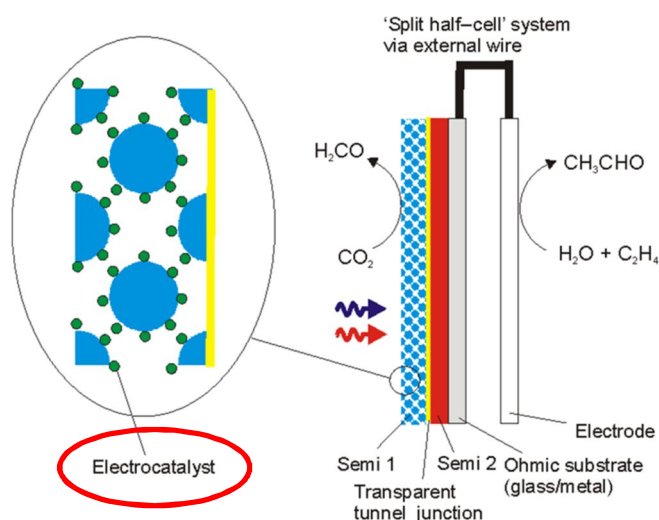


Figure 1.8: The schematic diagram for a potential device incorporating the various components necessary to construct a photo-electro-catalytic system capable of CO₂ reduction.⁴⁰

1.10. Method of Achieving the Aims of the Thesis

In order to fulfil aim (i) of the thesis three classes of transition metal containing compounds will be examined and evaluated. These are; metal complexes with

phosphine ligands, metal complexes containing bipyridine ligands and metal complexes with macrocyclic ligands. These can all be further sub divided by whether or not a semiconductor is attached to the complex, as is the case in some of the following examples. This section provides examples of catalysts and is by no means a comprehensive coverage.

1.10.1. Metal Complexes Containing Phosphine Ligands

The first group of complexes reviewed was those with phosphine ligands incorporated. Research on the phosphine ligand complexes has been carried out for many years and as such, there have been numerous papers published.^{12, 41-53}

Much of the work has been done by DuBois^{42, 43, 47-52} who has been working in the field of CO₂ reduction using phosphine based complexes for the last twenty years. After analysing complexes based on iron, cobalt, nickel and palladium it was determined that complexes of the type $[\text{Pd}(\text{triphosphine})(\text{CH}_3\text{CN})]^{2+}$ (**2**) are capable of electrochemically reducing CO₂ to CO. The numbers in bold e.g. (**2**) correspond to the numbered structures in Figure 1.9.

At low acid concentrations in which the acid is used as a source of protons, the catalytic rates are first order with respect to the catalyst and CO₂ and second order with respect to the acid. At higher acid concentrations, the catalytic rates become independent of the acid concentration, but remain first order with respect to the catalyst and CO₂. It has also been found that a weakly coordinating ligand such as acetonitrile is necessary for the catalytic cycle.^{48, 49, 52}

A mechanism for the catalytic cycle has been proposed and is shown in figure 1.9. After the initial injection of an electron (**3**), a CO₂ molecule is then able to coordinate to the palladium centre (**4**). Addition of a proton then occurs (**5**) followed by the addition of another electron (**6**). The labile solvent molecule is then lost (**7**). A final proton is then added (**8**), this then results in the cleavage of the C–O bond (**9**) due to the migration of the H₂O molecule. The final step of the cycle is then the loss of the H₂O and CO combined with the association of the solvent (**2**).

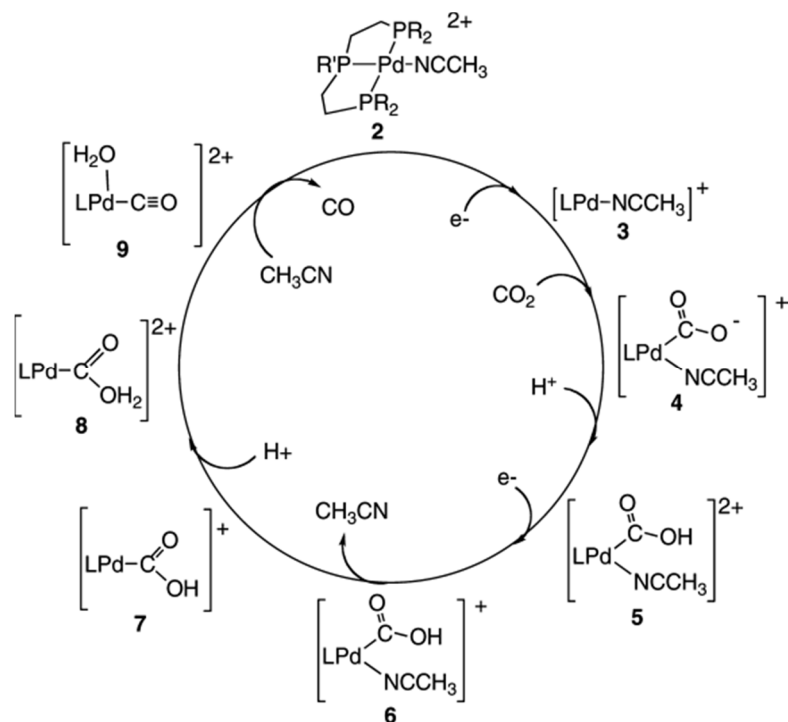


Figure 1.9: The proposed catalytic cycle for the reduction of CO₂ to CO using the DuBois palladium catalyst, L = triphosphine ligand.⁵¹

A second set of complexes which contain phosphine ligands was also reviewed and focuses on the work of Haines et al.^{41, 45} and more recently Kubiak et al.⁵⁴ This work involved the use of dinuclear copper complexes of the type shown below in Figure 1.10. These complexes were shown to have modest increases in current when a CO₂ atmosphere was present.

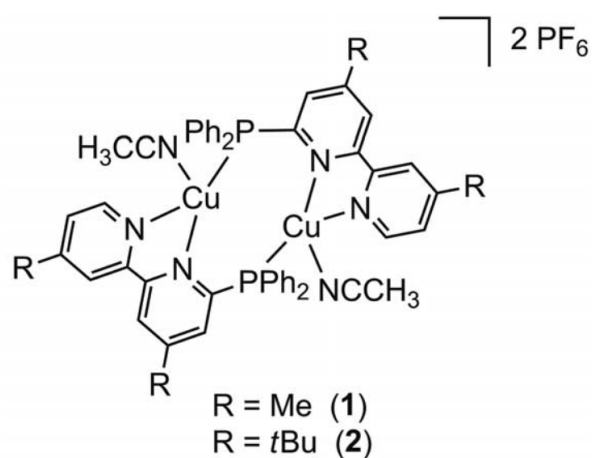


Figure 1.10: An example of a dinuclear copper complex capable of reducing CO₂.⁵⁴

Both the palladium complex and the copper complex seen in the literature were deemed suitable candidates for ligand modification to include an anchoring group in accordance with the fulfilment of the first part of aim (ii). The results of this work are detailed in chapter 3.

1.10.2. Metal Complexes Containing Bipyridine Ligands

The second class of compound is those containing bipyridine ligands. One of the first complexes of this class found to electro-catalytically reduce CO_2 was $\text{Re}(\text{bpy})(\text{CO})_3\text{Cl}$ ($\text{bpy} = 2,2'$ -bipyridine), which was reported in 1984 by Lehn et al.⁵⁵ They reported that CO_2 was successfully reduced to CO at -1.25 V vs. NHE, using a DMF:water (9:1) solution saturated with CO_2 , containing the catalyst and Et_4NCl . This produced CO with 98% current efficiency. They also noted that no CO was produced if the catalyst or CO_2 were absent. In a recent paper⁵⁶ a mechanism for the electro-reduction of CO_2 using Lehn's catalyst was proposed.

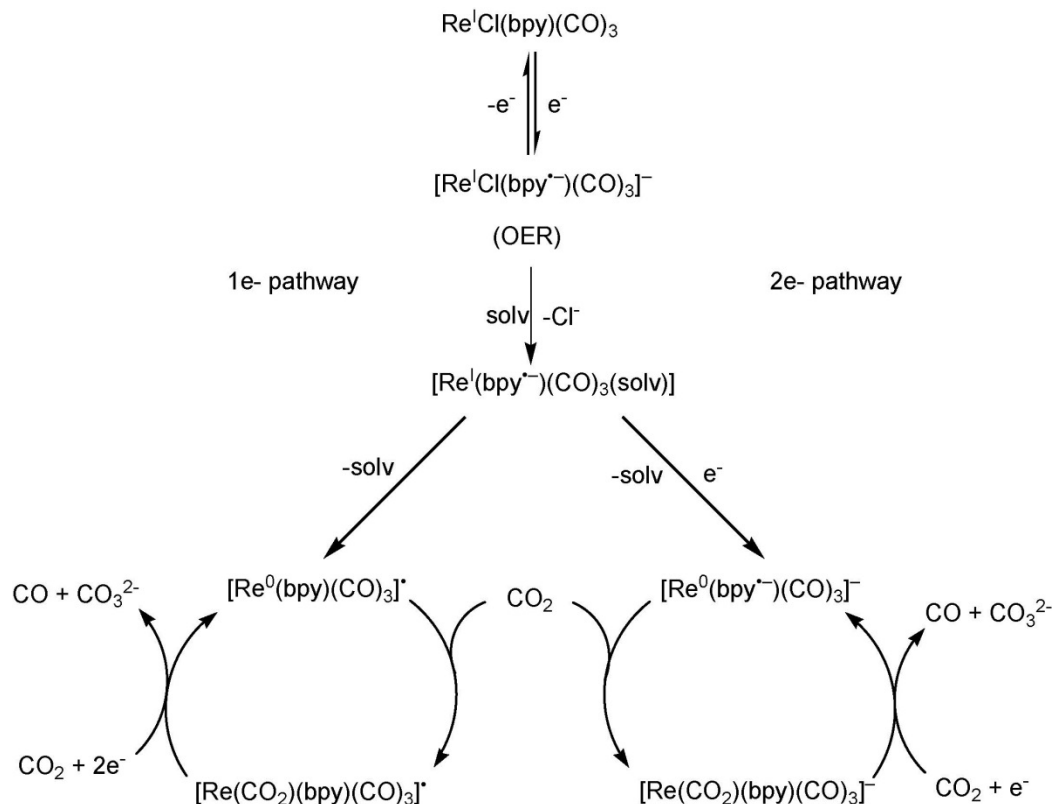


Figure 1.11: The proposed one and two-electron pathways for electrochemical CO_2 reduction.⁵⁶

Figure 1.11 shows the proposed simultaneous one and two-electron pathways leading to CO formation. Whilst the one electron reduction (OER) and $\text{fac-}[\text{Re}(\text{bpy})(\text{CO})_3]^-$ species have been observed using infrared spectro-electro-chemical techniques^{57, 58} neither of the proposed CO_2 adducts, $\text{fac-}[\text{Re}(\text{bpy})(\text{CO})_3(\text{CO}_2)]^+$ or $\text{fac-}[\text{Re}(\text{bpy})(\text{CO})_3(\text{CO}_2)]^-$ have been observed during catalysis.⁵⁶

Although the above papers discuss electro-reduction using Lehn's catalyst and its analogues, the complexes are also capable of catalysing photo-reduction.^{59, 60}

In the same paper that a mechanism for electro-reduction is proposed⁵⁶ a mechanism for the photo-reduction of CO_2 using an analogue of Lehn's catalyst is also proposed.

Figure 1.12 shows that after an initial photon interaction the chloride anion is removed. This then allows a solvent molecule to coordinate and an OER species is formed. The solvent molecule is then displaced and CO_2 coordinates in the form of a bridged dinuclear complex. Upon interaction with another photon and in the presence of an additional CO_2 molecule, the CO reduction product is formed along with CO_3^{2-} and the regeneration of the complex. However, there is again no clear evidence for formation of the CO_2 adducts or reduction of CO_2 by an outer sphere electron-transfer mechanism.

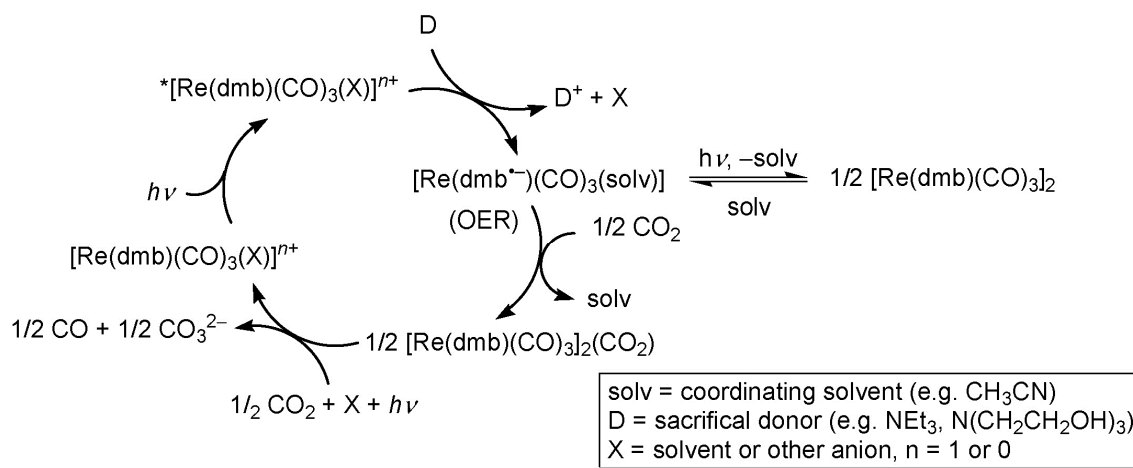


Figure 1.12: The proposed mechanism for the photo-reduction of CO_2 to CO using $\text{fac-ReCl}(\text{dmb})(\text{CO})_3$ ($\text{dmb} = 4,4'$ -dimethyl-2,2'-bipyridine).⁶¹

Ishitani et al.⁶¹ recently reported what effect substituting the chloride ligand by phosphorus ligands PR_3 ($\text{R} = \text{alkyl, alkoxy, or allyl group}$) has on the reduction process.

Their description of the mechanism is almost identical to that of Fujita et al.⁵⁶ in that after the initial photo excitation the ligand, P(OEt)₃ dissociates and forms the solvated complex [Re(bpy^{•-})(CO)₃(solv)]. Ishitani et al. also concurred with the mechanism and the formation of a dinuclear bridge. This work is of great importance because if we know the mechanism of reduction then it will enable us to begin to design new and hopefully better catalysts for CO₂ reduction.

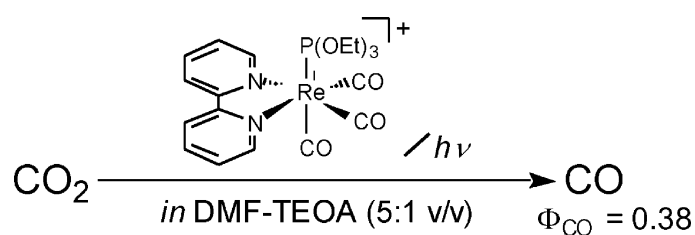


Figure 1.13: The photo-reduction of CO₂ to CO using fac-[Re(bpy)(CO)₃(PR₃)]⁺.⁶¹

Ishitani et al.⁶¹ also examined the mixed system of [Ru(bpy)₃]²⁺ and [Ru(bpy)₂(CO)₂]²⁺ in the presence of CO₂ and a light source (the [Ru(bpy)₃]²⁺ acts as a photosensitizer). They postulate that a one electron reduction (OER) species is being produced in the form of [Ru(II)(bpy^{•-})(bpy)₂]⁺. Reduction of CO₂ then proceeds via electron capture by the catalyst from the OER species, in which a CO₂ molecule coordinates to an open site on the ruthenium centre. This is produced by dissociation of one of the CO ligands after the reduction of [Ru(bpy)₂(CO)₂]²⁺. By controlling the pH of the solution, they are then able to control the outcome of the CO₂ reduction reaction, as shown in figure 1.14.

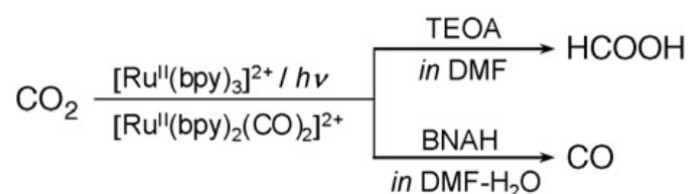


Figure 1.14: The different photo-reduction pathways of CO₂ depending on reaction conditions. TEOA = triethanolamine, BNAH = 1-benzyl-1,4-dihydronicotinamide.⁶¹

The mechanism for a closely related complex, $\text{Re}(\text{dmb})(\text{CO})_3(\text{COOH})$ has recently been explored by use of density functional theory and then supported with experimental work using isotopic labelling ($^{13}\text{CO}_2$). The proposed mechanism is shown below in Figure 1.15, however the analogous complex $\text{Re}(\text{bpy})(\text{CO})_3\text{COOH}$ is used.

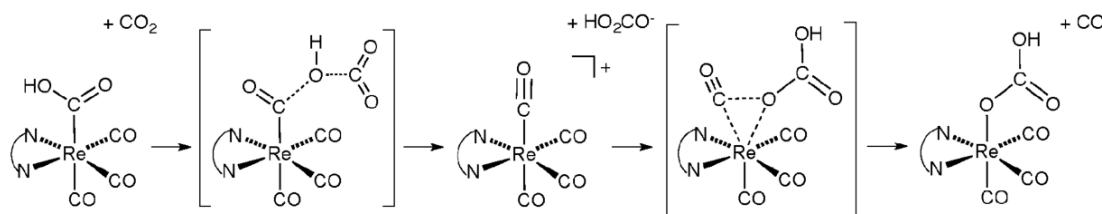


Figure 1.15: The proposed mechanism for the conversion of $\text{Re}(\text{bpy})(\text{CO})_3\text{COOH} + \text{CO}_2$ to $\text{Re}(\text{bpy})(\text{CO})_3\text{OCO}_2\text{H} + \text{CO}$. N–N = 2,2'-bipyridine.⁶²

This work is interesting because if we consider the mechanism mentioned by Kubiak et al.,²⁴ shown in Figure 1.16, it is possible to see an alternate pathway to the one shown above. This involves the $\text{Re}(\text{bpy})(\text{CO})_3\text{COOH}$ species, which they show interacting with H^+ , releasing water followed by CO and the cycle restarting. However, in Figure 1.15 they propose that $\text{Re}(\text{bpy})(\text{CO})_3\text{COOH}$ can interact with a CO_2 molecule, this results in a different pathway being followed, although CO is still released. This is significant because the mechanism in Figure 1.15 is not catalytic and even though CO is released, it is essentially a deactivation pathway for the catalyst. This means that because CO_2 is present in the cycle then over time it would be expected that the catalyst would degrade. When initially discussing catalyst requirements, degradation was identified as something we wanted to try to avoid as it limits catalyst lifetime. A possible remedy to this problem would be to limit the chance of CO_2 interacting with the COOH by adding substituents to the bipyridine ligand, whilst still allowing the H^+ to interact.

This leads nicely onto the work of Smieja and Kubiak^{59, 63} in which additional studies have been carried out on several analogues of the Lehn's catalyst.

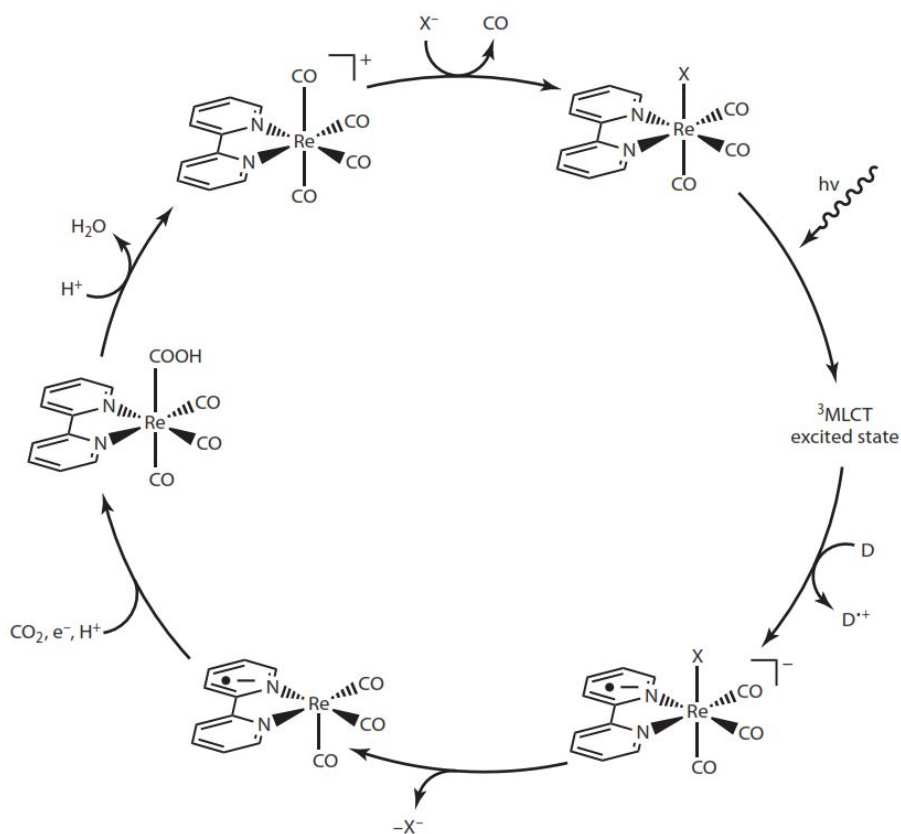


Figure 1.16: The proposed photocatalytic mechanism for CO production from a $\text{Re}(\text{bpy})(\text{CO})_3\text{X}$ catalyst. X is usually a halide.²⁴

In this work Smieja and Kubiak^{59, 63} examined the effect of electron donating and withdrawing groups in the 4,4' position of the bpy ligand (figure 1.17). It was then shown that **(A)** had no current enhancement when CO_2 was present. Lehn's catalyst **(B)** saw a 3.4 fold increase in peak current when CO_2 was present compared with argon. Complex **(C)** had a slightly larger increase and then complex **(D)** had an 18.4 fold increase in current under CO_2 , a reasonable improvement over the original catalyst **(B)**.

However, for complex **(E)** they noted virtually no increase in current under CO_2 even though **(E)** has the most negative reduction potential, which should create a more nucleophilic rhenium centre for CO_2 reduction. This was attributed to a possible π donor versus σ donor effect. Further investigation is currently on going with a variety of substituents in the 4, 4' positions.⁵⁹

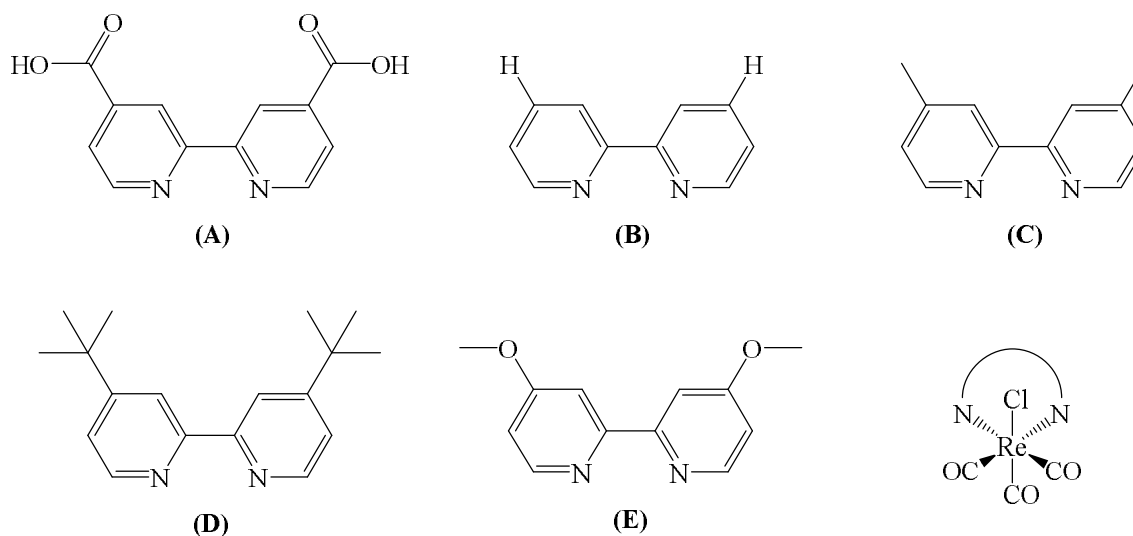


Figure 1.17: The different electron donating/withdrawing substituents in the 4,4' positions of the bipyridine ligand that were studied by Kubiak et al.: COOH **(A)** <H **(B)** <Me **(C)** <^tBu **(D)** <OCH₃ **(E)**.⁵⁹

From this paper, we learnt that it is possible to alter the catalytic current by altering the substituents on the bpy ligand, our work will look at incorporating these ideas when trying to design new catalysts

However work by others is still continuing on this type of complex, with a recent study⁶⁴ examining the structural and spectroscopic properties of different bipyridines with various substituents.

One of the newest areas of research found in the literature is the move from rhenium to manganese.⁶⁵ There are several advantages from doing this; on a practical level, manganese is significantly more abundant than rhenium. This would potentially allow the catalyst to be manufactured at a reduced cost, although this is more of a long-term consideration. Another advantage reported is the reduced overpotentials needed when compared to the analogous rhenium system. This was one of the selection criteria for a good catalyst. A disadvantage however is the need for Brønsted acids in order for catalysis to occur. Given that several different transition metal containing complexes are already under consideration when trying to fulfil the aims of the thesis it was decided

not to examine the manganese systems at this time. However, they are suggested as a possible area of future research in chapter 8.

1.10.3. Metal Complexes Anchored to Semiconductors

To assist in the fulfilment of aim (vi) and as part of the wider project aims, our collaborators were to model and design a semiconductor that would have a sufficient band gap to allow the reduction of CO₂ to one or more of its reduction products. As shown in Figure 1.18, there are several types of semiconductor that would fulfil this criterion.

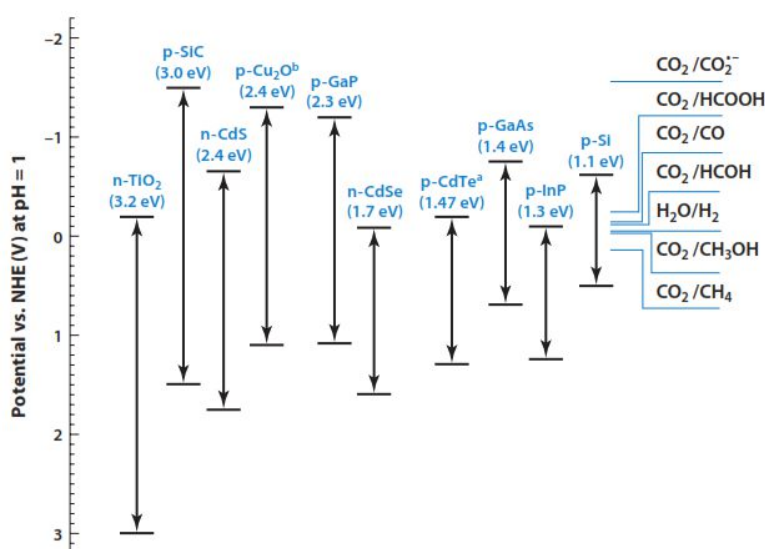


Figure 1.18: The position of the conduction and valence bands of several semiconductors at pH = 1 vs. a normal hydrogen electrode (NHE). Thermodynamic potentials for CO₂ reduction to different products at pH = 1 vs. a NHE are shown beside the band edge positions of semiconductors.²⁴

It was believed that one of these semiconductors or a composite material composed of several would form the core of the device shown in Figure 1.8 onto which the electrocatalyst being designed in this thesis would be anchored. However modelling and designing a suitable material proved more difficult in practice than expected. It was therefore necessary to return to the literature in order to find a suitable candidate. The sections below detail some of the ideas present in the literature, a few of which have

been used when fulfilling the aims of this thesis, aims which are guiding us towards our ultimate goal of an anchored photo-electro-catalytic system capable of CO₂ reduction.

Figure 1.19 is a schematic of the process of electron transfer to the catalyst. Firstly, a photon interacts with the semiconductor creating an electron hole pair, this electron is then transferred to the catalyst where the mechanisms discussed above lead to the reduction of CO₂ to CO. It is important to try to understand the electron transfer process, as was demonstrated in this paper.⁶⁶ In which they were able to achieve a threefold increase in current simply by modifying the surface of the electrode. Such information will be valuable in optimising the catalytic system.

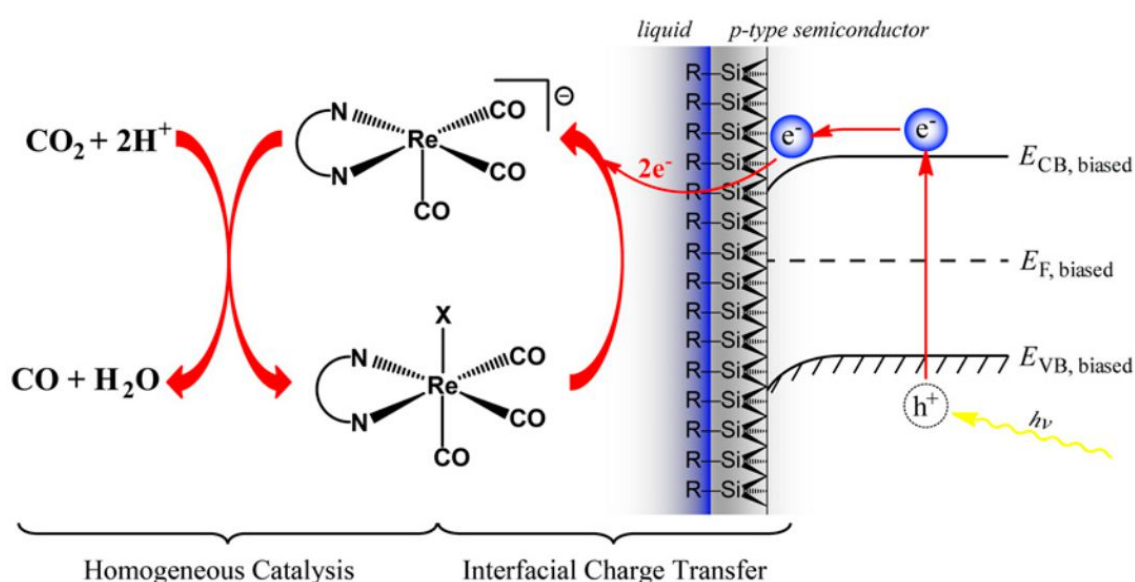


Figure 1.19: The schematic diagram for a device using a p-Si/Re(^tBu₂bpy)(CO)₃Cl semiconductor/molecular catalyst junction to photo-electro-chemically reduce CO₂.⁶⁶

We will now consider some examples in the literature^{63, 66} of anchoring the catalyst onto a semiconductor. This area of research is closely related to the previous one and involves modifying the bipyridine ligands so that they contain a group such as COOH or PO₃H. This modification would then enable them to be anchored to various semiconductors for example TiO₂^{67, 68} and N-Ta₂O₅.^{21, 69}

One example in the literature described the use of $[\text{Ru}(\text{dcbpy})_2(\text{CO})_2]^{2+}$ (dcbpy = 4,4'-dicarboxy-2,2'-bipyridine) coupled to a N-Ta₂O₅ (N = nitrogen doped) semiconductor.^{21, 35} In this system the semiconductor is acting as a photosensitizer. A photon is absorbed; the semiconductor then transfers an electron to the ruthenium complex, which is then able to reduce CO₂ to formic acid. It is interesting to note the similarities between this system and the one described earlier by Ishitani et al.⁶¹ The only real noticeable difference is that one uses $[\text{Ru}(\text{bpy})_3]^{2+}$ and the other uses N-Ta₂O₅ as the photosensitizer. The additions of the COOH groups, which are present to anchor the semiconductor to the complex, do not appear to effect the reduction of CO₂.

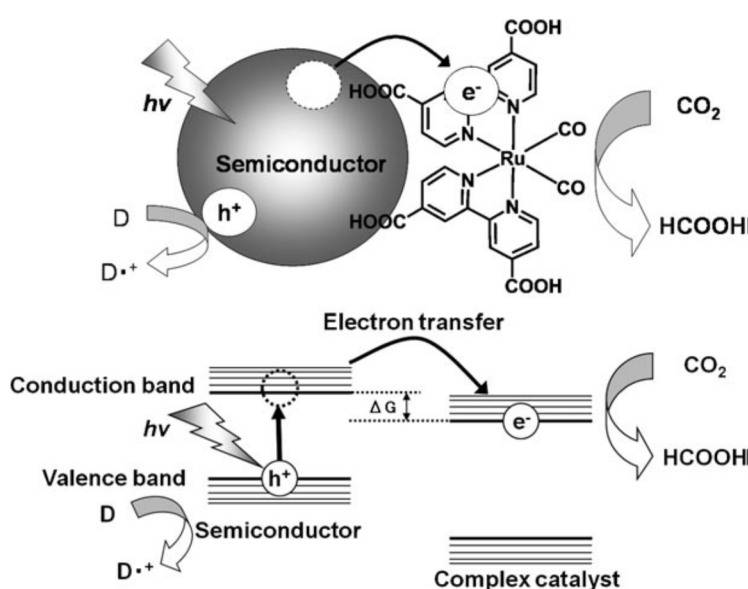


Figure 1.20: The schematic and energy diagram of hybrid photocatalysis under visible light with a semiconductor and a metal complex catalyst.²¹

As previously mentioned when looking to improve catalytic efficiency all aspects of the system need to be considered. Therefore, it would be ideal to be able to control the particle size and porosity of the semiconductor. Greater porosity increases the surface area of the semiconductor and will allow more of the catalyst to be anchored, which in turn increases the likelihood of CO₂ molecules coming into contact with the catalyst, resulting in an improved catalytic efficiency.

One way of achieving this is to construct mesoporous semiconductor spheres as was demonstrated by Suzuki et al.⁷⁰ This was done by using a new method of construction and resulted in spherical submicron-sized mesoporous tantalum oxide spheres.

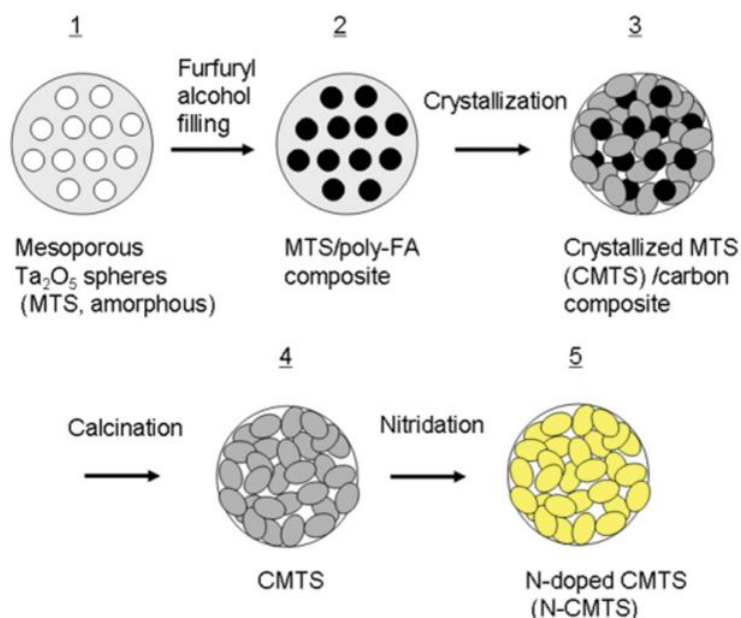


Figure 1.21: The procedure for the synthesis of nitrogen doped crystallized mesoporous tantalum pentoxide spheres (N-CMTS).⁷⁰

Although included in this literature review to help gain a complete picture of the field of research, this type of semiconductor synthesis was not carried out in this thesis. However, our collaborators performed work on mesoporous semiconductors as part of the wider project aims.

Armstrong et al. in their recent papers^{67, 71} described a unique approach in which they have taken a known complex, $[\text{Ru}(\text{bpy})_3]^{2+}$ and added PO_3H groups to attach it to TiO_2 , however they have then attached the TiO_2 onto a CO_2 -reducing enzyme, CODH I, see Figure 1.22

In this system the modified $[\text{Ru}(\text{bpy})_3]^{2+}$ is acting as the photosensitizer which then transfers the electrons through the TiO_2 and onto the enzyme. The enzyme then carries

out the reduction of CO₂ to CO. They reported that at pH 6 and 20 °C the visible light sensitized system produces ~5 μmol CO during 4 h of irradiation. Evaluating this on a per gram of TiO₂ basis gives an average turnover rate of 250 μmol of CO (g of TiO₂)⁻¹ h⁻¹. On a per mole of CODH I basis, the turnover rate is ~530 h⁻¹ (0.15 s⁻¹).⁶⁷

The system does suffer from a few problems though; firstly the conduction band of TiO₂ is only just sufficient for CO₂ reduction at CODH I (~ -0.52 V vs. SHE). Secondly, the enzyme is only weakly bound to the TiO₂. This is a problem because if the enzyme dissociates then CO₂ will not be able to be reduced due to incomplete electron transfer from the photosensitizer. These factors will have to be carefully considered when trying to build better systems in the future.

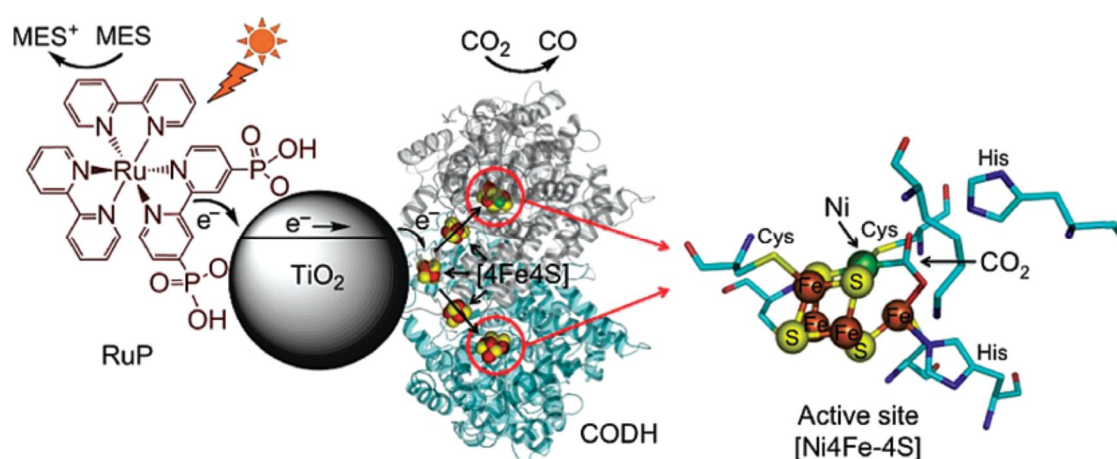


Figure 1.22: The CO₂ photoreduction system using Ch CODH I attached to RuP-modified TiO₂ nanoparticles. Ch CODH I represents the first of five carbon monoxide dehydrogenase (CODH) enzymes found in the anaerobic microbe *Carboxythermus hydrogenoformans* (Ch). The oxidized photosensitizer is recovered by the sacrificial electron donor 2-(N-morpholino)ethanesulfonic acid (MES).⁶⁷

1.10.4. Metal Complexes Containing Macrocyclic Ligands

The final class of compounds examined from the literature are those containing macrocyclic ligands.⁷²⁻⁷⁶ In 2002 Fujita et al. published their findings on cobalt and iron corroles and their ability to catalyse the reduction of CO₂ to CO.⁷⁷ Some of the complexes studied are shown in figure 1.23. They were found to reduce CO₂ to CO or produce H₂ in the presence of a sacrificial donor (Et₃N) and a photosensitizer (p-

terphenyl). However, the systems were not without their flaws, they suffered from high overpotentials and catalyst decomposition.

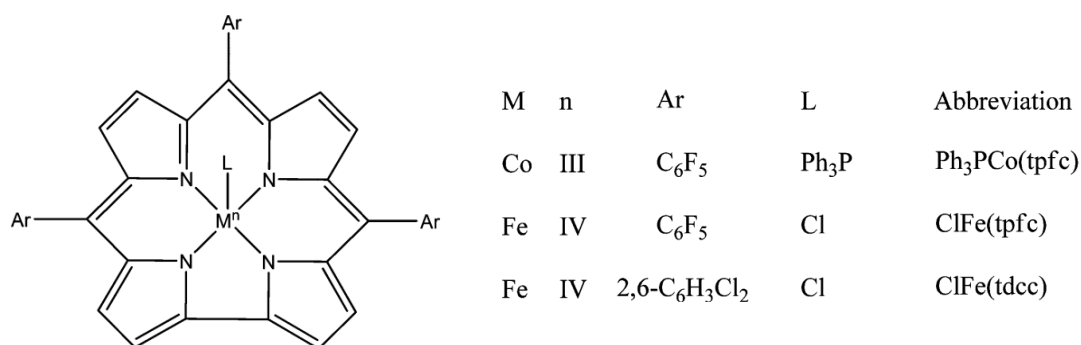


Figure 1.23: The Fujita metal corrole complexes for the photochemical reduction of CO₂ to CO.⁷⁷

In 2004 Toma et al.⁷⁸ reported on a series of porphyrin based ruthenium complexes that were then attached onto TiO₂ films. From their research they were able to conclude that when only two Ru(phen)₂Cl groups are present as opposed to four there is a better absorption of the complex onto the TiO₂ surface. This was attributed to the free pyridyl groups being able to anchor to the TiO₂. This better absorption resulted in a more efficient transfer of electrons to the conduction band of TiO₂.

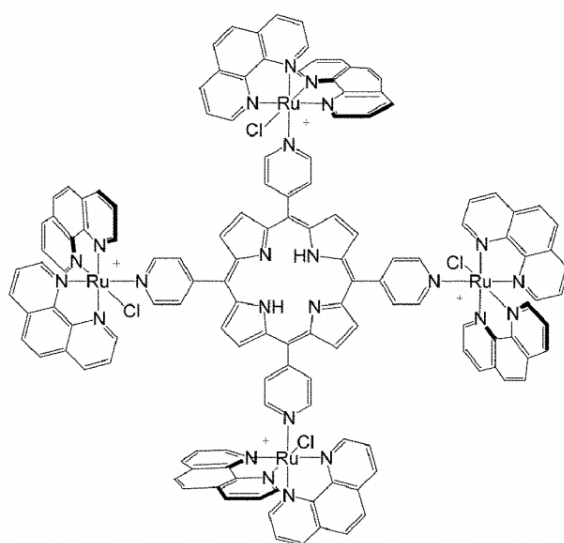


Figure 1.24: Four Ru(phen)₂Cl units coordinated to meso-tetrapyrrolylporphyrin, phen = phenanthroline.⁷⁸

complexes being purely electrocatalysts. The aim(s) being to take these compounds and modify them to contain an anchoring ligand, which would enable them to be attached onto a semiconductor of our choosing. Two different transition metal complexes were chosen from the literature and were synthesised, characterised and analysed. For full details and results of these complexes, see chapter 3.

Work on the second class of complex chosen has been ongoing for many years as shown by the great number of papers that have been published on the subject.^{30, 31, 80-86}

Recent literature has provided us with possible mechanisms for both the photo- and electro-reduction of CO₂ using the complex, Re(bpy)(CO)₃Cl, which will be important when trying to design analogues. However, there are numerous mechanisms currently present in the literature.^{24, 56, 61, 62, 87} Each of these is slightly different from the others although usually backed up by some form of experimental evidence. This demonstrates the need for further research to try to obtain an accurate mechanism.

The effect of varying the electron donating / withdrawing properties of substituents on the bipyridine ligand was also considered and will be helpful in fulfilling aims (ii) and (v).

Additionally, changing the metal from rhenium to manganese was briefly considered and advantages and disadvantages discussed.

Taking all of the information gained from the literature it was decided to focus on the ruthenium containing dicarbonyl systems as described by Sato et al. and rhenium containing bipyridyl systems as described by Lehn et al. This forms the basis of the second part of aim (ii) for which the work is presented and discussed fully in chapters 4 and 5 respectively. Our designs were then modified to incorporate the effects of changing the substituents on one of the bipyridine ligands, as shown by Kubiak et al., whilst still maintaining an anchoring group on the second bipyridine. The majority of the work concerning the ruthenium systems revolved around using carboxylate-containing ligands to anchor the complex on to the semiconductor. However, the use of

phosphonate containing ligands instead of carboxylate has also been considered and discussed, see chapter 4.

Research involving the use of analogues of Lehn's catalyst, which contain phosphonate anchoring groups has also been performed, this included electrochemical analysis and gas chromatography to identify any gaseous products as part of aims (iii) and (iv).

How the addition of a semiconductor effects the reduction of CO₂ was explored and some potential synthetic leads were discovered. A discussion of the different types of semiconductor available and any relevant properties they have was also carried out. This included the process of electron transfer at a surface interface, and using mesoporous materials to control particle size and porosity.

In accordance with aim (vi), literature looking at the best method for attaching the complexes onto the semiconductor was examined, although not shown above, the work is detailed and discussed in chapter 6.

The final class of compounds to be reviewed contained macrocycles, a few examples were shown along with a proposed mechanism for CO₂ reduction. This type of complex has not been examined in this thesis and has only been mentioned for completeness.

1.11. References

1. N. Armaroli and V. Balzani, *Angew. Chem. Int. Ed.*, 2007, **46**, 52–66.
2. *International Energy Outlook 2010*, US Department of Energy, Washington, DC, July 2010.
3. T. A. Napp, A. Gambhir, T. P. Hills, N. Florin and P. S. Fennell, *Renew. Sust. Energ. Rev.*, 2014, **30**, 616–640.
4. C. L. Quéré, T. Takahashi, E. T. Buitenhuis, C. Rödenbeck and S. C. Sutherland, *Global Biogeochem. Cycles*, 2010, **24**, GB4007.
5. T. Sueyoshi and M. Goto, *Energy Policy*, 2010, **38**, 5902–5911.
6. N. P. Gillett, V. K. Arora, K. Zickfeld, S. J. Marshall and W. J. Merryfield, *Nat. Geosci.*, 2011, **4**, 83–87.

7. A. A. Lacis, G. A. Schmidt, D. Rind and R. A. Ruedy, *Science*, 2010, **330**, 356–359.
8. A. Kelly, *Energy Environ.*, 2010, **21**, 611–632.
9. *IPCC Fourth Assessment Report: Climate Change 2007*.
10. S. C. Roy, O. K. Varghese, M. Paulose and C. A. Grimes, *ACS Nano*, 2010, **4**, 1259–1278.
11. S. Ardo and G. J. Meyer, *Chem. Soc. Rev.*, 2009, **38**, 115–164.
12. E. E. Benson, C. P. Kubiak, A. J. Sathrum and J. M. Smieja, *Chem. Soc. Rev.*, 2009, **38**, 89–99.
13. G. Centi and S. Perathoner, *Catal. Today*, 2009, **148**, 191–205.
14. J. Barber, *Chem. Soc. Rev.*, 2009, **38**, 185–196.
15. S. Parker, *Platinum(II) Diimine Acetylide Complexes: Synthesis and Elucidation of Their Photophysical Properties to Determine Their Potential for Storing Energy in a Charge Separated State*, MChem Thesis, University of Sheffield, 2010.
16. W. J. Youngblood, S.-H. A. Lee, K. Maeda and T. E. Mallouk, *Acc. Chem. Res.*, 2009, **42**, 1966–1973.
17. L. Hammarström and S. Hammes-Schiffer, *Acc. Chem. Res.*, 2009, **42**, 1859–1860.
18. M. Hambourger, G. F. Moore, D. M. Kramer, D. Gust, A. L. Moore and T. A. Moore, *Chem. Soc. Rev.*, 2009, **38**, 25–35.
19. B. P. Sullivan, *Platinum Met. Rev.*, 1989, **33**, 2–9.
20. H. Ishida, H. Tanaka, K. Tanaka and T. Tanaka, *J. Chem. Soc., Chem. Commun.*, 1987, 131–132.
21. S. Sato, T. Morikawa, S. Saeki, T. Kajino and T. Motohiro, *Angew. Chem. Int. Ed.*, 2010, **49**, 5101–5105.
22. G. R. Dey, *J. Nat. Gas Chem.*, 2007, **16**, 217–226.
23. A. P. Umpierre, E. de Jesús and J. Dupont, *ChemCatChem*, 2011, **3**, 1413–1418.
24. B. Kumar, M. Llorente, J. Froehlich, T. Dang, A. Sathrum and C. P. Kubiak, *Annu. Rev. Phys. Chem.*, 2012, **63**, 541–569.
25. P. Atkins and J. D. Paula, *Atkins Physical Chemistry*, 8th edn., Oxford University Press, 2006.
26. A. J. Bard and L. R. Faulkner, *Electrochemical Methods: Fundamentals and Applications*, 2nd edn., John Wiley & Sons, 2001.
27. *Electrochemistry*,
<http://alpha.chem.umb.edu/chemistry/ch612/documents/Echem.pdf>, Accessed 23/07/12.
28. D. F. Watson and G. J. Meyer, *Annu. Rev. Phys. Chem.*, 2005, **56**, 119–156.

29. P. Liska, N. Vlachopoulos, M. K. Nazeeruddin, P. Comte and M. Grätzel, *J. Am. Chem. Soc.*, 1988, **110**, 3686–3687.
30. C. Nasr, P. V. Kamat and S. Hotchandani, *J. Phys. Chem. B*, 1998, **102**, 10047–10056.
31. G. Ramakrishna, D. A. Jose, D. K. Kumar, A. Das, D. K. Palit and H. N. Ghosh, *J. Phys. Chem. B*, 2005, **109**, 15445–15453.
32. E. L. Aleksandrova and N. N. Khimich, *Semiconductors*, 2004, **38**, 1280–1283.
33. A. Listorti, B. O'Regan and J. R. Durrant, *Chem. Mater.*, 2011, **23**, 3381–3399.
34. S. Sato, T. Arai, T. Morikawa, K. Uemura, T. M. Suzuki, H. Tanaka and T. Kajino, *J. Am. Chem. Soc.*, 2011, **133**, 15240–15243.
35. T. M. Suzuki, H. Tanaka, T. Morikawa, M. Iwaki, S. Sato, S. Saeki, M. Inoue, T. Kajino and T. Motohiro, *Chem. Commun.*, 2011, **47**, 8673–8675.
36. K.-i. Yamanaka, S. Sato, M. Iwaki, T. Kajino and T. Morikawa, *J. Phys. Chem. C*, 2011, **115**, 18348–18353.
37. S. Sato, T. Morikawa, T. Kajino and O. Ishitani, *Angew. Chem. Int. Ed.*, 2013, **52**, 988–992.
38. C. D. Windle, E. Pastor, A. Reynal, A. C. Whitwood, Y. Vaynzof, J. R. Durrant, R. N. Perutz and E. Reisner, *Chem. Eur. J.*, 2015, **21**, 3746–3754.
39. G. Zeng, J. Qiu, Z. Li, P. Pavaskar and S. B. Cronin, *ACS Catal.*, 2014, **4**, 3512–3516.
40. *White Rose Solar CO₂ Network*, <http://www.hull.ac.uk/chemistry/WhiteRoseSolarCO2/>, Accessed 06-06-12.
41. R. J. Haines, R. E. Wittrig and C. P. Kubiak, *Inorg. Chem.*, 1994, **33**, 4723–4728.
42. B. D. Steffey, C. J. Curtis and D. L. DuBois, *Organometallics*, 1995, **14**, 4937–4943.
43. J. W. Raebiger, J. W. Turner, B. C. Noll, C. J. Curtis, A. Miedaner, B. Cox and D. L. DuBois, *Organometallics*, 2006, **25**, 3345–3351.
44. T. Kimura and Y. Uozumi, *Organometallics*, 2006, **25**, 4883–4887.
45. J. S. Field, R. J. Haines, C. J. Parry and S. H. Sookraj, *Polyhedron*, 1993, **12**, 2425–2428.
46. I. P. Beletskaya, A. V. Chuchuryukin, G. v. Koten, H. P. Dijkstra, G. P. M. v. Klink, A. N. Kashin, S. E. Nefedov and I. L. Eremenko, *Russ. J. Org. Chem.*, 2003, **39**, 1268–1281.
47. D. L. DuBois, *Comments Inorg. Chem.*, 1997, **19**, 307–325.
48. D. L. DuBois, A. Miedaner and R. C. Haltiwanger, *J. Am. Chem. Soc.*, 1991, **113**, 8753–8764.
49. A. Miedaner, B. C. Noll and D. L. DuBois, *Organometallics*, 1997, **16**, 5779–5791.

50. B. D. Steffey, A. Miedaner, M. L. Maciejewski-Farmer, P. R. Bernatis, A. M. Herring, V. S. Allured, V. Carperos and D. L. DuBois, *Organometallics*, 1994, **13**, 4844–4855.
51. M. R. DuBois and D. L. DuBois, *Acc. Chem. Res.*, 2009, **42**, 1974–1982.
52. P. R. Bernatis, A. Miedaner, R. C. Haltiwanger and D. L. DuBois, *Organometallics*, 1994, **13**, 4835–4843.
53. N. Selander and K. J. Szabó, *Chem. Rev.*, 2011, **111**, 2048–2076.
54. A. M. Lilio, K. A. Grice and C. P. Kubiak, *Eur. J. Inorg. Chem.*, 2013, 4016–4023.
55. J. Hawecker, J.-M. Lehn and R. Ziessel, *J. Chem. Soc., Chem. Commun.*, 1984, 328–330.
56. M. D. Doherty, D. C. Grills, J. T. Muckerman, D. E. Polyansky and E. Fujita, *Coord. Chem. Rev.*, 2010, **254**, 2472–2482.
57. F. P. A. Johnson, M. W. George, F. Hartl and J. J. Turner, *Organometallics*, 1996, **15**, 3374–3387.
58. E. E. Benson and C. P. Kubiak, *Chem. Commun.*, 2012, **48**, 7374–7376.
59. J. M. Smieja and C. P. Kubiak, *Inorg. Chem.*, 2010, **49**, 9283–9289.
60. J. Hawecker, J.-M. Lehn and R. Ziessel, *Helv. Chim. Acta*, 1986, **69**, 1990–2012.
61. H. Takeda and O. Ishitani, *Coord. Chem. Rev.*, 2010, **254**, 346–354.
62. J. Agarwal, B. C. Sanders, E. Fujita, H. F. Schaefer, T. C. Harrop and J. T. Muckerman, *Chem. Commun.*, 2012, **48**, 6797–6799.
63. B. Kumar, J. M. Smieja, A. F. Sasayama and C. P. Kubiak, *Chem. Commun.*, 2012, **48**, 272–274.
64. E. E. Benson, K. A. Grice, J. M. Smieja and C. P. Kubiak, *Polyhedron*, 2013, **58**, 229–234.
65. J. M. Smieja, M. D. Sampson, K. A. Grice, E. E. Benson, J. D. Froehlich and C. P. Kubiak, *Inorg. Chem.*, 2013, **52**, 2484–2491.
66. J. M. Smieja, E. E. Benson, B. Kumar, K. A. Grice, C. S. Seu, A. J. M. Miller, J. M. Mayer and C. P. Kubiak, *PNAS*, 2012, **109**, 15646–15650.
67. T. W. Woolerton, S. Sheard, E. Reisner, E. Pierce, S. W. Ragsdale and F. A. Armstrong, *J. Am. Chem. Soc.*, 2010, **132**, 2132–2133.
68. A. Grabulosa, M. Beley, P. C. Gros, S. Cazzanti, S. Caramori and C. A. Bignozzi, *Inorg. Chem.*, 2009, **48**, 8030–8036.
69. T. Morikawa, S. Saeki, T. Suzuki, T. Kajino and T. Motohiro, *Appl. Phys. Lett.*, 2010, **96**, 142111–142113.
70. T. M. Suzuki, T. Nakamura, S. Saeki, Y. Matsuoka, H. Tanaka, K. Yano, T. Kajino and T. Morikawa, *J. Mater. Chem.*, 2012, **22**, 24584–24590.

71. Y. S. Chaudhary, T. W. Woolerton, C. S. Allen, J. H. Warner, E. Pierce, S. W. Ragsdale and F. A. Armstrong, *Chem. Commun.*, 2012, **48**, 58–60.
72. A. J. Morris, G. J. Meyer and E. Fujita, *Acc. Chem. Res.*, 2009, **42**, 1983–1994.
73. C. D. Windle, M. W. George, R. N. Perutz, P. A. Summers, X.-Z. Sun and A. C. Whitwood, *Chem. Sci.*, 2015, **6**, 6847–6864.
74. C. D. Windle, M. V. Campian, A.-K. Duhme-Klair, E. A. Gibson, R. N. Perutz and J. Schneider, *Chem. Commun.*, 2012, **48**, 8189–8191.
75. C. Matlachowski, B. Braun, S. Tschierlei and M. Schwalbe, *Inorg. Chem.*, 2015, **54**, 10351–10360.
76. J. Schneider, K. Q. Vuong, J. A. Calladine, X.-Z. Sun, A. C. Whitwood, M. W. George and R. N. Perutz, *Inorg. Chem.*, 2011, **50**, 11877–11889.
77. J. Grodkowski, P. Neta, E. Fujita, A. Mahammed, L. Simkhovich and Z. Gross, *J. Phys. Chem. A*, 2002, **106**, 4772–4778.
78. A. F. Nogueira, A. L. B. Formiga, H. Winnischofer, M. Nakamura, F. M. Engelmann, K. Araki and H. E. Toma, *Photochem. Photobiol. Sci.*, 2004, **3**, 56–62.
79. J. Schneider, H. Jia, J. T. Muckerman and E. Fujita, *Chem. Soc. Rev.*, 2012, **41**, 2036–2051.
80. M. Bourrez, F. Molton, S. Chardon-Noblat and A. Deronzier, *Angew. Chem. Int. Ed.*, 2011, **50**, 9903–9906.
81. E. Fujita, *Coord. Chem. Rev.*, 1999, **185–186**, 373–384.
82. K. Sayama, H. Sugihara and H. Arakawa, *Chem. Mater.*, 1998, **10**, 3825–3832.
83. R. Ghanem, Y. Xu, J. Pan, T. Hoffmann, J. Andersson, T. Polívka, T. Pascher, S. Styring, L. Sun and V. Sundström, *Inorg. Chem.*, 2002, **41**, 6258–6266.
84. S. Chardon-Noblat, A. Deronzier, R. Ziessel and D. Zsoldos, *Inorg. Chem.*, 1997, **36**, 5384–5389.
85. J. Ettetdgui, Y. Diskin-Posner, L. Weiner and R. Neumann, *J. Am. Chem. Soc.*, 2011, **133**, 188–190.
86. Z.-Y. Bian, S.-M. Chi, L. Li and W. Fu, *J. Chem. Soc., Dalton Trans.*, 2010, **39**, 7884–7887.
87. J. Agarwal, R. P. Johnson and G. Li, *J. Phys. Chem. A*, 2011, **115**, 2877–2881.

2. Materials and General Procedures

All commercially available materials were of laboratory grade and were used without further purification unless stated.

Dry solvents were obtained from the Grubbs solvent system and kept under an inert atmosphere with 4 Å molecular sieves present to remove any further traces of water.

Air sensitive synthesis was performed using standard Schlenk techniques under an inert atmosphere of either nitrogen or argon.

Where a column was used in purification, silica, 60 Å mesh, from Fluorochem was used.

2.1. ¹H NMR Spectroscopy

¹H NMR was performed on either a 250 or 400 MHz Bruker Avance AV250/AV400 spectrometer. The samples were dissolved in CDCl₃, CD₂Cl₂ or DMSO-d₆ and filtered if necessary. The spectra were analysed using the software MestReNova 6 and were referenced to the residual solvent peak.¹

2.2. ¹⁹F NMR Spectroscopy

¹⁹F NMR was performed at 235 MHz on a Bruker Avance AV250 spectrometer. The samples were dissolved in DMSO-d₆ and filtered if necessary. An external reference of CFCl₃ was used. The spectra were analysed using the software MestReNova 6.

2.3. ³¹P NMR Spectroscopy

³¹P NMR was performed at 101 MHz on a Bruker Avance AV250 spectrometer. The samples were dissolved in CDCl₃, CD₂Cl₂ or DMSO-d₆ and filtered if necessary. An external reference of H₃PO₄ was used. The spectrometer automatically decoupled the ³¹P signals from ¹H signals. The spectra were analysed using the software MestReNova 6.

2.4. Mass Spectrometry

Mass spectra were obtained from the mass spectrometry service at the University of Sheffield. Electron ionisation (EI) mass spectrometry was performed on a VG Autospec magnetic sector instrument. Positive electrospray (ES^+) and negative electrospray (ES^-) was performed using a Waters LCT time of flight mass analyser. Matrix assisted laser desorption ionisation (MALDI) was performed using a Bruker Reflex III instrument fitted with a ToF mass analyser utilising a DCTB trans-2-[3-(4-tert-butylphenyl)-2-methyl-2-propenylidene]malononitrile matrix.

2.5. Elemental Analysis

Elemental microanalysis was performed by the Elemental analysis service at the University of Sheffield. Carbon, hydrogen and nitrogen analyses were performed using a Perkin Elmer 2400 Series II CHNS/O System.

2.6. UV-Vis Spectroscopy

UV-Vis spectroscopy was carried out on a Cary 50 Bio (200 – 1100 nm range) or Cary 5000 (175 – 3000 nm range) UV-Vis spectrophotometer using Cary WinUV Scan V3.00 software to record the data. The samples were run in either 1 cm or 1 mm quartz cuvettes at room temperature. The solvent used was dependant on the compound being analysed and is stated in the relevant figure captions. Spectra were obtained at 600 nm/min with a resolution of 0.42 – 0.63 nm.

2.7. Emission Spectroscopy

Emission spectroscopy was carried out on a Horiba Jobin Yvon Fluoromax-4 spectrofluorometer. The samples in DCM or DMF were degassed using the freeze-pump-thaw method with argon or were left under vacuum. See relevant figure captions for specific details on excitation wavelengths used. Resolution of spectra obtained was 1 nm. Integration time used was 0.5 s.

Excitation spectroscopy was carried out on the same instrument and using the same samples as the emission spectroscopy. The wavelengths used are contained in the relevant figure captions. Resolution of spectra obtained was 1 nm. Integration time used was 0.5 s.

2.8. Time-Resolved Emission Spectroscopy

Time-resolved emission (or emission lifetime) spectroscopy was carried out on an Edinburgh Instruments Mini-tau spectrometer using Time-Correlated Single Photon Counting (TCSPC). The samples in DCM or DMF were degassed using the freeze-pump-thaw method with argon or were left under vacuum. The samples were excited with a 405 nm, ca. 75 ps laser pulse. A bandpass filter allowing either 575 – 625 nm or 625 – 675 nm wavelengths was placed in between the sample and the detector. The instrument was controlled through the F900 software and set to 1024 channels mode. The duration between pulses was set on the laser control panel with the timescale of the experiment window set to match using the software. The duration of the counts acquisition time varied depending on the concentration of the sample and the number of counts generated by the sample. Lifetime values were obtained by exponential fitting using the F900 software.

2.9. IR Spectroscopy

IR spectroscopy was carried out either in the solid state using a FT IR Bruker Alpha or in solution using a Perkin Elmer Spectrum One FTIR spectrometer. Solution phase samples were in deuterated chloroform. Resolution of spectra obtained from solid state is 4 cm^{-1} , from the solution phase is 1 cm^{-1} .

2.10. Transient Absorption Spectroscopy

Transient absorption spectra were measured on a custom-built setup. The tripled output of a Q-switched Nd:YAG laser LS-2137U (LOTIS TII) was used as the excitation source (7 ns, 355 nm), while the probing was performed with a steady-state 150 W Hamamatsu Arc Xenon lamp. The probe beam was passed through a

monochromator before being detected by a custom-built detector unit, based on a FEU-118 photomultiplier tube. The detector current output was coupled into a Tektronix TDS 3032B digital oscilloscope and subsequently transferred to the computer. The instrumental response function is estimated at about 22 ns full width at half maximum. Sample solutions in CH₃CN were degassed by the freeze–pump–thaw technique in 10 mm quartz cells and subsequently saturated with argon. Sample solutions in water were deoxygenated with the freeze–pump–thaw technique (with careful freezing of the sample) in 10 mm quartz cells, and subsequently filled with argon. Sample solutions in DCM were degassed by the freeze–pump–thaw technique in 10 mm quartz cells and subsequently saturated with argon. The excitation energies and sample concentrations used were 2.5 – 5 mJ and 20 – 35 μM respectively.^{2,3}

2.11. Electrochemistry

Standard cyclic voltammetry was carried out using an Autolab Potentiostat 100 attached to a computer using GPES V4.9 software to record the data. The experiments were performed in a glass sample tube using a glassy carbon working electrode or a platinum disk electrode, a platinum wire counter electrode and a Ag/AgCl reference electrode under a N₂ or CO₂ atmosphere. 0.2 M of [NBu₄][PF₆] electrolyte was used when using DMF or acetonitrile and 0.4 M of [NBu₄][PF₆] electrolyte when using DCM. 2 mM solutions of the test compounds were used unless stated otherwise. The solution was saturated with either N₂ or CO₂ by bubbling the gas into the solution for a minimum of 30 minutes. The traces were obtained in the following way. The forward trace starts at 0 V vs. Ag/AgCl and progresses towards the maximum negative potential, usually about –2.5 V vs Ag/AgCl. Once it reaches this maximum the return trace progresses back to 0 V vs. Ag/AgCl and the scan is completed. Due to this, the current upon reaching the endpoint is always less negative than the starting point when at the same potential. E.g., when the start point is at 0 V the current is –8 μA and when the end point is at 0 V the current is –2 μA. All redox potentials quoted in the figures and results and discussion sections are vs. the ferrocene-ferrocenium couple (Fc/Fc⁺). Scan rates of 20 – 500 mVs⁻¹ were used, with the figure caption stating which was used to obtain the traces shown.

Bulk cyclic voltammetry was carried out using an Autolab Potentiostat 100 attached to a computer using GPES V4.9 software to record the data. The experiments were performed in a custom-made glass vessel. A platinum mesh working electrode, a platinum wire counter electrode and a Ag/AgCl reference electrode under a N₂ or CO₂ atmosphere. 0.2 M of [NBu₄][PF₆] electrolyte was dissolved in acetonitrile. 2 mM solutions of the compounds were used unless stated. The traces were obtained in a similar way to the method above, except that the potential was held at the maximum negative potential for a specified duration, see the relevant figure captions, before returning to the starting potential. All redox potentials quoted in the figures and results and discussion sections are versus the ferrocene-ferrocenium couple (Fc/Fc⁺).

2.12. Gas Chromatography

The experiments were performed on a Perkin Elmer Arnel Autosystem XL GC in TCD mode using hydrogen as the carrier gas and reference gas. The TCD compares the thermal conductivities of the reference gas and the carrier gas plus sample components. The column used was a Restek RT-M porous layer sieve 5 Å, length 30 m, inside diameter 0.53 mm. The machine was setup using a template designed by the technician. The template was loaded and then the machine was given a minimum of 30 minutes to equilibrate. Once this was complete, the sample could be injected using an airtight syringe. The machine would then run the sample and the data was recorded onto the computer. The template was set with the following parameters; the oven is set to 30 °C for 3 minutes, the temperature then increases 10 °C per minute until 100 °C and then held for 1 minute. The injector temperature is set to 100 °C. The flow rate of H₂ is set at 5 mL per minute. The detector is set to 100 °C.

A sample of helium was used to provide a reference retention time (t_0), which can be used to calculate the relative (corrected) retention times of the gases detected. This is done using the equation; $t'_R = t_R - t_0$, where t'_R is the relative retention time, t_R is the retention time of the gas detected and t_0 is the reference retention time. Using the instrument as described above, a reference retention time (t_0) of 1.6 minutes was obtained.

2.13. X-ray Photoelectron Spectroscopy (XPS)

The experiments were performed at the University of Leeds using a VG Escalab 250. The Escalab has a high intensity monochromated Al K-alpha source that can be focussed to a spot 120 – 600 μm in diameter on the sample. This allowed for high resolution XPS with a high signal to noise ratio. All the samples were prepared simultaneously and applied to a metal plate containing double-sided sticky tape. The plate was then inserted into a chamber of the machine. The chamber was then heated to 200 $^{\circ}\text{C}$ whilst evacuated down to around 1^{-10} atm, which took about 1.5 hours. Once this was completed, the samples were analysed over a period of several hours overnight and the results recorded by the computer.

2.14. References

1. G. R. Fulmer, A. J. M. Miller, N. H. Sherden, H. E. Gottlieb, A. Nudelman, B. M. Stoltz, J. E. Bercaw and K. I. Goldberg, *Organometallics*, 2010, **29**, 2176–2179.
2. S. Parker, *Platinum(II) Diimine Acetylide Complexes: Synthesis and Elucidation of Their Photophysical Properties to Determine Their Potential for Storing Energy in a Charge Separated State*, MChem Thesis, University of Sheffield, 2010.
3. S. P. Foxon, C. Green, M. G. Walker, A. Wragg, H. Adams, J. A. Weinstein, S. C. Parker, A. J. H. M. Meijer and J. A. Thomas, *Inorg. Chem.*, 2012, **51**, 463–471.

3. Metal Complexes Containing Phosphine Ligands as Potential Catalysts for CO₂ Reduction

3.1. Introduction

The first class of compounds considered for catalytic purposes during this research are transition metal complexes containing phosphine ligands. Specifically those that are in the form of either a pincer complex as shown in Figure 3.3 or as a dinuclear metal complex as shown in Figure 3.9. The pincer type complexes can be varied by changing the metal involved with numerous examples existing within the literature. Some of these include using iridium,^{1, 2} nickel,³⁻⁵ palladium,⁶⁻¹⁰ platinum,¹¹ rhenium,¹² ruthenium^{13, 14} and silver.¹⁵ Alternatively the tridentate pincer ligand itself can be changed e.g. using PCP, PNP, POP, PSP and PAsP donor sets.¹⁶ Literature on the phosphine containing dinuclear metal complexes is less varied with copper¹⁷⁻²² being the predominant metal used although some nickel²³ and palladium²⁴ examples do exist.

The work contained in this chapter focuses on using palladium as the metal in the pincer complex and copper in the dinuclear metal complex. These types of complexes were chosen as they were shown to selectively reduce CO₂ to a reduction product via an electrochemical route.^{23, 25} However, such palladium and copper complexes reported to date did not have anchoring groups incorporated.^{6, 8, 24, 26, 27} This work is in accordance with assisting the fulfilment of the aims of the thesis as follows;

- (i) To first reproduce known synthetic routes to obtain complexes for homogeneous electrocatalysis.
- (ii) The ligands were to be modified to include an anchoring group and enable attachment to a light harvesting semiconductor.
- (iii) To test the new complexes bearing anchoring groups to determine if their CO₂ reduction abilities were retained upon ligand modification, or ideally, enhanced.
- (iv) If the results from step 3 are positive, anchoring on the semiconductors and the building a heterogeneous system will be carried out with assistance from our collaborators.

The work in this chapter has been broken down and presented as two separate parts; the first part contains the synthesis, results and discussion for the palladium containing pincer complexes and a brief summary at the end. The second part provides details on the synthesis, results and discussion for the copper containing dinuclear complex and another brief summary at the end.

3.1.1. System Design

When designing these systems several criteria had to be taken into consideration. As already mentioned the complex needs to reduce CO₂ to a reduction product. This requires a source of electrons and the ability to store and subsequently use these electrons in the reduction process.^{8, 26, 27} The reduction products to be formed, as could be anticipated by analogy with the previous studies, are likely to be either CO or HC(O)OH i.e. the reduction products requiring two electrons. This is due to the singly charged nature of the pincer complex and the doubly charged nature of the dinuclear metal complex, which enables electrons to be stored before being used in the catalytic cycle. Reduction products requiring more than two electrons are not likely to be formed, for the reasons stated in chapter 1.

Another criterion was the ability for the solvent to disassociate from the metal during the catalytic cycle. In both the palladium pincer complex and the dinuclear copper metal complex this requirement is fulfilled by a labile CH₃CN ligand.^{28, 29}

A final criterion was the ability to add an anchoring group to the ligand of the complex, shown in Figure 3.1. For the PCP pincer complex the anchoring group would be added to the phenyl ring, shown below as R₁ or R₂, the anchoring group for the dinuclear copper metal complex would be added to position R₃. This will allow attachment to a light harvesting semiconductor which will provide the electrons used in the reduction process, eliminating the need for electrical current.

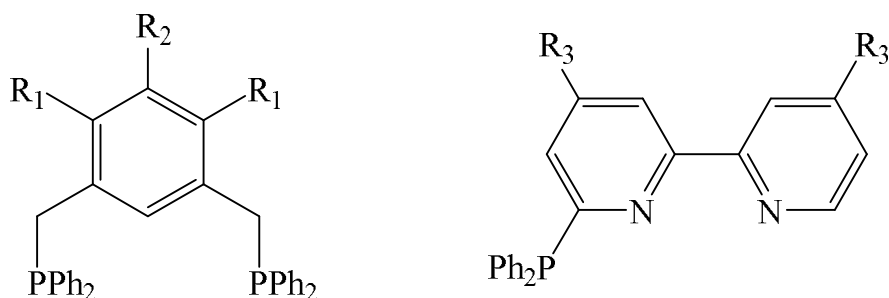


Figure 3.1: The possible sites to add an anchoring group to either the PCP pincer ligand, shown as R₁ and R₂ or the bipyridine ligand, shown as R₃.

By considering these criteria and selecting components that should fulfil them, it will result in two carefully designed systems, which should not only allow previous results to be verified, but builds upon and ideally improves previous work. This improvement is due to the replacement of electrical current with photocurrent. This is advantageous because when an appropriate semiconductor, i.e. a visible light absorbing one, is used then solar radiation can be utilised, which would provide potentially unlimited free energy and by consequence electrons to drive the CO₂ reduction process.

3.2. Synthesis and Characterisation of [Pd(PCP)(CH₃CN)][BF₄]

3.2.1. Synthetic Method

The previous section provided information as to why certain components were chosen when designing the system, this section gives brief information as to how the ligands were synthesised and then complexed to the metal.^{6, 16, 30} The pincer ligand was synthesised in two stages. Firstly, the phosphine was lithiated, and then a halogen substitution was performed using the lithiated product. Upon successful synthesis of the PCHP ligand, it was complexed to palladium by simple addition of a suitable palladium compound. This resulted in the desired final product of [Pd(PCP)(CH₃CN)][BF₄]. This was then used in the electrochemical experiments described in section 3.3.

3.2.2. Synthesis of 1,3-bis(diphenylphosphinomethyl) benzene (PCHP ligand)

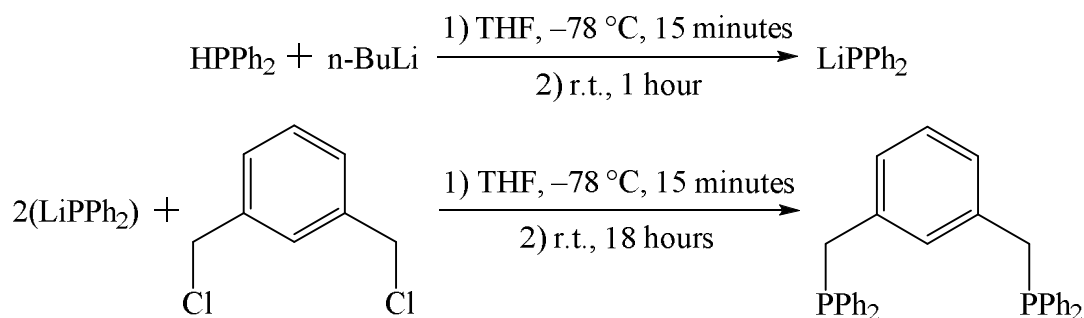


Figure 3.2: Reaction scheme showing the reagents and conditions required for the formation of PCHP ligand.

General method: HPPh₂ (1 mL, 5.75 mmol) was added to THF (10 mL) and cooled to -78°C before n-BuLi (2.5 mL, 2.5 M) was added drop wise via a syringe. The solution was stirred for 15 minutes before being allowed to warm up to room temperature and left stirring for 1 hour. This produced a red solution of LiPPh₂.

1,3-bis(chloromethyl)benzene (0.4930 g, 2.82 mmol) was degassed 3 times before THF (10 mL) was added via syringe. This was then transferred via cannula into the solution of LiPPh₂, which had been cooled to -78°C using an acetone/dry ice bath. The solution was stirred for 15 minutes, then allowed to warm up to room temperature before being left stirring for 18 hours. This resulted in a pale yellow solution. The solvent was removed by vacuum resulting in a white solid. The solid was dissolved in DCM (Grubbs, 50 mL), the solution transferred via a cannula into a column containing Celite (1 – 2 cm) whilst under a nitrogen atmosphere. The DCM from the filtrate was removed by vacuum resulting in a light yellow solid. Yield = 0.265 g, 0.56 mmol, 20%. ³¹P NMR (101 MHz, CDCl₃) δ -10.11 (s).

Synthetic comments: The PCHP ligand is highly air sensitive. The difference between the oxidised and non-oxidised form could be seen in the ³¹P NMR. The oxidised compound {containing P(V)} has a peak at around 30 ppm whilst the desired product has a peak at around -10 ppm, this allowed a quick way to determine if the product had formed.

3.2.3. Synthesis of [Pd(PCP)(CH₃CN)][BF₄]

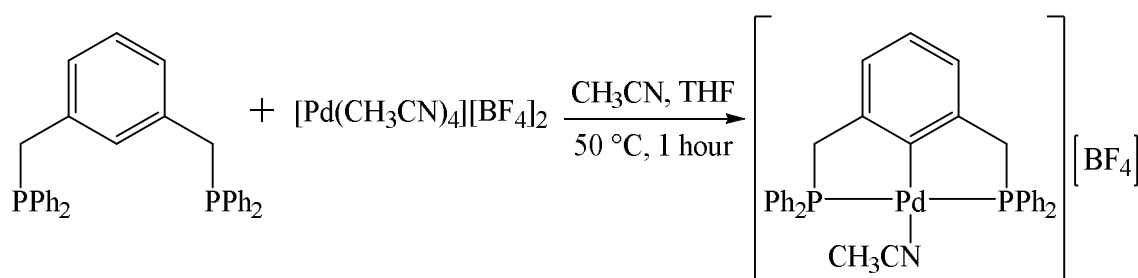


Figure 3.3: Reaction scheme showing the reagents and conditions required for the formation of [Pd(PCP)(CH₃CN)][BF₄].

General method: A solution of [Pd(CH₃CN)₄][BF₄]₂ (0.25 g, 0.56 mmol) in acetonitrile (20 mL) was prepared under a nitrogen atmosphere. PCHP (0.265 g, 0.56 mmol) was dissolved in THF (5 mL) and transferred via cannula into the flask containing the [Pd(CH₃CN)₄][BF₄]₂ solution. The solution was then heated to 50 °C and left stirring for 1 hour. This resulted in an orange brown solution. The solvent was removed under vacuum producing a brownish yellow solid. The solid was dissolved in hot acetone and then cooled. This resulted in black powder precipitating which was collected on filter paper. The liquid was collected and dried under vacuum producing a white solid. The complex was recrystallised by dissolving in hot acetone and then slowly allowing it to evaporate producing a white solid. The solid was dried under vacuum. Yield = 0.11 g, 28%. ³¹P NMR (101 MHz, CD₃CN) δ, 41.71 (s). This is the position expected as shown in the literature.⁹

3.3. Results and Discussion of [Pd(PCP)(CH₃CN)][BF₄]

3.3.1. Electrochemical Data for [Pd(PCP)(CH₃CN)][BF₄]

Cyclic voltammetry was performed on the complex in DMF, in the presence of N₂ or CO₂ using the standard cyclic voltammetry method described in chapter 2. The N₂ was bubbled into the solution using the in house supply. The CO₂ was provided by a cylinder containing the gas.

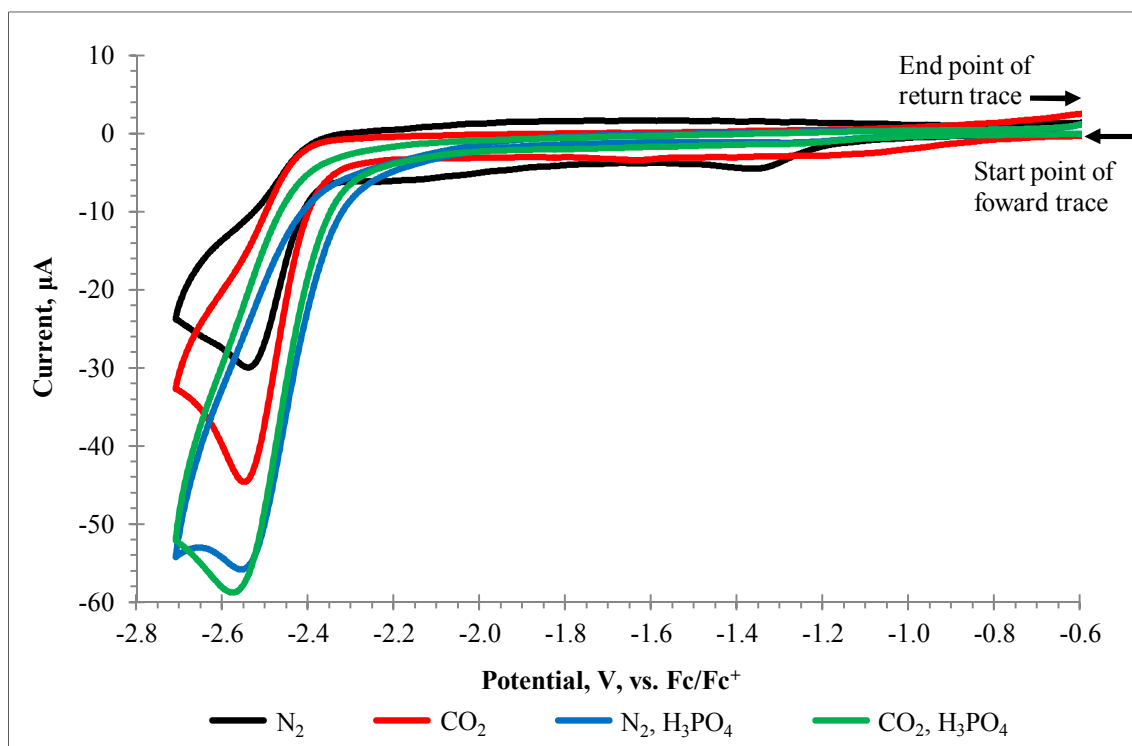


Figure 3.4: Cyclic voltammograms for $[\text{Pd}(\text{PCP})(\text{CH}_3\text{CN})][\text{BF}_4]$, 2 mM in DMF with 0.2 M $[\text{NBu}_4][\text{PF}_6]$, recorded at 50 mVs^{-1} , in the presence of N_2 or CO_2 , with and without H_3PO_4 , the potentials are reported vs. Fc/Fc^+ . The arrows show the start or end point and the direction of potential change.

Figure 3.4 shows that in a N_2 saturated solution, $[\text{Pd}(\text{PCP})(\text{CH}_3\text{CN})][\text{BF}_4]$ demonstrates a partially reversible redox couple at -2.48 V vs. Fc/Fc^+ . When CO_2 was bubbled into the solution, there was a slight increase in the current with the couple at -2.50 V vs. Fc/Fc^+ . This increase in current appears to correspond to the reduction of CO_2 , which was unexpected in the absence of acid, a source of protons. When H_3PO_4 acid was added, the current increased but by the same amount for both the N_2 and CO_2 saturated systems. A control experiment to investigate the breakdown of DMF in the presence of either N_2 or CO_2 , Figure 3.5, shows that there is virtually no difference between the cyclic voltammograms recorded when either of the two gases and when no compound is present. This rules out the increase in current under CO_2 being due to solvent breakdown.

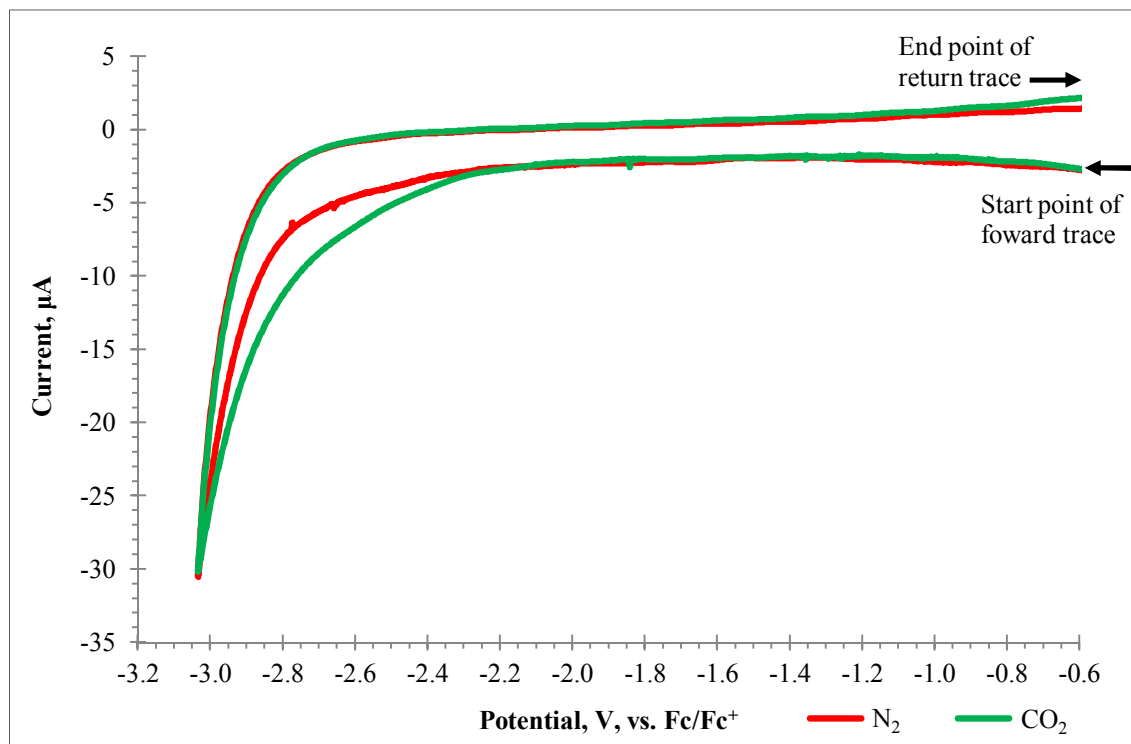


Figure 3.5: Cyclic voltammogram for DMF with 0.2 M [NBu₄][PF₆] at 100 mVs⁻¹, in the presence of N₂ or CO₂, reported vs. Fc/Fc⁺. The arrows show the start or end point and the direction of potential change.

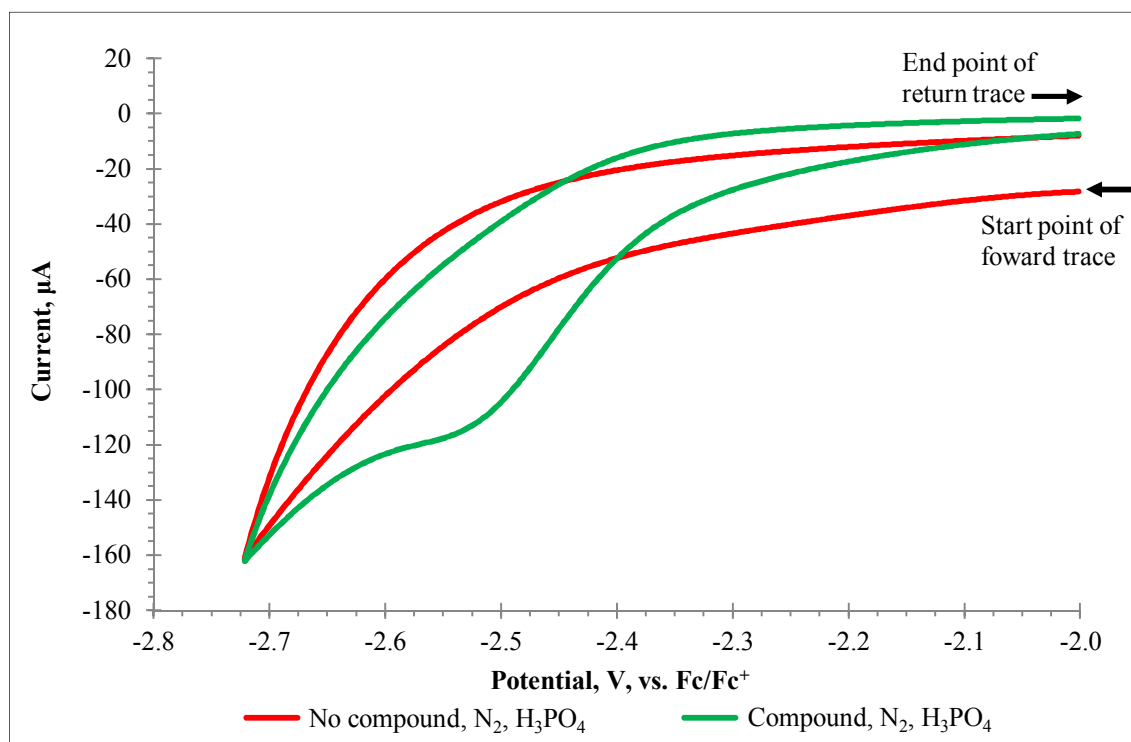


Figure 3.6: Cyclic voltammogram for DMF with 0.2 M [NBu₄][PF₆], recorded at 100 mVs⁻¹, in the presence of N₂ and H₃PO₄ both with and without the compound, [Pd(PCP)(CH₃CN)][BF₄], the potentials are reported vs. Fc/Fc⁺. The arrows show the start or end point and the direction of potential change.

The difference between electrochemical behaviour of the system having the compound with acid and having just acid, both under N₂, was also examined. Figure 3.6 shows the only change is the presence of a peak at -2.52 V when the compound is present. This indicates that the addition of acid should not cause an increase in the current seen when N₂ is present. However this is in conflict with the results obtained earlier which did show an increase in current in the presence of acid. All of these results show that the complex does not appear to behave as was described in the literature.²³

3.3.2. Summary

The palladium phosphine complexes were successfully produced using air-sensitive conditions. The activity of these compounds with regard to CO₂ reduction has been tested using cyclic voltammetry technique. An increase in anodic current was expected when the solution of the compound was saturated with CO₂. However, the results of the electrochemical experiments were difficult to interpret. Firstly, an increase of current was observed when the solution was saturated with CO₂ but without acid present – this observation was unexpected as, according to the literature data, a source of protons is required. On the other hand, in presence of acid, both the N₂ and CO₂ systems produced the same amount of current. Therefore, considering these unexpected observations, along with the difficulty of the synthesis and any potential synthetic modifications, it was decided to move away from this particular type of complex.

3.4. Synthesis and Characterisation of [Cu₂(μ-Ph₂Pbpy)₂(CH₃CN)₂][PF₆]₂

3.4.1. Synthetic Method

The complexes described here are based on 2,2'-bipyridyl ligand bearing a phosphine -PR₂ group in the 6-position. As with the synthesis of the pincer ligand described in section 3.2.2, the first step is the lithiation of the phosphine, Figure 3.7, followed by a halogen substitution reaction of the 6-Br-2,2'-bipyridine. This procedure results in a mono-substituted bipyridine with the phosphine in the 6-position. Two different methods for formation of the lithiated phosphine were performed, this was due to the phosphine oxidising during synthesis, as seen previously. Ultimately, method one was

deemed more successful. Upon successful synthesis of the ligand, complexation to copper was performed resulting in the desired dinuclear copper complex. Electrochemical experiments were then carried out with the results described in section 3.5.

3.4.2. Synthesis of 6-(diphenylphosphino)-2,2'-bipyridine (Method 1)

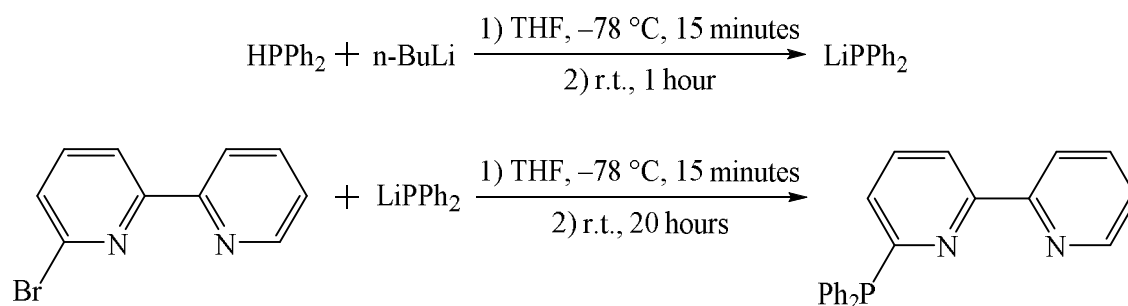


Figure 3.7: Reaction scheme showing the reagents and conditions required for the formation of 6-(diphenylphosphino)-2,2'-bipyridine.

General method: HPPh_2 (1 mL, 5.75 mmol) was added to THF (distilled, 10 mL) and cooled to -78°C before n-BuLi (2.5 mL, 2.5 M) was added drop wise via a syringe. The solution was stirred for 15 minutes before being allowed to warm up to room temperature and left stirring for 1 hour. This produced an orange/red solution of LiPPh_2 .

6-bromo-2,2'-bipyridine (0.4503 g, 1.92 mmol) was degassed 3 times, dissolved in THF (10 mL) and transferred via cannula into the solution of LiPPh_2 at -78°C . After 15 minutes, the solution was allowed to warm up to room temperature and stirred for a further 20 hours resulting in a red solution. HCl (10 mL, 2 M) followed by (4 mL of 35%) was added resulting in a yellow bottom layer and a colourless top layer. The organic and aqueous layers were separated. Ammonia solution was added to the aqueous layer to bring the pH to 10. Diethyl ether (50 mL) was added and another separation performed. The organic layer was dried with MgSO_4 , filtered and dried under vacuum. The resulting yellow oil was dissolved in chloroform and cold methanol to induce recrystallisation, none occurred so solvent was removed producing a light yellow

solid. Yield = 0.5393 g, crude. ^{31}P NMR (CDCl_3): 21.44, (s), -3.51 (s), -40.38 (s). The desired peak, -3.51 ppm was the largest component.

Synthetic comments: This product was difficult to isolate and had to be reacted with the copper complex whilst in the crude solid state.

3.4.3. Synthesis of 6-(diphenylphosphino)-2,2'-bipyridine (Method 2)

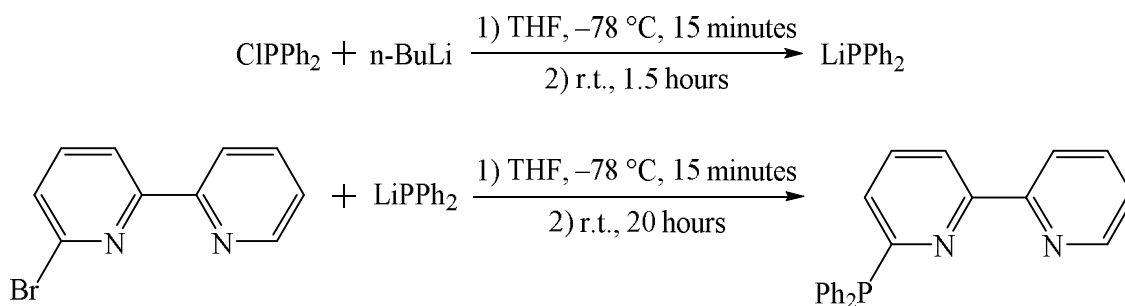


Figure 3.8: Alternative reaction scheme showing the reagents and conditions required for the formation of 6-(diphenylphosphino)-2,2'-bipyridine.

General method: ClPPh_2 (0.8 mL, 4.33 mmol) was added via syringe to THF (distilled, 10 mL). The solution was cooled to $-78\text{ }^\circ\text{C}$ using an acetone/dry ice bath before n-BuLi (3 mL, 2.5 M) was added drop wise producing an orange solution. The solution was warmed up to room temperature and left stirring for 1.5 hours. The solution was filtered under nitrogen and then cooled to $-78\text{ }^\circ\text{C}$.

6-bromo-2,2'-bipyridine (0.209 g, 0.88 mmol) was degassed 3 times, dissolved in THF (distilled, 10 mL) and added drop wise into the cooled solution of LiPPh_2 . After 15 minutes, the solution was allowed to warm up to room temperature and stirred for 20 hours resulting in a red solution. HCl (10 mL, 2 M) followed by (4 mL of 35%) was added resulting in the solution turning yellow. The organic and aqueous layers were separated. Ammonia solution was added to the aqueous layer to bring the pH to 10. Diethyl ether (50 mL) was added and another separation performed. The organic layer

was dried with MgSO_4 , filtered and dried under vacuum. This resulted in a brown oil product. ^{31}P NMR (CDCl_3): 31.73, (s), -15.98 (s), -24.26 (s).

Synthetic comments: The above alternate synthesis in which ClPPh_2 was used instead of HPPH_2 was attempted, however this reaction failed to produce any of the desired product.

3.4.4. Synthesis of $[\text{Cu}_2(\mu\text{-Ph}_2\text{Pbpy})_2(\text{CH}_3\text{CN})_2][\text{PF}_6]_2$

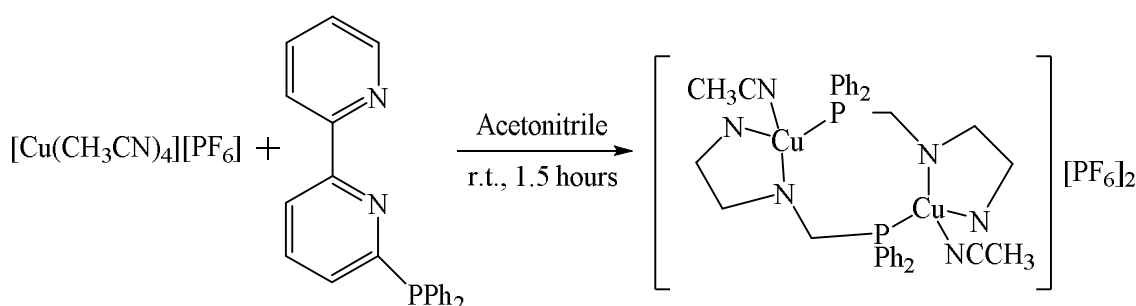


Figure 3.9: Reaction scheme showing the reagents and conditions required for the formation of the dinuclear copper complex, $[\text{Cu}_2(\mu\text{-Ph}_2\text{Pbpy})_2(\text{CH}_3\text{CN})_2][\text{PF}_6]_2$.

General method: $[\text{Cu}(\text{CH}_3\text{CN})_4][\text{PF}_6]$ (0.5905 g, 1.58 mmol), and bpyPPH_2 (0.5393 g, 1.58 mmol) were degassed 3 times before acetonitrile (Grubbs, 20 mL) was added via syringe. This produced an orange solution, which was stirred for 1.5 hours at room temperature. The solvent was partially removed on a rotary evaporator to leave a concentrated solution. The solution underwent slow diffusion into diethyl ether and left for 72 hours. This produced little product so more diethyl ether was added and the solid and liquid separated by centrifugation. The resulting yellow solid was dried using a high vacuum. Yield = 0.3563 g, 32%. ^1H NMR (250 MHz, CD_2Cl_2) δ 8.48 (d, $J = 8.3$ Hz), 8.37 (d, $J = 8.1$ Hz), 8.24 (t, $J = 7.9$ Hz), 8.09 (d, $J = 5.6$ Hz), 7.57 – 7.42 (m), 7.36 (t, $J = 6.3$ Hz), 7.06 (s), 1.57 (s). ^{31}P NMR (101 MHz, CD_2Cl_2) δ 10.43 (s). ^{31}P NMR (101 MHz, DMSO-d_6) δ 23.43 (s), 8.93 (s), 2.98 (s), -5.30 (s).

3.5. Results and Discussion of $[\text{Cu}_2(\mu\text{-Ph}_2\text{Pbpy})_2(\text{CH}_3\text{CN})_2][\text{PF}_6]_2$

3.5.1. Electrochemical Data for $[\text{Cu}_2(\mu\text{-Ph}_2\text{Pbpy})_2(\text{CH}_3\text{CN})_2][\text{PF}_6]_2$

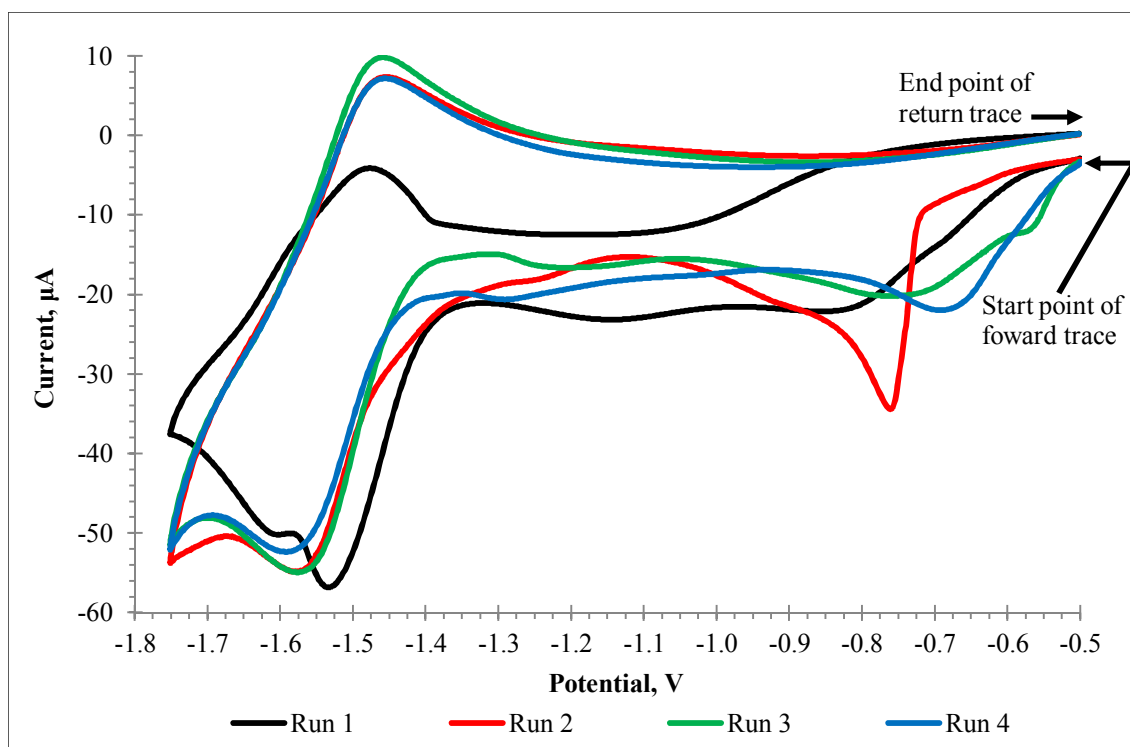


Figure 3.10: Successive cyclic voltammograms for $\text{Cu}_2(\mu\text{-Ph}_2\text{Pbpy})_2(\text{CH}_3\text{CN})_2$, 2 mM in distilled CH_3CN with 0.2 M $[\text{NBu}_4][\text{PF}_6]$, recorded at 100 mVs^{-1} , in the presence of N_2 . The arrows show the start or end point and the direction of potential change.

In order to assess the electrocatalytic properties of $[\text{Cu}_2(\mu\text{-Ph}_2\text{Pbpy})_2(\text{CH}_3\text{CN})_2][\text{PF}_6]_2$, cyclic voltammetry studies were performed in acetonitrile solution at r.t., Figure 3.10. However, it was noticed that successive scans at the same scan rate were resulting in progressively different traces. All the cyclic voltammetry traces show a redox couple at approximately -1.5 V ; but then they are otherwise not identical. The experiment was then stopped and the ^{31}P NMR was run again in DMSO-d_6 . This showed four peaks representing four different phosphorus environments showing the compound was decomposing which explained the inconsistency of the cyclic voltammetry results.

3.5.2. Summary

The target dinuclear copper(I) complex contained highly air sensitive phosphine ligands and proved rather difficult to handle. Thus, both the palladium and copper complexes containing phosphine ligands, in our hands, turned out to yield irreproducible results, which therefore hindered their further investigations for electrocatalysis. It is possible that work in a glove box would have alleviated these issues. Other classes of electrocatalysts described in the literature are based on diimine ligands that do not incorporate phosphine groups. These compounds, primarily ruthenium and rhenium derivatives, are discussed in chapters 4 and 5 respectively.

3.6. Consideration of Random and Systematic Errors

The measurement of a physical quantity or property usually has an associated error. This error arises from either the inability of the observer to differentiate between readings that differ by less than a certain amount or due to instrumental limitations or due to unpredictable fluctuations in environmental conditions. Generally, independent measurements taken by an instrument will differ by small random amounts. This is called random (or statistical) error and can usually be estimated and minimized through statistical analysis of repeated measurements. This type of error is assumed to fall on a Gaussian distribution around a mean value. By using various statistical calculations, it is possible to state the probability, usually 95%, of finding the true value within the upper and lower confidence limits. Random error can be further reduced by taking additional sets of data and calculating the standard error, however this comes at a cost of greatly increased work.

A second type of error exists in which all measurements are reproducibly inaccurate by the same amount and direction. E.g., a balance measures all masses as +0.001 g from their true value. This is called systematic error and usually results from either the instrument itself or user error of the instrument. Systematic errors are often difficult to detect and unlike random error cannot be reduced by statistical analysis of repeated measurements.

In the above sections, 3.3.1 and 3.5.1, the electrochemical data was discussed. The values obtained from the experiments could potentially be affected by random or

systematic error. Random error will be included in the concentration of the electrolyte and the mass of the complex used through use of the balance and measurement glassware. Systematic error will also occur with use of the glassware due to imperfections in its construction, however this is usually only around ± 0.1 mL for a 25 mL measuring cylinder. The balance is tared before each use so systematic error should be negligible. There will also be an associated random and systematic error with the potentiostat. The potential is calculated relative to a reference electrode and could be subject to systematic error; however, this will then be significantly reduced by using an additional reference, ferrocene. The potentiostat is capable of measuring current at the nano amp scale whilst all of our measurements are on the micro amp scale, this would suggest that any error is going to be orders of magnitude less than our measurements. Taking into account all of these sources of error and their potential size it is unlikely that they will have any significant impact on our results and conclusions.

3.7. References

1. P. Kang, C. Cheng, Z. Chen, C. K. Schauer, T. J. Meyer and M. Brookhart, *J. Am. Chem. Soc.*, 2012, **134**, 5500–5503.
2. T. J. Schmeier, G. E. Dobereiner, R. H. Crabtree and N. Hazari, *J. Am. Chem. Soc.*, 2011, **133**, 9274–9277.
3. B. J. Boro, E. N. Duesler, K. I. Goldberg and R. A. Kemp, *Inorg. Chem.*, 2009, **48**, 5081–5087.
4. S. Chakraborty, J. Zhang, Y. J. Patel, J. A. Krause and H. Guan, *Inorg. Chem.*, 2013, **52**, 37–47.
5. S. Chakraborty, Y. J. Patel, J. A. Krause and H. Guan, *Polyhedron*, 2012, **32**, 30–34.
6. N. Selander and K. J. Szabó, *Chem. Rev.*, 2011, **111**, 2048–2076.
7. J. Aydin and K. J. Szabó, *Org. Lett.*, 2008, **13**, 2881–2884.
8. T. Kimura and Y. Uozumi, *Organometallics*, 2006, **25**, 4883–4887.
9. I. P. Beletskaya, A. V. Chuchuryukin, G. v. Koten, H. P. Dijkstra, G. P. M. v. Klink, A. N. Kashin, S. E. Nefedov and I. L. Eremenko, *Russ. J. Org. Chem.*, 2003, **39**, 1268–1281.
10. J. A. Therrien, M. O. Wolf and B. O. Patrick, *Inorg. Chem.*, 2014, **53**, 12962–12972.
11. M. A. Bennett, H. Jin and A. C. Willis, *J. Organomet. Chem.*, 1993, **451**, 249–256.

12. M. Vogt, A. Nerush, Y. Diskin-Posner, Y. Ben-David and D. Milstein, *Chem. Sci.*, 2014, **5**, 2043–2051.
13. P. Dani, B. Richter, G. P. M. v. Klink and G. v. Koten, *Eur. J. Inorg. Chem.*, 2001, 125–131.
14. P. Steenwinkel, S. Kolmschot, R. A. Gossage, P. Dani, N. Veldman, A. L. Spek and G. v. Koten, *Eur. J. Inorg. Chem.*, 1998, 477–483.
15. F. Caruso, M. Camalli, J. H. Rimml and L. M. Venanzi, *Inorg. Chem.*, 1995, **34**, 673–679.
16. B. D. Steffey, A. Miedaner, M. L. Maciejewski-Farmer, P. R. Bernatis, A. M. Herring, V. S. Allured, V. Carperos and D. L. DuBois, *Organometallics*, 1994, **13**, 4844–4855.
17. M. Maekawa, M. Munakata, S. Kitagawa and T. Yonezawa, *Bull. Chem. Soc. Jpn.*, 1991, **64**, 2286–2288.
18. A. M. Lilio, K. A. Grice and C. P. Kubiak, *Eur. J. Inorg. Chem.*, 2013, 4016–4023.
19. R. J. Haines, R. E. Wittrig and C. P. Kubiak, *Inorg. Chem.*, 1994, **33**, 4723–4728.
20. J. H. Satcher and A. L. Balch, *Inorg. Chem.*, 1995, **34**, 3371–3373.
21. S.-M. Kuang, Z.-Z. Zhang, Q.-G. Wang and T. C. W. Mak, *J. Chem. Soc., Dalton Trans.*, 1998, 1115–1119.
22. J. S. Field, R. J. Haines, C. J. Parry and S. H. Sookraj, *Polyhedron*, 1993, **12**, 2425–2428.
23. E. E. Benson, C. P. Kubiak, A. J. Sathrum and J. M. Smieja, *Chem. Soc. Rev.*, 2009, **38**, 89–99.
24. B. D. Steffey, C. J. Curtis and D. L. DuBois, *Organometallics*, 1995, **14**, 4937–4943.
25. M. R. DuBois and D. L. DuBois, *Acc. Chem. Res.*, 2009, **42**, 1974–1982.
26. A. Miedaner, B. C. Noll and D. L. DuBois, *Organometallics*, 1997, **16**, 5779–5791.
27. J. W. Raebiger, J. W. Turner, B. C. Noll, C. J. Curtis, A. Miedaner, B. Cox and D. L. DuBois, *Organometallics*, 2006, **25**, 3345–3351.
28. P. R. Bernatis, A. Miedaner, R. C. Haltiwanger and D. L. DuBois, *Organometallics*, 1994, **13**, 4835–4843.
29. D. L. DuBois, A. Miedaner and R. C. Haltiwanger, *J. Am. Chem. Soc.*, 1991, **113**, 8753–8764.
30. M. Gagliardo, N. Selander, N. C. Mehendale, G. v. Koten, R. J. M. K. Gebbink and K. J. Szabó, *Chem. Eur. J.*, 2008, **14**, 4800–4809.

4. Ruthenium Complexes Containing Bipyridine Ligands as Potential Catalysts for CO₂ Reduction

4.1. Introduction

The second class of compounds that were studied for catalytic purposes during this research were ruthenium metal complexes containing one or more diimine ligands on which the substituents could be varied. This allowed for control of the sterics and electronics of the complexes. Generic structures can be seen in Figure 4.1 and Figure 4.2. There has already been extensive research for these types of complexes in the context of photocatalysis. The work reported in the literature can be primarily divided into two groups; complexes without anchoring groups¹⁻¹⁶ and complexes containing anchoring groups¹⁷⁻²³ allowing for attachment to a semiconductor. The anchoring group used is usually a carboxylate²⁴⁻³⁷ or a phosphonate.^{17, 38-45}

The work presented in this chapter covers both groups of complexes, with several syntheses producing “anchorless” complexes. However, in keeping with the overall objective of the research the anchorless complexes are usually intermediates of the final desired complex that does contain an anchoring group. All of the complexes shown in this chapter have two CO ligands attached to the ruthenium and the reasons for this are discussed below in 4.1.1.

The aims of this chapter are the same as chapter 3 but focus on the ruthenium containing complexes mentioned in the overall aims of the thesis;

- (i) To identify and reproduce known synthetic routes to obtain complexes for homogeneous electrocatalysis.
- (ii) To modify the ligands to include an anchoring group and enable attachment to a light harvesting semiconductor.
- (iii) To test the new complexes bearing anchoring groups to determine if their CO₂ reduction abilities were retained upon ligand modification, or ideally, enhanced.
- (iv) If the results from step 3 are positive, anchoring on the semiconductors and the building a heterogeneous system will be carried out with assistance from our collaborators.

4.1.1. System Design

The purpose of this work was to start from reproducing the work of Sato et al.^{24, 46} on a ruthenium(II) catalyst and then use the knowledge gained during the synthesis to either modify the complex in some way, or use the same complex but anchor it to different semiconductors. These complexes were chosen for the following reasons;

When choosing a catalytic system, several criteria had to be taken into consideration. Primarily the complex needs to reduce CO₂ to a reduction product. This requires a source of electrons and the ability to store and subsequently use these electrons in the reduction process.⁴⁷⁻⁴⁹ The reduction products to be formed, as could be anticipated by analogy with the previous studies, are likely to be either CO or HC(O)OH i.e. the reduction products requiring two electrons. This is due to the doubly charged nature of the ruthenium metal complex, which enables electrons to be stored before being used in the catalytic cycle. Reduction products requiring more than two electrons are not likely to be formed, for the reasons stated in chapter 1. In the work of Sato et al.^{24, 46} the primary product was HC(O)OH.

Another criterion was the presence of a reaction site for the conversion of CO₂ into the reaction product. For these complexes, it is believed to be the CO ligand. There are benefits to having CO ligands; they act as good IR reporters often allowing quick and easy access to structural information of the complex due to how many bands are present in the IR spectrum. Another advantage is their ability for back bonding from the metal centre ($d\pi \rightarrow \pi^*$). This allows the metal to transfer electron density to the CO ligand helping to stabilise the complex when receiving electrons from the semiconductor.

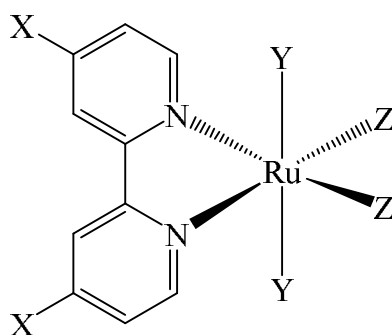


Figure 4.1: A generic representation of the ruthenium containing complex with one diimine ligand. X can be any substituent e.g. Me or ^tbutyl. Y is usually chloride. Z is CO.

A final criterion was the ability to add an anchoring group to the ligand of the complex. As seen in Figure 4.1 and Figure 4.2 as either X or X and Y respectively. This will allow attachment to a light harvesting semiconductor which will provide the electrons used in the reduction process, eliminating the need for electrical current.

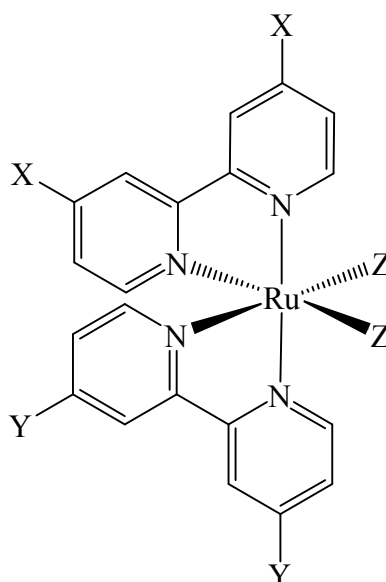


Figure 4.2: A generic representation of the ruthenium containing complex with two diimine ligands. X and Y can be any substituent e.g. Me or ^tbutyl. Z is usually CO.

From these two figures, it can be seen that there is a wide variety of customisation that can be performed on these complexes, allowing them to be tuned to fulfil the aims of the research.

After considering these criteria, the work of Sato et al. was decided as a good starting point from which to build and improve upon.

Some of the changes attempted include adding electron withdrawing groups to the diimine as these had been shown in the literature to result in an increase in catalytic efficiency of the complexes.^{50, 51} Another modification was the addition of $-CH_2-$ spacer groups in between the anchoring groups and the ligand.⁵²⁻⁵⁴

4.2. Synthesis and Characterisation of Bis-dcbpy Ruthenium Dicarbonyl Complexes (Route 1)

4.2.1. Synthetic Method

Section (iv) provided information as to why certain components were chosen when designing the system; this section gives brief information as to how the ligands were synthesised, complexed to the metal and carbonyls attached.

The chloride analogue of the complex was synthesised using standard literature methods.⁵⁵ With the *cis*-dichloro-bis-4,4'-dicarboxy-2,2'-bipyridine ruthenium complex synthesised it was believed that the chlorides could be substituted for carbonyls simply by bubbling CO into the solution for several hours. The reaction was monitored by IR spectroscopy. After 5 hours however, the bubbling was stopped because no metal carbonyl bands had appeared.

After the initial attempt to substitute the chlorides for carbonyl groups had failed it was decided to substitute the chlorides for triflate groups, which should be more labile and therefore substitute for carbonyls when CO is bubbled into the solution. This did not occur, therefore the attempt to make the ruthenium bis-dcbpy dicarbonyl complex by route one was deemed a failure and another route were devised. However, useful synthetic techniques were learnt and were used for other synthetic routes.

4.2.2. Synthesis of $\text{Ru}(\text{dcbpy})_2\text{Cl}_2$

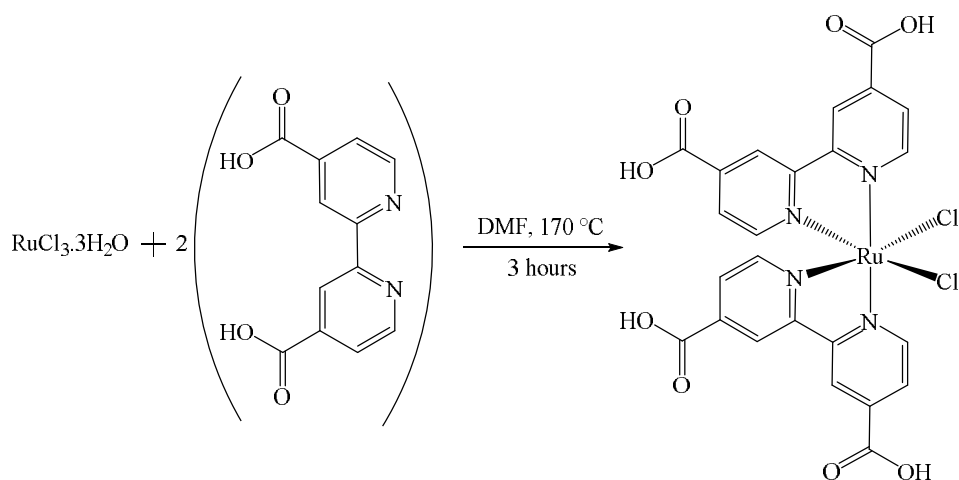


Figure 4.3: Reaction scheme showing the reagents and conditions required for the formation of *cis*-dichloro-bis-4,4'-dicarboxy-2,2'-bipyridine ruthenium(II).

General method: $\text{RuCl}_3 \cdot x\text{H}_2\text{O}$ (0.106 g, 0.41 mmol) and 2,2'-bipyridine-4,4'-dicarboxylic acid (0.1907 g, 0.78 mmol) were degassed in a flask 3 times before DMF (Grubbs, 20 mL) was added. The flask was wrapped in foil, heated to 180 °C using an oil bath and the solution stirred. Reaction was monitored by UV-Vis spectroscopy in ethanol (316, 412, 563 nm). Solution was heated for 3 hours before being allowed to cool to room temperature. The solution was then filtered and the solvent removed under vacuum at 75 °C. HCl (4 mL, 2 M) was added and the solution stirred for 4 hours whilst in the dark. Solution containing precipitate was filtered and washed with acetone. Residual solvent was removed from solid product under vacuum. Yield = 0.227 g, 85%. ^1H NMR (400 MHz, DMSO-d_6) δ 10.10 (d, $J = 5.8$ Hz, 2H), 9.08 (s, 2H), 8.91 (s, 2H), 8.24 (d, $J = 5.8$ Hz, 2H), 7.76 (d, $J = 6.0$ Hz, 2H), 7.50 (dd, $J = 6.0, 1.5$ Hz, 2H). ToF MS ES^- : m/z 659 (M^-).

Synthetic comments: The synthesis was straightforward, in which the reagents reacted together in DMF at 180 °C for 3 hours in the dark. It was kept in the dark in order to prevent the trans-conformation from forming. The reaction was monitored via UV-Vis spectroscopy with bands at 565, 414, and 316 nm in the ratio of 1:1.05:3.33 appearing upon completion. The DMF was then removed under the high vacuum whilst being heated to 75 °C. HCl (2 M) was then added and the solution stirred in the dark for 4 hours. It was not completely clear as to the purpose of this step, perhaps to make sure all of the acid groups were fully protonated. The ^1H NMR showed six signals due to the cis-configuration which means that the two sides of the bipyridine rings are inequivalent.^{25, 55} The product can be purified further by recrystallisation using DMF and acetone, which removes trace impurities. ^1H NMR (400 MHz, DMSO-d_6) δ 10.09 (d, $J = 5.9$ Hz, 2H), 9.08 (s, 2H), 8.90 (s, 2H), 8.23 (dd, $J = 5.9, 1.6$ Hz, 2H), 7.75 (d, $J = 6.0$ Hz, 2H), 7.49 (dd, $J = 6.0, 1.6$ Hz, 2H).

4.2.3. Synthesis of $\text{Ru}(\text{dcbpy})_2\text{CO}_2$ (Method 1)

$\text{Ru}(\text{dcbpy})\text{Cl}_2$ (0.0203 g, 0.03 mmol) was dissolved in ethanol (25 mL), CO was bubbled into the solution. The solution was monitored by IR spectroscopy every hour. After five hours, no metal CO stretches had appeared and so the bubbling was stopped.

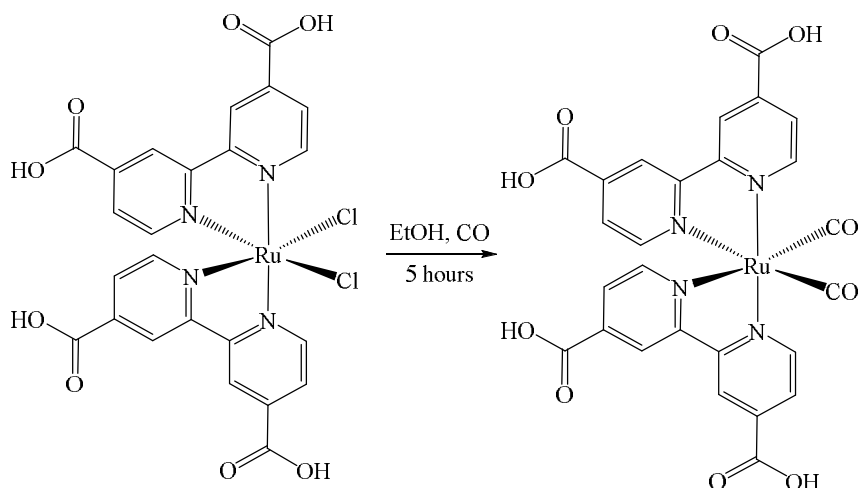


Figure 4.4: Reaction scheme showing the reagents and conditions required for the formation of cis-dicarbonyl-bis-4,4'-dicarboxy-2,2'-bipyridine ruthenium(II).

4.2.4. Synthesis of $\text{Ru}(\text{dcbpy})_2(\text{SO}_3\text{CF}_3)_2$

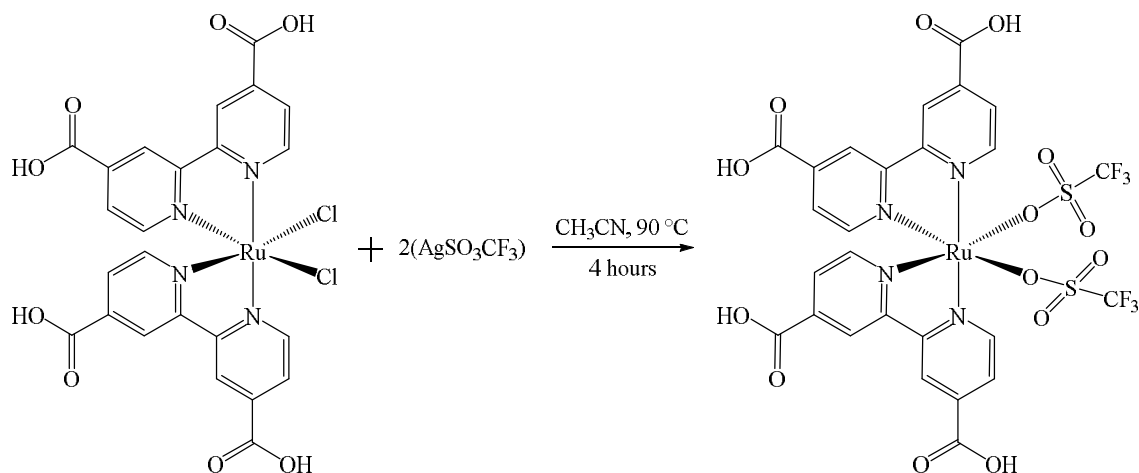


Figure 4.5: Reaction scheme showing the reagents and conditions required for the formation of cis-ditriflate-bis-4,4'-dicarboxy-2,2'-bipyridine ruthenium(II).

General method: $\text{Ru}(\text{dcbpy})_2\text{Cl}_2$ (0.1061 g, 0.16 mmol) and AgSO_3CF_3 (0.085 g, 0.33 mmol) were degassed 3 times in the dark before acetonitrile (40 mL) was added. The solution was then heated to 90 °C for 4 hours whilst maintaining dark conditions. Solution was then filtered through Celite under a nitrogen atmosphere. The solution was then concentrated to ~ 3 mL, diethyl ether (50 mL) was added to induce precipitation. The red / brown solid was collected on a sinter, washed with diethyl ether (15 mL) and

dried. Yield = 0.0224 g, 16%. $^1\text{H NMR}$ (400 MHz, DMSO-d_6) δ 9.56 (d, $J = 5.8$ Hz, 2H), 9.31 (d, $J = 0.6$ Hz, 2H), 9.15 (d, $J = 0.6$ Hz, 2H), 8.29 (dd, $J = 5.8, 1.4$ Hz, 2H), 7.84 (d, $J = 5.6$ Hz, 2H), 7.71 (dd, $J = 6.0, 1.3$ Hz, 2H).

Synthetic comments: Several attempts were made to synthesise this product but were mostly unsuccessful. It was unclear as to why this was the case, one batches' $^1\text{H NMR}$ showed a very impure product whilst another showed only small amounts of product present. A possible explanation is that the silver triflate had somehow decomposed despite carrying out the reaction in the dark and was therefore unable to react with the ruthenium compound. The small amounts of product that did form during the reaction were used in the next step of bubbling CO into the solution.

4.2.5. Synthesis of $\text{Ru}(\text{dcbpy})_2\text{CO}_2$ (Method 2)

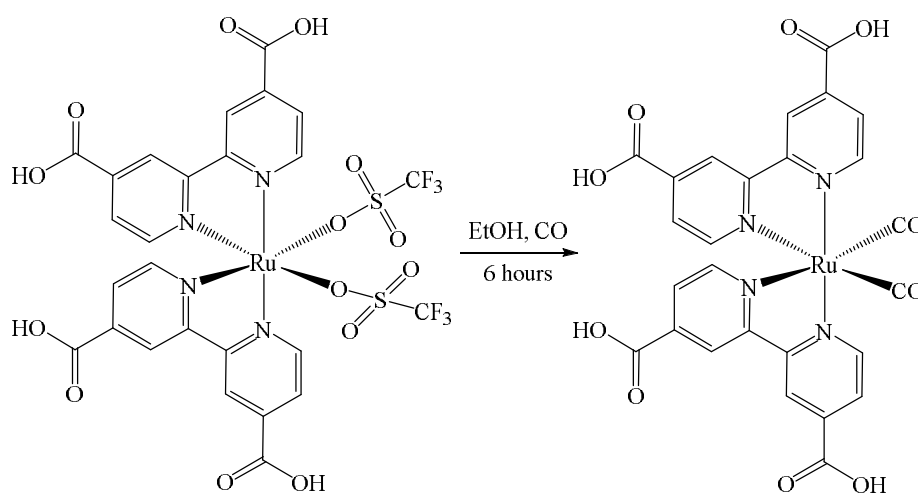


Figure 4.6: Reaction scheme showing the reagents and conditions required for the formation of cis-dicarbonyl-bis-4,4'-dicarboxy-2,2'-bipyridine ruthenium(II).

The reaction was setup in the same way as the previous CO bubbling experiment. $\text{Ru}(\text{dcbpy})(\text{SO}_3\text{CF}_3)_2$ (crude, 0.014 g, 0.016 mmol) was dissolved in ethanol (5 mL), and CO was bubbled into the solution. The solution was monitored by IR spectroscopy every hour. After six hours, no metal CO stretch(s) had appeared and so the bubbling was stopped.

4.3. Synthesis and Characterisation of Bis-dcbpy Ruthenium Dicarbonyl Complexes (Route 2)

4.3.1. Synthetic Method

Due to the difficulties described above in trying to add carbonyl groups to the complex, the problem was solved by adding the carbonyl groups first and then adding the diimine ligands to the complex. As will be seen in later sections this method allows for a high degree of customisability when producing these types of complex.

One of the published sources suggested the addition of a dcbpy ligand in methanol to the metal carbonyl precursor.¹¹ Although the dcbpy ligand was not very soluble, it was believed that it would react as a suspension. The dcbpy did not react with the ruthenium compound in methanol, however the reaction was found to occur in THF. ¹H NMR showed that there was still some of the free ligand present and we have been unable to purify the crude product. It was suggested that using Sephadex LH-20 would have been able to purify the crude product, however due to a limited consumables budget this was not attempted and thus the product was left as crude.

The crude material, Ru(CO)₂Cl₂(dcbpy) as obtained from the previous step was used in the next step of the reaction in which the chlorides were substituted for triflates. The purpose of the substitution was to add labile groups, which could then be exchanged for another diimine ligand.

The attempt to make ruthenium bis-dcbpy dicarbonyl complex by route two was slightly more successful than route one, as carbonyl groups are present on the metal complex. However, the synthesis of the triflate species was not successfully completed, as only starting materials were recovered from the reaction.

4.3.2. Synthesis of [Ru(CO)₂Cl₂]_n

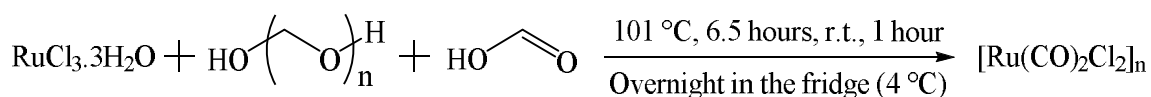


Figure 4.7: Reaction scheme showing the reagents and conditions required for the formation of dicarbonyl-dichloro ruthenium(II) oligomer.

General method: Paraformaldehyde (1.008 g, 33.5 mmol) and $\text{RuCl}_3 \cdot x\text{H}_2\text{O}$ (2.0216 g, 9.746 mmol) were degassed 3 times before deaerated formic acid (97%, 50 mL) was added. The solution was stirred at 101 °C for 6.5 hours, during which the solution changed from a dark brown to a clear orange colour. The solution was then allowed to cool to room temperature before being placed in the fridge (4 °C) overnight, resulting in a golden yellow coloured solution. The solvent was removed under vacuum. Hexane (25 mL) was then used to wash the product, the supernatant was decanted and the product dried under vacuum. Yield = 2.172 g, 98%. FTIR: $\nu(\text{CO})$, 2061, 2010 cm^{-1} .

Synthetic comments: The reaction is relatively straightforward although care must be taken when doing reactions in neat formic acid. The reaction was monitored visually by colour change, starting from a dark brown, to a dark green to a clear orange colour. The reaction mixture was then placed in the fridge overnight to complete the formation of the complex, resulting in a golden yellow solution. The formic acid was then removed using a rotary evaporator (in a fume cupboard) and the solid washed with hexane and dried under vacuum. In the original paper,¹¹ a steam bath was used to remove the formic acid. This method was attempted first however after 4 hours the formic acid did not appear to be being removed and so the rotary evaporator was used instead.

4.3.3. Synthesis of $\text{Ru}(\text{CO})_2\text{Cl}_2(\text{dcbpy})$

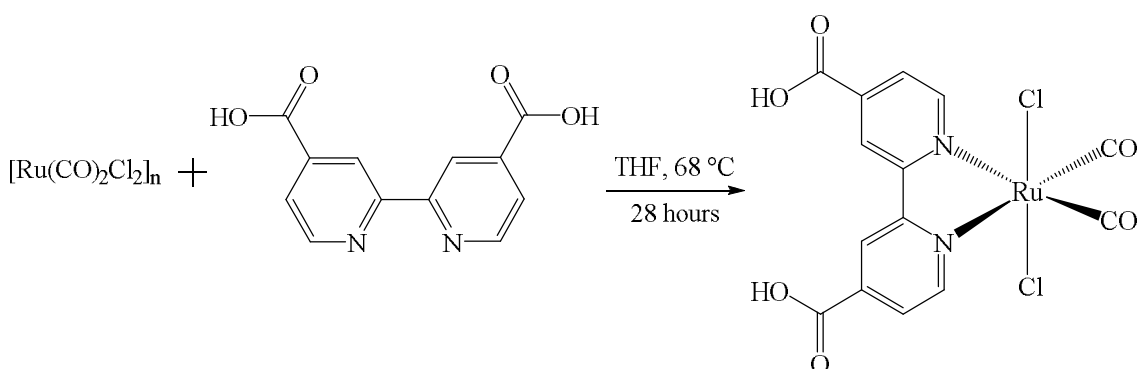


Figure 4.8: Reaction scheme showing the reagents and conditions required for the formation of trans-dichloro-cis-dicarbonyl-4,4'-dicarboxy-2,2'-bipyridine ruthenium(II).

General method: dcbpy (0.2630 g, 1 mmol) and $[\text{Ru}(\text{CO})_2\text{Cl}_2]_n$ (0.2638 g, 1.1 mmol) were degassed 3 times before THF (deaerated, 20 mL) was added. Solution was wrapped in foil, heated to 68 °C and stirred for 28 hours. The solution was cooled to room temperature before the solvent was removed on the rotary evaporator. Hexane (50 mL) was used to wash the solid before being dried. Crude yield = 0.5025 g. ^1H NMR (400 MHz, DMSO-d_6) δ 9.44 (d, $J = 5.6$ Hz, 2H), 9.20 (s, 2H), 8.22 (dd, $J = 5.6, 1.6$ Hz, 2H). Product was not purified and still had starting material present in a ratio of 5:1 (product:starting material) $\{^1\text{H}$ NMR δ 8.92 (d, $J = 5.5$ Hz, 2H), 8.85 (s, 2H), 7.92 (dd, $J = 4.9, 1.6$ Hz, 2H) $\}$.⁵⁵

Synthetic comments: Several attempts to synthesise the desired complex were performed using the literature method.¹¹ Each time unreacted dcbpy was collected on the sinter. This appears to have been caused by solubility issues with the dcbpy in methanol. A modification was then made to change the solvent to THF resulting in product formation although some dcbpy starting material remained unconsumed.

4.3.4. Synthesis of $\text{Ru}(\text{CO})_2(\text{dcbpy})(\text{SO}_3\text{CF}_3)_2$

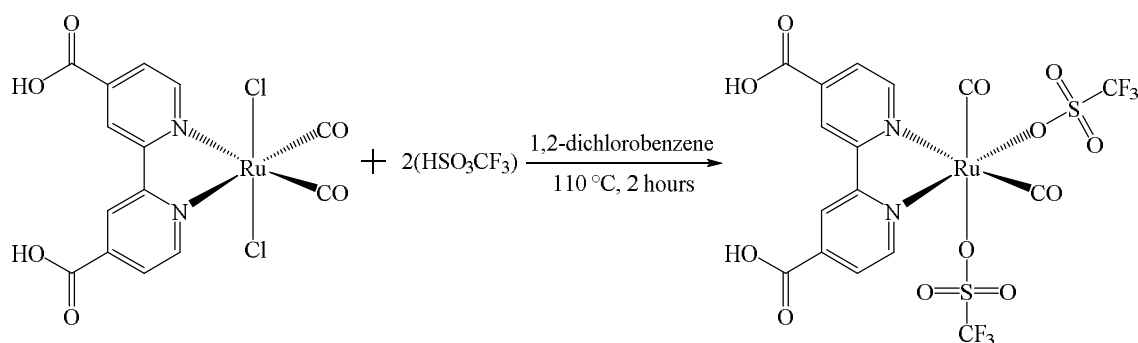


Figure 4.9: Reaction scheme showing the reagents and conditions required for the formation of cis-dicarbonyl-ditriflate-4,4'-dicarboxy-2,2'-bipyridine ruthenium(II).

General method: Crude $\text{Ru}(\text{dcbpy})(\text{CO})_2\text{Cl}_2$ (0.1547 g) was added to 1,2-dichlorobenzene (40 mL). Argon was bubbled into the solution for 30 minutes before HSO_3CF_3 (0.2 mL) was added drop wise via a glass pipette. The solution was heated to 110 °C and left stirring for 2 hours. The solution was cooled to room temperature;

diethyl ether (40 mL) was added and then placed in an ice bath for 1 hour. The solution was filtered through a sinter and washed with diethyl ether (50 mL), water (25 mL), diethyl ether (50 mL). The solid was then collected. Yield = 0.0195 g. ^1H NMR (250 MHz, DMSO- d_6) δ 8.92 (dd, $J = 5.0, 0.7$ Hz, 2H), 8.85 (d, $J = 0.7$ Hz, 2H), 7.92 (dd, $J = 4.9, 1.6$ Hz, 2H). This matches the free dcbpy ligand that was present in the crude starting material.

Synthetic comments: Multiple attempts were made to synthesise this compound with various conditions, including using methanol instead of 1,2-dichlorobenzene and AgSO_3CF_3 instead of HSO_3CF_3 . None of the attempts was successful, resulting in only recovery of starting materials.

4.4. Synthesis and Characterisation of $^t\text{Bu}_2\text{bpy}$ Ruthenium Dicarbonyl Complexes

4.4.1. Synthetic Method

Due to the highly customisable nature of these complexes, it is possible to attach the diimine ligands in any order desired. This section details the attachment of a t butyl-bipyridine ligand instead of the dcbpy ligand. This was done to overcome the reaction failure that occurs in the chloride substitution stage when the dcbpy ligand is present. However, this approach was also unsuccessful.

A previously published paper⁷ detailed conditions for which triflate substitution was not necessary to attach a second diimine ligand and so this approach was tried. An ethanol:water, 1:1 mixture was used as the solvent. However, the ^1H NMR showed that the reaction had failed as all that was recovered was dcbpy starting material.

Another paper⁵⁶ was found in which the details of a modified synthesis were provided. In this paper a mixture of ethanol and water was also used but in a 2:1 ratio. In order to test the method an unsubstituted bipyridine (bpy) was used instead of dcbpy. The method was followed as described but the ^1H NMR only showed $\text{Ru}(\text{CO})_2(^t\text{Bu}_2\text{bpy})\text{Cl}_2$ starting material was collected. Therefore, it was concluded that

the problem was with the ^tbutyl complex itself rather than the dcbpy being insoluble or unreactive.

The ^tbutyl-bipyridine containing complexes were chosen due to improved catalytic efficiency however, they have proved rather difficult to prepare. The preliminary step, obtaining Ru(CO)₂(^tBu₂bpy)Cl₂ was successful. However, no success was made with the further stages even after varying the synthesis.

4.4.2. Synthesis of Ru(CO)₂Cl₂(^tBu₂bpy)

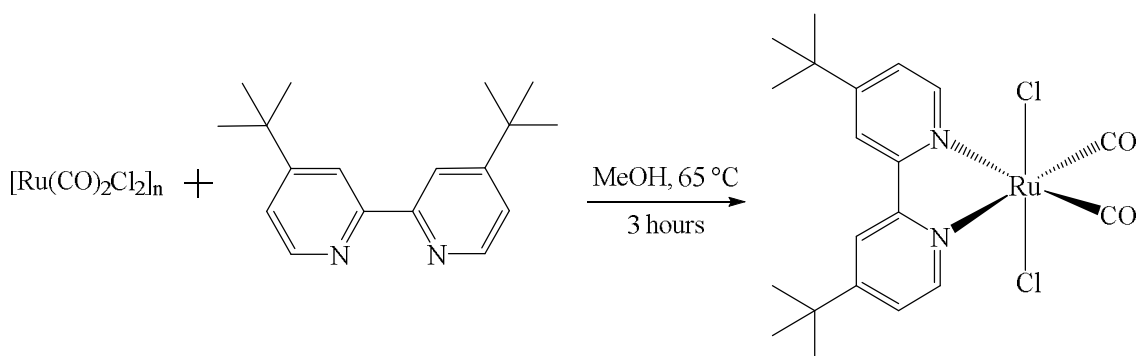


Figure 4.10: Reaction scheme showing the reagents and conditions required for the formation of trans-dichloro-cis-dicarbonyl-4,4'-tert-butyl-2,2'-bipyridine ruthenium(II).

General method: ^tBu₂bpy (1.7719 g, 6.6 mmol) and Ru(CO)₂Cl₂ (1.0041 g, 4.4 mmol) were degassed 3 times before methanol (deaerated, 20 mL) was added. Solution was heated to 65 °C and stirred for 3 hours resulting in the solution changing colour from orange to a pale yellow. The solution was cooled to room temperature before the solid product was collected on a sinter. Yield = 0.8508 g, 39%. ¹H NMR (400 MHz, CDCl₃) δ 9.06 (d, *J* = 5.8 Hz, 2H), 8.13 (d, *J* = 1.8 Hz, 2H), 7.62 (dd, *J* = 5.9, 2.0 Hz, 2H), 1.44 (s, 18H).

Synthetic comments: The synthesis of this complex was quick and simple although the yield of reaction was slightly lower than expected, at 39%. This may be due to the bulkiness of the ^tbutyl groups; perhaps a longer reaction time would improve the yield.

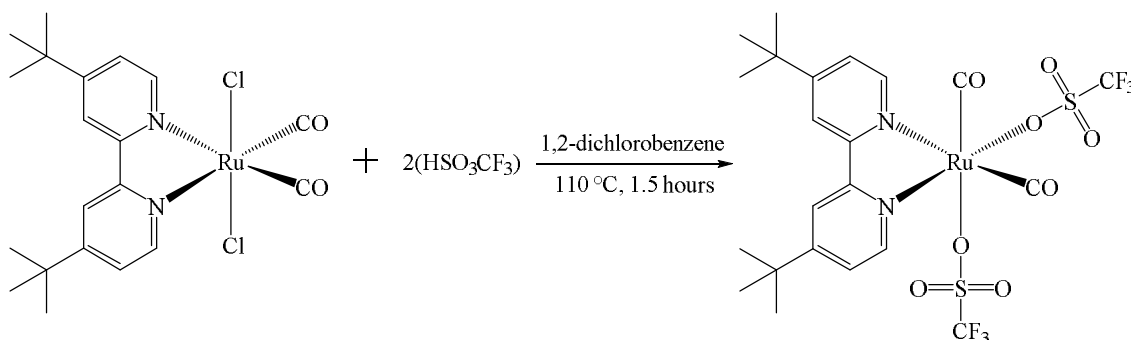
4.4.3. Synthesis of $\text{Ru}(\text{CO})_2(\text{}^t\text{Bu}_2\text{bpy})(\text{SO}_3\text{CF}_3)_2$ 

Figure 4.11: Reaction scheme showing the reagents and conditions required for the formation of cis-dicarbonyl-ditriflate-4,4'-tert-butyl-2,2'-bipyridine ruthenium(II).

General method: $\text{Ru}(\text{CO})_2\text{Cl}_2(\text{}^t\text{Bu}_2\text{bpy})$ (0.3004 g, 0.6 mmol) was dissolved in 1,2-dichlorobenzene (75 mL), argon was bubbled through the solution for 45 minutes. HSO_3CF_3 (0.5 mL) was added via syringe. The yellow solution was heated to 110 °C and stirred for 1.5 hours. The solution was cooled using an ice bath, diethyl ether (75 mL) was added and the solution left stirring for an additional hour. The solid was then collected on a sinter and washed with diethyl ether (10 mL), water (10 mL), diethyl ether (10 mL) Yield = 0.039 g. ^1H NMR (400 MHz, CDCl_3) δ 8.87 (d, $J = 5.7$ Hz, 2H), 8.50 (d, $J = 1.5$ Hz, 2H), 7.70 (dd, $J = 5.7, 1.8$ Hz, 2H), 1.46 (s, 18H).

Synthetic comments: Two attempts have been carried out to synthesise this complex, during the first attempt product appeared to have formed as a shift in the ^1H NMR was observed between the chloride and triflate product signals, however no metal carbonyl bands were observed in the FT IR spectrum from a solid sample of the triflate product. The second attempt yielded no collectable amount of product. The failure of this reaction may again have been due to the bulkiness of the t butyl groups. The bulkiness could be important due to the rearrangement that occurs when substituting chlorides for triflates, in this case from trans to cis. If the t butyl groups are preventing the triflate from successfully attacking the ruthenium centre then this may explain the reaction failure. The size of the triflate group may also be preventing a successful reaction for the same reason.

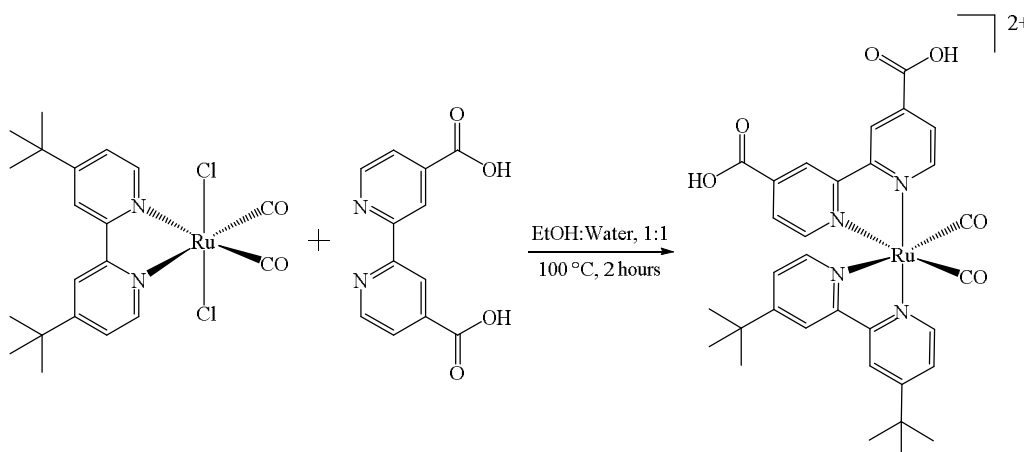
4.4.4. Synthesis of $\text{Ru}(\text{CO})_2(\text{}^t\text{Bu}_2\text{bpy})(\text{dcbpy})$ 

Figure 4.12: Reaction scheme showing the reagents and conditions required for the formation of cis-dicarbonyl-4,4'-tert-butyl-2,2'-bipyridine-4,4'-dicarboxy-2,2'-bipyridine ruthenium(II).

General method: $\text{Ru}(\text{CO})_2\text{Cl}_2(\text{}^t\text{Bu}_2\text{bpy})$ (0.0513 g, 0.1 mmol) and dcbpy (0.0264 g, 0.11 mmol) were degassed three times. Ethanol (deaerated, 20 mL) and water (deaerated, 20 mL) were added via syringe. The solution was heated to 100 °C for 2 hours. A saturated solution of NH_4PF_6 (10 mL) was added resulting in a colour change from yellow to pink. The solution was filtered and the solid collected. Yield = 0.0173 g. ^1H NMR (400 MHz, DMSO-d_6) δ 8.89 (d, $J = 5.0$ Hz, 1H), 8.84 (s, 1H), 7.90 (dd, $J = 4.9, 1.5$ Hz, 1H). This matches the dcbpy starting material.

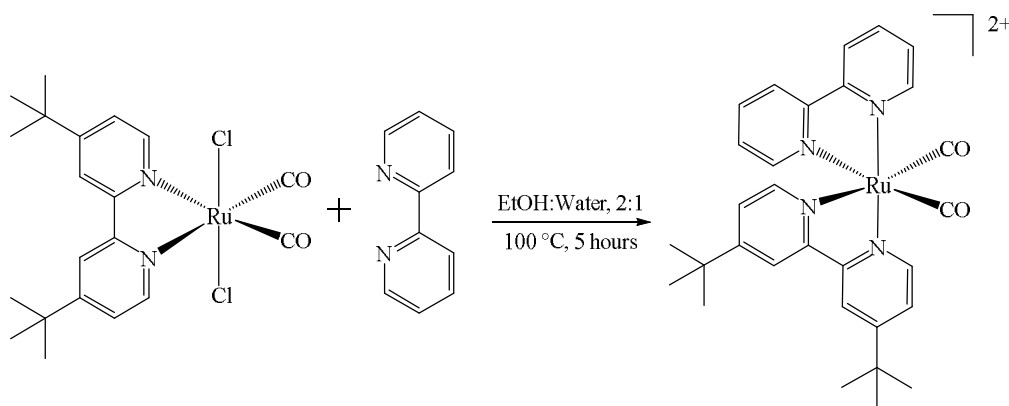
4.4.5. Synthesis of $\text{Ru}(\text{CO})_2(\text{}^t\text{Bu}_2\text{bpy})(\text{bpy})$ 

Figure 4.13: Reaction scheme showing the reagents and conditions required for the formation of cis-dicarbonyl-4,4'-tert-butyl-2,2'-bipyridine-2,2'-bipyridine ruthenium(II).

General method: $\text{Ru}(\text{CO})_2\text{Cl}_2(^t\text{Bu}_2\text{bpy})$ (0.0517 g, 0.1 mmol) and bpy (0.0254 g, 0.11 mmol) were degassed three times. Ethanol (deaerated, 10 mL) and water (deaerated, 5 mL) were added via syringe. The solution was heated to 100 °C for 5 hours. Solution was cooled to room temperature before being evaporated to dryness. Water (30 mL) was then used to dissolve the solid with any undissolved solid being collected (0.0406 g). The solution was added to a saturated KPF_6 solution (20 mL) with the precipitate being collected on a sinter. (0.0350 g) ^1H NMR (400 MHz, DMSO-d_6) δ 9.08 (d, $J = 5.9$ Hz, 2H), 8.79 (d, $J = 1.8$ Hz, 2H), 7.81 (dd, $J = 5.9, 2.0$ Hz, 2H), 1.45 (s, 18H). ^1H NMR (400 MHz, CDCl_3) δ 9.07 (d, $J = 5.9$ Hz, 2H), 8.13 (d, $J = 1.9$ Hz, 2H), 7.63 (dd, $J = 5.9, 2.0$ Hz, 2H), 1.44 (s, 18H). This matches the $\text{Ru}(\text{CO})_2\text{Cl}_2(^t\text{Bu}_2\text{bpy})$ starting material.

Synthetic comments: An additional attempt was made using this method but the reaction was left for 24 hours to see if increased reaction time resulted in product formation however only starting materials were recovered.

4.5. Synthesis and Characterisation of Bpy Ruthenium Dicarbonyl Complexes

4.5.1. Synthetic Method

Since the synthesis of the complex bearing a bulky t butyl substituted bipyridine was not successful, it was decided to employ bipyridine ligands that are less sterically hindered. With this in mind, both unsubstituted and 4,4'-dimethyl-2,2'-bipyridine was used as one of the diimine ligands, the second diimine ligand bearing an anchoring group.

The synthetic procedure published previously¹¹ was used, Figure 4.14. The desired product, $\text{Ru}(\text{bpy})(\text{CO})_2\text{Cl}_2$, with two Cl-ligands being in the trans position, was formed and isolated, as shown by ^1H NMR, Figure 4.15, albeit in a somewhat low yield (16%).

Continuing to follow the procedure described in the literature, the substitution of the chloride ligands for triflate groups was performed.

The preparation of $\text{Ru}(\text{CO})_2(\text{bpy})(\text{SO}_3\text{CF}_3)_2$ has not been as successful as was hoped. This was primarily due to the unforeseen decomposition of the triflate containing species. It is believed that if the reaction was performed again but additional water was used to remove all of the excess triflic acid then the product should be stable and the next stage of the synthesis can be carried out. However, it was decided to focus on preparing an analogous dimethyl bipyridine complex instead as it may have increased solubility, and would also be a new compound.

4.5.2. Synthesis of $\text{Ru}(\text{CO})_2\text{Cl}_2(\text{bpy})$

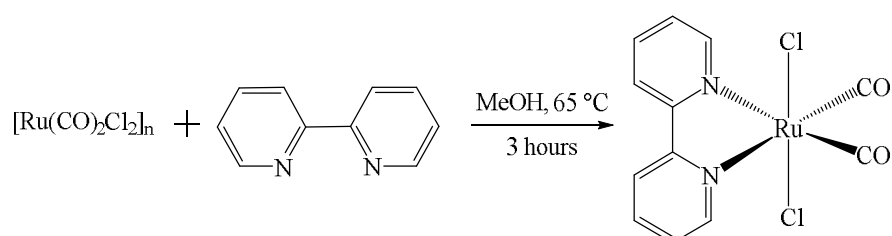


Figure 4.14: Reaction scheme showing the reagents and conditions required for the formation of trans-dichloro-cis-dicarbonyl-2,2'-bipyridine ruthenium(II).

General method: bpy (0.5013 g, 3.2 mmol) and $\text{Ru}(\text{CO})_2\text{Cl}_2$ (0.5165 g, 2.27 mmol) were degassed 3 times before methanol (deaerated, 25 mL) was added. Solution was heated to 65 °C and stirred for 3 hours under N_2 . The solution was cooled to room temperature before the solid product was collected on a sinter. Yield = 0.1410 g, 16%. ^1H NMR (400 MHz, DMSO-d_6) δ 9.23 (d, $J = 5.3$ Hz, 2H), 8.80 (d, $J = 8.2$ Hz, 2H), 8.38 (td, $J = 7.9, 1.3$ Hz, 2H), 7.88 – 7.82 (m, 2H).

Synthetic comments: Although not previously mentioned, these mono-diimine complexes have a trans-(Cl), cis-(CO) configuration, due to competition by the CO ligands for π -back-bonding from the metal d-orbitals. This is supported by Figure 4.15, which shows there are only four proton environments in the aromatic region as would be expected for a symmetric, trans-(Cl), cis-(CO) configuration.

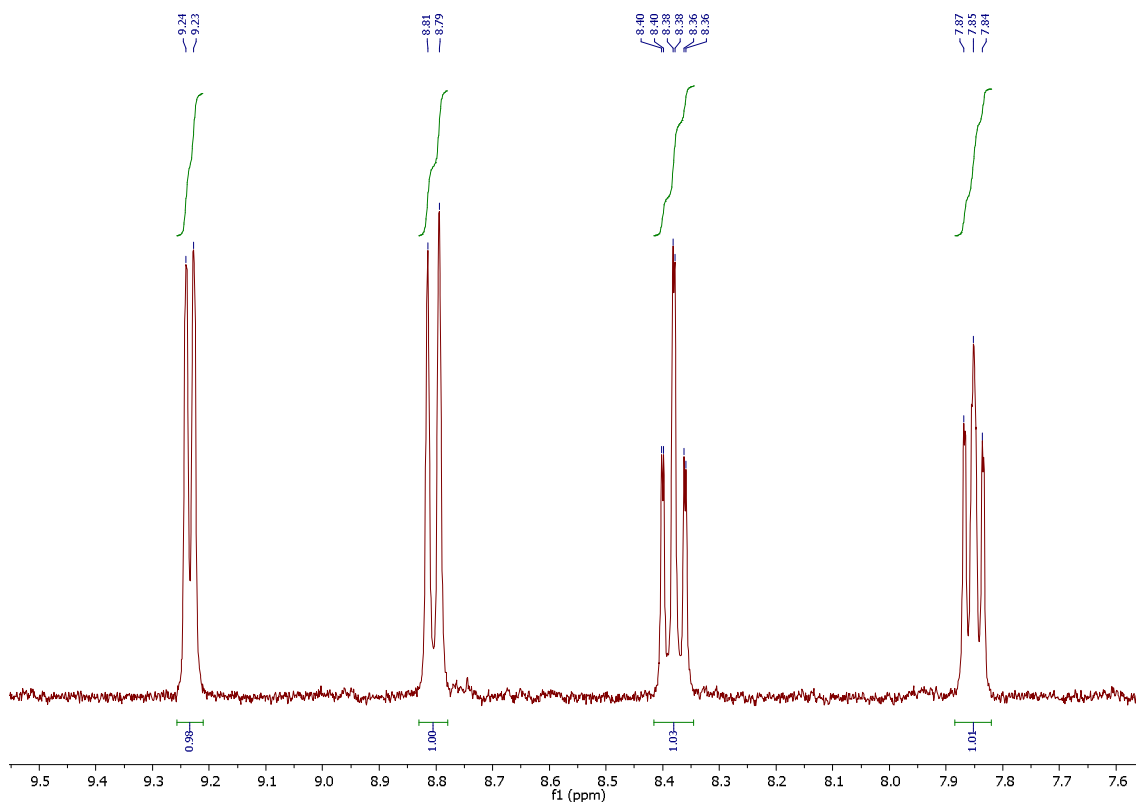


Figure 4.15: ^1H NMR (400 MHz, DMSO-d_6 , 300 kelvin) of $\text{Ru}(\text{CO})_2\text{Cl}_2(\text{bpy})$ focusing on the aromatic region of the spectrum to highlight the four different proton environments. The integration shows each environment contains the same number of protons, as expected for the trans-chloride product.

4.5.3. Synthesis of $\text{Ru}(\text{CO})_2(\text{bpy})(\text{SO}_3\text{CF}_3)_2$

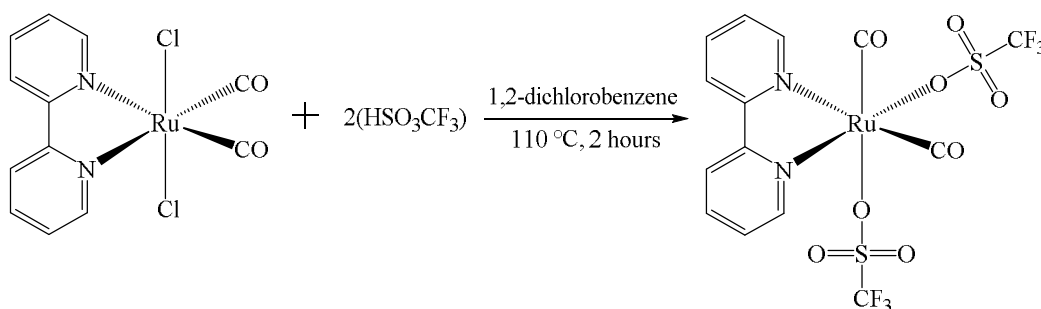


Figure 4.16: Reaction scheme showing the reagents and conditions required for the formation of cis-dicarbonyl-ditriflate-2,2'-bipyridine ruthenium(II).

$\text{Ru}(\text{CO})_2\text{Cl}_2(\text{bpy})$ (0.1041 g, 0.3 mmol) was dissolved in 1,2-dichlorobenzene (40 mL), argon was bubbled through the solution for 30 minutes. HSO_3CF_3 (0.3 mL) was added via a glass pipette. The solution was heated to 110 °C and stirred for 2 hours

under argon. The solution was cooled using an ice bath, diethyl ether (75 mL) was added and the solution left stirring for 3 hours. The solid was then collected on a sinter and washed with diethyl ether (10 mL), water (10 mL), diethyl ether (10 mL) resulting in a white product. Yield = 0.16 g, 87%. ^1H NMR (400 MHz, DMSO- d_6) δ 9.37 (d, J = 5.3 Hz), 8.96 (d, J = 4.7 Hz), 8.90 (d, J = 8.4 Hz), 8.82 (d, J = 8.0 Hz), 8.71 (d, J = 4.8 Hz), 8.63 – 8.48 (m), 8.41 (t, J = 7.9 Hz), 8.17 – 8.11 (m), 8.07 (d, J = 4.1 Hz), 8.02 (t, J = 6.6 Hz), 7.96 (d, J = 9.6 Hz), 7.83 (s), 7.80 (t, J = 6.1 Hz).

Synthetic comments: The synthesis appeared to have worked, as the product was the correct colour, creamy white. However, the product started to decompose due to residual triflic acid. This was deduced only after the solid product became liquid over several days even though it is supposed to be air stable. This was unfortunate, as it was believed that product had been washed with sufficient water, which removes the acid. Therefore, future reactions will be washed with excess water or try to use less acid in the reaction.

4.6. Synthesis and Characterisation of Me_2bpy Ruthenium Dicarbonyl Complexes

4.6.1. Synthetic Method

The synthetic procedure was taken from the same literature source¹¹ which detailed the procedure for preparing complexes bearing the unsubstituted bipyridine. Again, the product was formed cleanly, as shown by ^1H NMR, Figure 4.18. Over the course of several attempts the yield increased from 27% to 67%.

The preparation of $\text{Ru}(\text{CO})_2\text{Cl}_2(\text{Me}_2\text{bpy})$, and its conversion to $\text{Ru}(\text{CO})_2(\text{Me}_2\text{bpy})(\text{SO}_3\text{CF}_3)_2$ were successful, however, the addition of the second diimine ligand was not successful. This occurred even after incorporating the lessons learnt previously about using THF rather than the standard methanol solvent.

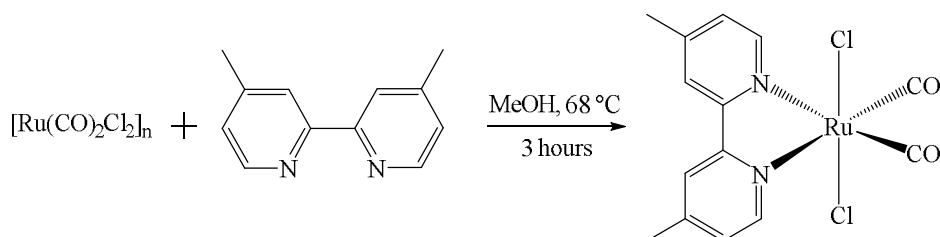
4.6.2. Synthesis of $\text{Ru}(\text{CO})_2\text{Cl}_2(\text{Me}_2\text{bpy})$ 

Figure 4.17: Reaction scheme showing the reagents and conditions required for the formation of trans-dichloro-cis-dicarbonyl-4,4'-dimethyl-2,2'-bipyridine ruthenium(II).

General method: Me_2bpy (0.5044 g, 2.73 mmol) and $\text{Ru}(\text{CO})_2\text{Cl}_2$ (0.7582 g, 3.33 mmol) were degassed 3 times before methanol (deaerated, 25 mL) was added. Solution was heated to 68 °C and stirred for 3 hours under N_2 . The solution was cooled to room temperature before the light yellow product was collected on a sinter. Yield = 0.7490 g, 67%. ^1H NMR (400 MHz, DMSO-d_6) δ 9.03 (d, $J = 5.7$ Hz, 2H), 8.64 (s, 2H), 7.66 (d, $J = 5.7$ Hz, 2H), 2.58 (s, 6H). MS EI^+ : m/z 412 (M^+) 384 ($\text{M}-\text{CO}^+$) 356 ($\text{M}-2\text{CO}^+$).

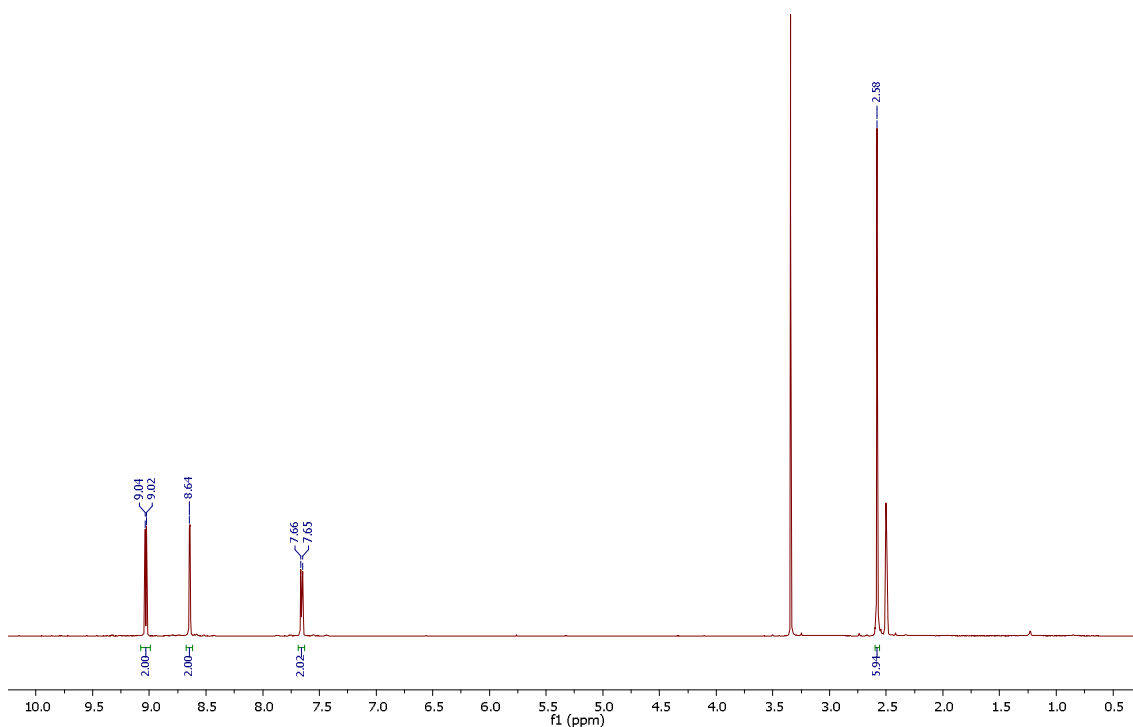


Figure 4.18: ^1H NMR (400 MHz, DMSO-d_6 , 300 kelvin) of $\text{Ru}(\text{CO})_2\text{Cl}_2(\text{Me}_2\text{bpy})$ showing the three aromatic environments and the methyl environment. Integration and number of environments is as expected for the trans-chloride product.

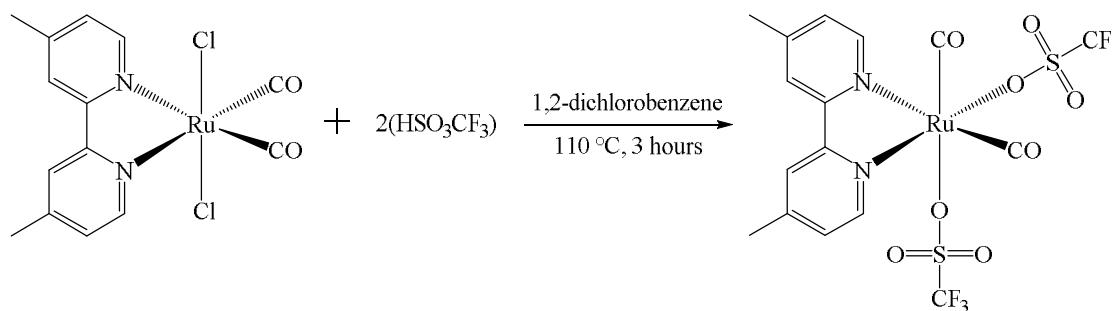
4.6.3. Synthesis of $\text{Ru}(\text{CO})_2(\text{Me}_2\text{bpy})(\text{SO}_3\text{CF}_3)_2$ 

Figure 4.19: Reaction scheme showing the reagents and conditions required for the formation of cis-dicarbonyl-ditriflate-4,4'-dimethyl-2,2'-bipyridine ruthenium(II).

General method: $\text{Ru}(\text{CO})_2\text{Cl}_2(\text{Me}_2\text{bpy})$ (0.2997 g, 0.722 mmol) was dissolved in 1,2-dichlorobenzene (80 mL), argon was bubbled through the solution for 1 hour. HSO_3CF_3 (1 mL) was added drop wise via a glass pipette. The solution was heated to 110 °C and stirred for 3 hours. The solution was cooled using an ice bath, diethyl ether (80 mL) was added and the solution left stirring for 1 hour. The solid was then collected on a sinter and washed with diethyl ether (100 mL), water (50 mL), diethyl ether (100 mL) resulting in a white product. Yield = 0.2381 g, 52%. ^1H NMR (400 MHz, DMSO-d_6) δ 8.78 – 8.75 (m, 2H), 8.73 (d, $J = 5.8$ Hz, 1H), 8.70 (d, $J = 1.9$ Hz, 1H), 7.84 (dd, 1H), 7.65 (dd, $J = 6.1, 2.3$ Hz, 1H), 2.65 (s, 3H), 2.59 (s, 3H). FTIR: $\nu(\text{CO})$, 2099, 2027 cm^{-1} . MS EI^+ : m/z 640 (M^+).

Synthetic comments: As previously mentioned excess water was used when washing the solid product to ensure all of the triflic acid was removed.

During the synthesis of successive batches, it was noticed that there were differences in the number and intensities of the signals in the ^1H and ^{19}F NMR. This can be seen clearly in the ^{19}F NMR. To investigate the differences a fresh sample was prepared using a batch synthesised as described above. The ^{19}F NMR was performed straight away resulting in the following; ^{19}F NMR (235 MHz, DMSO-d_6) δ -77.78. The sample was then rerun a few hours later resulting in the following; ^{19}F NMR (235 MHz, DMSO-d_6) δ -76.34, -77.78, in a 1:2 ratio. The ^1H NMR also changes over time; ^1H

NMR (250 MHz, DMSO- d_6) δ 8.80 – 8.73 (m, 2.19H), 8.71 (d, $J = 5.1$ Hz, 1.57H), 8.53 (d, $J = 5.8$ Hz, 0.67H), 7.96 (d, $J = 5.9$ Hz, 0.65H), 7.84 (d, $J = 5.9$ Hz, 0.62H), 7.64 (d, $J = 6.2$ Hz, 1.32H), 2.64 (s, 3H), 2.59 (s, 3H).

The literature^{11, 57} suggests that the complex is in the cis-(OTf), cis-(CO) configuration and is partially supported by the IR spectrum which shows two signals as expected for a cis-(CO) configuration. However as mentioned above the ^{19}F NMR initially shows a single environment suggesting the OTf groups are in the trans-(OTf) configuration. When in solution a rearrangement maybe occurring over time resulting in the formation of the cis-(OTf), cis-(CO) configuration. This is shown in the ^{19}F NMR by the eventual appearance of two signals in a 1:1 ratio.

4.6.4. Synthesis of $[\text{Ru}(\text{CO})_2(\text{Me}_2\text{bpy})(\text{dcbpy})]^{2+}$

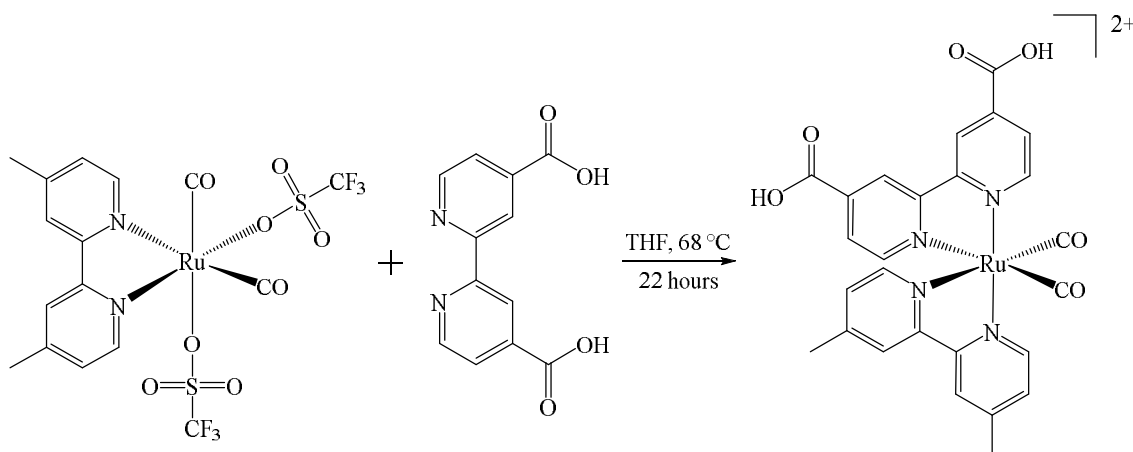


Figure 4.20: Reaction scheme showing the reagents and conditions required for the formation of cis-dicarbonyl-4,4'-dimethyl-2,2'-bipyridine-4,4'-dicarboxy-2,2'-bipyridine ruthenium(II).

General method: $\text{Ru}(\text{CO})_2(\text{Me}_2\text{bpy})(\text{SO}_3\text{CF}_3)_2$ (0.0511 g, 0.08 mmol) and dcbpy (0.0298 g, 0.12 mmol) were degassed 3 times before THF (deaerated, 15 mL) was added via syringe. The solution was heated to reflux (68 °C) and stirred for 22 hours. The solution was cooled to room temperature and filtered. This resulted in a white solid. Yield = 0.033 g. ^1H NMR (400 MHz, DMSO- d_6) δ 8.91 (d, $J = 5.0$ Hz, 1H), 8.85 (s, 1H), 7.91 (dd, $J = 4.9, 1.5$ Hz, 1H).

Synthetic comments: Using the earlier lessons of reacting dcbpy in THF the next stage of the synthesis, adding a second diimine, was performed. However, even using this modified method the reaction was unsuccessful. The ^1H NMR of the solid product collected matches the dcbpy starting material. The solvent from the filtrate was then removed and the remaining solid analysed by ^1H NMR but the desired product could not be identified.

4.7. Synthesis and Characterisation of Phosphonate Ruthenium Dicarbonyl Complexes

4.7.1. Synthetic Method

Whilst work was continuing on the carboxylic acid anchor containing complexes it was decided to look at phosphonic acid anchoring groups. Initial work was started on $(\text{Et}_2\text{O}_3\text{P})_2\text{bpy}$. However work on this ligand was suspended due to the publication of a paper by Suzuki et al.¹⁸ in which this ligand, attached to $\text{Ru}(\text{CO})_2\text{bpy}(\text{L})$ was used in a system with N-Ta₂O₅, which is what we had planned to do.

In order to produce a novel system it was decided to look at a phosphonic acid containing ligand that had a $-\text{CH}_2-$ spacer between the phosphorus and the bipyridine. The synthesis of the ligand was performed by Dr Stuart Archer using the method described in a paper by G J. Meyer et al.²¹

Synthesis of the titled complex was performed using the now familiar method of substituting labile triflate groups for a second diimine. The ^1H NMR is slightly unclear as to whether the desired complex has been produced. There are only 10 clear signals when 12 would be expected if both sides of both diimines were inequivalent however, the integration shows 12 protons are present leading to the conclusion that several of the signals are overlapping. The ^1H NMR is virtually identical for all attempts therefore whatever is being produced is done so consistently.

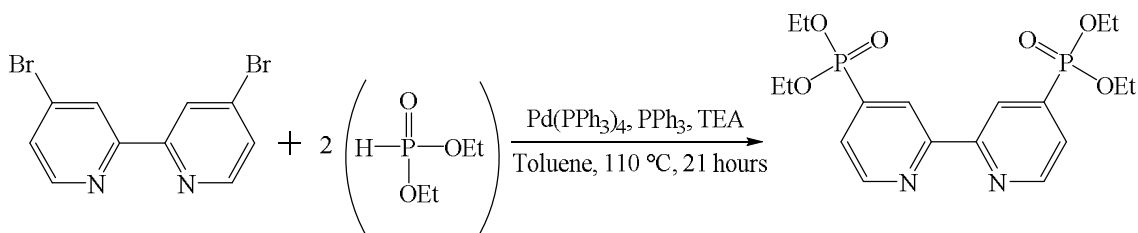
4.7.2. Synthesis of $(\text{Et}_2\text{O}_3\text{P})_2\text{bpy}$ 

Figure 4.21: Reaction scheme showing the reagents and conditions required for the formation of 4,4'-(diethylphosphonate)-2,2'-bipyridine.^{40, 58}

General method: 4,4'-dibromo-2,2'-bipyridine (0.3002 g, 0.96 mmol), PPh_3 (2.5165 g, 9.6 mmol) and $\text{Pd}(\text{PPh}_3)_4$ were degassed three times before toluene (10 mL), TEA (0.3 mL) and diethyl phosphate (0.3 mL, 2.3 mmol) were added. The reaction was heated to 110 °C and left stirring for 21 hours, during which the solution changed colour from brown to a clear yellow. The solution was cooled to room temperature, ammonium hydroxide (10 mL), water (20 mL) was added, and an organic-aqueous separation performed. The organic layer was dried with MgSO_4 , filtered and the solvent removed by rotary evaporation. Product was purified on a silica column, eluent; DCM, followed by DCM:MeOH; 99:1. Unreacted PPh_3 (2.3 g) and product (0.26 g, 64%) were obtained. ^1H NMR (400 MHz, CDCl_3) δ 8.86 – 8.81 (m, 2H), 8.80 – 8.78 (m, 1H), 8.77 – 8.74 (m, 1H), 7.74 (dd, $J = 4.8, 1.4$ Hz, 1H), 7.71 (dd, $J = 4.8, 1.4$ Hz, 1H), 7.69 (t, $J = 1.3$ Hz, 2H), 7.68 (t, $J = 1.7$ Hz, 3H), 7.66 (t, $J = 1.3$ Hz, 3H), 7.65 (t, $J = 1.7$ Hz, 3H), 7.57 (dd, $J = 2.9, 1.4$ Hz, 1H), 7.55 (q, $J = 2.2$ Hz, 3H), 7.53 (dt, $J = 3.9, 1.9$ Hz, 2H), 7.49 – 7.47 (m, 4H), 7.46 (dd, $J = 2.9, 1.3$ Hz, 5H), 7.44 (dd, $J = 2.9, 1.2$ Hz, 2H), 4.28 – 4.09 (m, 8H), 1.36 (dt, $J = 7.1, 3.7$ Hz, 12H).

Synthetic comments: ^1H NMR showed too many signals to identify the product successfully. Synthesis was repeated by another group member, Dr Stuart Archer but with modified column conditions, silica, chloroform:MeOH; 99:1. This resulted in pure product being obtained. ^1H NMR (400 MHz, CDCl_3) δ 8.84 (t, $J = 5.1$ Hz, 2H), 8.80 (s, 1H), 8.76 (s, 1H), 7.75 (dd, $J = 4.8, 1.3$ Hz, 1H), 7.72 (dd, $J = 4.8, 1.3$ Hz, 1H), 4.30 – 4.10 (m, 8H), 1.37 (t, $J = 7.1$ Hz, 12H).

This showed that the product had been synthesised during the initial attempt but had not been fully purified under the original column conditions used.

4.7.3. Synthesis of $\text{Ru}(\text{CO})_2(\text{Me}_2\text{bpy})\{\text{bpy}(\text{CH}_2\text{PO}_3\text{Et}_2)_2\}$

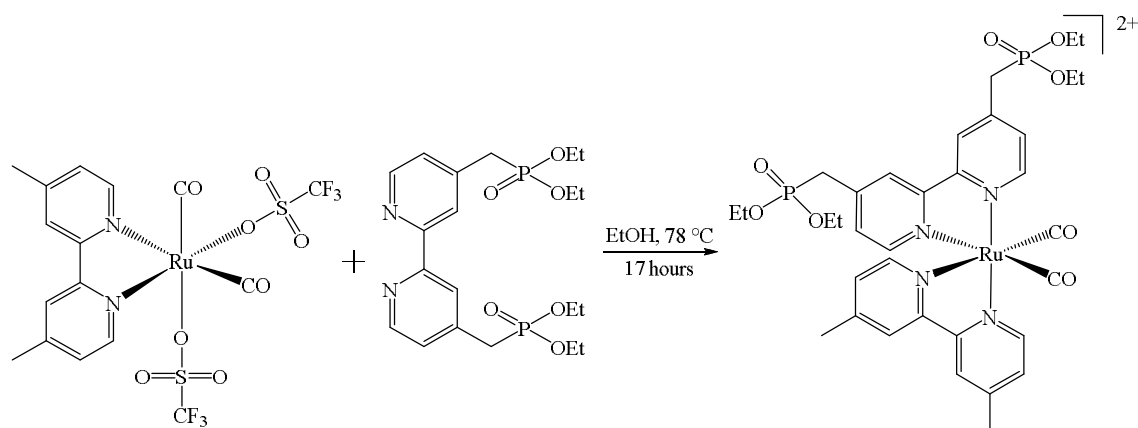


Figure 4.22: Reaction scheme showing the reagents and conditions required for the formation of cis-dicarbonyl-4,4'-bis(diethylmethylphosphonate)-2,2'-bipyridine-4,4'-dimethyl-2,2'-bipyridine ruthenium(II).

General method: $\text{Ru}(\text{CO})_2(\text{Me}_2\text{bpy})(\text{SO}_3\text{CF}_3)_2$ (0.1515 g, 0.237 mmol) and $\text{bpy}(\text{CH}_2\text{PO}_3\text{Et}_2)_2$ (0.1169 g, 0.256 mmol) were degassed three times before ethanol (deaerated, 30 mL) was added via syringe. The solution was heated to reflux (78 °C) and stirred for 17 hours. The solution was cooled to room temperature and the solvent removed by rotary evaporation. The solid was dissolved in boiling water (25 mL), filtered and the solution added to a saturated solution of NH_4PF_6 (5 mL). The precipitate was then filtered and washed with ether. This resulted in a light brown solid. Yield = 0.2057 g, 80%. ^1H NMR (400 MHz, DMSO-d_6) δ 9.18 (d, $J = 5.9$ Hz, 1H), 9.06 (d, $J = 5.8$ Hz, 1H), 8.80 (d, $J = 1.8$ Hz, 1H), 8.74 – 8.67 (m, 2H), 8.61 (s, 1H), 7.91 (dd, $J = 5.1, 3.0$ Hz, 1H), 7.87 (dd, $J = 6.0, 1.7$ Hz, 1H), 7.54 – 7.46 (m, 1H), 7.43 (dd, $J = 6.2, 2.7$ Hz, 2H), 7.22 (d, $J = 5.8$ Hz, 1H), 4.10 (ddd, $J = 8.6, 6.9, 4.7$ Hz, 4H), 3.93 (ddd, $J = 10.5, 8.7, 7.0$ Hz, 4H), 3.57 (s, 2H), 3.51 (s, 2H), 2.68 (s, 3H), 2.48 (s, 3H), 1.24 (td, $J = 7.0, 3.8$ Hz, 6H), 1.05 (dt, $J = 13.6, 7.0$ Hz, 6H). ^{31}P NMR (101 MHz, DMSO-d_6) δ 23.12, 22.99. ToF MS ES^+ : m/z 399 (M^{2+}). {The $\text{bpy}(\text{CH}_2\text{PO}_3\text{Et}_2)_2$ ligand was synthesised using the method shown in chapter 5, figure 5.4.}

4.7.4. Synthesis of $\text{Ru}(\text{CO})_2(\text{Me}_2\text{bpy})\{\text{bpy}(\text{CH}_2\text{PO}_3\text{H}_2)_2\}$

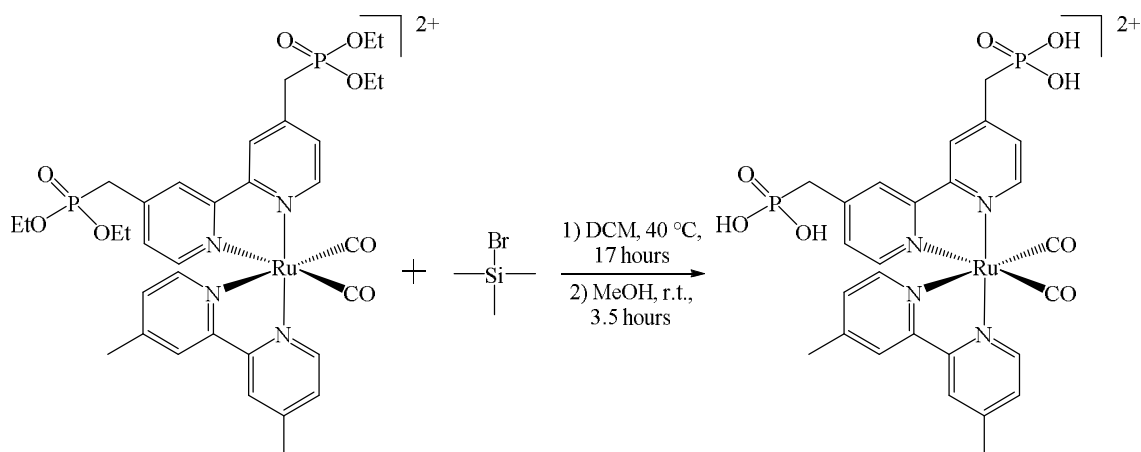


Figure 4.23: Reaction scheme showing the reagents and conditions required for the formation of cis-dicarbonyl-4,4'-bis(methylphosphonate)-2,2'-bipyridine-4,4'-dimethyl-2,2'-bipyridine ruthenium(II).

$\text{Ru}(\text{CO})_2(\text{Me}_2\text{bpy})\{\text{bpy}(\text{CH}_2\text{PO}_3\text{Et}_2)_2\}$ (0.2057 g, 0.258 mmol) was degassed three times before DCM (Grubbs, 30 mL) was added via syringe. Trimethylsilyl bromide (2 mL) was then injected slowly by syringe. The reaction was heated to reflux (40 °C) and stirred for 17 hours. MeOH (45 mL) was then added via syringe. The solution was cooled to room temperature and left stirring for 3.5 hours. The solution was filtered and the solvents removed on the rotary evaporator. The product was then purified by recrystallisation in DMF/diethyl ether. Yield = 0.168 g, 95%. ^1H NMR (400 MHz, DMSO-d_6) δ 9.14 (d, $J = 6.0$ Hz, 1H), 9.06 (d, $J = 5.8$ Hz, 1H), 8.85 (s, 1H), 8.76 (s, 2H), 8.65 (s, 1H), 7.89 (d, $J = 5.9$ Hz, 2H), 7.50 (d, $J = 5.7$ Hz, 1H), 7.46 (d, $J = 5.9$ Hz, 1H), 7.38 (d, $J = 5.9$ Hz, 1H), 7.27 (d, $J = 5.9$ Hz, 1H), 3.27 (s, 2H), 3.21 (s, 2H), 2.68 (s, 3H), 2.48 (s, 3H). ^{31}P NMR (101 MHz, DMSO-d_6) δ 16.89, 16.75.

4.8. Results and Discussion of Phosphonate Ruthenium Dicarbonyl Complexes

4.8.1. Photophysical Data for $\text{Ru}(\text{CO})_2(\text{Me}_2\text{bpy})\{\text{bpy}(\text{CH}_2\text{PO}_3\text{Et}_2)_2\}$

Figure 4.24 shows the UV-Vis spectrum of $\text{Ru}(\text{CO})_2(\text{Me}_2\text{bpy})\{\text{bpy}(\text{CH}_2\text{PO}_3\text{Et}_2)_2\}$ in DCM. The three bands at 253, 304 and 314 nm are due to $\pi \rightarrow \pi^*$ transitions. There are then two other, lower intensity, bands that are difficult to see on this scale, but can be

seen easier in Figure 4.25 and are at 350 and 420 nm. The band at 420 nm is attributed to the main MLCT transition. The band at 350 nm could be a higher-lying MLCT or another intraligand transition.

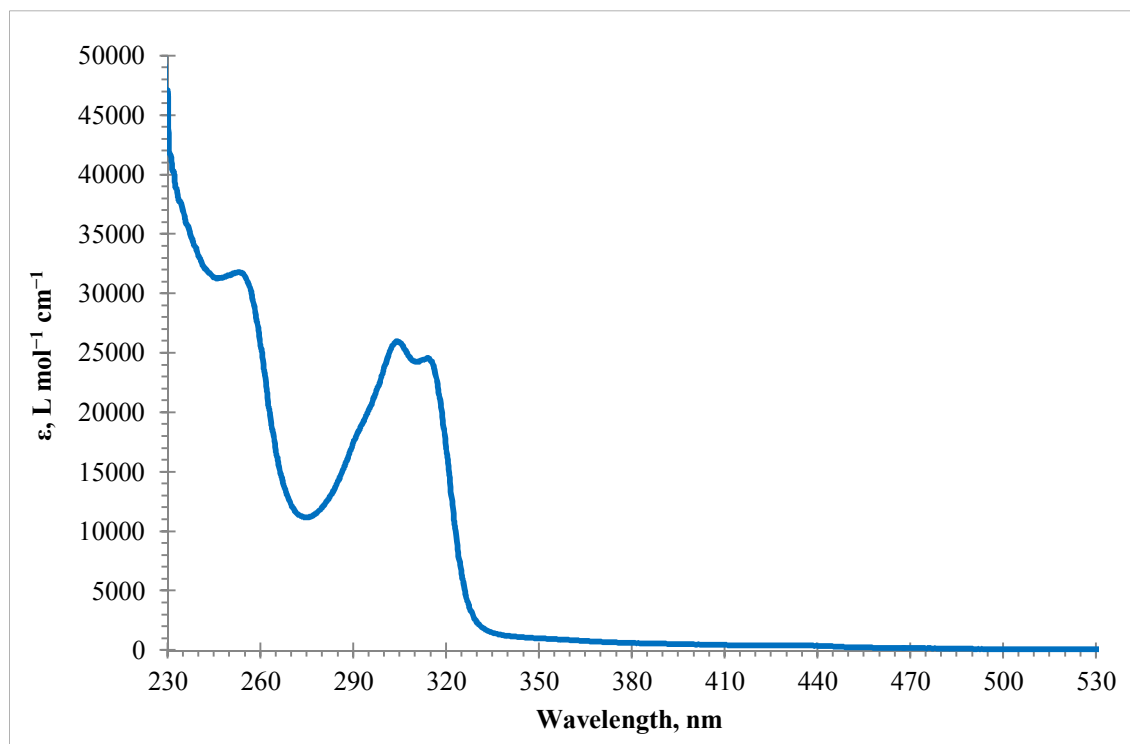


Figure 4.24: The UV-Vis spectrum, of $\text{Ru}(\text{CO})_2(\text{Me}_2\text{bpy})\{\text{bpy}(\text{CH}_2\text{PO}_3\text{Et}_2)_2\}$ in DCM.

Figure 4.25 shows the UV-Vis, emission and excitation spectra for the complex. The MLCT band at 420 nm was excited to provide the emission spectrum, from this a single emission process is observed, however this emission is very weak. The excitation spectrum appears to have the same spectral shape as the UV-Vis suggesting that the emission does in fact come from the complex and not an impurity of some sort.

Figure 4.26 shows the emission lifetime data for the complex in DMF. This was obtained using the mini- τ instrument with a 5 μs delay between pulses and a bandpass filter of 625 – 675 nm. It is a relatively straight line in half-logarithmic coordinates, representing a single decay process occurring from the MLCT state back directly to the ground state. This process has a lifetime of 744 ± 74 ns.

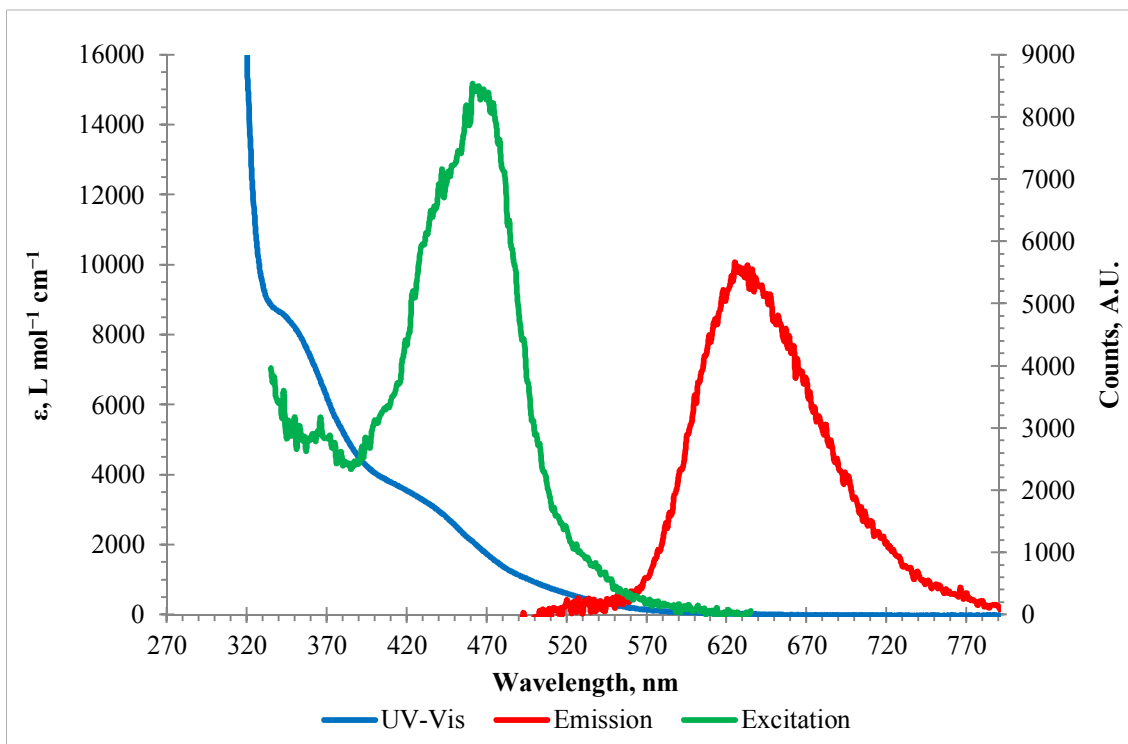


Figure 4.25: The UV-Vis, emission and excitation spectra of $\text{Ru}(\text{CO})_2(\text{Me}_2\text{bpy})\{\text{bpy}(\text{CH}_2\text{PO}_3\text{Et}_2)_2\}$ in DMF. The excitation spectra were registered at 645 nm; the emission spectra were obtained under 420 nm excitation.

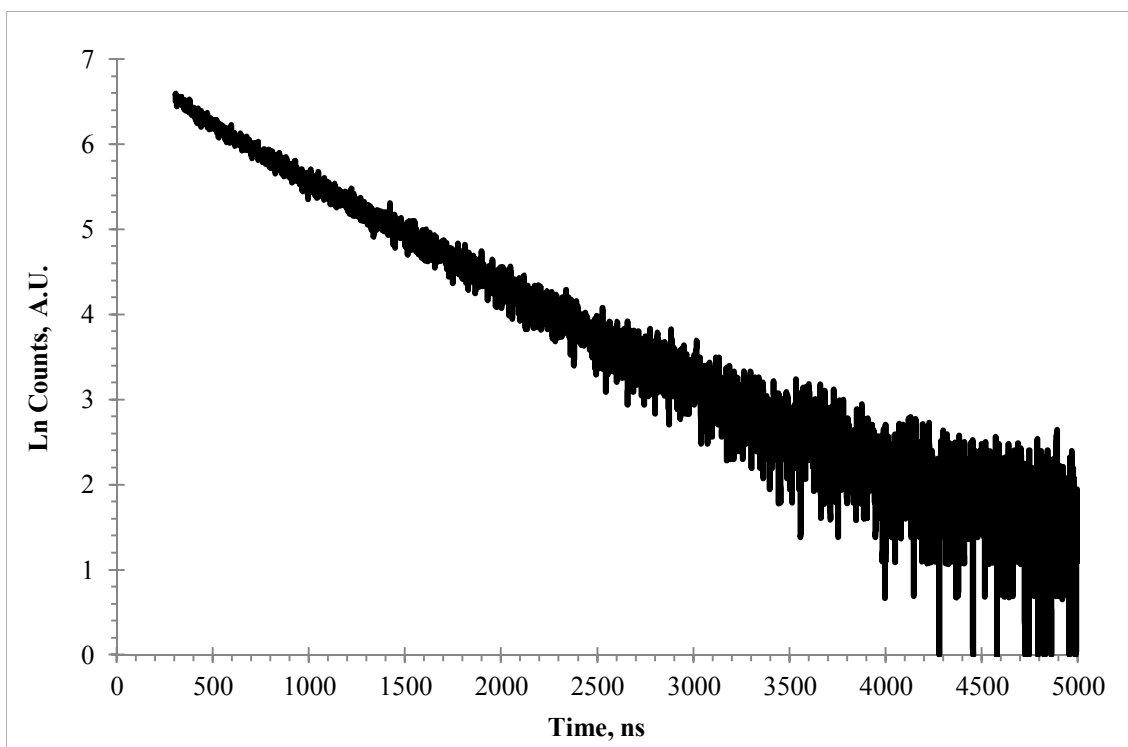


Figure 4.26: Lifetime trace of $\text{Ru}(\text{CO})_2(\text{Me}_2\text{bpy})\{\text{bpy}(\text{CH}_2\text{PO}_3\text{Et}_2)_2\}$, in DMF, recorded in the spectral range 625 – 675 nm, 5 μs timescale, excitation with ca. 75 ps, 405 nm laser pulse.

4.8.2. Electrochemical Data for $\text{Ru}(\text{CO})_2(\text{Me}_2\text{bpy})\{\text{bpy}(\text{CH}_2\text{PO}_3\text{Et}_2)_2\}$

Tests for electrocatalytic activity of all new complexes have been performed following a standard protocol:

- (i) Cyclic voltammetry of 2 mM solution saturated with N_2 .
- (ii) Cyclic voltammetry of the same solution saturated with CO_2 .
- (iii) Cyclic voltammetry of the same solution re-saturated with N_2 .

In all cases, control experiments included background scans (electrolyte only, no Ru complexes) under N_2 and CO_2 , although these are not always shown in the figures below. All potentials were measured vs. Ag/AgCl^+ , and reported vs. Fc/Fc^+ .

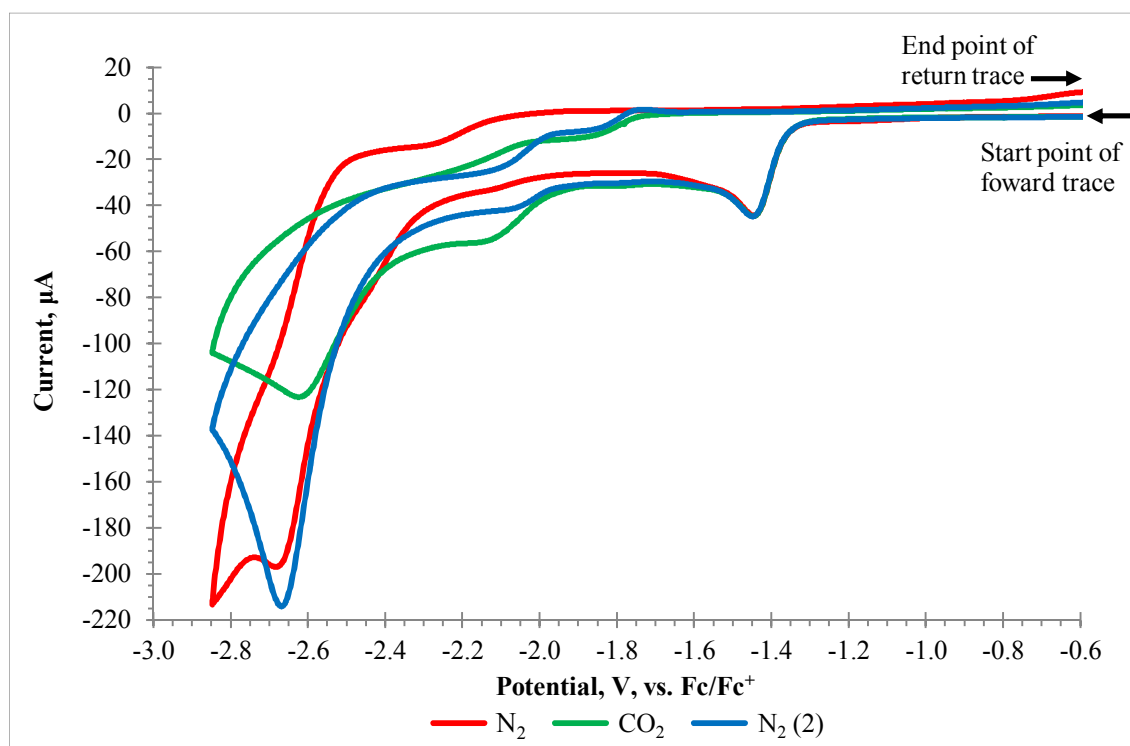


Figure 4.27: Cyclic voltammograms for $\text{Ru}(\text{CO})_2(\text{Me}_2\text{bpy})\{\text{bpy}(\text{CH}_2\text{PO}_3\text{Et}_2)_2\}$, 2 mM in DMF with 0.2 M $[\text{Bu}_4\text{N}][\text{PF}_6]$, recorded at 100 mVs^{-1} , in the presence of N_2 or CO_2 , the potentials are reported vs. Fc/Fc^+ . The arrows show the start or end point and the direction of potential change.

Figure 4.27 shows the results from the cyclic voltammetry experiment in which the complex was used in both a nitrogen saturated solution, and a CO_2 saturated solution. Saturation was achieved by bubbling the desired gas into the solution for up to 45

minutes. The red line is when the solution is saturated with nitrogen, the nitrogen is then replaced with CO₂, the green line. The CO₂ is then changed back to nitrogen, the blue line. There is an irreversible couple at -1.45 V in all three traces. When CO₂ is present in the system a slight increase in current can be seen at -2.12 V, however when the solution is resaturated with nitrogen the current decreases slightly although it does not go back to the value of the first run. One possible explanation is that not all of the CO₂ was purged, although given the usual time of 45 minutes purging, this seems unlikely.

4.8.3. Photophysical Data for Ru(CO)₂(Me₂bpy){bpy(CH₂PO₃H₂)₂}

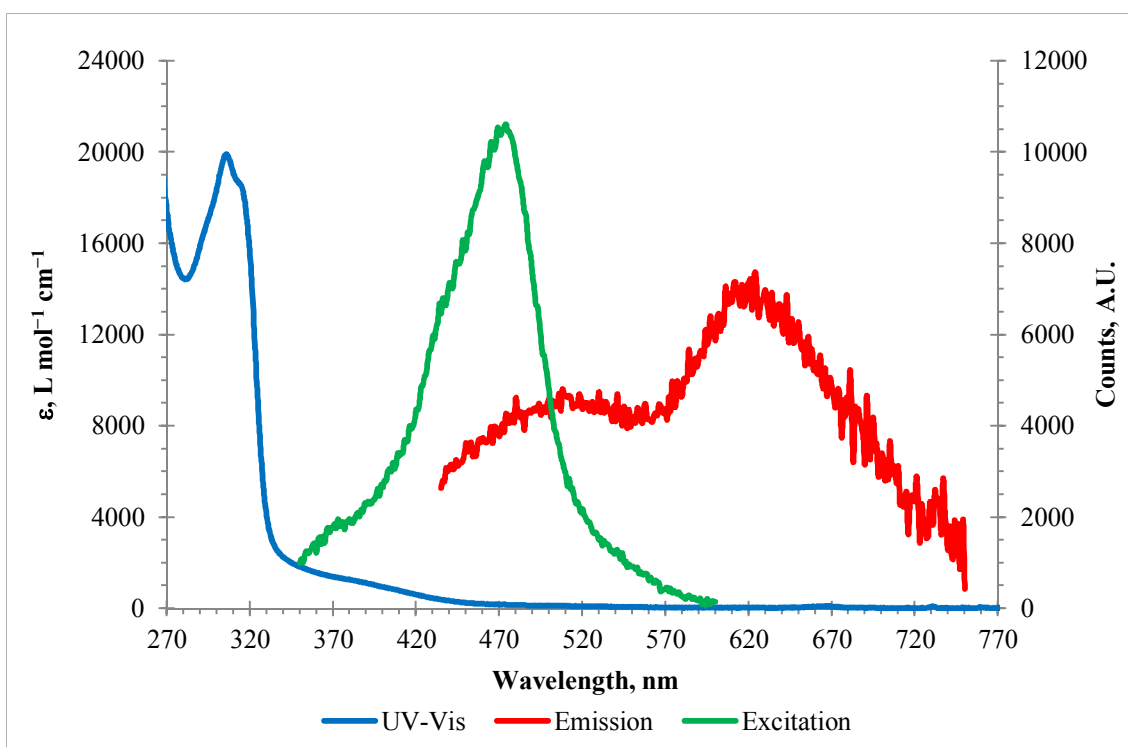


Figure 4.28: The UV-Vis, emission and excitation spectra of Ru(CO)₂(Me₂bpy){bpy(CH₂PO₃H₂)₂} in DMF. The excitation spectra were registered at 620 nm; the emission spectra were obtained under 380 nm excitation. Emission and excitation spectra were normalised.

Figure 4.28 shows the UV-Vis, emission and excitation spectra for Ru(CO)₂(Me₂bpy){bpy(CH₂PO₃H₂)₂}. There are two $\pi \rightarrow \pi^*$ bands, 305 and 315 nm visible in this solvent. There is then an MLCT band present at 380 nm. This band was used to excite the complex and generate the emission spectrum as show in the red line.

This emission is extremely weak but appears to show a two-component system. This is unexpected as the ester analogue had only one component. The first is believed to be the $^3\text{MLCT}$. It is unknown as to what this second component could be. When trying to get lifetime data for the decay processes to help us understand the components, we were only able to collect background signal even under long sampling times. The excitation spectrum also presents a difficulty as the position of the band does not appear to correlate to any band in the UV-Vis, this would usually suggest an impurity despite the recrystallisation. Another possibility is a band with a very low absorption is present but could not be seen at this concentration. A rerun of this experiment was planned however, electrochemical experiments were performed in the meantime resulting in the decision to cease work on this class of complex.

4.8.4. Electrochemical Data for $\text{Ru}(\text{CO})_2(\text{Me}_2\text{bpy})\{\text{bpy}(\text{CH}_2\text{PO}_3\text{H}_2)_2\}$

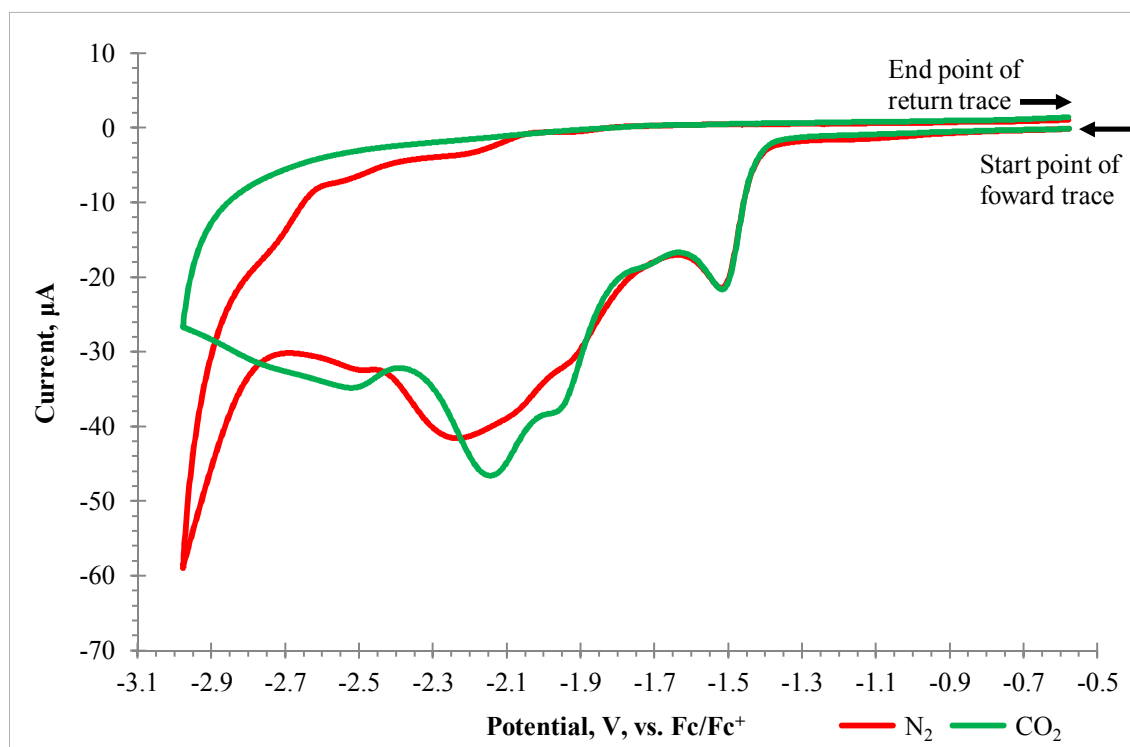


Figure 4.29: Cyclic voltammograms for $\text{Ru}(\text{CO})_2(\text{Me}_2\text{bpy})\{\text{bpy}(\text{CH}_2\text{PO}_3\text{H}_2)_2\}$, 2 mM in DMF with 0.2 M $[\text{Bu}_4\text{N}][\text{PF}_6]$, recorded at 100 mVs^{-1} , in the presence of N_2 or CO_2 , the potentials are reported vs. Fc/Fc^+ .

The arrows show the start or end point and the direction of potential change.

Figure 4.29 shows the results from the cyclic voltammetry experiment in which the current generated when the solution is saturated with nitrogen is compared to when the solution is saturated with CO₂. The results are simple to understand although disappointing. Under the same conditions except the gas involved, it is clear that there is no increase in current when CO₂ is in the solution. This is in contrast with the ester analogue, which did show a small increase.

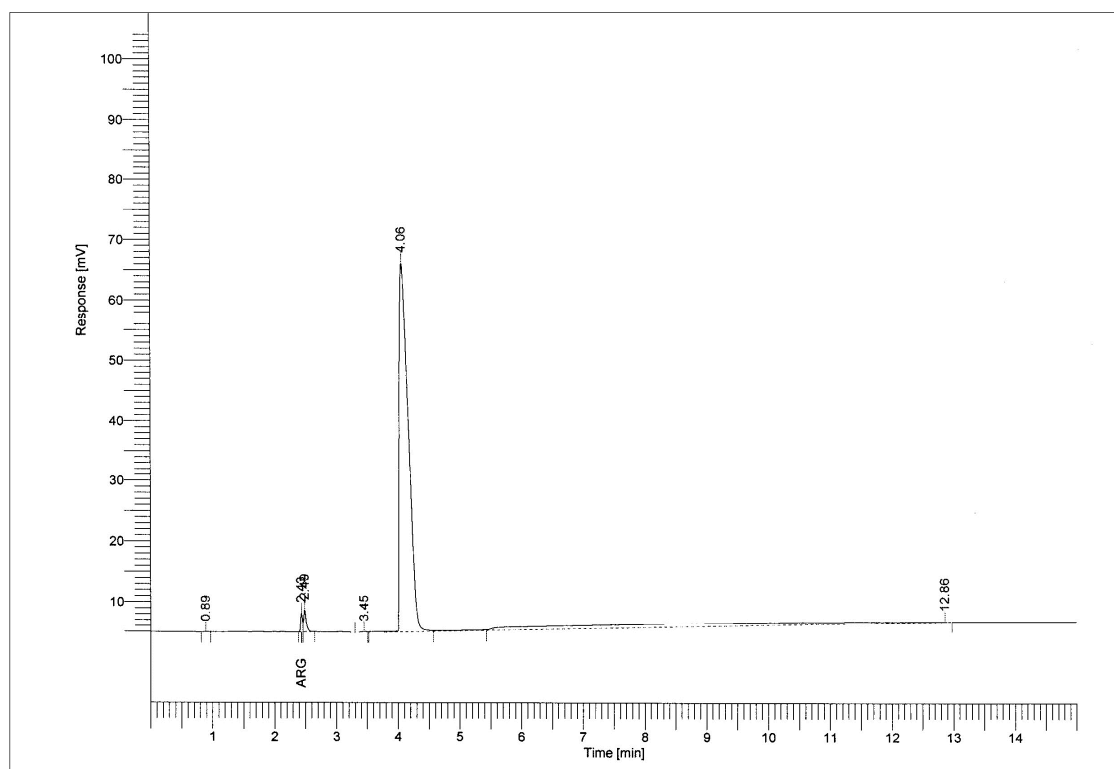


Figure 4.30: A gas chromatogram of a sample taken from the headspace of the electrolysis vessel, in which a solution of $\text{Ru}(\text{CO})_2(\text{Me}_2\text{bpy})\{\text{bpy}(\text{CH}_2\text{PO}_3\text{H}_2)_2\}$, 2 mM in CH_3CN with 0.2 M $[\text{Bu}_4\text{N}][\text{PF}_6]$, before a potential had been applied, and under a N_2 atmosphere, was present.

In order to make sure no reduction of CO₂ is occurring a two-part experiment was devised, the first part is the use of a bulk electrolysis setup in which the complex is electrolysed firstly under a N_2 and then a CO₂ atmosphere. The second half of the experiment involves the use of a gas chromatograph to identify the gases being produced. The results of the nitrogen atmosphere GC experiments are shown in Figure 4.30 and Figure 4.31. These show that there is no CO present in the headspace before

the potential has been applied, nor is there any CO when the headspace is sampled again after a potential of -2.5 V has been applied for 1 hour. This is as expected as there was no source of CO_2 for the complex to reduce to CO.

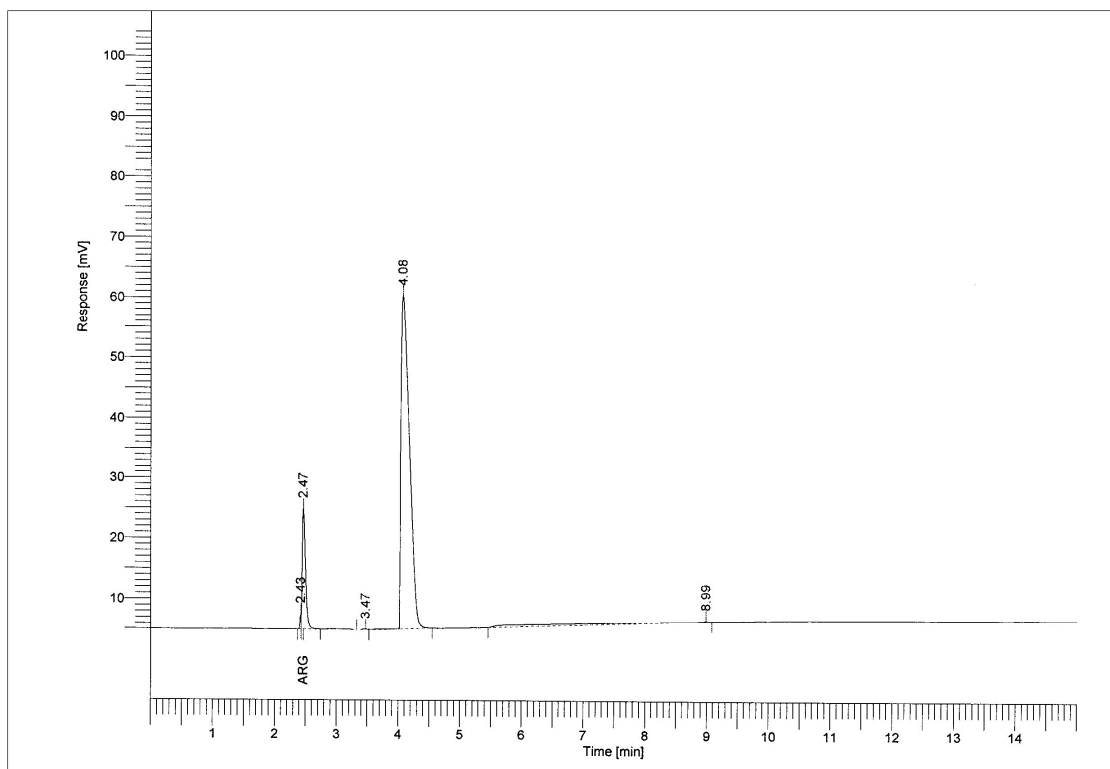


Figure 4.31: A gas chromatogram of a sample taken from the headspace of the electrolysis vessel, in which a solution of $\text{Ru}(\text{CO})_2(\text{Me}_2\text{bpy})\{\text{bpy}(\text{CH}_2\text{PO}_3\text{H}_2)_2\}$, 2 mM in CH_3CN with 0.2 M $[\text{Bu}_4\text{N}][\text{PF}_6]$, after a potential of -2.5 V had been applied for 1 hour, and under a N_2 atmosphere, was present.

Figure 4.32 and Figure 4.33 are the results from the experiment when there was a CO_2 atmosphere present. These show that both before and after a potential has been applied there is no detectable amount of CO present in the headspace. This was somewhat expected given the results from Figure 4.29 which showed no increase in current when CO_2 was present, although it was disappointing nevertheless.

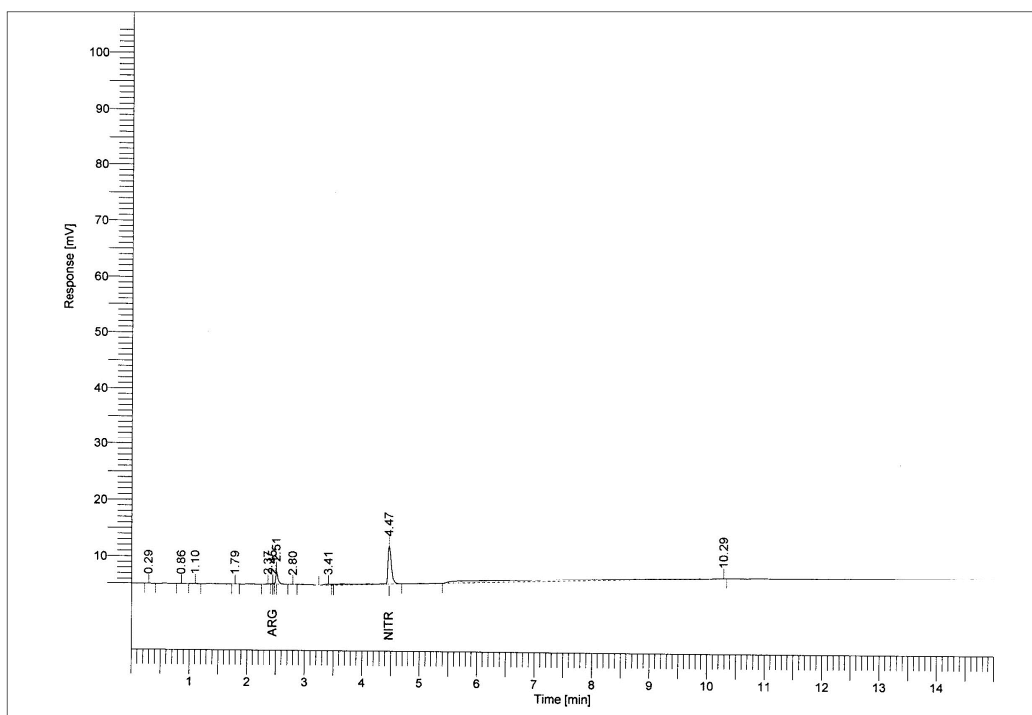


Figure 4.32: A gas chromatogram of a sample taken from the headspace of the electrolysis vessel, in which a solution of $\text{Ru}(\text{CO})_2(\text{Me}_2\text{bpy})\{\text{bpy}(\text{CH}_2\text{PO}_3\text{H}_2)_2\}$, 2 mM in CH_3CN with 0.2 M $[\text{Bu}_4\text{N}][\text{PF}_6]$, before a potential had been applied, and under a CO_2 atmosphere, was present.

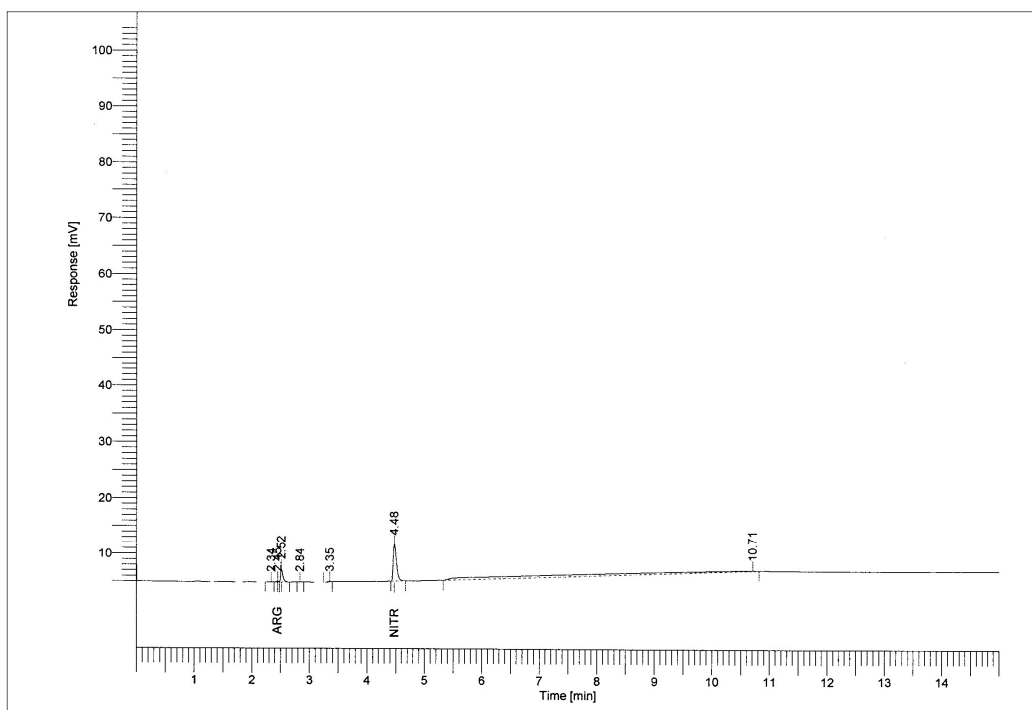


Figure 4.33: A gas chromatogram of a sample taken from the headspace of the electrolysis vessel, in which a solution of $\text{Ru}(\text{CO})_2(\text{Me}_2\text{bpy})\{\text{bpy}(\text{CH}_2\text{PO}_3\text{H}_2)_2\}$, 2 mM in CH_3CN with 0.2 M $[\text{Bu}_4\text{N}][\text{PF}_6]$, after a potential of -2.5 V had been applied for 1 hour, and under a CO_2 atmosphere, was present.

4.8.5. Summary

The overall summary for these phosphonate containing class of ruthenium compounds is that a successful electrocatalyst has not been synthesised. From a synthetic point of view, the desired complexes were made, although the synthesis does require a multistep process in which the complex has to be assembled one ligand at a time. The results on attempted electrocatalysis using the ester- and acid derivatives, $\text{Ru}(\text{CO})_2(\text{Me}_2\text{bpy})\{\text{bpy}(\text{CH}_2\text{PO}_3\text{Et}_2)_2\}$ and $\text{Ru}(\text{CO})_2(\text{Me}_2\text{bpy})\{\text{bpy}(\text{CH}_2\text{PO}_3\text{H}_2)_2\}$, indicate no electrocatalytic reduction of CO_2 to CO . The UV-Vis spectrum of the ester derivative suggests that as the MLCT band was at 420 nm then the complex may not have the desired reduction potentials for CO_2 reduction. However, the cyclic voltammetry results showed a small increase in current when a solution of the complex was saturated with CO_2 . Work therefore continued and the complex was hydrolysed to the acid derivative. Unfortunately, the results from the cyclic voltammetry, Figure 4.29, show that there is no increase in current when CO_2 is present in solution, nor can any CO be detected by GC experiments. On this basis, the complex does not pass the objective of reducing CO_2 to CO . It was therefore concluded to move towards the more promising rhenium based systems.

4.9. Consideration of Random and Systematic Errors

In the above sections, 4.8.1–5, the photophysical and electrochemical data was discussed. The values obtained from these experiments could potentially be affected by random or systematic error. During the determination of the photophysical properties, it is likely that random errors have occurred during measurement collection in addition to those present during sample preparation. The balance is capable of weighing to ± 0.0001 g and has an enclosed case to reduced atmospheric pressure fluctuations. Vibrations are dampened by the presence of shock absorbers, further reducing random errors. This will result in minimal random errors associated with any mass values. Systematic error should also be minimal due to taring of the balance before each use. The error for the volume of a solution used is likely to be negligible due to the use of microlitre syringes for extinction coefficient determination, assuming proper calibration. Random errors caused by the instruments themselves are unlikely to be of concern as they are capable

of measuring to 3 – 4 decimal places, thus our values will have more error due to simple rounding than because of random error. This is not true however for the potential systematic error for which great care must be taken to properly zero the instruments and subsequently perform suitable background scans to subtract from the actual scans. This removes both the sample cuvette and the solvent signals allowing for measurement of the actual sample.

For the electrochemical experiments, random error will be included in the concentration of the electrolyte and the mass of the complex used through use of the balance and measurement glassware. Systematic error will also occur with use of the glassware due to imperfections in its construction, however this is usually only around ± 0.1 mL for a 25 mL measuring cylinder. As stated above errors arising from mass determinations should be negligible. There will also be an associated random and systematic error with the potentiostat. The potential is calculated relative to a reference electrode and could be subject to systematic error; however, this will then be significantly reduced by using an additional reference, ferrocene. The potentiostat is capable of measuring current at the nano amp scale whilst all of our measurements are on the micro amp scale, this would suggest that any error is going to be orders of magnitude less than our measurements.

The gas chromatography experiments will be subject to random error, however given the apparent sensitivity of the detector these errors should be negligible compared to rounding errors. Systematic error due to there being an offset from zero present is potentially of greater concern for these experiments. The offset can be positive or negative resulting in more or less gas being recorded than was actually present. However after numerous experiments were performed whilst testing the CO₂ reduction properties of the complexes mentioned in this chapter and others, it would appear that any offset is usually negligible when compared to the size of signal being detected.

Taking into account all of these sources of error and their potential size it is unlikely that they will have any significant impact on our results or conclusions. Therefore, repeat readings were often not necessary hence; no statistical analysis could be performed.

4.10. References

1. A. J. Morris, G. J. Meyer and E. Fujita, *Acc. Chem. Res.*, 2009, **42**, 1983–1994.
2. K. A. Kumar, K. L. Reddy, S. Vidhisha and S. Satyanarayana, *Appl. Organomet. Chem.*, 2009, **23**, 409–420.
3. H. Takeda and O. Ishitani, *Coord. Chem. Rev.*, 2010, **254**, 346–354.
4. A. Inagakia and M. Akita, *Coord. Chem. Rev.*, 2010, **254**, 1220–1239.
5. M. D. Doherty, D. C. Grills, J. T. Muckerman, D. E. Polyansky and E. Fujita, *Coord. Chem. Rev.*, 2010, **254**, 2472–2482.
6. K. Rangan, S. M. Arachchige, J. R. Brown and K. J. Brewer, *Energy Environ. Sci.*, 2009, **2**, 410–419.
7. S. Losse, H. Görls, R. Groarke, J. G. Vos and S. Rau, *Eur. J. Inorg. Chem.*, 2008, 4448–4452.
8. H. Ishida, T. Terada, K. Tanaka and T. Tanaka, *Inorg. Chem.*, 1990, **29**, 905–911.
9. M.-N. Collomb-Dunand-Sauther, A. Deronzier and R. Ziessel, *Inorg. Chem.*, 1994, **33**, 2961–2967.
10. S. Chardon-Noblat, M.-N. Collomb-Dunand-Sauthier, A. Deronzier, R. Ziessel and D. Zsoldos, *Inorg. Chem.*, 1994, **33**, 4410–4412.
11. P. A. Anderson, G. B. Deacon, K. H. Haarmann, F. R. Keene, T. J. Meyer, D. A. Reitsma, B. W. Skelton, G. F. Strouse, N. C. Thomas, J. A. Treadway and A. H. White, *Inorg. Chem.*, 1995, **34**, 6145–6157.
12. B. Gholamkhash, H. Mametsuka, K. Koike, T. Tanabe, M. Furue and O. Ishitani, *Inorg. Chem.*, 2005, **44**, 2326–2336.
13. J. Hawecker, J.-M. Lehn and R. Ziessel, *J. Chem. Soc., Chem. Commun.*, 1983, 536–538.
14. H. Ishida, H. Tanaka, K. Tanaka and T. Tanaka, *J. Chem. Soc., Chem. Commun.*, 1987, 131–132.
15. H. Ohtsu, K. Tsuge and K. Tanaka, *J. Photochem. Photobiol., A*, 2015, **313**, 163–167.
16. K. Kobayashi, T. Kikuchi, S. Kitagawa and K. Tanaka, *Angew. Chem. Int. Ed.*, 2014, **53**, 11813–11817.
17. M. Orlandi, R. Argazzi, A. Sartorel, M. Carraro, G. Scorrano, M. Bonchio and F. Scandola, *Chem. Commun.*, 2010, **46**, 3152–3154.
18. T. M. Suzuki, H. Tanaka, T. Morikawa, M. Iwaki, S. Sato, S. Saeki, M. Inoue, T. Kajino and T. Motohiro, *Chem. Commun.*, 2011, **47**, 8673–8675.
19. S. Ardo and G. J. Meyer, *Chem. Soc. Rev.*, 2009, **38**, 115–164.
20. C. D. Windle and R. N. Perutz, *Coord. Chem. Rev.*, 2012, **256**, 2562–2570.
21. I. Gillaizeau-Gauthier, F. Odobel, M. Alebbi, R. Argazzi, E. Costa, C. A. Bignozzi, P. Qu and G. J. Meyer, *Inorg. Chem.*, 2001, **40**, 6073–6079.

22. C. She, J. Guo, S. Irle, K. Morokuma, D. L. Mohler, H. Zabri, F. Odobel, K.-T. Youm, F. Liu, J. T. Hupp and T. Lian, *J. Phys. Chem. A*, 2007, **111**, 6832–6842.
23. K. Maeda, R. Kuriki, M. Zhang, X. Wang and O. Ishitani, *J. Mater. Chem. A*, 2014, **2**, 15146–15151.
24. S. Sato, T. Morikawa, S. Saeki, T. Kajino and T. Motohiro, *Angew. Chem. Int. Ed.*, 2010, **49**, 5101–5105.
25. X.-H. Wu, S. Wang, Y. Guo, Z.-Y. Xie, L. Han and Z.-H. Jiang, *Chin. J. Chem.*, 2008, **26**, 1939–1943.
26. E. Fujita, *Coord. Chem. Rev.*, 1999, **185–186**, 373–384.
27. A. C. Lees, B. Evrard, T. E. Keyes, J. G. Vos, C. J. Kleverlaan, M. Alebbi and C. A. Bignozzi, *Eur. J. Inorg. Chem.*, 1999, 2309–2317.
28. G. Wolfbauer, A. M. Bond and D. R. MacFarlane, *Inorg. Chem.*, 1999, **38**, 3836–3846.
29. M. K. Nazeeruddin, S. M. Zakeeruddin, R. Humphry-Baker, M. Jirousek, P. Liska, N. Vlachopoulos, V. Shklover, C.-H. Fischer and M. Grätzel, *Inorg. Chem.*, 1999, **38**, 6298–6305.
30. R. Ghanem, Y. Xu, J. Pan, T. Hoffmann, J. Andersson, T. Polívka, T. Pascher, S. Styring, L. Sun and V. Sundström, *Inorg. Chem.*, 2002, **41**, 6258–6266.
31. M. Zhou, G. P. Robertson and J. Roovers, *Inorg. Chem.*, 2005, **44**, 8317–8325.
32. A. Grabulosa, M. Beley, P. C. Gros, S. Cazzanti, S. Caramori and C. A. Bignozzi, *Inorg. Chem.*, 2009, **48**, 8030–8036.
33. P. G. Bomben, K. C. D. Robson, P. A. Sedach and C. P. Berlinguette, *Inorg. Chem.*, 2009, **48**, 9631–9643.
34. S. Kämper, A. Paretzki, J. Fiedler, S. Zálíš and W. Kaim, *Inorg. Chem.*, 2012, **51**, 2097–2104.
35. E. Eskelinen, S. Luukkanen, M. Haukka, M. Ahlgrén and T. A. Pakkanen, *J. Chem. Soc., Dalton Trans.*, 2000, 2745–2752.
36. R. J. Ellingson, J. B. Asbury, S. Ferrere, H. N. Ghosh, J. R. Sprague, T. Lian and A. J. Nozik, *J. Phys. Chem. B*, 1998, **102**, 6455–6458.
37. K. Kilså, E. I. Mayo, B. S. Brunshwig, H. B. Gray, N. S. Lewis and J. R. Winkler, *J. Phys. Chem. B*, 2004, **108**, 15640–15651.
38. J. J. Concepcion, J. W. Jurss, M. K. Brennaman, P. G. Hoertz, A. O. T. Patrocínio, N. Y. M. Iha, J. L. Templeton and T. J. Meyer, *Acc. Chem. Res.*, 2009, **42**, 1954–1965.
39. W. J. Youngblood, S.-H. A. Lee, K. Maeda and T. E. Mallouk, *Acc. Chem. Res.*, 2009, **42**, 1966–1973.
40. M. Montalti, S. Wadhwa, W. Y. Kim, R. A. Kipp and R. H. Schmehl, *Inorg. Chem.*, 2000, **39**, 76–84.
41. H. Zabri, I. Gillaizeau, C. A. Bignozzi, S. Caramori, M.-F. Charlot, J. Cano-Boquera and F. Odobel, *Inorg. Chem.*, 2003, **42**, 6655–6666.

42. V. Penicaud, F. Odobel and B. Bujoli, *Tetrahedron Lett.*, 1998, **39**, 3689–3692.
43. F. Yoshitomi, K. Sekizawa, K. Maeda and O. Ishitani, *ACS Appl. Mater. Interfaces*, 2015, **7**, 13092–13097.
44. K. Maeda, K. Sekizawa and O. Ishitani, *Chem. Commun.*, 2013, **49**, 10127–10129.
45. M. R. Norris, J. J. Concepcion, C. R. K. Glasson, Z. Fang, A. M. Lapides, D. L. Ashford, J. L. Templeton and T. J. Meyer, *Inorg. Chem.*, 2013, **52**, 12492–12501.
46. K.-i. Yamanaka, S. Sato, M. Iwaki, T. Kajino and T. Morikawa, *J. Phys. Chem. C*, 2011, **115**, 18348–18353.
47. T. Kimura and Y. Uozumi, *Organometallics*, 2006, **25**, 4883–4887.
48. A. Miedaner, B. C. Noll and D. L. DuBois, *Organometallics*, 1997, **16**, 5779–5791.
49. J. W. Raebiger, J. W. Turner, B. C. Noll, C. J. Curtis, A. Miedaner, B. Cox and D. L. DuBois, *Organometallics*, 2006, **25**, 3345–3351.
50. T.-J. J. Kinnunen, M. Haukka, M. Nousiainen, A. Patrikka and T. A. Pakkanen, *J. Chem. Soc., Dalton Trans.*, 2001, 2649–2654.
51. E. Eskelinen, M. Haukka, T.-J. J. Kinnunen and T. A. Pakkanen, *J. Electroanal. Chem.*, 2003, **556**, 103–108.
52. S. Lense, K. I. Hardcastle and C. E. MacBeth, *J. Chem. Soc., Dalton Trans.*, 2009, 7396–7401.
53. Z.-Y. Bian, S.-M. Chi, L. Li and W. Fu, *J. Chem. Soc., Dalton Trans.*, 2010, **39**, 7884–7887.
54. K. Koike, S. Naito, S. Sato, Y. Tamaki and O. Ishitani, *J. Photochem. Photobiol., A*, 2009, **207**, 109–114.
55. M. K. Nazeeruddin and M. Grätzel, in *Inorganic Syntheses*, ed. D. Coucouvanis, John Wiley & Sons, Inc., 2002, vol. 33, pp. 185–189.
56. D. Mulhern, S. Brooker, H. Görls, S. Rau and J. G. Vos, *J. Chem. Soc., Dalton Trans.*, 2006, 51–57.
57. D. S. C. Black, G. B. Deacon and N. C. Thomas, *Aust. J. Chem.*, 1982, **35**, 2445–2453.
58. M. Pikulski, J. J. Wilson, A. Aguilar and J. S. Brodbelt, *Anal. Chem.*, 2006, **78**, 8512–8517.

5. Rhenium Complexes Containing Bipyridine Ligands as Potential Catalysts for CO₂ Reduction

5.1. Introduction

In this chapter, work on a new series of compounds in which rhenium is used instead of ruthenium for the purpose of catalytic CO₂ reduction is shown. Rhenium catalysts for CO₂ reduction have been known for many years.¹⁻⁸ However, in order to increase selectivity, stability and of course catalytic activity, along with a reduction in the catalyst's costs, improvements to the existing systems and development of new classes of catalysts need to be made. As seen in chapter 4 the literature can be divided into two groups; complexes without anchoring groups^{4, 8-19} and complexes containing anchoring groups^{5, 20, 21} allowing for attachment to a semiconductor. The anchoring group used is usually a carboxylate^{5, 22-24} or a phosphonate.^{20, 22-27}

The systems we have decided to modify are rhenium tricarbonyl chloride diimine complexes and we have focused on phosphonic acid as an anchoring group. The phosphonate group is an alternative to the better studied carboxylic acid containing anchor ligands. They have different affinities to various semiconductors, and for instance are known to have faster rates of electron injection than carboxylates to TiO₂.²²

The aims of this chapter are the same as chapter 3 and 4 but focusing on the rhenium containing complexes mentioned in the primary thesis aims;

- (i) To identify and reproduce known synthetic routes to obtain complexes for homogeneous electrocatalysis.
- (ii) To modify the ligands to include an anchoring group and enable attachment to a light harvesting semiconductor.
- (iii) To test the new complexes bearing anchoring groups to determine if their CO₂ reduction abilities were retained upon ligand modification, or, ideally, enhanced.
- (iv) If the results from step 3 are positive, anchoring on the semiconductors and the building a heterogeneous system will be carried out with assistance from our collaborators.

The work contained in this chapter has been the most successful and significant progress has been made towards our overall goal. The chapter has therefore been broken down into several parts, each part corresponding to a separate aim of the thesis (iii – v). The first part details the work on the ester containing rhenium complex (aim iii), its synthesis, results and discussion and a summary. The second part discusses the work on the hydrolysis product (aim iv), its synthesis, results and discussion and a summary. The last part presents the results and discussion and a final summary for the comparisons made between several rhenium complex analogues (aim iv and v).

5.1.1. System Design

The purpose of this work was to start from reproducing the work of Lehn et al.¹⁻³ and then improve and expand upon the work by modifying the compound to contain an anchoring group to enable the attachment of a semiconductor. Lehn's catalyst can be seen in Figure 5.1 when X = H. As mentioned in chapter 4 there are several considerations to take into account when choosing a suitable catalyst;

The complex needs to be able to catalytically reduce CO₂ to a reduction product. This requires a source of electrons and the ability to store and subsequently use these electrons in the reduction process. In a homogeneous system the electrons will most likely be provided by an electrical current. In a heterogeneous system the electrons will be provided by the semiconductor upon absorption of light, i.e. a photocurrent. The reduction product for Lehn's catalyst is CO, one of the reduction products requiring 2 electrons, the other being HC(O)OH.

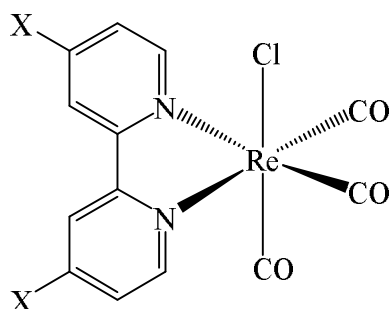


Figure 5.1: A generic representation of the rhenium complex containing one diimine ligand. X can be any substituent e.g. H, Me or ^tbutyl. Lehn's catalyst is when X = H.¹

Another criterion was the presence of a reaction site for the conversion of CO₂ into the reaction product. For these complexes, it is believed to be the Cl ligand.

Figure 5.2 shows the process that occurs during the 2-electron reduction during which the chloride ligand is removed and a 5-coordinate anion is produced. It is this anion that is believed to be the catalytically active species.¹⁶

The presence of the CO ligands is thought to be beneficial; they act as good IR reporters often allowing quick and easy access to structural information of the complex due to how many bands are present in the IR spectrum. Another advantage is their ability for back bonding from the metal centre ($d\pi \rightarrow \pi^*$). This allows the metal to transfer electron density to the CO ligand helping to stabilise the complex when receiving electrons from the semiconductor.

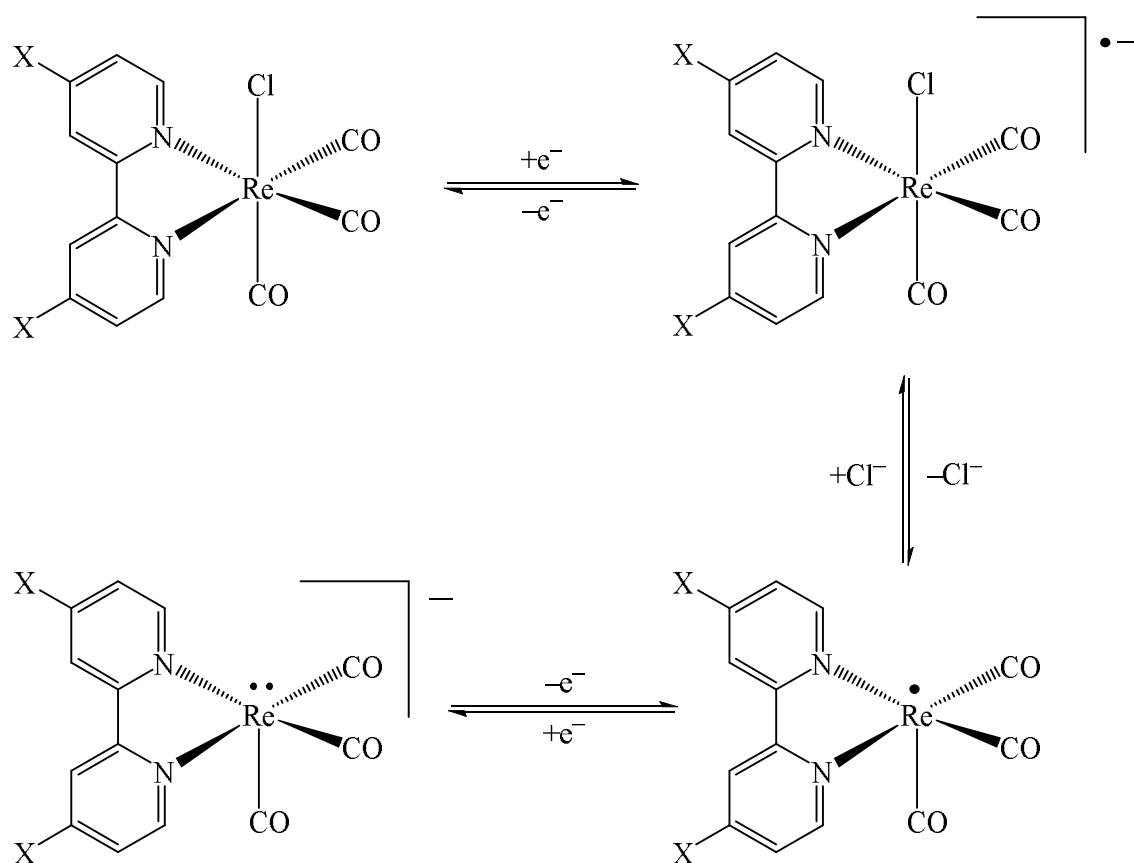


Figure 5.2: The first reduction of the initial species to the radical anion. A ligand to metal charge transfer then occurs resulting in the loss of the chloride. A second reduction to a 5 coordinate anion occurs resulting in the catalytically active species.¹⁶

A final criterion was the ability to add an anchoring group to the ligand of the complex. This will allow attachment to a light harvesting semiconductor that will provide the electrons used in the reduction process, eliminating the need for electrical current and replacing it with photocurrent.

After considering these criteria, it is clear that Lehn's catalyst is a good foundation from which to build and improve upon. Using the lessons learnt in chapter 4 it was decided to add a $-\text{CH}_2-$ spacer between the anchoring group and the ligand in these rhenium complexes.²⁸⁻³⁰

Figure 5.3 shows the desired compound, which incorporates all of the criteria that have been discussed.

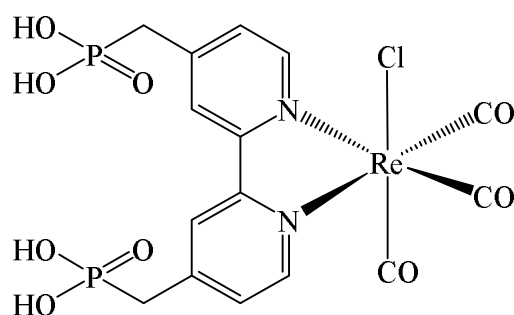


Figure 5.3: The desired rhenium complex containing the phosphonate anchoring group connected to the diimine with a $-\text{CH}_2-$ spacer.

5.2. Synthesis and Characterisation of $\text{Re}(\text{CO})_3\text{Cl}\{\text{bpy}(\text{CH}_2\text{PO}_3\text{Et}_2)_2\}$

5.2.1. Synthetic Method

Section 5.1.1 provided information as to why certain components were chosen when designing the system, this section gives brief information as to how the ligands were synthesised and then complexed to the metal. The synthesis of the ligand was performed by Dr Stuart Archer using the method described in a paper by G. J. Meyer et al.³¹ This was a five step process starting from the dimethyl bipyridine, converting it to the acid, then the ester, then an alkyl alcohol, then an alkyl halide and finally to the phosphonate. The synthesis is shown in

Figure 5.4. The complexation was then achieved by refluxing the ligand and rhenium pentacarbonyl in toluene overnight. The product was obtained by use of a counter solvent to precipitate the product.

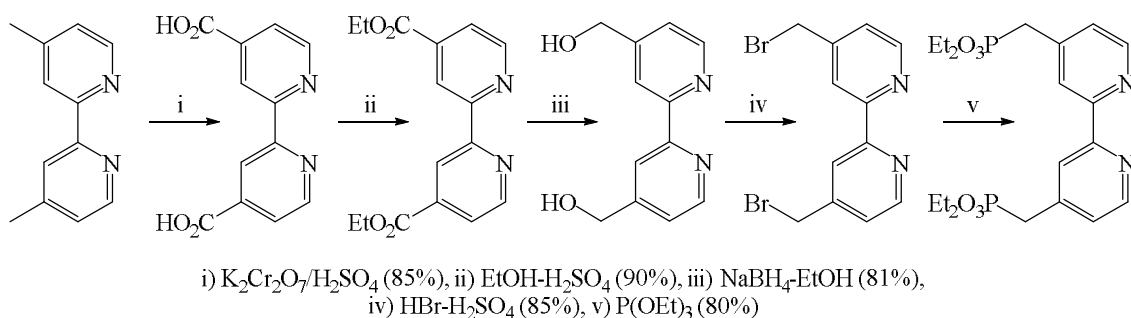


Figure 5.4: Reaction scheme showing the reagents and conditions required for the formation of 4,4'-bis(diethylmethylphosphonate)-2,2'-bipyridine.

5.2.2. Synthesis of $\text{Re}(\text{CO})_3\text{Cl}\{\text{bpy}(\text{CH}_2\text{PO}_3\text{Et}_2)\}$

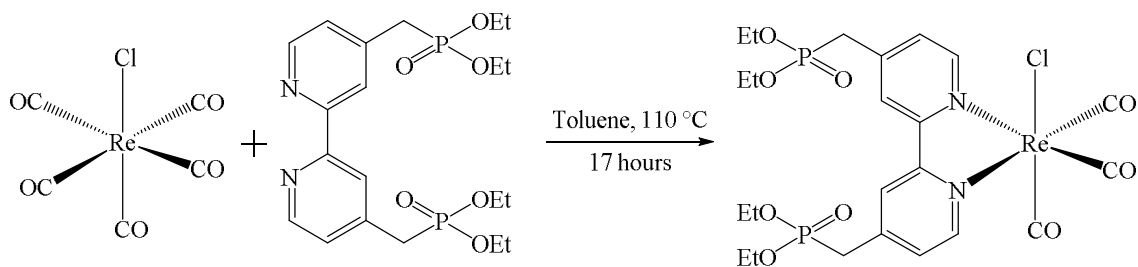


Figure 5.5: Reaction scheme showing the reagents and conditions required for the formation of tricarbonyl-chloro-4,4'-bis(diethylmethylphosphonate)-2,2'-bipyridine rhenium(I).

General method: $\text{Re}(\text{CO})_5\text{Cl}$ (0.1598 g, 0.442 mmol) and $\text{bpy}(\text{CH}_2\text{PO}_3\text{Et}_2)_2$ (0.2239 g, 0.491 mmol) were degassed 3 times with argon before toluene (deaerated, 30 mL) was added via syringe. Solution was heated to 110 °C and stirred for 16 hours. A colour change from colourless to yellow to orange was observed. The solution was cooled to room temperature resulting in the solution changing back to a yellow colour. Diethyl ether (200 mL) was added to induce precipitation. The solids were collected on a sinter. Yield = 0.29 g, 88%. ^1H NMR (400 MHz, $\text{DMSO}-d_6$) δ 8.96 (d, $J = 5.7$ Hz, 2H), 8.55 (s, 2H), 7.66 (dd, $J = 3.8, 1.9$ Hz, 2H), 4.10 – 3.98 (m, 8H), 3.65 (s, 2H), 3.59 (s, 2H), 1.20 (td, $J = 7.0, 1.0$ Hz, 12H). ^{31}P NMR (101 MHz, $\text{DMSO}-d_6$) δ 23.42. MALDI MS: m/z 762 (M^+)

Synthetic comments: The synthesis of this complex was straightforward due to the solubility of the reagents, the product was precipitated using a counter solvent and no

further purification was required. The purity was confirmed by ^1H and ^{31}P NMR spectra, and was perceived sufficient for future studies.

5.3. Results and Discussion of $\text{Re}(\text{CO})_3\text{Cl}\{\text{bpy}(\text{CH}_2\text{PO}_3\text{Et}_2)_2\}$

5.3.1. Photophysical Data for $\text{Re}(\text{CO})_3\text{Cl}\{\text{bpy}(\text{CH}_2\text{PO}_3\text{Et}_2)_2\}$

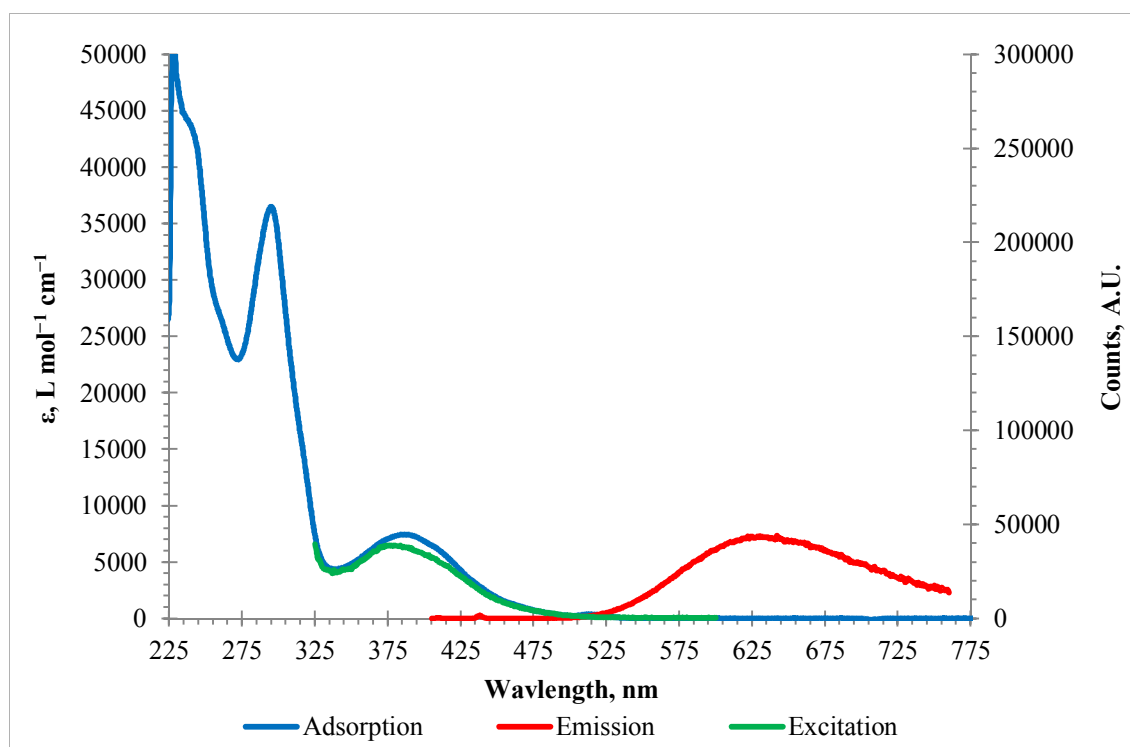


Figure 5.6: The UV-Vis, emission and excitation spectra of $\text{Re}(\text{CO})_3\text{Cl}\{\text{bpy}(\text{CH}_2\text{PO}_3\text{Et}_2)_2\}$ in DCM, normalised. The excitation spectra were registered at 631 nm; the emission spectra were obtained under 387 nm excitation.

Figure 5.6 shows the UV-Vis spectrum in blue with the MLCT band at 387 nm, and then two $\pi \rightarrow \pi^*$ bands at 242 and 229 nm. The red line is the emission profile, which has been scaled to match the MLCT band. This has its maximum at 631 nm. The green line is the excitation spectrum, as is shown it matches the UV-Vis spectrum indicating that the emission seen is from the complex and not from a trace impurity. The excitation spectrum was also scaled to match the UV-Vis spectrum.

As with other rhenium(I) complexes, $\text{Re}(\text{CO})_3\text{Cl}\{\text{bpy}(\text{CH}_2\text{PO}_3\text{Et}_2)_2\}$ is expected to emit in solution at r.t. from an excited state of largely $^3\text{MLCT}$ origin. It is interesting to

see whether replacing of the carboxylate with the phosphonate in this class of complexes changes the photophysics (lifetime, energy of the lowest excited state) in any notable way. Figure 5.6 shows that the complex does emit in solution at r.t., with the emission maximum at 631 nm. This is similar to $\text{Re}(\text{CO})_3\text{Cl}\{\text{bpy}(\text{COOEt})_2\}$, the closest carboxylate analogue in the literature, which has an emission maximum of 600 nm.

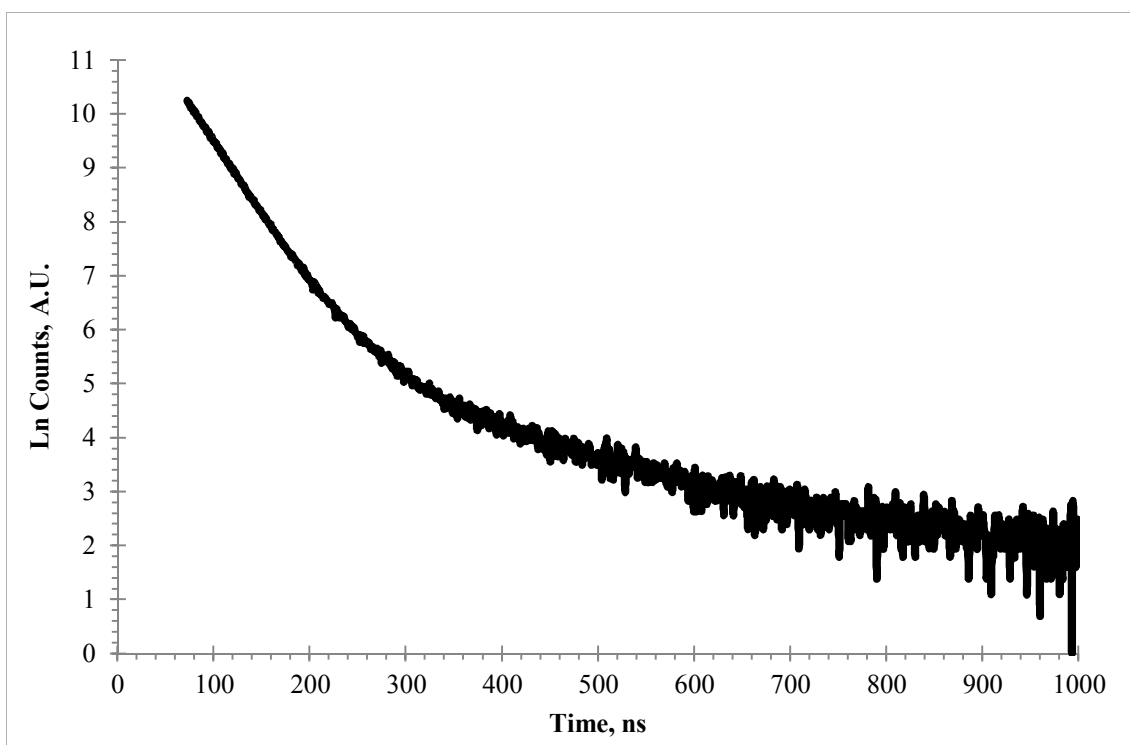


Figure 5.7: Lifetime trace of $\text{Re}(\text{CO})_3\text{Cl}\{\text{bpy}(\text{CH}_2\text{PO}_3\text{Et}_2)_2\}$, in DCM, recorded in the spectral range 575 – 625 nm, 1 μs timescale, excitation with ca. 75 ps, 405 nm laser pulse.

Figure 5.7 shows the emission lifetime data for $\text{Re}(\text{CO})_3\text{Cl}\{\text{bpy}(\text{CH}_2\text{PO}_3\text{Et}_2)_2\}$ in DCM. This was obtained using the mini- τ instrument with a 1 μs delay between pulses and a bandpass filter of 575 – 625 nm. The data was fitted using a 2-component exponential, which provided lifetime values of 36 ± 4 ns and 155 ± 16 ns of which the first component represents 99.6% of the relative contribution. This first component compares well with the literature values for $\text{Re}(\text{CO})_3\text{Cl}(\text{bpy})$ and $\text{Re}(\text{CO})_3\text{Cl}(\text{Me}_2\text{bpy})$ which are, 39 ± 4 ns and 49 ± 5 ns respectively.³² This suggests that it is actually a single decay process occurring from the $^3\text{MLCT}$ to the ground state.

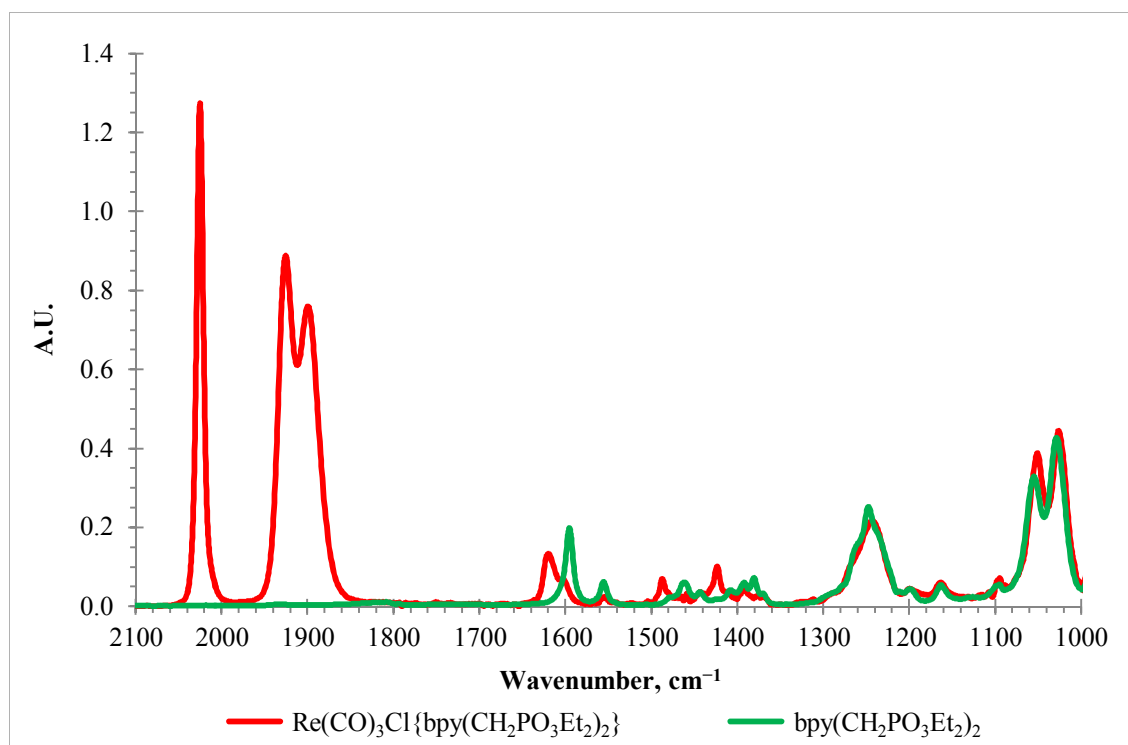


Figure 5.8: Comparison of IR spectra of $\text{Re}(\text{CO})_3\text{Cl}\{\text{bpy}(\text{CH}_2\text{PO}_3\text{Et}_2)_2\}$ and $\text{bpy}(\text{CH}_2\text{PO}_3\text{Et}_2)_2$ in CDCl_3 .

Figure 5.8 shows the solution state IR spectra of $\text{Re}(\text{CO})_3\text{Cl}\{\text{bpy}(\text{CH}_2\text{PO}_3\text{Et}_2)_2\}$ and the free ligand $\text{bpy}(\text{CH}_2\text{PO}_3\text{Et}_2)_2$ in CDCl_3 . The spectra were taken in CDCl_3 instead of CHCl_3 because CHCl_3 has a large absorbance at 1200 cm^{-1} which is where the P=O stretching vibration occurs. The spectra have been scaled to show a clear comparison. The spectrum of the complex shows the intra-ligand vibrations are mainly unaffected due to coordination to the metal centre. However, the IR spectrum of the complex has three additional bands present in the high frequency region due to CO-groups. The trans-CO (a)symmetric stretch is at 2025 cm^{-1} , whilst the two bands attributed to the cis-CO symmetric and asymmetric stretches are at 1926 and 1900 cm^{-1} . Additionally, the Re–N and Re–C stretching vibrations are expected in the low frequency region, $< 500\text{ cm}^{-1}$; however, this region was not investigated in detail.

Table 5.1: IR spectrum data for $\text{Re}(\text{CO})_3\text{Cl}\{\text{bpy}(\text{CH}_2\text{PO}_3\text{Et}_2)_2\}$ and $\text{bpy}(\text{CH}_2\text{PO}_3\text{Et}_2)_2$ in CDCl_3 .

Compound	Frequency, cm^{-1}	Stretching vibration
bpy(CH ₂ PO ₃ Et ₂) ₂	1029	C–H
	1055	C–H
	1248	P=O
	1595	Aromatic C=C
Re(CO) ₃ Cl{bpy(CH ₂ PO ₃ Et ₂) ₂ }	1027	C–H
	1051	C–H
	1243	P=O
	1620	Aromatic C=C
	1900	cis-CO symmetric
	1926	cis-CO symmetric
	2025	trans-CO (a)symmetric

5.3.2. Electrochemical Data for Re(CO)₃Cl{bpy(CH₂PO₃Et₂)₂}

Tests for electrocatalytic activity of all new complexes have been performed following a standard protocol:

- (i) Cyclic voltammetry of 2 mM solution saturated with N₂.
- (ii) Cyclic voltammetry of the same solution saturated with CO₂.
- (iii) Cyclic voltammetry of the same solution re-saturated with N₂.

In all cases, control experiments included background scans (electrolyte only, no rhenium complexes) under N₂ and CO₂, although these are not always shown in the figures below. All potentials were measured vs. Ag/AgCl⁺ and reported vs. Fc/Fc⁺.

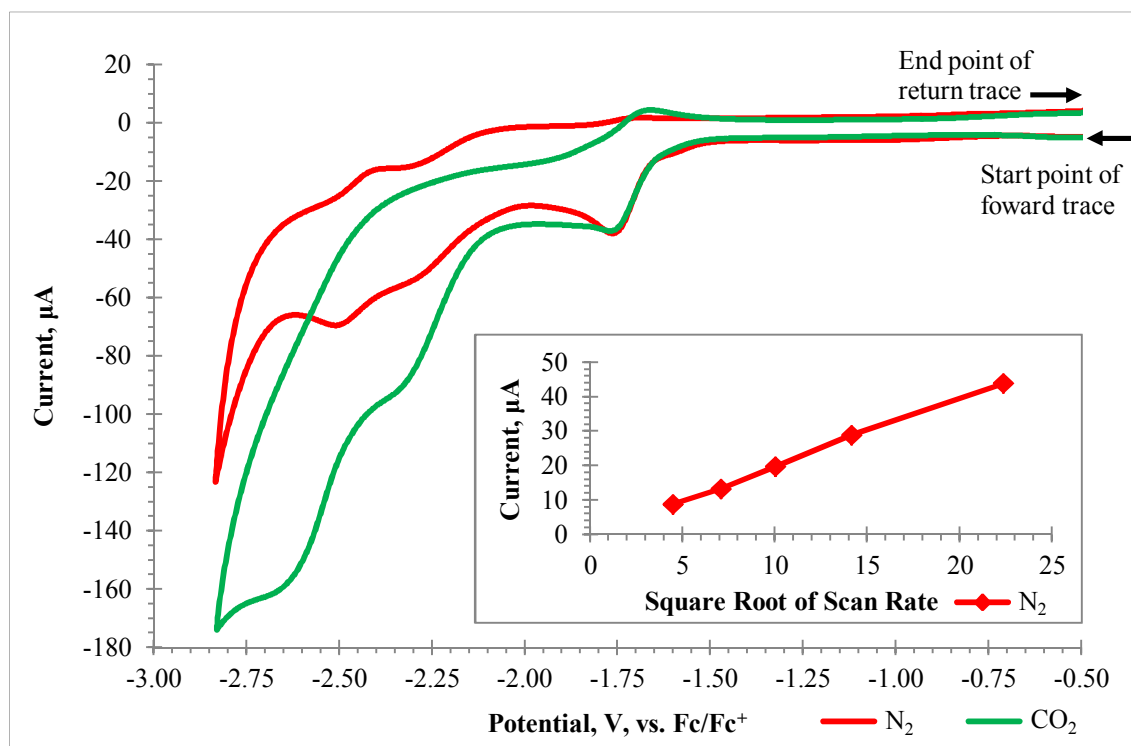


Figure 5.9: Cyclic voltammograms for $\text{Re}(\text{CO})_3\text{Cl}\{\text{bpy}(\text{CH}_2\text{PO}_3\text{Et}_2)_2\}$, 2 mM in CH_3CN with 0.2 M $[\text{Bu}_4\text{N}][\text{PF}_6]$, recorded at 100 mVs^{-1} , in the presence of N_2 or CO_2 , the potentials reported vs. Fc/Fc^+ . The arrows show the start or end point and the direction of potential change. A graph showing the linearity of the current with respect to $v^{1/2}$ is inset. Note the increase in current in the presence of CO_2 .

Figure 5.9 shows the results from the cyclic voltammetry experiment in which $\text{Re}(\text{CO})_3\text{Cl}\{\text{bpy}(\text{CH}_2\text{PO}_3\text{Et}_2)_2\}$ was used in both a nitrogen saturated solution and a carbon dioxide saturated solution. Saturation was achieved by bubbling the desired gas into the solution for up to 45 minutes. Both recorded traces show a redox couple at -1.7 V . The nitrogen system has partially reversible couples at -2.2 V and -2.45 V . The CO_2 system has two irreversible couples at -2.35 V and -2.62 V . For the first couple in both systems the same amount of current is produced, however, for the other couples there is an increase in the current of $\sim 2 - 2.5$ times between the solutions saturated with CO_2 vs. nitrogen. This increase could be attributed to a catalytic current although it is unclear as to why there are two redox couples. One possible explanation is the solvent breaks down easier in the CO_2 saturated system and so we see an increase in current. Another explanation could be we are reducing the CO_2 directly i.e. $\text{CO}_2 + e^-$ to $\text{CO}_2^{\cdot-}$ due to the very negative potentials. However, since neither of those effects is observed in the

control experiments that contain solvent and electrolyte only, neither of those explanations are likely. The literature¹⁶ does not given any indication as the experiments described within do not go to as negative potentials.

The inset graph shows that when the solution is saturated with nitrogen, the 2nd reduction process is diffusion controlled and is reversible. This is governed by the Cottrell equation.³³

$$I = k(v^{1/2})$$

Where I represents the current, k is a collection of constants and v is the scan rate. The graph shows that as the scan rate increases the current increases as a linear relationship with respect to $v^{1/2}$. This means that the current is diffusion controlled, confirming that the process is reversible.

However, for the 2nd reduction couple, when the solution is saturated with CO₂, two competing processes occur. The first is the process described by the Cottrell equation i.e. as scan rate increases so does current. The second process however is that at lower scan rates higher current will be generated; this is because the compound spends longer at the catalytic potential and so more current is generated.

This can be seen in Figure 5.10, the lower scan rates are generating more current that would be expected if the process were entirely diffusion controlled. This shows that catalytic current is being produced during the experiment.

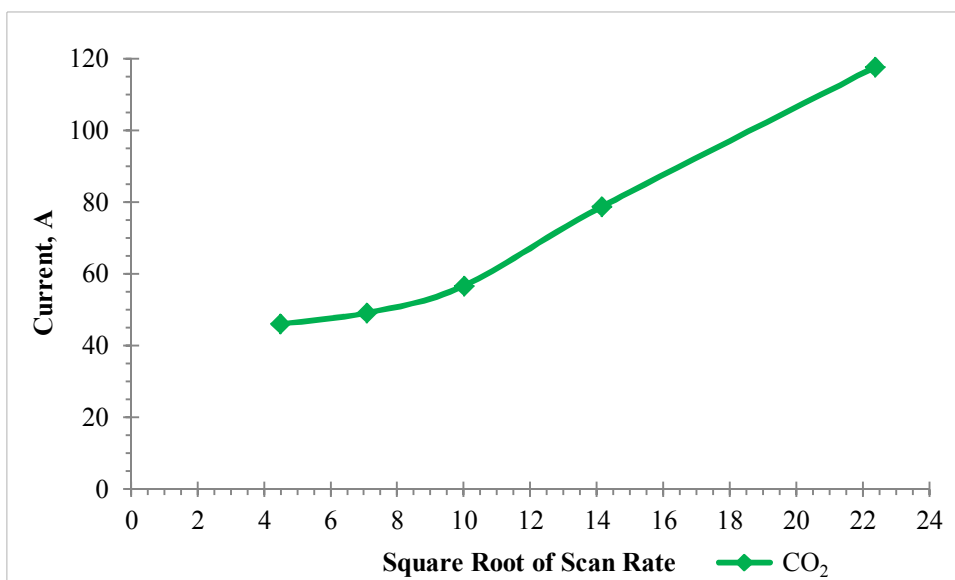


Figure 5.10: A graph showing the non-linearity of the current with respect to $v^{1/2}$ when the solution is saturated with CO_2 .

Table 5.2: Electrochemical data for $\text{Re}(\text{CO})_3\text{Cl}\{\text{bpy}(\text{CH}_2\text{PO}_3\text{Et}_2)_2\}$, reported vs. Fc/Fc^+ .

Gas present in solution	Redox process	$E_{p,a}$, V	$E_{p,c}$, V	$E^{1/2}$, V
Saturated with N_2	1 st reduction	-1.76	-1.69	-1.72
Saturated with N_2	2 nd reduction	-2.51	-2.38	-2.44
Saturated with CO_2	1 st reduction	-1.77	-1.66	-1.71
Saturated with CO_2	2 nd reduction	-2.35	No return wave observed	
Saturated with CO_2	3 rd reduction	-2.62	No return wave observed	

5.3.3. Summary

The complex has been successfully synthesised. Photophysical and electrochemical experiments have been performed. The results from these experiments are very encouraging, the electrochemical data from the cyclic voltammetry shows that catalytic current is being produced when CO_2 is present in solution. The next step is to hydrolyse the ester to the acid derivative and see if the results remain the same.

5.4. Synthesis and Characterisation of $\text{Re}(\text{CO})_3\text{Cl}\{\text{bpy}(\text{CH}_2\text{PO}_3\text{H}_2)_2\}$

5.4.1. Synthetic Method

To convert the ester product, $\text{Re}(\text{CO})_3\text{Cl}\{\text{bpy}(\text{CH}_2\text{PO}_3\text{Et}_2)_2\}$ to the acid, trimethylsilyl bromide (TMSBr) was used to hydrolyse the ester groups. The first step involved the production of a silyl ester before the hydrolysis to the acid product. Due to the presence of phosphonate groups, ^{31}P NMR was used to determine whether the hydrolysis had been successful.

5.4.2. Synthesis of $\text{Re}(\text{CO})_3\text{Cl}\{\text{bpy}(\text{CH}_2\text{PO}_3\text{H}_2)_2\}$

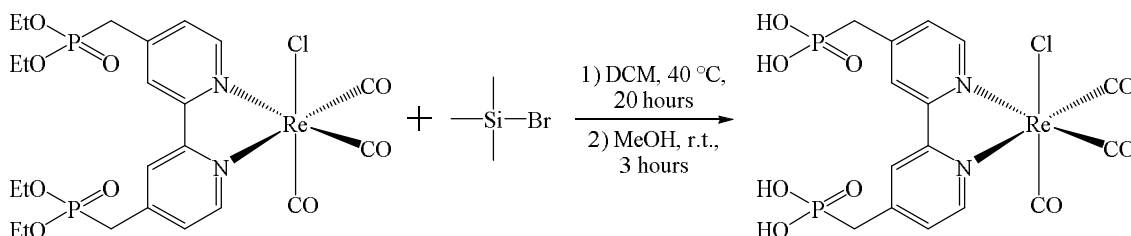


Figure 5.11: Reaction scheme showing the reagents and conditions required for the formation of tricarbonyl-chloro-4,4'-bis(methylphosphonate)-2,2'-bipyridine rhenium(I).

General method: $\text{Re}(\text{CO})_3\text{Cl}\{\text{bpy}(\text{CH}_2\text{PO}_3\text{Et}_2)_2\}$ (0.0403 g, 0.053 mmol) was degassed 3 times before being dissolved in DCM (Grubbs, 10 mL). TMSBr (0.5 mL) was added via a syringe, resulting in a colour change from yellow to orange. The solution was refluxed at 40 °C for 20 hours. Methanol (15 mL) was added via syringe, which changed the solution from orange to yellow. The solution was allowed to cool to room temperature and stirred for 3 hours. The solution was filtered using filter paper and the solvent removed on the rotary evaporator. ^1H NMR (400 MHz, DMSO-d_6) δ 8.92 (d, $J = 5.6$ Hz, 2H), 8.54 (s, 2H), 7.62 (d, $J = 5.2$ Hz, 2H), 3.34 (s, 2H), 3.28 (s, 2H). ^{31}P NMR (101 MHz, DMSO-d_6) δ 17.30 (s). Elemental Analysis; Calculated (%) of $\text{C}_{15}\text{H}_{14}\text{ClN}_2\text{O}_9\text{P}_2\text{Re}$: C, 27.72; H, 2.17; N, 4.31. Found: C, 25.25; H, 2.80; N, 5.18.

Synthetic comments: The synthesis of this reaction was reasonably simple although care was required when handling the TMSBr reagent. The ^1H and ^{31}P NMR showed that

the complex had been completely converted from the ester to acid as seen by the loss of the ester protons and the presence of only one phosphorus environment.

5.5. Results and Discussion of $\text{Re}(\text{CO})_3\text{Cl}\{\text{bpy}(\text{CH}_2\text{PO}_3\text{H}_2)_2\}$

5.5.1. Photophysical Data for $\text{Re}(\text{CO})_3\text{Cl}\{\text{bpy}(\text{CH}_2\text{PO}_3\text{H}_2)_2\}$

Figure 5.12 shows the UV-Vis spectrum in blue with the MLCT band at 371 nm, and then two $\pi \rightarrow \pi^*$ bands at 317 and 291 nm. The red line is the emission profile, which was collected under deaerated conditions. This has its maximum at 584 nm. The green line is the excitation spectrum, normalised, as is shown it matches the UV-Vis spectrum indicating that the emission seen is from the complex and not from a trace impurity. These results are analogous to those of the $\text{Re}(\text{CO})_3\text{Cl}\{\text{bpy}(\text{CH}_2\text{PO}_3\text{Et}_2)_2\}$, with only the positions of the bands changing as opposed to the spectral shape, as seen in

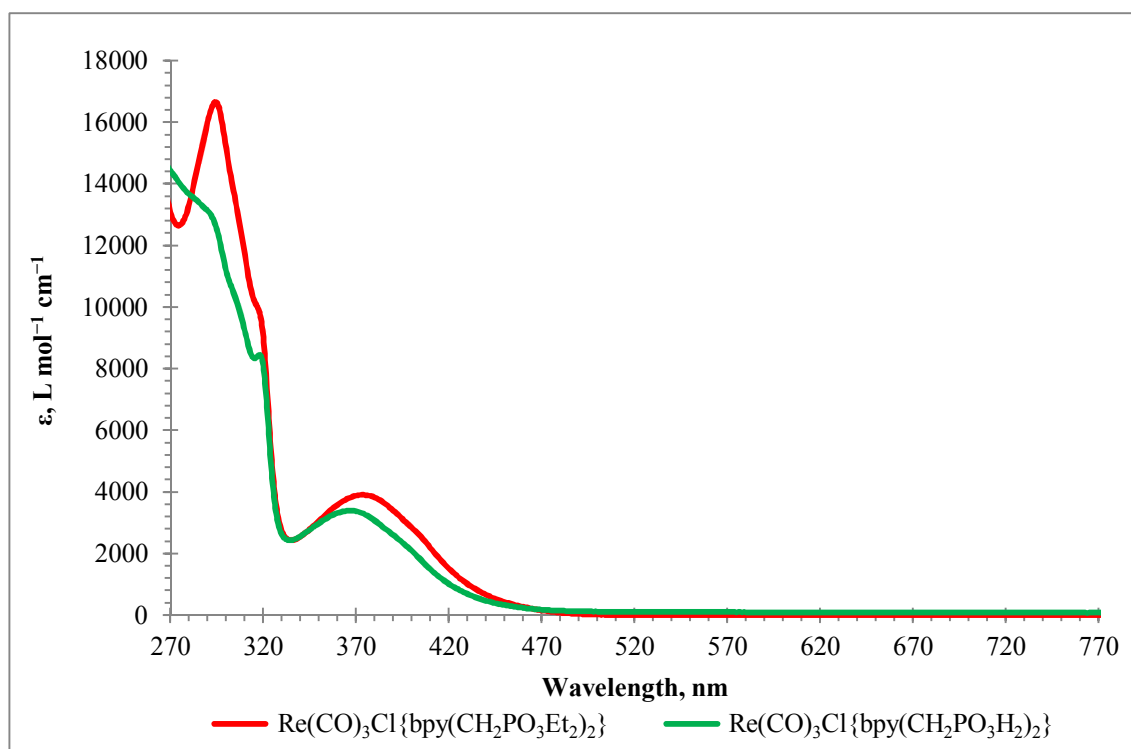


Figure 5.13 and Figure 5.14.

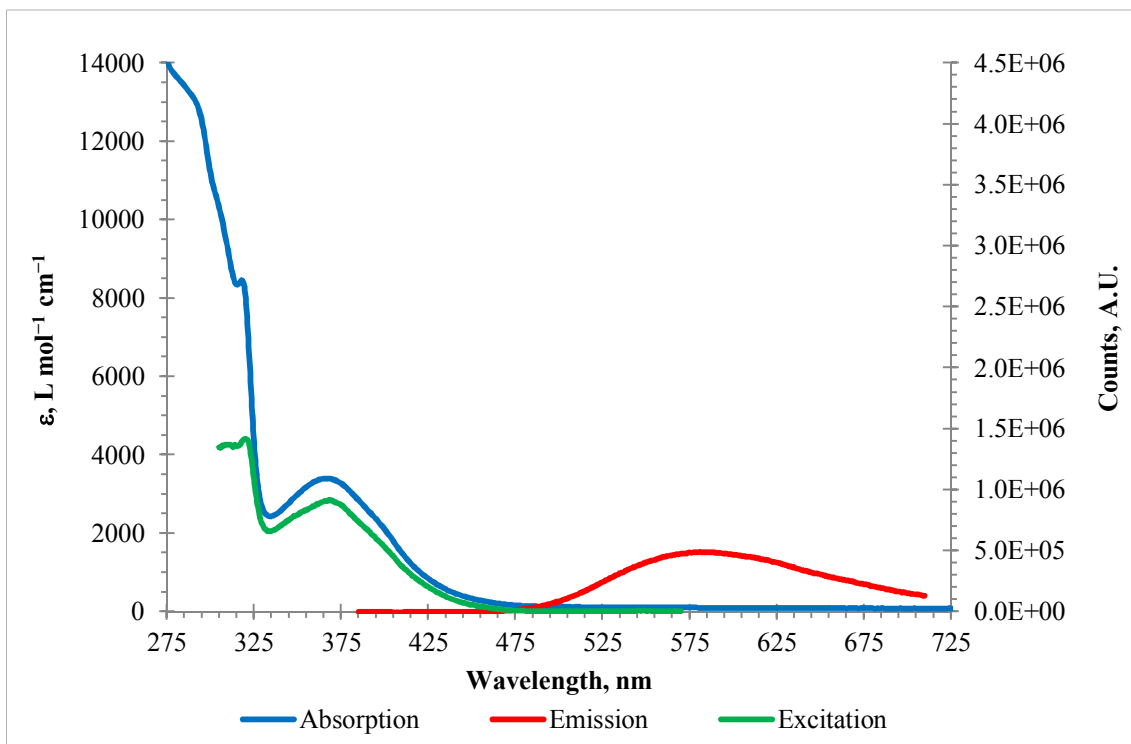


Figure 5.12: The UV-Vis, emission and excitation spectra of $\text{Re}(\text{CO})_3\text{Cl}\{\text{bpy}(\text{CH}_2\text{PO}_3\text{H}_2)_2\}$ in DMF, normalised. The excitation spectra were registered at 584 nm; the emission spectra were obtained under 364 nm excitation.

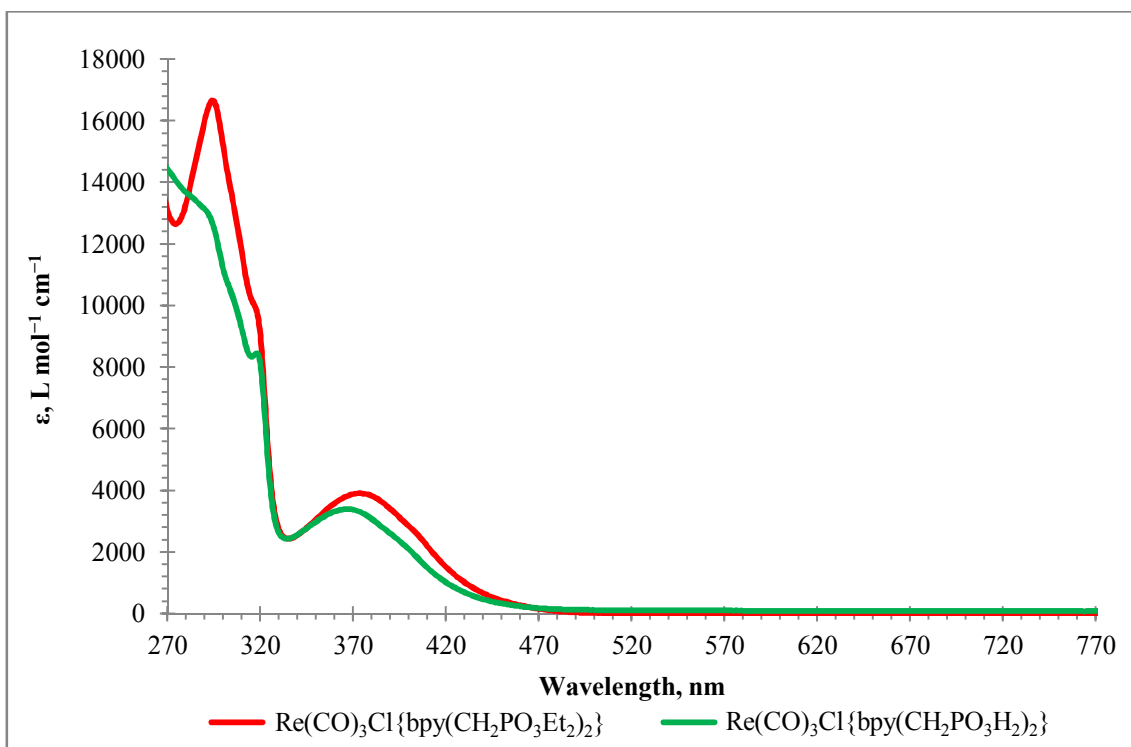


Figure 5.13: Comparison of UV-Vis spectra of $\text{Re}(\text{CO})_3\text{Cl}\{\text{bpy}(\text{CH}_2\text{PO}_3\text{Et}_2)_2\}$ and $\text{Re}(\text{CO})_3\text{Cl}\{\text{bpy}(\text{CH}_2\text{PO}_3\text{H}_2)_2\}$, both in DMF.

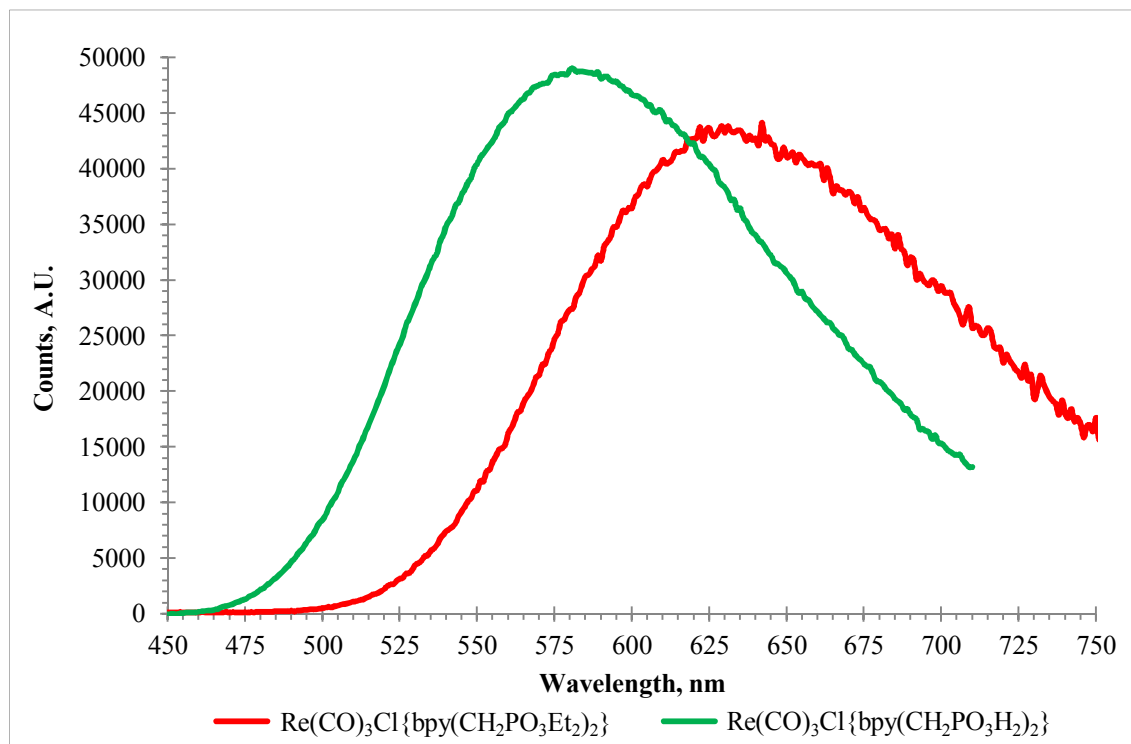


Figure 5.14: Comparison of emission spectra of $\text{Re}(\text{CO})_3\text{Cl}\{\text{bpy}(\text{CH}_2\text{PO}_3\text{Et}_2)_2\}$ and $\text{Re}(\text{CO})_3\text{Cl}\{\text{bpy}(\text{CH}_2\text{PO}_3\text{H}_2)_2\}$.

Figure 5.15 shows the FT IR spectrum from a solid sample of $\text{Re}(\text{CO})_3\text{Cl}\{\text{bpy}(\text{CH}_2\text{PO}_3\text{H}_2)_2\}$. The main peaks are the OH at 3350 cm^{-1} . The trans-CO (a)symmetric stretch is at 2024 cm^{-1} and the two bands attributed to the cis-CO symmetric and asymmetric stretches are at 1903 and 1888 cm^{-1} . As with the UV-Vis, emission and excitation spectra, the IR spectra for $\text{Re}(\text{CO})_3\text{Cl}\{\text{bpy}(\text{CH}_2\text{PO}_3\text{H}_2)_2\}$ and $\text{Re}(\text{CO})_3\text{Cl}\{\text{bpy}(\text{CH}_2\text{PO}_3\text{Et}_2)_2\}$ are analogous with only a small change in the position of some of the bands.

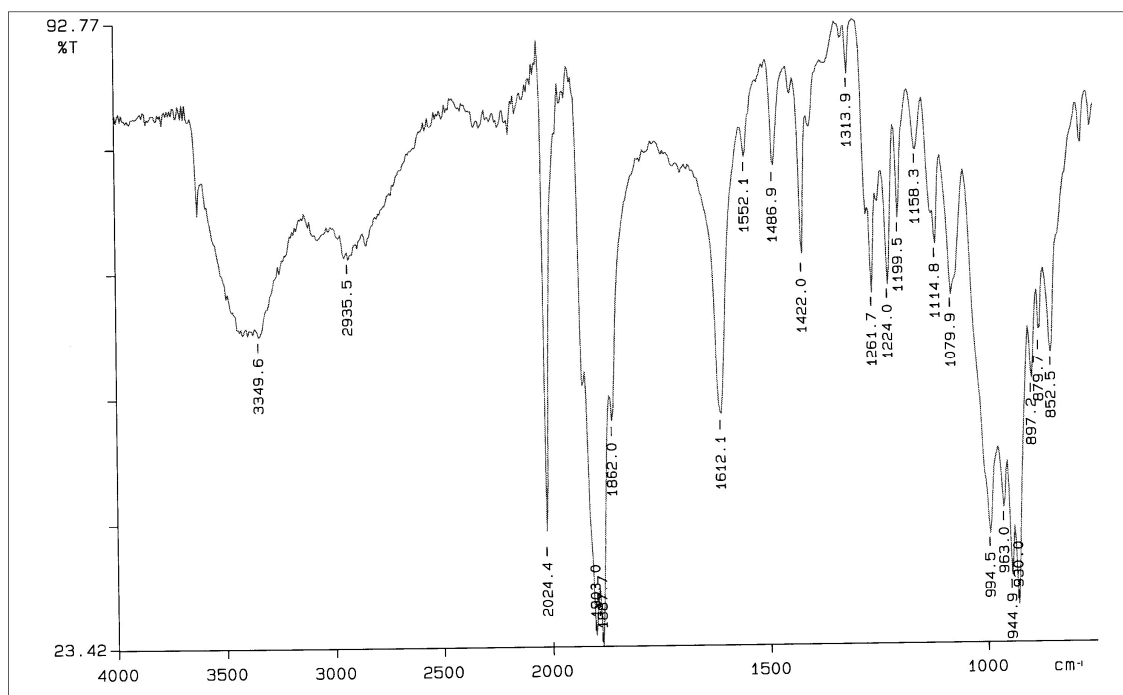


Figure 5.15: FT IR spectrum from a solid sample of $\text{Re}(\text{CO})_3\text{Cl}\{\text{bpy}(\text{CH}_2\text{PO}_3\text{H}_2)_2\}$.

Figure 5.16 shows the emission lifetime data for $\text{Re}(\text{CO})_3\text{Cl}\{\text{bpy}(\text{CH}_2\text{PO}_3\text{H}_2)_2\}$ in DMF. This was obtained using the mini- τ instrument with a 2 μs delay between pulses and a bandpass filter of 575 – 625 nm. The data was fitted using a 2 component exponential which provided lifetime values of 26 ± 3 ns and 119 ± 12 ns, 83% and 17% relative contribution respectively. This is comparable to the ester analogue showing that the lifetime of the complex does not change in any significant way upon hydrolysis of the ancillary ester group. This is as expected, given that the $-\text{PO}(\text{OEt})_2$ group is “decoupled” from the MLCT transition by a $-\text{CH}_2-$ spacer.

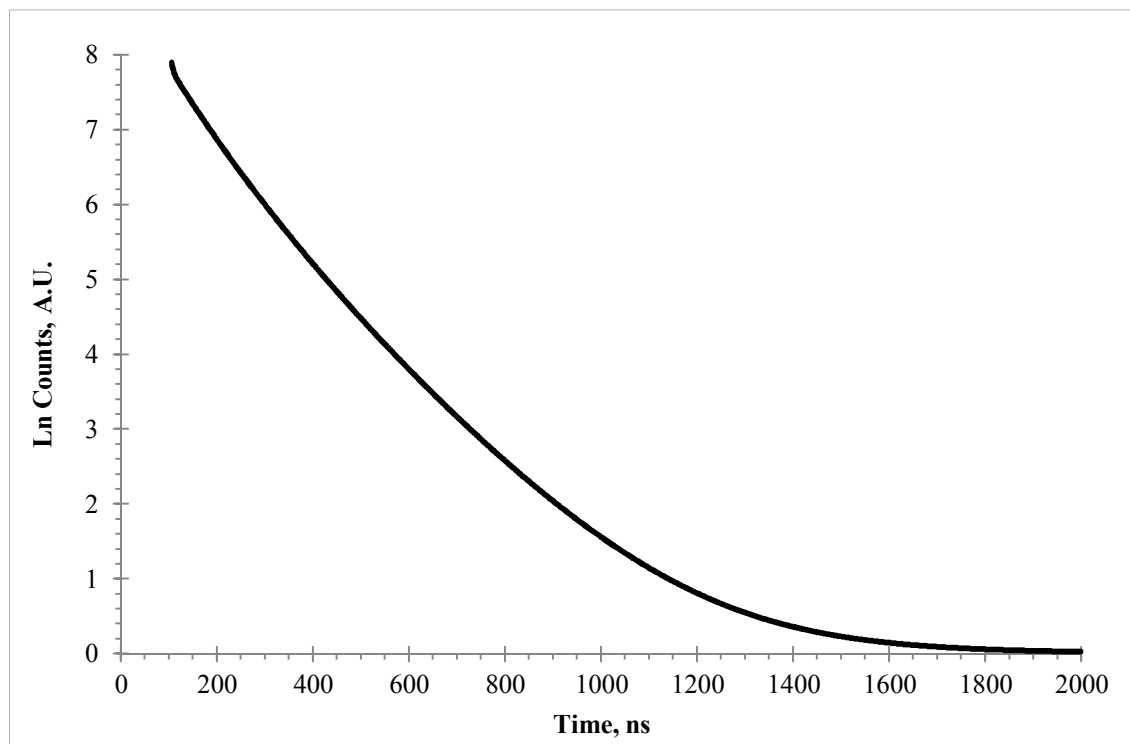


Figure 5.16: Lifetime trace of $\text{Re}(\text{CO})_3\text{Cl}\{\text{bpy}(\text{CH}_2\text{PO}_3\text{H}_2)_2\}$, in DMF, recorded in the spectral range 575 – 625 nm, 2 μs timescale, excitation with ca. 75 ps, 405 nm laser pulse.

5.5.2. Electrochemical Data for $\text{Re}(\text{CO})_3\text{Cl}\{\text{bpy}(\text{CH}_2\text{PO}_3\text{H}_2)_2\}$

Figure 5.17 shows the results from the cyclic voltammetry experiment in which $\text{Re}(\text{CO})_3\text{Cl}\{\text{bpy}(\text{CH}_2\text{PO}_3\text{H}_2)_2\}$ was used in both a nitrogen saturated solution and a carbon dioxide saturated solution. Saturation was achieved by bubbling the desired gas into the solution for up to 45 minutes. The couples for this complex are significantly more difficult to identify than those of the ester analogue. It is not clear as to why this is the case. The experiment was repeated a few times but the results were the same. However, there is still an increase in current when the system is saturated with CO_2 , which is desired. The second reduction peak for CO_2 appears to be at -2.14 V. The lack of clarity in the couples has also prevented us from checking whether the process is diffusion controlled using the Cottrell equation and if the current increase can be classed as catalytic.

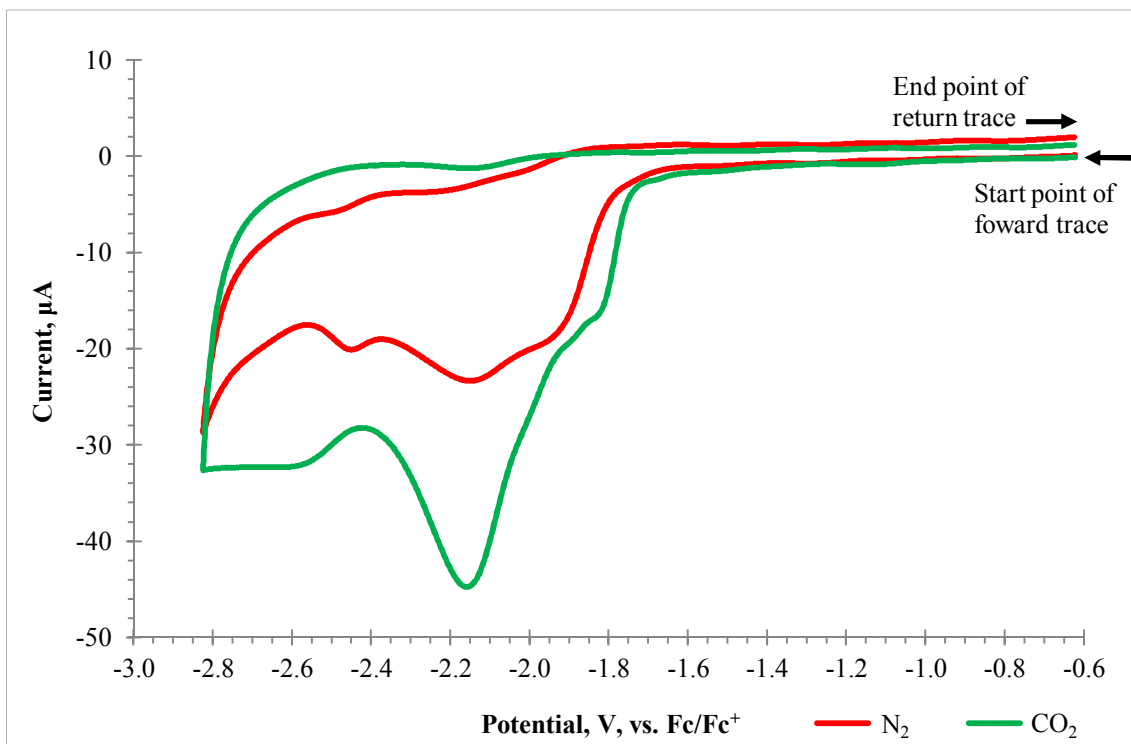


Figure 5.17: Cyclic voltammograms for $\text{Re}(\text{CO})_3\text{Cl}\{\text{bpy}(\text{CH}_2\text{PO}_3\text{H}_2)_2\}$, 2 mM in DMF with 0.2 M $[\text{Bu}_4\text{N}][\text{PF}_6]$, recorded at 100 mVs^{-1} , in the presence of N_2 or CO_2 , the potentials are reported vs. Fc/Fc^+ . The arrows show the start or end point and the direction of potential change. Note the increase in current in the presence of CO_2 .

The next section of results details the experiments carried out to try to quantify the volume of CO being produced during the reduction of CO_2 . In order to do this a two-part experiment was devised. The first part is the use of a bulk electrolysis setup in which the complex, $\text{Re}(\text{CO})_3\text{Cl}\{\text{bpy}(\text{CH}_2\text{PO}_3\text{H}_2)_2\}$, is electrolysed, firstly in the presence of N_2 and then with CO_2 . The second half of the experiment involves the use of a gas chromatograph to identify the gases being produced during the electrolysis. The results of the GC experiments are shown in Figure 5.18 and Figure 5.19. In Figure 5.18 the complex has been added to a N_2 saturated solution, the sample of the headspace is then removed and analysed by GC. This provides a baseline for comparison. The bulk electrolysis equipment is then reassembled and a potential of -2.3 V is applied for 1 hour. The headspace is then sampled again, with the results shown in Figure 5.19. As expected, there is no production of CO as there was no CO_2 present in the system.

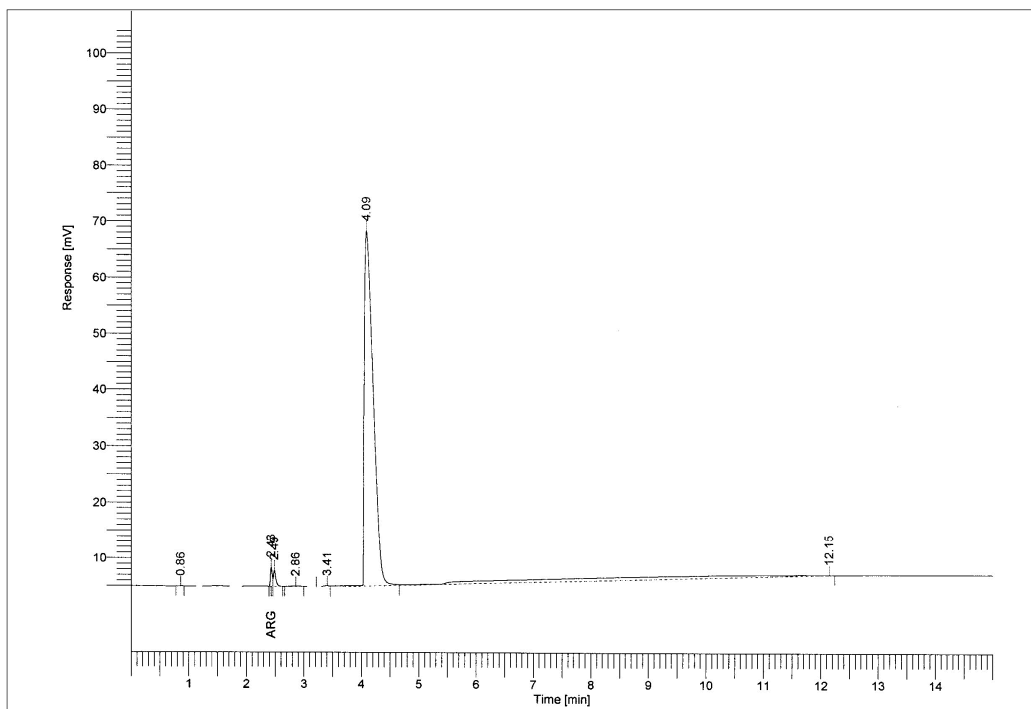


Figure 5.18: A gas chromatogram of a sample taken from the headspace of the electrolysis vessel, in which a solution of $\text{Re}(\text{CO})_3\text{Cl}\{\text{bpy}(\text{CH}_2\text{PO}_3\text{H}_2)_2\}$, 2 mM in CH_3CN with 0.2 M $[\text{Bu}_4\text{N}][\text{PF}_6]$, before a potential has been applied, and under a N_2 atmosphere, was present.

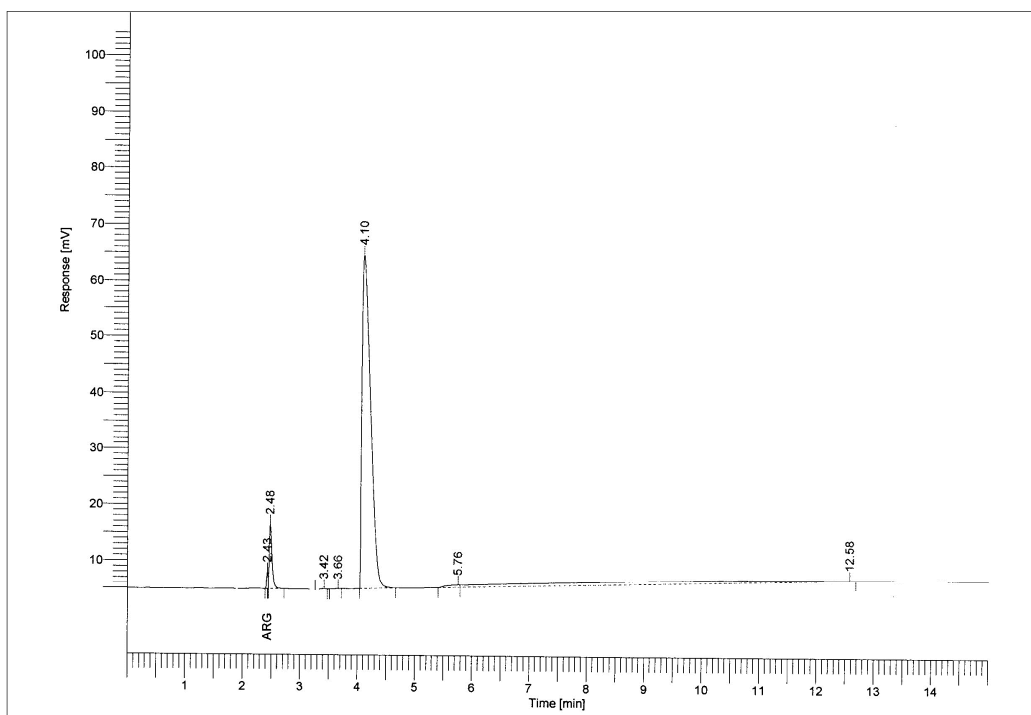


Figure 5.19: A gas chromatogram of a sample taken from the headspace of the electrolysis vessel, in which a solution of $\text{Re}(\text{CO})_3\text{Cl}\{\text{bpy}(\text{CH}_2\text{PO}_3\text{H}_2)_2\}$, 2 mM in CH_3CN with 0.2 M $[\text{Bu}_4\text{N}][\text{PF}_6]$, after a potential of -2.3 V had been applied for 1 hour, and under a N_2 atmosphere, was present.

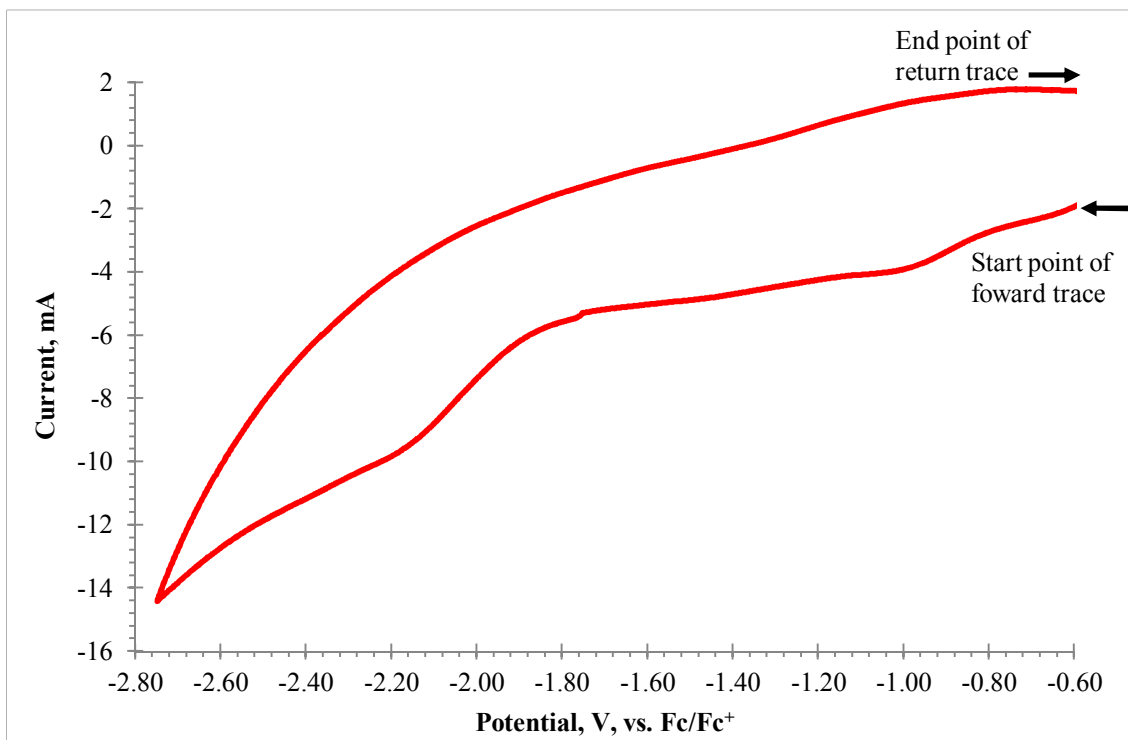


Figure 5.20: Bulk cyclic voltammogram for $\text{Re}(\text{CO})_3\text{Cl}\{\text{bpy}(\text{CH}_2\text{PO}_3\text{H}_2)_2\}$, 0.5 mM in CH_3CN with 0.2 M $[\text{Bu}_4\text{N}][\text{PF}_6]$, recorded at 100 mVs^{-1} , in the presence of CO_2 , the potentials are reported vs. Fc/Fc^+ . The arrows show the start or end point and the direction of potential change.

The experiment was carried out using the bulk cyclic voltammetry method and with the solution saturated with CO_2 instead of N_2 . Figure 5.20 shows the cyclic voltammogram recorded during the bulk electrocatalytic CO_2 reduction with $\text{Re}(\text{CO})_3\text{Cl}\{\text{bpy}(\text{CH}_2\text{PO}_3\text{H}_2)_2\}$.

Figure 5.21 shows the composition of the headspace prior to electrolysis, with Figure 5.22 detailing the results after 1 hour of electrolysis. From this, it can be seen that a small amount of CO has been produced during the hour. In order to try to quantify the volume, a gas cylinder in which the components and amounts are already known is needed. A 2% CO , 2% CH_4 , 96% N_2 mixture was used for this purpose. From this, the area under the curve in the gas chromatogram trace could be converted to a $\text{CO}\%$. It was calculated that this complex, $\text{Re}(\text{CO})_3\text{Cl}\{\text{bpy}(\text{CH}_2\text{PO}_3\text{H}_2)_2\}$, converted $6 \pm 0.6\%$ of the headspace to CO , after a potential of -2.3 V was applied for 1 hour.

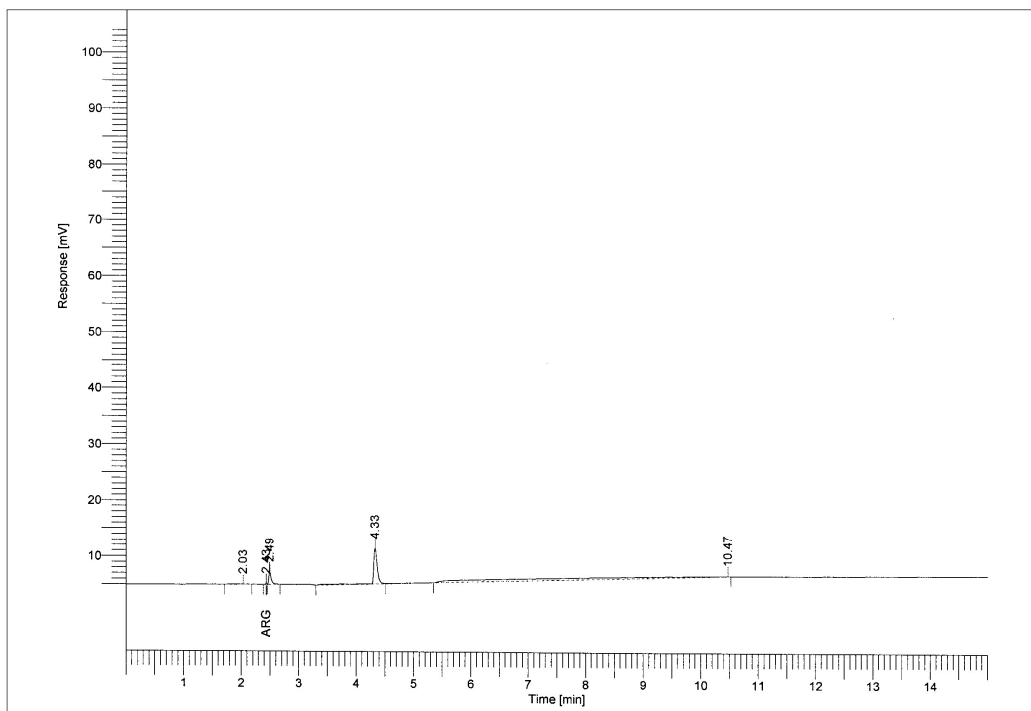


Figure 5.21: A gas chromatogram of a sample taken from the headspace of the electrolysis vessel, in which a solution of $\text{Re}(\text{CO})_3\text{Cl}\{\text{bpy}(\text{CH}_2\text{PO}_3\text{H}_2)_2\}$, 2 mM in CH_3CN with 0.2 M $[\text{Bu}_4\text{N}][\text{PF}_6]$, before a potential had been applied, and under a CO_2 atmosphere, was present.

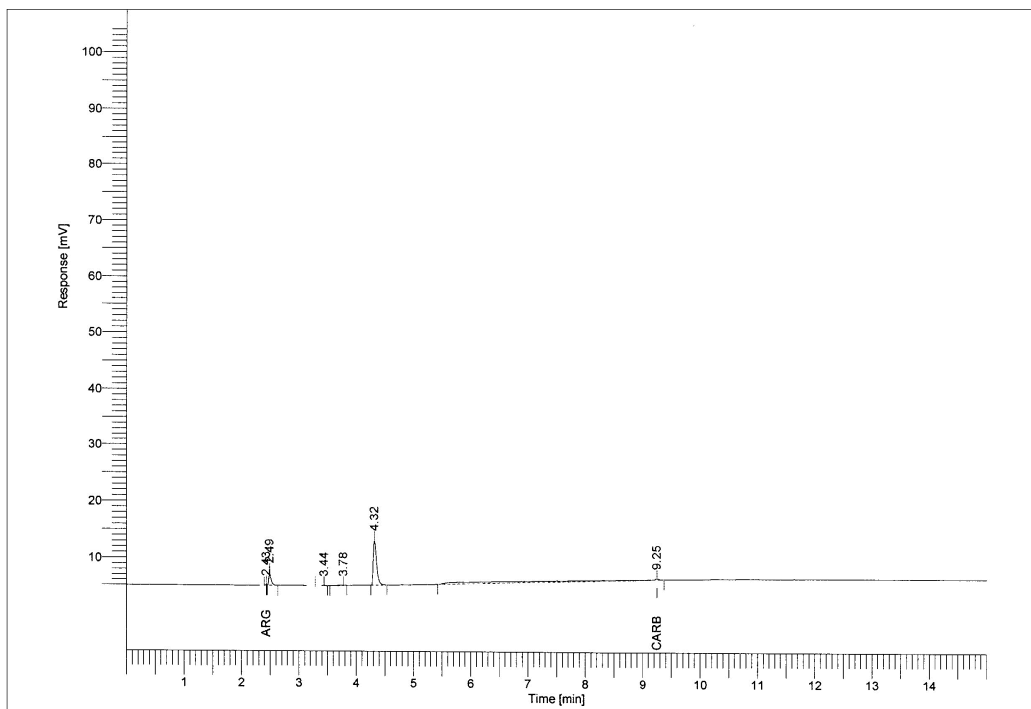


Figure 5.22: A gas chromatogram of a sample taken from the headspace of the electrolysis vessel, in which a solution of $\text{Re}(\text{CO})_3\text{Cl}\{\text{bpy}(\text{CH}_2\text{PO}_3\text{H}_2)_2\}$, 2 mM in CH_3CN with 0.2 M $[\text{Bu}_4\text{N}][\text{PF}_6]$, after a potential of -2.3 V has been applied for 1 hour, and under a CO_2 atmosphere, was present.

5.5.3. Summary

The desired complex, $\text{Re}(\text{CO})_3\text{Cl}\{\text{bpy}(\text{CH}_2\text{PO}_3\text{H}_2)_2\}$ was synthesised by hydrolysis of the corresponding ester analogue. The same array of photophysical and electrochemical experiments were then performed on the complex. These showed that the acid-bearing complex is capable of reducing CO_2 to CO when a potential of -2.3 V is applied, resulting in $6 \pm 0.6\%$ of CO being produced within 1 hour.

5.6. Results and Discussion of Rhenium Complex Analogues

5.6.1. Photophysical Data for Rhenium Complex Analogues

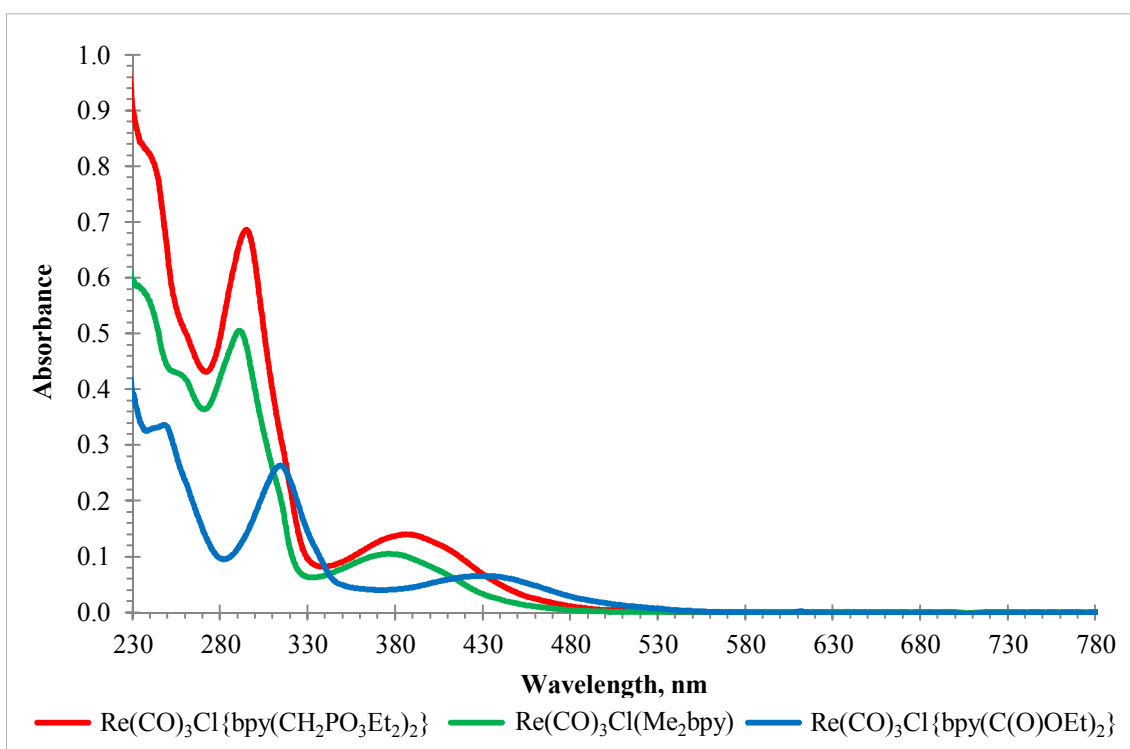


Figure 5.23: The UV-Vis spectra of $\text{Re}(\text{CO})_3\text{Cl}\{\text{bpy}(\text{CH}_2\text{PO}_3\text{Et}_2)_2\}$, $\text{Re}(\text{CO})_3\text{Cl}(\text{Me}_2\text{bpy})$, and $\text{Re}(\text{CO})_3\text{Cl}\{\text{bpy}(\text{C}(\text{O})\text{OEt})_2\}$, all in DCM.

To assist in explaining the results obtained from the electrochemical experiments the UV-Vis absorption spectrum of the three complexes was obtained, Figure 5.23. These show that the methyl and phosphonate complexes have very similar absorption profiles, i.e., the energies of their lowest $^1\text{MLCT}$ states are very close to one another. The carbonate ester also has a similar spectral shape but the $^1\text{MLCT}$ is red shifted to 428 nm.

5.6.2. Electrochemical Data for Rhenium Analogues

The next set of figures show the cyclic voltammetry results obtained for analogues of the rhenium complex. Both a methyl substituted bipyridine and a bipyridine carboxylate ester have been studied. This is due to their presence already in the literature¹⁶ and provides the opportunity to reproduce the papers results and see how known systems behave on our experimental setup.

The complexes studied were $\text{Re}(\text{CO})_3\text{Cl}(\text{Me}_2\text{bpy})$ and $\text{Re}(\text{CO})_3\text{Cl}\{\text{bpy}(\text{C}(\text{O})\text{OEt})_2\}$, both were already synthesised, purified and available in the lab.

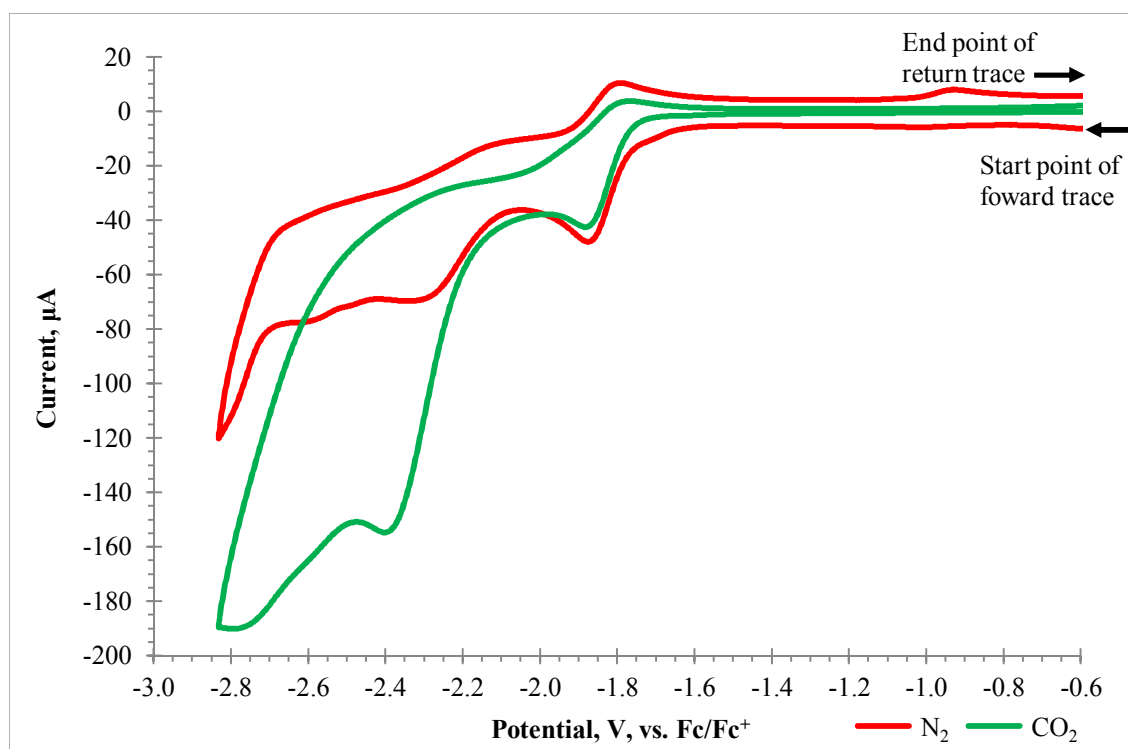


Figure 5.24: Cyclic voltammograms for $\text{Re}(\text{CO})_3\text{Cl}(\text{Me}_2\text{bpy})$, 2 mM in CH_3CN with 0.2 M $[\text{Bu}_4\text{N}][\text{PF}_6]$, recorded at 100 mVs^{-1} , in the presence of N_2 or CO_2 , the potentials are reported vs. Fc/Fc^+ . The arrows show the start or end point and the direction of potential change.

Figure 5.24 shows the results obtained for the $\text{Re}(\text{CO})_3\text{Cl}(\text{Me}_2\text{bpy})$ complex in both the N_2 , and CO_2 saturated solutions. Similar to the previously studied complex there is a reversible couple for the first reduction, at -1.83 V , in both the N_2 , and CO_2 system. The N_2 system has a partially reversible couple at -2.2 V . There may also be a second

irreversible reduction at -2.58 V but it is very hard to distinguish, unlike the $\text{Re}(\text{CO})_3\text{Cl}\{\text{bpy}(\text{CH}_2\text{PO}_3\text{Et}_2)_2\}$, which had a much clearer couple. There is then a large increase in the current for the second reduction of the CO_2 system, at -2.4 V. This corresponds to the current increase seen for the $\text{Re}(\text{CO})_3\text{Cl}\{\text{bpy}(\text{CH}_2\text{PO}_3\text{Et}_2)_2\}$ complex, although, as could be anticipated due to the difference in the reduction potential between the two complexes, the current enhancement is larger for the methyl complex. The results for Me complex match those reported previously in the literature.¹⁶

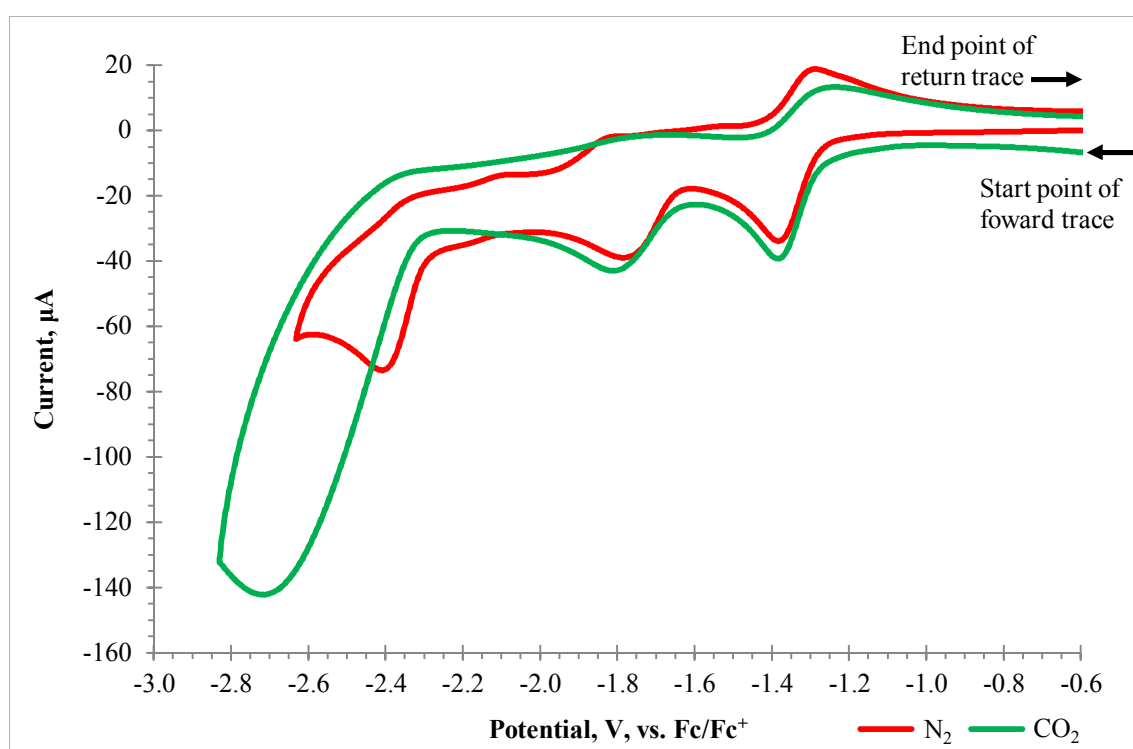


Figure 5.25: Cyclic voltammograms for $\text{Re}(\text{CO})_3\text{Cl}\{\text{bpy}(\text{C}(\text{O})\text{OEt}_2)_2\}$, 2 mM in CH_3CN with 0.2 M $[\text{Bu}_4\text{N}][\text{PF}_6]$, recorded at 100 mVs^{-1} , in the presence of N_2 or CO_2 , the potentials are reported vs. Fc/Fc^+ .

The arrows show the start or end point and the direction of potential change.

Figure 5.25 shows the results collected for $\text{Re}(\text{CO})_3\text{Cl}\{\text{bpy}(\text{C}(\text{O})\text{OEt}_2)_2\}$ complex which was studied in identical conditions to the previous complexes. The first reversible reduction couple occurs at -1.31 V in both the N_2 , and CO_2 saturated systems. In the N_2 system, there is an irreversible reduction process at -1.8 V and a reversible couple at -2.37 V. For the CO_2 containing system there is an increase in current with a peak at

-2.72 V. It is not clear if this is due to a catalytic CO₂ reduction process, it is several hundred mV from where couples attributed to the process are in other similar complexes. To help summarise the results from the electrochemical experiments a comparison between the different complexes in both N₂, and CO₂ is shown in Figure 5.26 and Figure 5.27 respectively.

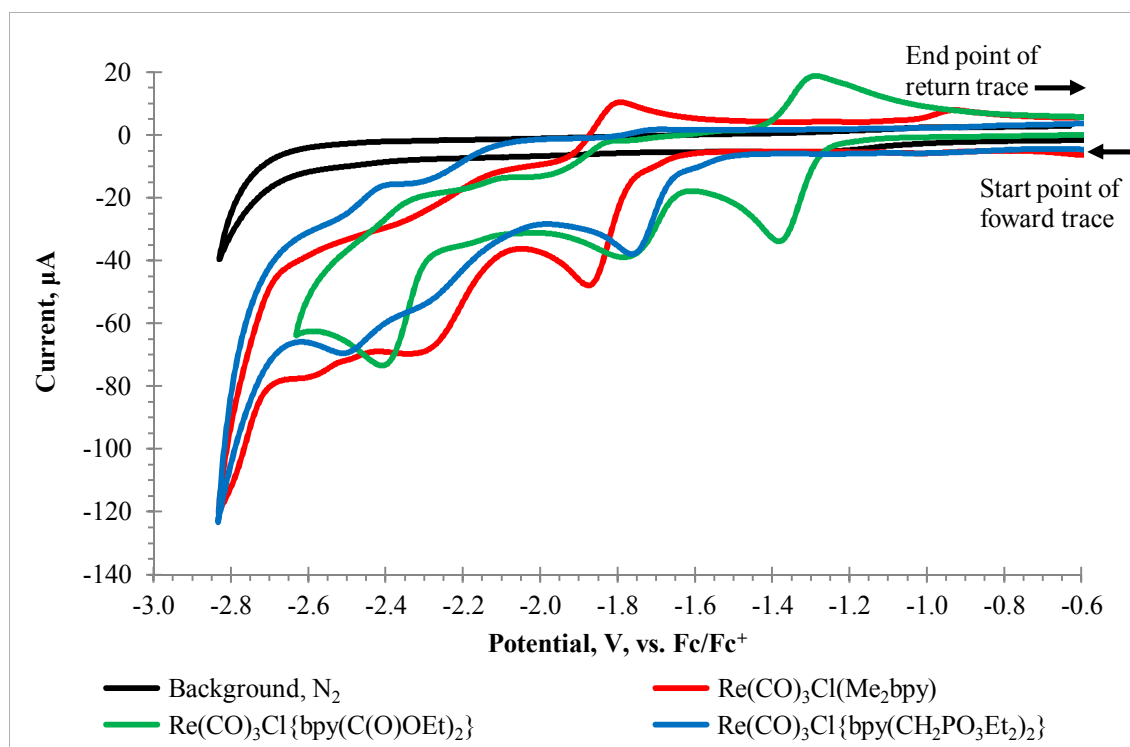


Figure 5.26: Cyclic voltammograms for several rhenium complexes, 2 mM in CH₃CN with 0.2 M [Bu₄N][PF₆], recorded at 100 mVs⁻¹, in the presence of N₂, the potentials are reported vs. Fc/Fc⁺. The arrows show the start or end point and the direction of potential change.

Figure 5.26 shows how the position of the first reduction couple changes for the different complexes. The methyl and phosphonate complexes have a second reduction at the same potential with the ester complex needing a slightly more negative potential for the reduction to occur. The black line is the control scan of the background – solvent and electrolyte, but no metal complex and shows that no current is observed other than at very negative potentials due to solvent break down.

Figure 5.27 helps to summarise the results obtained for the complexes in CO₂ saturated solutions. The first reduction does not appear to change significantly between the N₂, and CO₂ systems and so will not be mentioned further. For the second reduction, where the current increases, the differences between the different complexes can be clearly seen. As previously mentioned the methyl, and phosphonate complexes have a second reduction at the same potential however, the methyl complex produces more current at the same potential under the same conditions. At the same potential, it can also be seen that the ester complex produces little to no current.

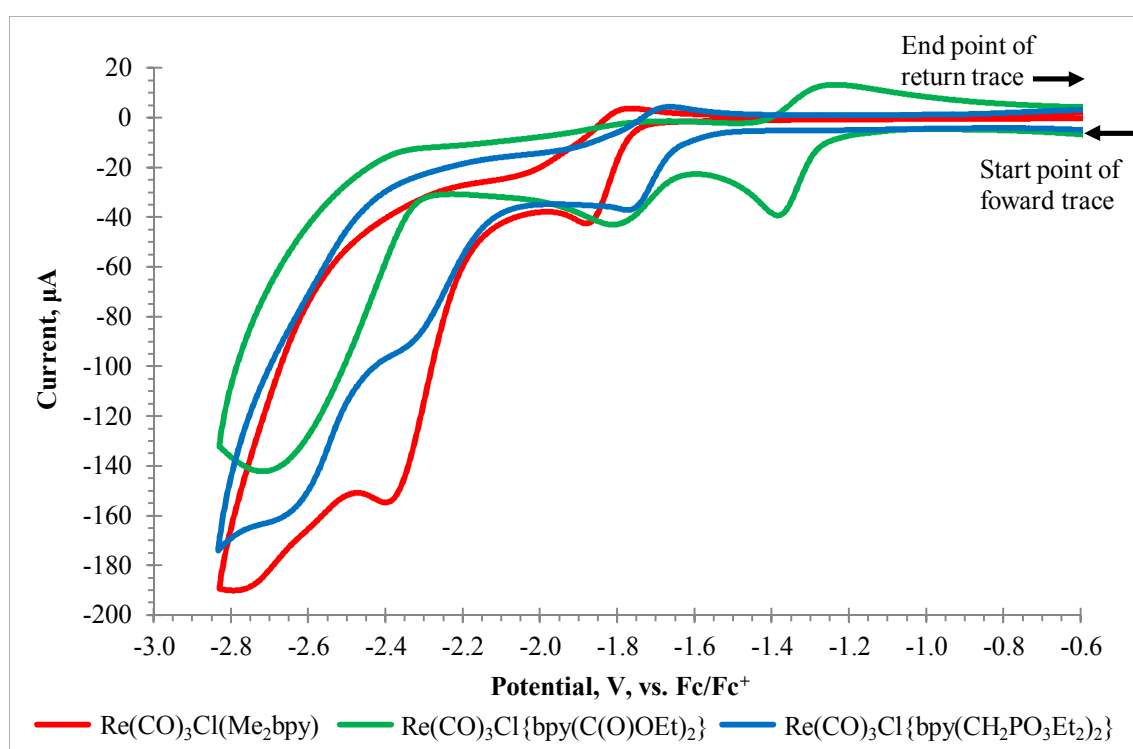


Figure 5.27: Cyclic voltammograms for several rhenium complexes, 2 mM in CH₃CN with 0.2 M [Bu₄N][PF₆], recorded at 100 mVs⁻¹, in the presence of CO₂, the potentials are reported vs. Fc/Fc⁺. The arrows show the start or end point and the direction of potential change.

As seen previously in Figure 5.23, the absorption spectrum of the rhenium complex containing an accepting -C(O)OEt group has the MLCT absorption band at lower energies than both the Me₂bpy, and bpy(CH₂PO₃Et₂)₂ containing complexes. This is consistent with a ca. 400 mV less negative potential required to reduce the compound. In fact, the difference in the positions of the MLCT absorption bands are very close to

the difference in reduction potentials for these complexes, as shown in Figure 5.26, Figure 5.27, and summarised in Table 5.3.

Table 5.3: Position of the $^1\text{MLCT}$ band and of the first redox couple for the various rhenium complexes studied in this chapter, in DCM at r.t., reported vs. Fc/Fc^+ .

Compound	Position of $^1\text{MLCT}$ band, nm	Position of first redox couple, V, vs. Fc/Fc^+
$\text{Re}(\text{CO})_3\text{Cl}(\text{Me}_2\text{bpy})$	376	-1.84
$\text{Re}(\text{CO})_3\text{Cl}\{\text{bpy}(\text{C}(\text{O})\text{OEt})_2\}$	428	-1.31
$\text{Re}(\text{CO})_3\text{Cl}\{\text{bpy}(\text{CH}_2\text{PO}_3\text{Et}_2)_2\}$	384	-1.71
$\text{Re}(\text{CO})_3\text{Cl}\{\text{bpy}(\text{CH}_2\text{PO}_3\text{H}_2)_2\}$	371	-1.93

From Figure 5.28 a clear linear trend can be seen between the position of the first reduction and the position of the MLCT band. This information is useful as it shows that by tuning the position of the MLCT band through ligand modification we are also tuning the position of the reduction potentials, which allows us to design better catalysts. A similar result can be seen in Figure 5.29, which shows the relationship between the emission maximum and reduction potentials.

This observation is important for two reasons. Firstly, it means that introducing an anchoring group onto a bipyridyl ligand is possible without compromising its photophysical, electrochemical, and consequently electrocatalytic properties. This is shown by the comparison between the Me_2bpy , already known to be electrocatalytically active, and $\text{bpy}(\text{CH}_2\text{PO}_3\text{Et}_2)_2$ containing complexes. Both of which have similar MLCT bands and reduction potentials implying that the $\text{bpy}(\text{CH}_2\text{PO}_3\text{Et}_2)_2$ containing complex will also be electrocatalytically active. The excited state lifetimes obtained from the emission data also show that these compounds behave in a nearly identical way.

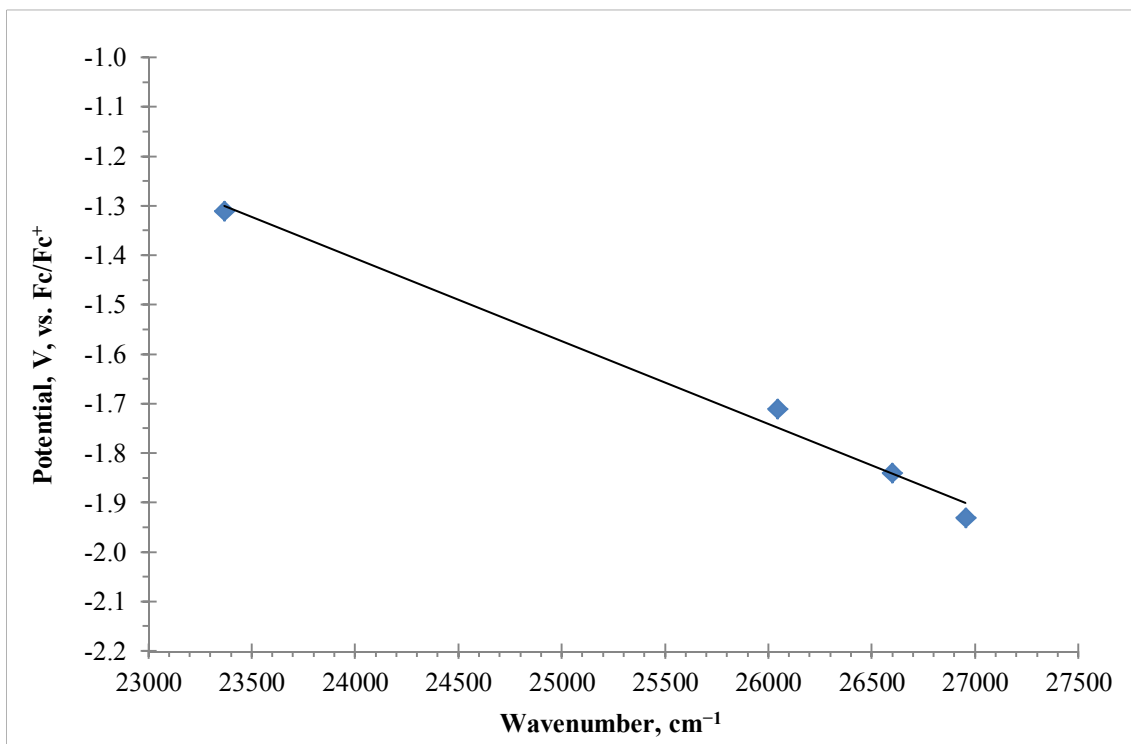


Figure 5.28: A plot of the potential of the first reduction vs. the MLCT band in the UV-Vis spectrum, for the rhenium complexes studied in this chapter.

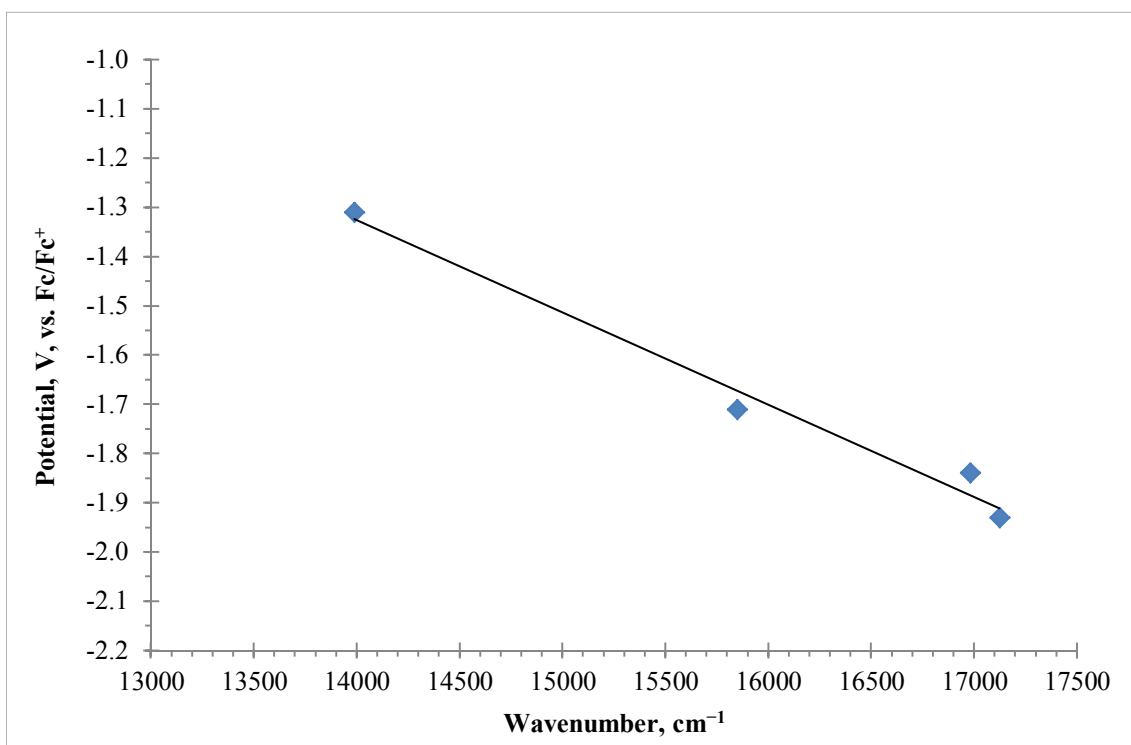


Figure 5.29: A plot of the potential of the first reduction vs. the emission maximum, for the rhenium complexes studied in this chapter.

Secondly, by comparing the $\text{bpy}(\text{CH}_2\text{PO}_3\text{Et}_2)_2$ containing complex with the $\text{C}(\text{O})\text{OEt}$ containing complex we can see that the $-\text{CH}_2-$ spacer acts as an “insulator” between the anchor group and the bipyridine. This is shown by the difference in position of the MLCT band and subsequently reduction potential.

These observations reveal the compound, $\text{Re}(\text{CO})_3\text{Cl}\{\text{bpy}(\text{CH}_2\text{PO}_3\text{H}_2)_2\}$, combines the advantages of a high-energy LUMO³⁴ and hence capable to reduce CO_2 , with possessing an anchoring group, allowing for attachment to a semiconductor.

In order to assess how efficient the phosphonate rhenium catalyst is, and to compare its electrocatalytic performance with the previously studied analogues, a comparative study with the rhenium complex bearing a Me_2bpy ligand was carried out. The same experiments as previous, bulk electrolysis followed by gas chromatogram analysis were performed on the Me_2bpy containing complex. The results are shown in Figure 5.30, Figure 5.31 and Figure 5.32.

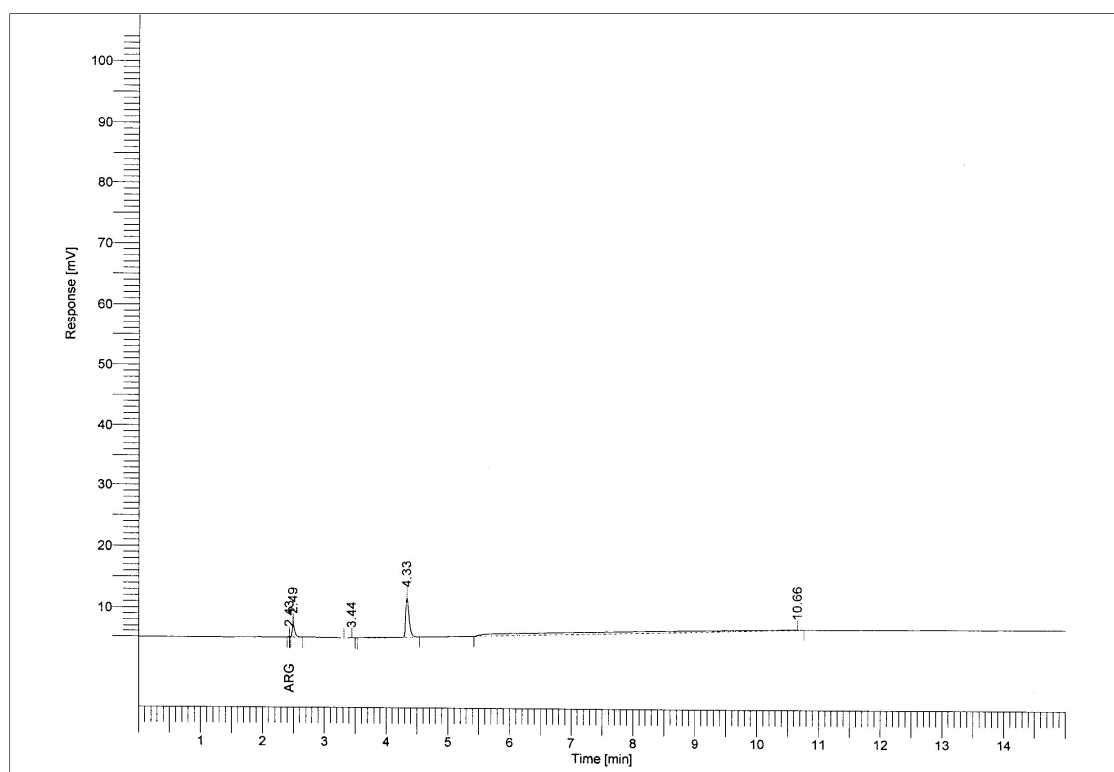


Figure 5.30: A gas chromatogram of a sample taken from the headspace of the electrolysis vessel, in which a solution of $\text{Re}(\text{CO})_3\text{Cl}(\text{Me}_2\text{bpy})$, 2 mM in CH_3CN with 0.2 M $[\text{Bu}_4\text{N}][\text{PF}_6]$, before potential has been applied, and under a CO_2 atmosphere, was present.

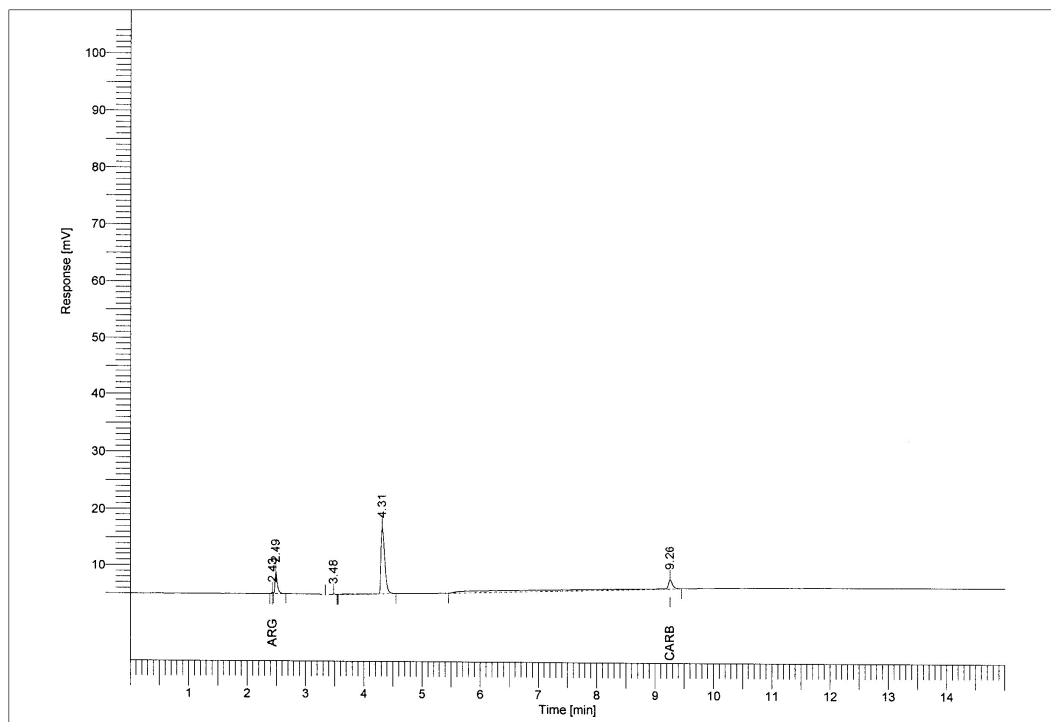


Figure 5.31: A gas chromatogram of a sample taken from the headspace of the electrolysis vessel, in which a solution of $\text{Re}(\text{CO})_3\text{Cl}(\text{Me}_2\text{bpy})$, 2 mM in CH_3CN with 0.2 M $[\text{Bu}_4\text{N}][\text{PF}_6]$, after a potential of -2.3 V had been applied for 1 hour, and under a CO_2 atmosphere, was present

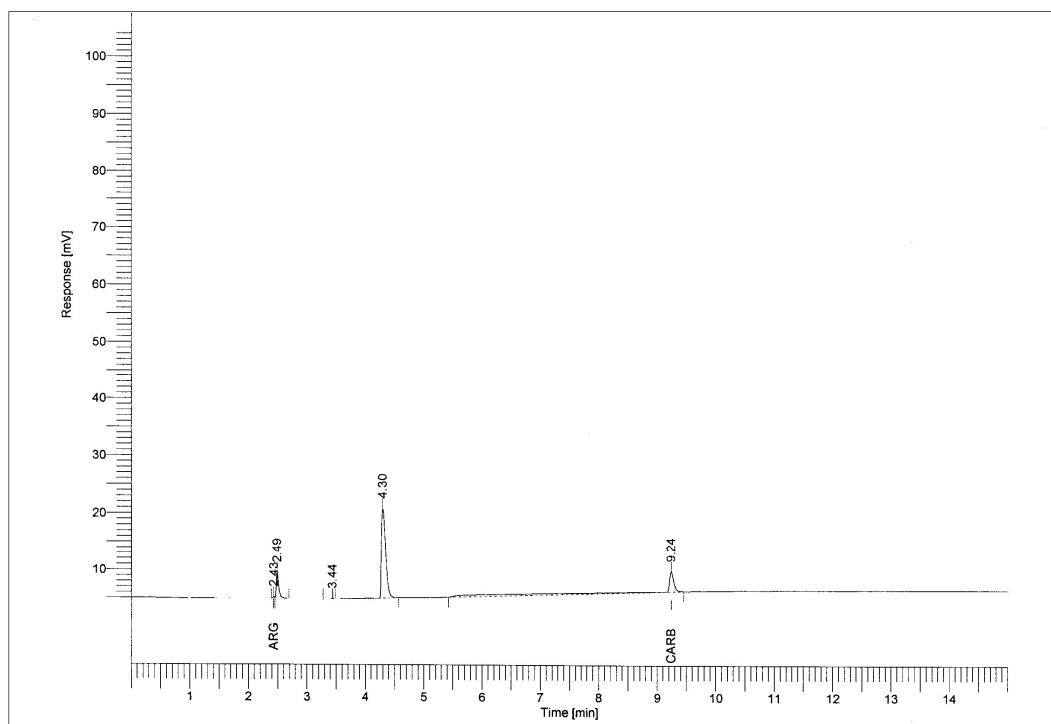


Figure 5.32: A gas chromatogram of a sample taken from the headspace of the electrolysis vessel, in which a solution of $\text{Re}(\text{CO})_3\text{Cl}(\text{Me}_2\text{bpy})$, 2 mM in CH_3CN with 0.2 M $[\text{Bu}_4\text{N}][\text{PF}_6]$, after a potential of -2.3 V had been applied for 2 hours, and under a CO_2 atmosphere, was present

These results show that, as expected, without potential being applied there is no CO production from the Me₂bpy complex. After 1 hour and then 2 hours of electrolysis at -2.3 V, (100 mV overpotential from the 2nd redox couple) $7 \pm 0.7\%$ and $8 \pm 0.8\%$ respectively of CO was produced.

5.6.3. Summary

A series of comparisons with complexes from the literature was performed. This showed that Re(CO)₃Cl(Me₂bpy) is capable of producing $7 \pm 0.7\%$ CO within 1 hour. This is obviously a larger volume of CO than our complex; however, our complex contains a ligand capable of anchoring on to a semiconductor and therefore has the potential to be powered by light rather than electric current. This means that we are closer to achieving the objective of the thesis and can move onto the final aim of attaching the complex to a semiconductor.

5.7. Consideration of Random and Systematic Errors

In the above sections, the photophysical and electrochemical data was discussed. The values obtained from these experiments could potentially be affected by random or systematic error. During the determination of the photophysical properties, it is likely that random errors have occurred during measurement collection in addition to those present during sample preparation. The balance is capable of weighing to ± 0.0001 g and has an enclosed case to reduced atmospheric pressure fluctuations. Vibrations are dampened by the presence of shock absorbers, further reducing random errors. This will result in minimal random errors associated with any mass values. Systematic error should also be minimal due to taring of the balance before each use. The error for the volume of a solution used is likely to be negligible due to the use of microlitre syringes for extinction coefficient determination, assuming proper calibration. Random errors caused by the instruments themselves are unlikely to be of concern as they are capable of measuring to 3 – 4 decimal places, thus our values will have more error due to simple rounding than because of random error. This is not true however for the potential systematic error for which great care must be taken to properly zero the instruments and subsequently perform suitable background scans to subtract from the actual scans. This

removes both the sample cuvette and the solvent signals allowing for measurement of the actual sample.

For the electrochemical experiments, random error will be included in the concentration of the electrolyte and the mass of the complex used through use of the balance and measurement glassware. Systematic error will also occur with use of the glassware due to imperfections in its construction, however this is usually only around ± 0.1 mL for a 25 mL measuring cylinder. As stated above errors arising from mass determinations should be negligible. There will also be an associated random and systematic error with the potentiostat. The potential is calculated relative to a reference electrode and could be subject to systematic error; however, this will then be significantly reduced by using an additional reference, ferrocene. The potentiostat is capable of measuring current at the nano amp scale whilst all of our measurements are on the micro amp scale, this would suggest that any error is going to be orders of magnitude less than our measurements.

The gas chromatography experiments will be subject to random error however given the apparent sensitivity of the detector these errors should be negligible compared to rounding errors. Systematic error due to there being an offset from zero present is potentially of greater concern for these experiments. The offset can be positive or negative resulting in more or less gas being recorded than was actually present. However, after numerous experiments were performed whilst testing the CO₂ reduction properties of the complexes mentioned in this chapter and others, it would appear that any offset is usually negligible when compared to the size of signal being detected.

Taking into account all of these sources of error and their potential size it is unlikely that they will have any significant impact on our results or conclusions. Therefore, repeat readings were often not necessary hence; no statistical analysis could be performed.

5.8. References

1. J. Hawecker, J.-M. Lehn and R. Ziessel, *J. Chem. Soc., Chem. Commun.*, 1983, 536–538.
2. J. Hawecker, J.-M. Lehn and R. Ziessel, *J. Chem. Soc., Chem. Commun.*, 1984, 328–330.
3. J. Hawecker, J.-M. Lehn and R. Ziessel, *Helv. Chim. Acta*, 1986, **69**, 1990–2012.
4. B. Gholamkhash, H. Mametsuka, K. Koike, T. Tanabe, M. Furue and O. Ishitani, *Inorg. Chem.*, 2005, **44**, 2326–2336.
5. C. L. Anfuso, R. C. Snoeberger, A. M. Ricks, W. Liu, D. Xiao, V. S. Batista and T. Lian, *J. Am. Chem. Soc.*, 2011, **133**, 6922–6925.
6. Y. Hayashi, S. Kita, B. S. Brunshwig and E. Fujita, *J. Am. Chem. Soc.*, 2003, **125**, 11976–11987.
7. H. Takeda, K. Koike, H. Inoue and O. Ishitani, *J. Am. Chem. Soc.*, 2008, **130**, 2023–2031.
8. J. Agarwal, R. P. Johnson and G. Li, *J. Phys. Chem. A*, 2011, **115**, 2877–2881.
9. A. J. Morris, G. J. Meyer and E. Fujita, *Acc. Chem. Res.*, 2009, **42**, 1983–1994.
10. E. E. Benson, M. D. Sampson, K. A. Grice, J. M. Smieja, J. D. Froehlich, D. Friebe, J. A. Keith, E. A. Carter, A. Nilsson and C. P. Kubiak, *Angew. Chem. Int. Ed.*, 2013, **52**, 4841–4844.
11. B. Kumar, M. Llorente, J. Froehlich, T. Dang, A. Sathrum and C. P. Kubiak, *Annu. Rev. Phys. Chem.*, 2012, **63**, 541–569.
12. B. Kumar, J. M. Smieja, A. F. Sasayama and C. P. Kubiak, *Chem. Commun.*, 2012, **48**, 272–274.
13. E. E. Benson and C. P. Kubiak, *Chem. Commun.*, 2012, **48**, 7374–7376.
14. M. D. Doherty, D. C. Grills, J. T. Muckerman, D. E. Polyansky and E. Fujita, *Coord. Chem. Rev.*, 2010, **254**, 2472–2482.
15. H. Takeda and O. Ishitani, *Coord. Chem. Rev.*, 2010, **254**, 346–354.
16. J. M. Smieja and C. P. Kubiak, *Inorg. Chem.*, 2010, **49**, 9283–9289.
17. B. Probst, M. Guttentag, A. Rodenberg, P. Hamm and R. Alberto, *Inorg. Chem.*, 2011, **50**, 3404–3412.
18. B. Kumar, J. M. Smieja and C. P. Kubiak, *J. Phys. Chem. C*, 2010, **114**, 14220–14223.
19. Y. Kou, Y. Nabetani, D. Masui, T. Shimada, S. Takagi, H. Tachibana and H. Inoue, *J. Am. Chem. Soc.*, 2014, **136**, 6021–6030.
20. C. D. Windle and R. N. Perutz, *Coord. Chem. Rev.*, 2012, **256**, 2562–2570.
21. K. D. DuBois, H. He, C. Liu, A. S. Vorushilov and G. Li, *J. Mol. Catal. A: Chem.*, 2012, **363–364**, 208–213.

22. C. She, J. Guo, S. Irle, K. Morokuma, D. L. Mohler, H. Zabri, F. Odobel, K.-T. Youm, F. Liu, J. T. Hupp and T. Lian, *J. Phys. Chem. A*, 2007, **111**, 6832–6842.
23. C. She, N. A. Anderson, J. Guo, F. Liu, W.-H. Goh, D.-T. Chen, D. L. Mohler, Z.-Q. Tian, J. T. Hupp and T. Lian, *J. Phys. Chem. B*, 2005, **109**, 19345–19355.
24. C. She, J. Guo and T. Lian, *J. Phys. Chem. B*, 2007, **111**, 6903–6912.
25. J. Guo, C. She and T. Lian, *J. Phys. Chem. C*, 2007, **111**, 8979–8987.
26. F. P. A. Johnson, M. W. George, F. Hartl and J. J. Turner, *Organometallics*, 1996, **15**, 3374–3387.
27. V. Penicaud, F. Odobel and B. Bujoli, *Tetrahedron Lett.*, 1998, **39**, 3689–3692.
28. S. Lense, K. I. Hardcastle and C. E. MacBeth, *J. Chem. Soc., Dalton Trans.*, 2009, 7396–7401.
29. Z.-Y. Bian, S.-M. Chi, L. Li and W. Fu, *J. Chem. Soc., Dalton Trans.*, 2010, **39**, 7884–7887.
30. K. Koike, S. Naito, S. Sato, Y. Tamaki and O. Ishitani, *J. Photochem. Photobiol., A*, 2009, **207**, 109–114.
31. I. Gillaizeau-Gauthier, F. Odobel, M. Alebbi, R. Argazzi, E. Costa, C. A. Bignozzi, P. Qu and G. J. Meyer, *Inorg. Chem.*, 2001, **40**, 6073–6079.
32. D. Uner and M. M. Oymak, *Catal. Today*, 2012, **181**, 82–88.
33. F. G. Cottrell, *Z. Phys. Chem.*, 1903, **42**, 385–431.
34. Y. Kuramochi, K. Fukaya, M. Yoshida and H. Ishida, *Chem. Eur. J.*, 2015, **21**, 10049–10060.

6. Metal Complexes Anchored to Semiconductors

6.1. Introduction

Once a complex that is capable of reducing CO₂ to CO had been identified, the next step was to anchor it to a semiconductor. There are several different semiconductors available to choose from. The most commonly studied in the literature is TiO₂,¹⁻³ with the earlier work often involving the type one systems⁴⁻¹³ mentioned in the introduction chapter and the more recent work concerning the type two systems¹⁴⁻²⁰ of which this thesis has focused. There are also a couple of examples using only TiO₂ as the reduction agent.^{21, 22} Other light absorbing semiconductors include; tantalum oxides, undoped, Ta₂O₅^{23, 24} or nitrogen-doped, N-Ta₂O₅,²⁵⁻²⁷ a tantalum oxynitride, (CaTaO₂N)²⁸ and a polymeric carbon nitride (C₃N₄).^{29, 30}

The work presented in this chapter primarily involves the use of TiO₂ and tantalum oxides in conjunction with the rhenium complex, Re(CO)₃Cl{bpy(CH₂PO₃H₂)₂}, from chapter 5 that was shown to be catalytically active for the purpose of CO₂ reduction. Several different types of experiment were carried out; some involving TiO₂ slides, TiO₂ powder, and doped or undoped Ta₂O₅. Other experiments involved model complexes such as PtCl₂(dcbpy), and the free ligand dcbpy. These experiments were designed to fulfil the aims of the chapter and ultimately the aims of the thesis.

The aims of this chapter are derived from the primary thesis aim (vi) which can be broken down into several smaller aims;

- (i) To identify the most efficient electrocatalyst from those evaluated in the previous chapters.
- (ii) To then establish a method of anchoring the electrocatalyst to a semiconductor, either TiO₂ or Ta₂O₅ or N-Ta₂O₅.
- (iii) To determine if anchoring has been successful.
- (iv) If the results from step 3 are positive, the building of a heterogeneous system will be carried out with assistance from our collaborators.

6.1.1. System Design

In the previous chapters a series of transition metal complexes were synthesised, characterised and their potential for catalytically reducing CO_2 to CO was tested and discussed. From this work a rhenium complex, $\text{Re}(\text{CO})_3\text{Cl}\{\text{bpy}(\text{CH}_2\text{PO}_3\text{H}_2)_2\}$, was identified as being the most suitable for electrochemical reduction of CO_2 . Through the fulfilment of the aims of the thesis thus far, the rhenium complex in addition to its catalytic properties also contains an anchoring group that will allow attachment to a semiconductor. The anchor group for this complex is a phosphonic acid group that is attached to a bipyridine through a $-\text{CH}_2-$ spacer.

This phosphonate anchor group is analogous to a carboxylate anchor group however they have different affinities to various semiconductors, and for instance are known to have faster rates of electron injection into TiO_2 than carboxylates.³¹ For carboxylates several different modes of attachment to the semiconductor are possible.^{32, 33} These include a monodentate, a bidentate, and a bridging mode as shown in Figure 6.1.

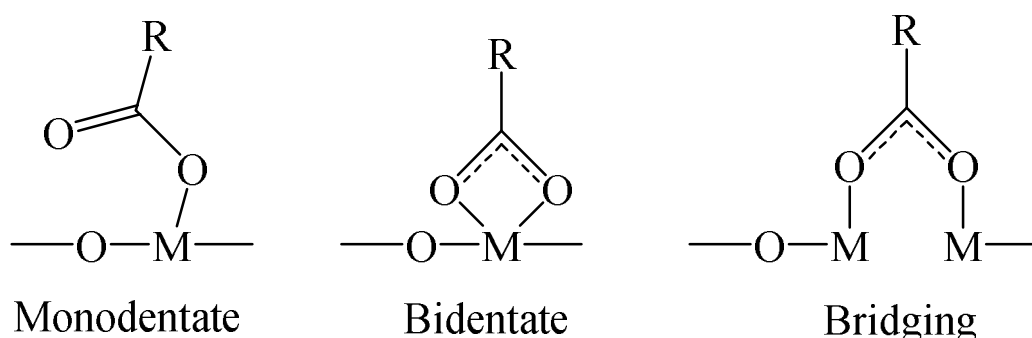


Figure 6.1: Examples of several possible modes of carboxylate binding to a metal oxide surface. M refers to the metal, R can be any ligand.^{32,33}

Attachment through phosphonates is very similar but there are several different variations of the bidentate mode available as seen in Figure 6.2. Tridentate modes are also possible although generally not with TiO_2 . In Figure 6.2, modes 1 – 3 are typical of TiO_2 whilst modes 4 – 5 would be expected for polyoxotitanates (Ti_4L_4 -based cages).³⁴

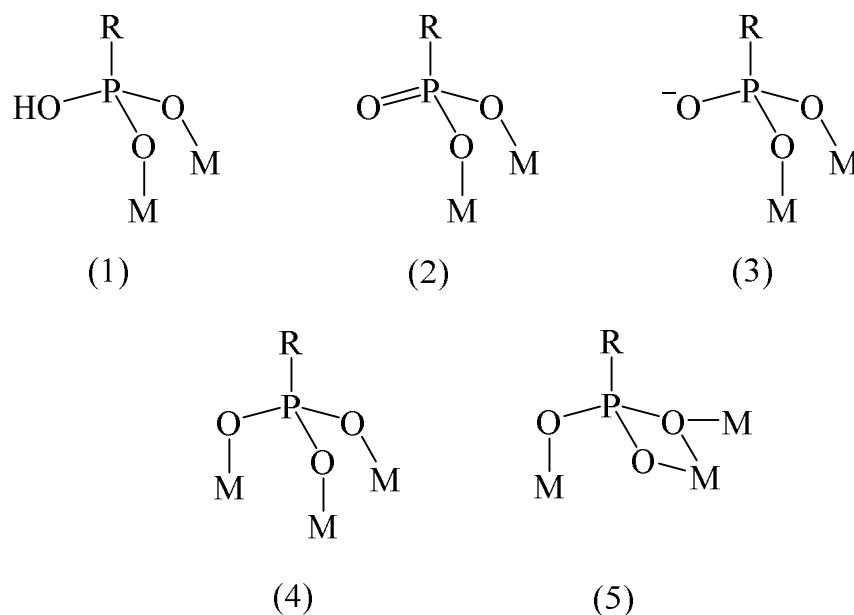


Figure 6.2: Examples of several possible modes of phosphonate binding to a metal oxide surface. M refers to the metal, R can be any ligand.³⁴

The modes of binding should not change when considering tantalum oxides as opposed to TiO_2 as they are both metal oxides capable of attaching to an anchor group.

Having established the purpose of the anchor group present on the complex and identified its potential modes of binding, the choice of semiconductor itself can be considered. TiO_2 is an abundant metal oxide found readily in the Earth's crust. This allows for a low cost, which is a potential consideration when designing a system, although it is only a small factor at this stage of the research. The band gap of unmodified TiO_2 is 3.2 eV,³⁵ which means that it only absorbs ultraviolet light, hence its white colouration. This is a problem when trying to design a photo-electro-system as visible region light is required in order to maximise solar absorption and improve catalytic efficiency. However, TiO_2 anatase has shown the potential for surface modification through surface preparation conditions resulting in a bandgap of 2 eV.³⁵ This results in a shift into the red region of the spectrum and would be far more suitable for a solar light absorbing device.

Another light absorbing semiconductor is tantalum oxide, Ta_2O_5 , which similarly to TiO_2 , is a white, UV absorbing material, with a band gap of 3.7 eV.³⁶ This again puts it

outside of the useful range. However, by using nitrogen doping it is possible to alter the band gap and reduce it to 1.8 eV,³⁶ putting it inside the visible region. The level of doping is controllable through synthetic conditions allowing for further tuning of the band gap as evidenced by the different absorption profiles seen visually through differing colouration of the material, e.g. yellow or orange.

Therefore, both TiO₂ and doped tantalum oxide appear to be suitable candidates for incorporation with the novel rhenium complex to produce a photo-electro-catalytic system capable of CO₂ reduction.

6.1.2. Experimental Design

Aims (ii) and (iii) of this chapter require the establishment of methodologies for the anchoring the complex to a semiconductor and to determine if the anchoring has been successful. Presented below are the details of the preparation of samples and the results of the subsequent experiments designed to determine the success of the preparation method. This includes the use of TiO₂ or nitrogen-doped tantalum oxide, N-Ta₂O₅, and anchoring the rhenium complex to it. Model compounds have also been used with the N-Ta₂O₅ and the results are presented. UV-Vis absorption was used as the primary method of determining if the complex has been anchored to the semiconductor. However, XPS analysis has also been performed on a variety of samples containing either raw tantalum oxide, doped and undoped, or with the rhenium complex, Re(CO)₃Cl{bpy(CH₂PO₃H₂)₂} attached.

6.2. Anchoring Re(CO)₃Cl{bpy(CH₂PO₃H₂)₂} onto TiO₂

TiO₂ slides that we had in the laboratory were used. These are a thin film of TiO₂ that has been adhered to a glass slide. The purpose of the test was to determine if the Re(CO)₃Cl{bpy(CH₂PO₃H₂)₂} complex would anchor to TiO₂ and to try to determine how much complex had been attached. The initial results showed the complex was absorbed onto the TiO₂ but we were unable to measure the amount directly.

A different approach of measuring the concentration of complex absorbed onto the TiO₂ was then carried out. This was achieved by analysing the concentration of

complex left in the supernatant. We initially had difficulty monitoring the anchoring of complexes onto semiconductors. However, with guidance from our collaborators, it was determined that the problem was the concentration of complex was too high for the amount of semiconductor being used. Once this was significantly reduced, the expected results were forthcoming.

6.2.1. Preparation of $\text{Re}(\text{CO})_3\text{Cl}\{\text{bpy}(\text{CH}_2\text{PO}_3\text{H}_2)_2\}$ onto TiO_2

Experiment 1 – General method: A 1.5 mM solution of $\text{Re}(\text{CO})_3\text{Cl}\{\text{bpy}(\text{CH}_2\text{PO}_3\text{H}_2)_2\}$ in DMSO was prepared. The solution was applied using a pipette; the slide was covered with a watch glass to prevent contamination and was left overnight. The next day the solution was removed from the slide, which was then washed with water and then acetone before being allowed to dry. In Figure 6.3, a faint yellow colouring can be seen on the slide, where before there was no colour visible.



Figure 6.3: A glass slide with a TiO_2 film on which $\text{Re}(\text{CO})_3\text{Cl}\{\text{bpy}(\text{CH}_2\text{PO}_3\text{H}_2)_2\}$ has been anchored onto overnight.

Experiment 2 – General method: $\text{Re}(\text{CO})_3\text{Cl}\{\text{bpy}(\text{CH}_2\text{PO}_3\text{H}_2)_2\}$ (0.65 mg, 10 μmol) was dissolved in DMF (25 mL). UV-Vis spectroscopy was then performed on the solution. TiO_2 (0.5 g) was then added to the solution. The solution was stirred for 1 hour before being centrifuged and a light yellow powder collected. The supernatant was collected and a UV-Vis spectrum was obtained.

6.2.2. Results and Discussion of $\text{Re}(\text{CO})_3\text{Cl}\{\text{bpy}(\text{CH}_2\text{PO}_3\text{H}_2)_2\}$ onto TiO_2

The results from experiment 1 were encouraging, in that the previously colourless slide now shows a faint yellow colouring. UV-Vis spectroscopy was attempted on the slide but it was not possible to position it in exactly the same place both before and after absorption of the complex. This resulted in different amounts of UV-Vis absorption due to the solid nature of the TiO_2 . From this it was determined that the best way to monitor the amounts of complex absorbed onto the surface would be by analysing the supernatant rather than the TiO_2 directly.

The results from experiment 2 are shown in

Figure 6.4. In which we were able to monitor the uptake of $\text{Re}(\text{CO})_3\text{Cl}\{\text{bpy}(\text{CH}_2\text{PO}_3\text{H}_2)_2\}$ from solution onto a TiO_2 powder, 25 Å particle size. As can be seen, before the TiO_2 powder was added there is a strong absorption band at 372 nm. After 1 hour, the solution has clearly undergone a dramatic reduction in absorption. This could be seen visually as well as in the UV-Vis spectrum as the solution went from a bright yellow colour to a colourless solution within 1 hour.

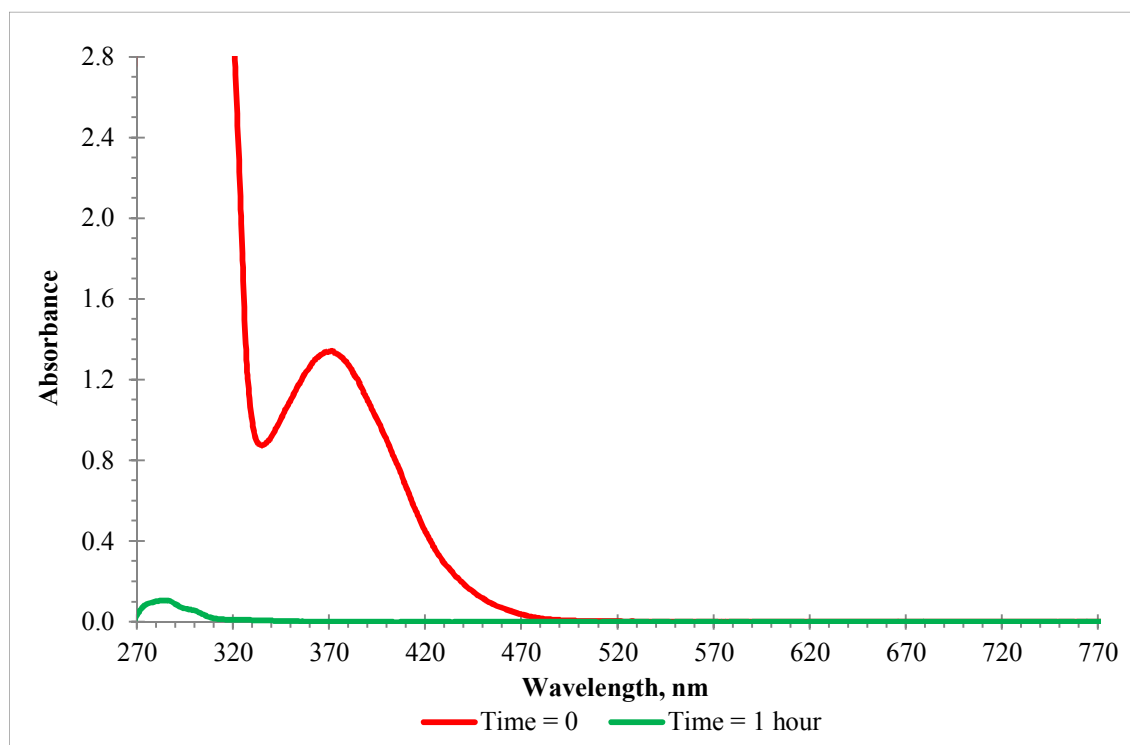


Figure 6.4: The UV-Vis spectrum of $\text{Re}(\text{CO})_3\text{Cl}\{\text{bpy}(\text{CH}_2\text{PO}_3\text{H}_2)_2\}$, 0.1 μmol per 5 mg of TiO_2 in DMF, before, and 1 hour after the TiO_2 was added.

6.3. Anchoring Complexes onto N-Ta₂O₅

This next section details the work performed whilst trying to anchor various compounds to a nitrogen-doped semiconductor, N-Ta₂O₅. This semiconductor was seen in the work of Sato et al.²⁶ in combination with their ruthenium catalyst. Due to the semiconductor absorbing in visible region we decided to use it ourselves but in conjunction with our rhenium catalyst to produce a new heterogeneous system.

Some preliminary work using the free ligand dcbpy and a platinum complex was carried out in order to test the viability of the semiconductor and establish a method for monitoring the attachment of the rhenium complex.

6.3.1. Preparation of N-Ta₂O₅

The N-Ta₂O₅ (nitrogen-doped Ta₂O₅) was synthesised by Dr Robert Mitchell, at the University of York. Ta₂O₅ was doped by adding NH₃ gas to the reacting furnace. The temperature was raised by 5 °C per minute until a temperature of 700 °C was reached. This was maintained for 3 hours before being allowed to cool.

6.3.2. Preparation of Dcbpy onto N-Ta₂O₅

General method: dcbpy (9.1 mg, 0.0375 mmol) was dissolved in DMSO (25 mL). A UV-Vis spectrum of the solution was obtained. N-Ta₂O₅ (50 mg) was added to the solution and the solution stirred for 1 hour. The solution was then centrifuged and the UV-Vis spectrum of the supernatant was collected.

6.3.3. Results and Discussion of Dcbpy onto N-Ta₂O₅

Figure 6.5 details the results of the initial trial work carried out to determine if it was possible to monitor the anchoring of a ligand onto a semiconductor using UV-Vis absorption spectroscopy. This test involved the use of the ligand dcbpy, 1.5 mM, the doped semiconductor, N-Ta₂O₅ and DMSO as the solvent. The solutions UV-Vis

spectrum was taken before the semiconductor was added and can be seen as the red line in Figure 6.5. The N-Ta₂O₅ was then added and the solution stirred for 1 hour. The solution was then centrifuged and the UV-Vis spectrum of the supernatant was collected, seen as the green line. As is shown there is clearly a decrease in the absorption for one of the bands, this suggests that the ligand has been able to anchor on to the semiconductor, reducing its concentration in solution hence the decrease in absorption. This was quite promising, however, more work was needed to try to determine if the success was due to only the free ligand being present or whether the different solvent used had any effect on anchoring.

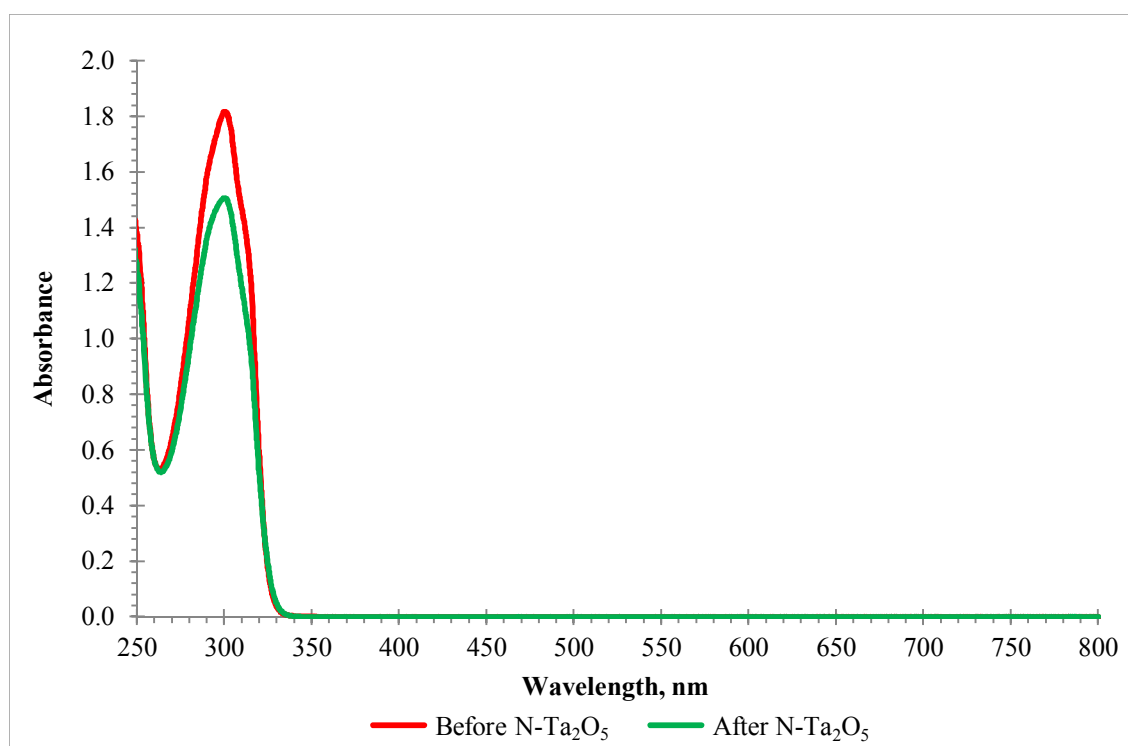


Figure 6.5: The UV-Vis spectra of dcbpy, 1.5 mM in DMSO, before, and after N-Ta₂O₅ was added.

6.3.4. Preparation of PtCl₂(dcbpy) onto N-Ta₂O₅

The next series of experiments involved dcbpy but complexed to platinum. The PtCl₂(dcbpy) was synthesised by Dr Paul Scattergood and was pure upon receiving.

Experiment 3 – General method: $\text{PtCl}_2(\text{dcbpy})$ (5.06 mg, 0.01 mmol) was dissolved in DMF (10 mL). A UV-Vis spectrum of the solution was obtained. $\text{N-Ta}_2\text{O}_5$ (50 mg) was added to the solution and the solution stirred for a set time (15 minutes, 90 minutes, 18 hours). The solution was either carefully decanted or centrifuged for 15 minutes before a sample of the supernatant was taken and the UV-Vis spectrum obtained.

Experiment 4 – General method: $\text{PtCl}_2(\text{dcbpy})$ (2.53 mg, 0.005 mmol) was dissolved in DMF (10 mL). A UV-Vis spectrum of the solution was obtained. $\text{N-Ta}_2\text{O}_5$ (50 mg) was added to the solution and the solution stirred for a set time (1, 2, 3, and 4 hours). The solution was centrifuged for 15 minutes before a sample was taken. After 4 hours, TEA was added and the solution left for an additional hour before another UV-Vis spectrum was obtained. As an additional check, the solution was left stirring for 3 days before a final UV-Vis spectrum was obtained.

6.3.5. Results and Discussion of $\text{PtCl}_2(\text{dcbpy})$ onto $\text{N-Ta}_2\text{O}_5$

Figure 6.6 shows the results of experiment 3, the work carried out to determine if it was possible to monitor the anchoring of a desired metal complex onto a semiconductor using UV-Vis absorption spectroscopy. It shows the absorption spectrum of the $\text{PtCl}_2(\text{dcbpy})$ before the semiconductor was added and then at several different time intervals after the semiconductor was added. As can be seen there is no change in the absorbance spectrum for any of the traces. There are two possible explanations for this, either the complex did not anchor onto the semiconductor or the change in absorbance is too small to be seen on our instrument.

Figure 6.7 is a repeat of the previous experiment but the time intervals are more regular and the solution was centrifuged rather than decanted in order to obtain a sample for testing. As the figure shows, there is no change in absorption after 4 hours. TEA was then added to try and deprotonate all of the acid groups to provide the best chance of anchoring. However even after 3 days in solution, there was no marked decrease in the absorption spectrum. There are a few small changes in the spectrum i.e. a blue shift and

a change in intensity for some of the bands but these are attributed to the presence of the TEA rather than the effect of the complex anchoring on to the semiconductor.

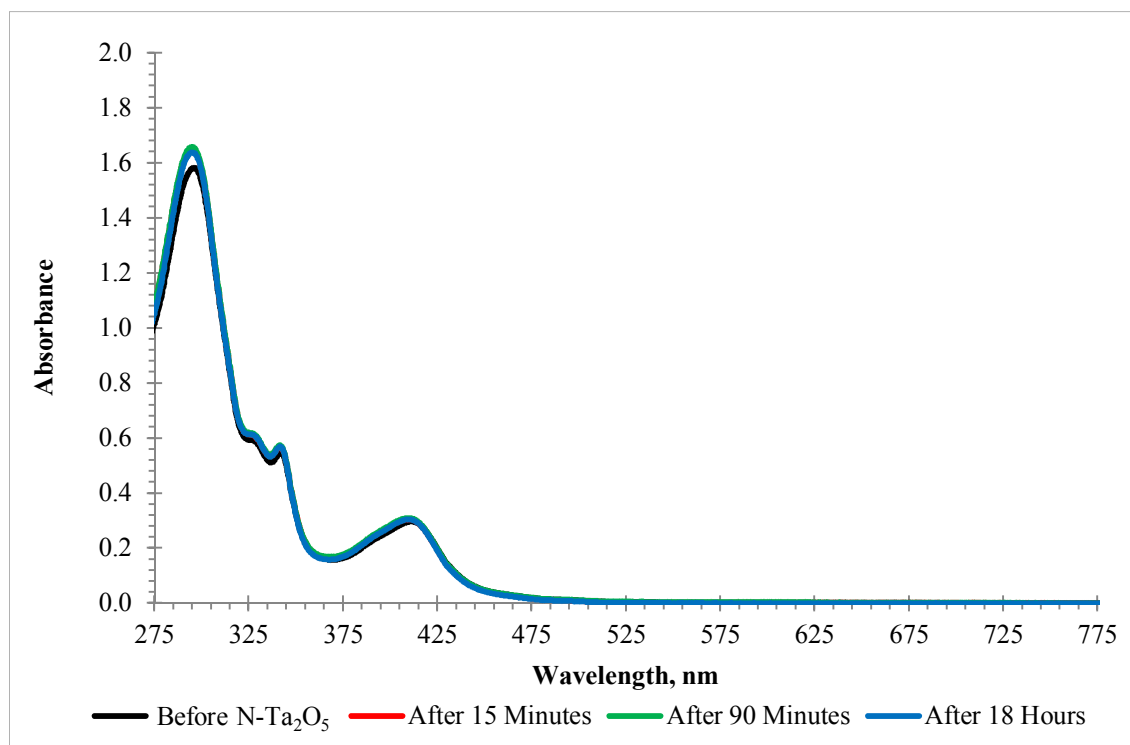


Figure 6.6: The UV-Vis spectra of PtCl₂(dcbpy), 1 mM in DMF with and without N-Ta₂O₅ at different time delays.

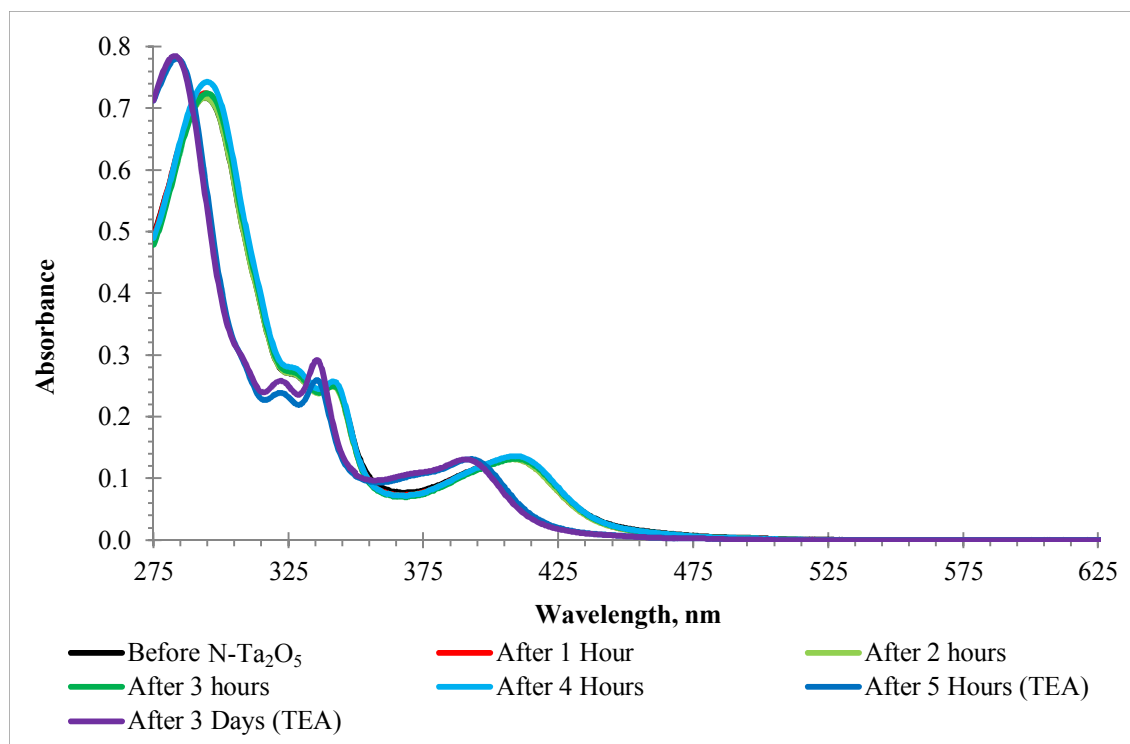


Figure 6.7: The UV-Vis spectra of $\text{PtCl}_2(\text{dcbpy})$, 0.5 mM in DMF with and without N- Ta_2O_5 and with and without TEA at different time delays.

6.3.6. Preparation of $\text{Re}(\text{CO})_3\text{Cl}\{\text{bpy}(\text{CH}_2\text{PO}_3\text{H}_2)_2\}$ onto N- Ta_2O_5

Despite not initially being able to fully monitor uptake of complexes being anchored on to the semiconductors, it was possible to do so visually. This is shown in Figure 6.8, although the yellow colouration is only slight. These samples were prepared using a method similar to the one outlined earlier. A solution of the complex, $\text{Re}(\text{CO})_3\text{Cl}\{\text{bpy}(\text{CH}_2\text{PO}_3\text{H}_2)_2\}$, 2 mM in DMSO was prepared. This was then added to the Ta_2O_5 semiconductor, they were then stirred overnight. The powder was then extracted by centrifuge, washed with water then acetone, resulting in a light yellow powder.

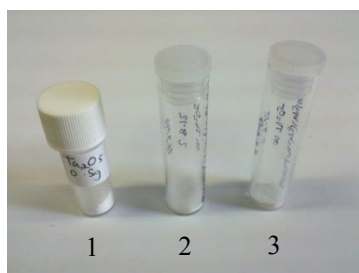


Figure 6.8: Tube 1 contains a sample of raw Ta_2O_5 . Tubes 2 – 3 contain samples of Ta_2O_5 that have had $\text{Re}(\text{CO})_3\text{Cl}\{\text{bpy}(\text{CH}_2\text{PO}_3\text{H}_2)_2\}$ anchored onto the surface.



Figure 6.9: Tube 1 contains a sample of raw N- Ta_2O_5 . Tube 2 contains a sample of N- Ta_2O_5 that has had $\text{Re}(\text{CO})_3\text{Cl}\{\text{bpy}(\text{CH}_2\text{PO}_3\text{H}_2)_2\}$ anchored onto the surface.

The sample shown in Figure 6.9 was prepared in an identical manner to that described above except that N- Ta_2O_5 was used instead of Ta_2O_5 . It was difficult to

observe visually whether the anchoring process was successful as the initial N-Ta₂O₅ is an orange powder.

6.4. X-ray Photoelectron Spectroscopy (XPS)

Another method of determining whether a complex is anchored to the surface of the semiconductor is to use XPS. Each element on the periodic table has a unique fingerprint of binding energy peaks that allow the element to be identified. These peaks arise from the electron configuration of the atom and therefore because each element has a different electron configuration so too is the pattern of binding energy peaks different. Using this information and the amount of electrons detected for each peak it is possible to work out the relative percentages of each element within the sample. In order to maximise the number of samples that can be run in any one session they are all prepared simultaneously.

6.4.1. Preparation of XPS Samples

The solid sample is applied to a piece of double-sided tape, the other side of which is attached to a metal plate. Once all of the samples, in this case 9, are ready, they are placed within the vacuum chamber of the machine. The chamber is capable of producing an ultra-high vacuum, less than 10⁻¹⁰ atm, and is then heated to 200 °C. This eliminates any traces of water or other volatile substances either in the chamber or on the samples. This level of vacuum is needed so that only the electrons generated by the X-ray source hitting the sample are present. If there are any other molecules present, they could interact with the electrons before they reach the detector and produce inaccurate results.

Multiple samples are prepared using the method outlined in section 6.3.6, these were given the following abbreviations;

N-Ta₂O₅ – This is the raw nitrogen-doped Ta₂O₅ semiconductor powder.

N-Ta₂O₅RuOH – This is the nitrogen-doped Ta₂O₅ semiconductor with the ruthenium complex, Ru(CO)₂(Me₂bpy){bpy(CH₂PO₃H₂)₂} attached.

N-Ta₂O₅ReOH – This is the nitrogen-doped Ta₂O₅ semiconductor with the rhenium complex, Re(CO)₃Cl{bpy(CH₂PO₃H₂)₂} attached.

N-Ta₂O₅ReOH-B – Same as above but using a basic solution (NaOH, pH 9) to attach the Re(CO)₃Cl{bpy(CH₂PO₃H₂)₂} complex.

ReOH – This is the free Re(CO)₃Cl{bpy(CH₂PO₃H₂)₂} complex.

Ta₂O₅ – This is the raw undoped Ta₂O₅ semiconductor powder.

Ta₂O₅RuOH – This is the undoped Ta₂O₅ semiconductor with ruthenium complex, Ru(CO)₂(Me₂bpy){bpy(CH₂PO₃H₂)₂} attached.

Ta₂O₅ReOH – This is the undoped Ta₂O₅ semiconductor with rhenium complex, Re(CO)₃Cl{bpy(CH₂PO₃H₂)₂} attached.

Ta₂O₅ReOH-B – This is the same as above but using a basic solution (NaOH, pH 9) to attach the Re(CO)₃Cl{bpy(CH₂PO₃H₂)₂} complex.

6.4.2. Results and Discussion of XPS Samples

Table 6.1: The relative elemental abundance of each element present within the samples analysed using XPS.

Sample Identifier	Elemental abundance, %												
	Br 3d	C 1s	Ca 2p	Cl 2p	F 1s	N 1s	Na 1s	O 1s	P 2p	Re 4f	Ru 3d	Ta 4f	Zn 2p
N-Ta ₂ O ₅		28.5				7.9		37.8				25.9	
N-Ta ₂ O ₅ RuOH		34.4				7.5		35.0	1.4		0.6	21.1	
N-Ta ₂ O ₅ ReOH		28.7				6.6		37.4	1.9	2.6		22.9	
N-Ta ₂ O ₅ ReOH-B		29.7	2.6	0.2	4.4	6.2	0.3	35.2	0.0	1.7		18.9	0.7
ReOH	3.0	59.5				6.1		22.9	5.8	2.6			
Ta ₂ O ₅		28.1				1.8		46.8				23.3	

Ta ₂ O ₅ RuOH		26.7		0.2		1.5		48.0	1.4		0.3	21.8	
Ta ₂ O ₅ ReOH		25.5		0.4		0.9		48.3	1.4	3.0		20.5	
Ta ₂ O ₅ ReOH-B		30.3	1.8	0.1		19.3	0.2	32.9	0.0	1.3		13.8	0.3

This technique is highly sensitive and often elements are detected that are not expected to be in the sample. For example, the ReOH sample contains bromine, which is present because the hydrolysis of the ester required TMSBr and despite purification, there is evidently some still present in the sample. The samples that were prepared under basic conditions have Ca and Na and Zn present. All of these can be explained due to the use of water in the preparation, obviously the water used was not completely deionised. However, the main elements that are important are Re and Ru, these are present or absent in the samples that they should be. This provides evidence that allows us to say with reasonable certainty that the complexes have been successfully anchored onto the semiconductors.

Now that a method for attaching the complex to the semiconductor has been established, the next step was to perform a series of electrochemical and GC experiments using both the complex that works, $\text{Re}(\text{CO})_3\text{Cl}\{\text{bpy}(\text{CH}_2\text{PO}_3\text{H}_2)_2\}$ and the N-Ta₂O₅ semiconductor together. To this end, our collaborators were going to send an electrode made from N-Ta₂O₅, this would then have the complex anchored onto its surface using the method described above. The electrode would then be used in the bulk electrolysis setup and the results from the GC analysis collected and processed. Unfortunately, this electrode could not be produced at this time. This means that at present the complex $\text{Re}(\text{CO})_3\text{Cl}\{\text{bpy}(\text{CH}_2\text{PO}_3\text{H}_2)_2\}$ and the N-Ta₂O₅ semiconductor have not been tested together and so there are no results to show or discuss at present.

6.5. Summary

The purpose of the work in this chapter was to examine how the anchoring groups can be attached to the semiconductor, N-Ta₂O₅, we are currently using. Work on TiO₂ was also carried out as the material was readily available in the lab. The work using TiO₂ was promising, with both visible observations and UV-Vis spectra providing evidence of anchoring on the TiO₂ surface. Work on the N-Ta₂O₅ and Ta₂O₅ semiconductor was also presented and after some initial failure when using DMF as the solvent, attachment does appear to occur when using DMSO instead. This was demonstrated both visually and by the process of XPS, which was able to identify rhenium present on the surface of the semiconductor. Electrochemical and GC experiments were then planned to be carried out using the rhenium complex and the N-Ta₂O₅ semiconductor in conjunction with each other, but we are unable to present that work at this time. However, it should be possible to do so in future if a suitable electrode can be constructed.

6.6. Consideration of Random and Systematic Errors

In the above sections, the photophysical data was discussed. The values obtained from these experiments could potentially be affected by random or systematic error. During the determination of the photophysical properties, it is likely that random errors have occurred during measurement collection in addition to those present during sample preparation. The balance is capable of weighing to ± 0.0001 g and has an enclosed case to reduced atmospheric pressure fluctuations. Vibrations are dampened by the presence of shock absorbers, further reducing random errors. This will result in minimal random errors associated with any mass values. Systematic error should also be minimal due to taring of the balance before each use. The error for the volume of a solution used is likely to be negligible due to the use of microlitre syringes for extinction coefficient determination, assuming proper calibration. Random errors caused by the instruments themselves are unlikely to be of concern as they are capable of measuring to 3 – 4 decimal places thus our values will have more error due to simple rounding than because of random error. This is not true however for the potential systematic error for which great care must be taken to properly zero the instruments and subsequently

perform suitable background scans to subtract from the actual scans. This removes both the sample cuvette and the solvent signals allowing for measurement of the actual sample.

The XPS technique is extremely sensitive as demonstrated by the detection of elements present in the sample that were not expected to be there. This sensitivity in combination with the technique itself requiring an extremely high vacuum, thus eliminating environmental fluctuations, means that random errors are unlikely to be of any concern. Systematic errors may arise due to the sample area tested being very small. This could result in a misrepresentation of how much of a particular element is present if it is concentrated in a particular area. However, due to the samples being in powder form prior to being adhere to the sample plate for testing, it is reasonable to assume that the elements are evenly distributed throughout the sample.

Taking into account all of these sources of error and their potential size it is unlikely that they will have any significant impact on our results or conclusions. Therefore, repeat readings were often not necessary hence, no statistical analysis could be performed.

6.7. References

1. J. B. Asbury, A. J. Nozik, R. J. Ellingson, H. N. Ghosh, S. Ferrere and T. Lian, *J. Phys. Chem. B*, 1999, **103**, 3110–3119.
2. S. A. Trammell, J. A. Moss, J. C. Yang, B. M. Nakhle, C. A. Slate, F. Odobel, M. Sykora, B. W. Erickson and T. J. Meyer, *Inorg. Chem.*, 1999, **38**, 3665–3669.
3. A. F. Nogueira, A. L. B. Formiga, H. Winnischofer, M. Nakamura, F. M. Engelmann, K. Araki and H. E. Toma, *Photochem. Photobiol. Sci.*, 2004, **3**, 56–62.
4. S. Uchida, Y. Yamamoto, Y. Fujishiro, A. Watanabe, O. Ito and T. Sato, *J. Chem. Soc., Faraday Trans.*, 1997, **93**, 3229–3234.
5. C. Nasr, P. V. Kamat and S. Hotchandani, *J. Phys. Chem. B*, 1998, **102**, 10047–10056.
6. K. Hara, H. Sugihara, Y. Tachibana, A. Islam, M. Yanagida, K. Sayama and H. Arakawa, *Langmuir*, 2001, **17**, 5992–5999.
7. R. Ghanem, Y. Xu, J. Pan, T. Hoffmann, J. Andersson, T. Polívka, T. Pascher, S. Styring, L. Sun and V. Sundström, *Inorg. Chem.*, 2002, **41**, 6258–6266.

8. H. Zabri, I. Gillaizeau, C. A. Bignozzi, S. Caramori, M.-F. Charlot, J. Cano-Boquera and F. Odobel, *Inorg. Chem.*, 2003, **42**, 6655–6666.
9. C. She, J. Guo and T. Lian, *J. Phys. Chem. B*, 2007, **111**, 6903–6912.
10. X.-H. Wu, S. Wang, Y. Guo, Z.-Y. Xie, L. Han and Z.-H. Jiang, *Chin. J. Chem.*, 2008, **26**, 1939–1943.
11. S. Ardo and G. J. Meyer, *Chem. Soc. Rev.*, 2009, **38**, 115–164.
12. A. Grabulosa, M. Beley, P. C. Gros, S. Cazzanti, S. Caramori and C. A. Bignozzi, *Inorg. Chem.*, 2009, **48**, 8030–8036.
13. T. W. Woolerton, S. Sheard, E. Reisner, E. Pierce, S. W. Ragsdale and F. A. Armstrong, *J. Am. Chem. Soc.*, 2010, **132**, 2132–2133.
14. C. L. Anfuso, R. C. Snoberger, A. M. Ricks, W. Liu, D. Xiao, V. S. Batista and T. Lian, *J. Am. Chem. Soc.*, 2011, **133**, 6922–6925.
15. S. Qin, F. Xin, Y. Liu, X. Yin, W. Ma and H. Nöth, *J. Colloid Interface Sci.*, 2011, **356**, 257–261.
16. T. J. LaTempa, S. Rani, N. Bao and C. A. Grimes, *Nanoscale*, 2012, **4**, 2245–2250.
17. L. Liu, H. Zhao, J. M. Andino and Y. Li, *ACS Catal.*, 2012, **2**, 1817–1828.
18. M. Oftadeh, A. Aghtar, M. Salavati-Niasari, M. N. Esfahani and N. Mir, *J. Iran. Chem. Soc.*, 2012, **9**, 143–149.
19. G. Zeng, J. Qiu, Z. Li, P. Pavaskar and S. B. Cronin, *ACS Catal.*, 2014, **4**, 3512–3516.
20. C. D. Windle, E. Pastor, A. Reynal, A. C. Whitwood, Y. Vaynzof, J. R. Durrant, R. N. Perutz and E. Reisner, *Chem. Eur. J.*, 2015, **21**, 3746–3754.
21. G. R. Dey, *J. Nat. Gas Chem.*, 2007, **16**, 217–226.
22. A. Dhakshinamoorthy, S. Navalon, A. Corma and H. Garcia, *Energy Environ. Sci.*, 2012, **5**, 9217–9233.
23. W.-J. Chun, A. Ishikawa, H. Fujisawa, T. Takata, J. N. Kondo, M. Hara, M. Kawai, Y. Matsumoto and K. Domen, *J. Phys. Chem. B*, 2003, **107**, 1798–1803.
24. R. Nashed, W. M. I. Hassan, Y. Ismail and N. K. Allam, *Phys. Chem. Chem. Phys.*, 2013, **15**, 1352–1357.
25. T. Morikawa, S. Saeki, T. Suzuki, T. Kajino and T. Motohiro, *Appl. Phys. Lett.*, 2010, **96**, 142111–142113.
26. S. Sato, T. Morikawa, S. Saeki, T. Kajino and T. Motohiro, *Angew. Chem. Int. Ed.*, 2010, **49**, 5101–5105.
27. T. M. Suzuki, T. Nakamura, S. Saeki, Y. Matsuoka, H. Tanaka, K. Yano, T. Kajino and T. Morikawa, *J. Mater. Chem.*, 2012, **22**, 24584–24590.
28. F. Yoshitomi, K. Sekizawa, K. Maeda and O. Ishitani, *ACS Appl. Mater. Interfaces*, 2015, **7**, 13092–13097.

29. K. Maeda, K. Sekizawa and O. Ishitani, *Chem. Commun.*, 2013, **49**, 10127–10129.
30. K. Maeda, R. Kuriki, M. Zhang, X. Wang and O. Ishitani, *J. Mater. Chem. A*, 2014, **2**, 15146–15151.
31. C. She, J. Guo, S. Irle, K. Morokuma, D. L. Mohler, H. Zabri, F. Odobel, K.-T. Youm, F. Liu, J. T. Hupp and T. Lian, *J. Phys. Chem. A*, 2007, **111**, 6832–6842.
32. K. Kilså, E. I. Mayo, B. S. Brunshwig, H. B. Gray, N. S. Lewis and J. R. Winkler, *J. Phys. Chem. B*, 2004, **108**, 15640–15651.
33. K. Westermark, H. Rensmo, A. C. Lees, J. G. Vos and H. Siegbahn, *J. Phys. Chem. B*, 2002, **106**, 10108–10113.
34. Y. Chen, E. Trzop, J. D. Sokolow and P. Coppens, *Chem. Eur. J.*, 2013, **19**, 16651–16655.
35. C. Dette, M. A. Pérez-Osorio, C. S. Kley, P. Punke, C. E. Patrick, P. Jacobson, F. Giustino, S. J. Jung and K. Kern, *Nano Lett.*, 2014, **14**, 6533–6538.
36. R. Jinnouchi, A. V. Akimov, S. Shirai, R. Asahi and O. V. Prezhdo, *J. Phys. Chem. C*, 2015, **119**, 26925–26936.

7. Collaborations and Publications

7.1. Introduction

In addition to the primary work detailed in the previous chapters of this thesis, several other research projects have also been carried out, all in the broad area of photochemistry of coordination compounds. These have taken the form of collaborations with other research groups within the chemistry department at the University of Sheffield or with other members of our research group. These collaborations proved highly successful and have resulted in several publications in peer reviewed internationally recognised journals. Other work has been presented at various symposia during the course of the thesis.

This research was conducted in parallel with the studies of the catalysts for CO₂ reduction. The potential of transition metal complexes as photocatalysts / photo-electrocatalysts has long been known. To this end, it was interesting to investigate light-induced processes in several complexes related to, but not directly designed for, photo-electro-catalysis.

These include ruthenium(II) complexes for the purpose of DNA binding {with Prof. J. A. Thomas, publication (i)}, studies of electron and energy transfer in iridium(III) complexes and their lanthanide based d-f dyads {with Prof. M. D. Ward, publications (ii, iii)}. Publication (iv) details the work on furthering our understanding of the dynamics of the initial stages of vibrational energy transfer in ruthenium(II) bipyridine complexes that are similar to those described in chapter 4, and indeed are a derivative of the famous “N3” dye for dye-sensitised solar cells. The references to the full papers, a brief outline, and a summary of my contributions to these studies are given below.

7.2. Collaborations

7.2.1. Publication (i)

Synthesis, Characterization, and DNA Binding Properties of Ruthenium(II) Complexes Containing the Redox Active Ligand Benzo[i]dipyrido[3,2-a,2'3'-c]phenazine-11,16-quinone. S. P. Foxon, C. Green, M. G. Walker, A. Wragg, H.

Adams, J. A. Weinstein, S. C. Parker, A. J. H. M. Meijer and J. A. Thomas, *Inorg. Chem.*, 2012, **51**, 463–471.

Work in the Thomas group has for a number of years focused on ruthenium(II) complexes,^{1,2} including their propensity for DNA binding.^{3,4} Previous work in the field has concerned ruthenium complexes containing a conjugated, flat, intercalating ligand, dppz (dipyrido[3,2-a:2',3'-c]phenazine) or dppn (benzo[i]-dipyrido[3,2-a:2',3'-c]phenazine). The dppz complexes in particular exhibit an interesting “light switch effect” whereby no luminescence is observed in water due to the excited states being quenched by water molecules through interaction with the N-atoms of the phenazine part. Whereas emission is switched “on” in acetonitrile, or in DNA where intercalation protects the compound from interactions with water molecules. Overall, ruthenium(II) polypyridyl complexes have rich photophysical properties involving several close-lying excited states, some or all of the may be not emissive and therefore require methods such as transient absorption spectroscopy, to investigate their dynamics.

The purpose of this work was to investigate the photophysical, electrochemical, and DNA binding properties of three new qdppn containing ruthenium complexes to enable a comparison between these new intercalators and their dppn analogues. Qdppn (benzo[i]dipyrido[3,2-a:2',3'-c]phenazine-11,16-quinone) is a quinone containing analogue, with the quinone component capable of functioning as a reversible $2e^-$ redox couple and possesses good acceptor properties.

The paper reported that a new, higher yielding method of synthesis was established for the qdppn ligand. A series of hexagonal channels that are occupied by anions and solvent molecules were identified from the X-ray crystal structure of the complex, $[\text{Ru}(\text{phen})_2(\text{qdppn})](\text{PF}_6)_2$ (phen = 1,10-phenanthroline). These channels are the result of a combination of π - π stacking between the phen and qdppn ligands, and anion-ligand hydrogen bonding. Photophysical experiments demonstrated the new qdppn complexes lack of luminescence and their poor singlet oxygen sensitization capabilities. Electrochemical studies were performed, revealing low-lying qdppn-based unoccupied

orbitals. Density functional theory (DFT) calculations predicted the presence of a charge separated state involving the quinone moiety of qdppn. Time-resolved studies were conducted to try to confirm this prediction. The DNA binding properties of the qdppn complexes were also examined, with the binding affinities found to be comparable with the previously studied dppn analogues.

Summary of our contribution – Nanosecond flash photolysis experiments on $[\text{Ru}(\text{phen})_2(\text{qdppn})]^{2+}$ [6] as both the $[\text{PF}_6]^-$ and $[\text{Cl}]^-$ salts in CH_3CN , and water were performed. A hypothesis was suggested that a charge-separated state located on the quinone moiety of the coordinated qdppn was being produced. However, our results showed that on a time scale from 22 ns and longer, no ground state bleaches or transient signals were observed in the range from 380 to 700 nm. Thus, a formation of long-lived charge-separated excited state in these complexes was disproved. These studies were conducted under an excitation wavelength of 355 nm, using the custom-built nanosecond flash photolysis set-up as described in the paper and in chapter 2 of this thesis.

7.2.2. Publication (ii)

d→*f* Energy Transfer in Ir(III)/Eu(III) Dyads: Use of a Naphthyl Spacer as a Spatial and Energetic “Stepping Stone”. D. Sykes, S. C. Parker, I. V. Sazanovich, A. Stephenson, J. A. Weinstein, and M. D. Ward, *Inorg. Chem.*, 2013, **52**, 10500–10511.

For several years, work in the Ward group has revolved around transition metal complexes⁵⁻⁹ and lanthanide containing dyads. One potential application of this work is creating white light from a single molecule. Another application is for cellular imaging, taking advantage of the differing time scales and wavelengths that the d and f block components both luminesce at, e.g., Eu(III) in the visible region and Yb(III) or Nd(III) in the near-IR regions.

The main question of this paper was to identify and try to understand the mechanism of $d \rightarrow f$ energy-transfer. It was suggested that an intermediate charge-transfer state was contributing to the overall process. However, this was a "dark" state, which could not be detected by emission spectroscopy. Therefore, flash photolysis experiments were performed on a series of luminescent complexes based on $\{\text{Ir}(\text{phpy})_2\}$ (phpy = cyclometallating anion of 2-phenylpyridine) or $\{\text{Ir}(\text{F}_2\text{phpy})_2\}$ (F_2phpy = cyclometallating anion of 2-(2',4'-difluorophenyl)pyridine) units, with an additional 3-(2-pyridyl)-pyrazole (pypz) ligand. Coordination of an $\{\text{Eu}(\text{hfac})_3\}$ unit (hfac = 1,1,1,5,5,5-hexafluoro-pentane-2,4-dionate) to the pypz binding site affords Ir-naphthyl-Eu triads, enabling observation of the $d \rightarrow f$ energy-transfer mechanism.

Crystal structures for several of the complexes were reported in the paper. These show that the naphthyl group can sit close to the Ir core and participate in a π -stacking interaction with a coordinated phpy or F_2phpy ligand. This has an interesting effect on the luminescence lifetimes, with the $\{\text{Ir}(\text{phpy})_2(\text{pypz})\}$ complexes showing typical Ir-based emission, but with lengthened lifetimes due to the interaction with the stacked naphthyl group. However, the luminescence for the $\{\text{Ir}(\text{F}_2\text{phpy})_2(\text{pypz})\}$ complexes is nearly quenched. This is because the presence of the F_2phpy ligand results in a blue shift of the ${}^3\text{MLCT}/{}^3\text{LC}$ luminescence of the Ir unit from 477 to 455 nm. This higher energy state is then quenched by the formation of a long-lived naphthyl-centred triplet (${}^3\text{nap}$) state that is detectable by transient absorption spectroscopy. This means that in the $\{\text{Ir}(\text{F}_2\text{phpy})_2\}$ -naphthyl-Eu triad, the initial $\text{Ir} \rightarrow {}^3\text{nap}$ energy-transfer step is followed by a second, slower, ${}^3\text{nap} \rightarrow \text{Eu}$ energy-transfer step. Whereas in the $\{\text{Ir}(\text{phpy})_2\}$ -naphthyl-Eu triad, due to ${}^3\text{nap}$ state being unavailable, the energy transfer occurs directly from the $\text{Ir} \rightarrow \text{Eu}$ instead of via the ${}^3\text{nap}$ intermediate.

Summary of our contribution – In order to test the “dark” state hypothesis, flash photolysis studies were performed on the d-block metal complexes and their Ln-containing dyads. The flash photolysis method allows us to detect absorption spectra of excited states, and is not reliant on the states being emissive. The studies were performed in DCM, at a concentration of 0.1 – 0.3 mM, under an excitation wavelength

of 355 nm. The results (shown in Fig. 5, 6 and Table 4 in the paper) supported the hypothesis of an intermediate, "dark" state, participating in the mechanism of energy transfer for the fluorinated complexes. During the experiments, a large amount of time-resolved spectroscopic data from the various complexes studied was acquired. This was analysed using the Origin Pro package and the built-in global fit procedure, which yielded the spectra and the lifetimes of the various excited states involved, and assisted in creating the overall picture of light-induced processes in these molecules.

7.2.3. Publication (iii)

Sensitisation of Eu(III)- and Tb(III)-based luminescence by Ir(III) units in Ir/lanthanide dyads: evidence for parallel energy-transfer and electron-transfer based mechanisms. D. Sykes, A. J. Cankut, N. M. Ali, A. Stephenson, S. J. P. Spall, S. C. Parker, J. A. Weinstein and M. D. Ward., *Dalton Trans.*, 2014, **43**, 6414–6428.

Energy transfer between the iridium chromophore and the lanthanide ions in the d-f dyads was hypothesised to occur in parallel with the process of electron transfer. Establishing whether these processes did indeed occur in parallel formed the basis of the paper.

The paper details the synthesis and characterisation of a series of Ir(III) complexes to which Eu, Tb or Gd was bound. Photophysical studies of the Ir-Ln (Ln = Tb, Eu) dyads were used to help establish the energy-transfer or electron-transfer mechanisms. The mechanism of photoinduced electron-transfer (PET) was observed in the Ir-Gd dyads where direct Ir→Gd energy-transfer is not possible. This PET quenches the Ir-based luminescence and generates a short-lived charge separated $[\text{Ir}^{4+}]^{\bullet-}(\text{pyrazolyl-pyridine})^{\bullet-}$ state. However, in the Ir-Eu, and Ir-Tb dyad systems, a direct Dexter-type Ir→Ln energy-transfer occurs in addition to the PET process. This is seen with time-resolved luminescence measurements, which show fast and slow rise-time components, associated with the photoinduced electron-transfer and Dexter-based energy-transfer

mechanisms respectively, thus demonstrating that the two mechanisms occur in parallel with each other.

Summary of our contribution – As with the previous paper our contribution was to employ time resolved flash photolysis in order to obtain spectra and lifetime values of any excited state(s) formed upon visible excitation. These data were essential for establishing the presence and identify the energy-transfer and electron transfer processes. The studies were performed in DCM, at a concentration of 0.1 – 0.3 mM, under an excitation wavelength of 355 nm. The experiments generated a large amount of time-resolved spectroscopic data from the various complexes studied. This was again analysed using the Origin Pro package and the built-in global fit procedure; which yielded the spectra and the lifetimes of the various excited states involved. These results, shown in Table 5, Fig. 10, 11 and 12 in the paper, confirm the existence of two parallel mechanisms, a photoinduced electron transfer pathway and Dexter-based energy-transfer pathway.

7.2.4. Publication (iv)

Vibrational energy transfer dynamics in ruthenium polypyridine transition metal complexes. M. Fedoseeva, M. Delor, S. C. Parker, I. V. Sazanovich, M. Towrie, A.W. Parker, and J. A. Weinstein, *Phys. Chem. Chem. Phys.*, 2015, **17**, 1688–1696.

During the last few years, work in the Weinstein group has focused on platinum(II) containing complexes¹⁰⁻¹⁴ and their photophysical properties. More recent work however has included other transition metal complexes including copper¹⁵, rhenium¹⁶ and ruthenium¹⁷ as well as the work contained in this thesis.

The purpose of the research was to gain understanding of the dynamics of the initial stages of vibrational energy transfer in order to improve the performance of solar devices or photocatalysis.

This paper details the experiments and subsequent results from a ruthenium(II) bipyridine complex, $\text{Ru}(4,4'-(\text{COOEt})_2-2,2'\text{-bpy})_2(\text{NCS})_2$, that is analogous to the complexes presented in chapter 4 of this thesis. The studied complex is also a close relative of the well-known “N3” dye that has previously been used in dye-sensitised solar cells. The paper investigates both the vibrational energy transport in the ground and the electronic excited state. These experiments were performed using the relatively new technique of ultrafast two-dimensional infrared spectroscopy. This revealed that the Ruthenium atom acts a “bottleneck” for the energy transfer from the small ligands with high-energy vibrational stretching frequencies, making the process less favourable and lowering the efficiency of vibrational energy flow in the complex. When comparing the vibrational relaxation times in the electronic ground state with those of the excited state, it was found that the latter was significantly faster. This was attributed to a reduction in the structural and thermodynamic barriers due to an increase in the degree of vibrational coupling between CN and Ru–N modes in the excited state. This effect has been observed previously in similar complexes such as, $\text{Re}(4,4'-(\text{COOEt})_2-2,2'\text{-bpy})(\text{CO})_3\text{Cl}$, and may be common for transition-metal complexes with heavy central atoms in general.

Summary of our contribution – Our contribution to the work was the synthesis of the $\text{Ru}(4,4'-(\text{COOEt})_2-2,2'\text{-bpy})_2(\text{NCS})_2$ which was the primary complex studied in the paper. This involved preparing the ligand, complexation to ruthenium(II) centre and column purification. The method was adapted from the supporting information of a paper by Wolfbauer et al.¹⁸

$\text{RuCl}_3 \cdot 3\text{H}_2\text{O}$ (0.156 g, 0.597 mmol) and 2,2'-bipyridine-4,4'-diethylester (0.350 g, 1.166 mmol) were degassed 3 times under argon, after that dimethylformamide (DMF, Grubbs, argon saturated, 20 mL) was added via syringe. The resulting solution was then heated to 130 °C and stirred for 2.5 hours. The reaction temperature was then lowered to 80 °C and NH_4NCS (0.9984 g, 13.116 mmol) was added to the reaction mixture, which was left stirring for another hour. The DMF was then removed under the vacuum, whilst keeping the reaction mixture at 80 °C. Afterwards MeOH (50 mL) was added

and the resulting solution stirred overnight. The solvent was then removed on a rotary evaporator, yielding a red-purple solid product. The product was dissolved in dichloromethane (DCM), filtered and the remaining solid washed with more DCM until the washings became colourless; this procedure removed excess NH_4NCS , which is insoluble in DCM. Excess DCM was removed from the filtrate using a rotary evaporator to approx. 10 mL. This solution was purified using a silica packed column with DCM:ethyl acetate, 5:1 mobile phase. 0.149 g (0.182 mmol, 31% yield) of dark purple product was obtained. ^1H NMR (400 MHz, DMSO-d_6) δ 9.46 (d, $J = 5.8$ Hz, 2H), 9.24 (s, 2H), 9.07 (s, 2H), 8.48 – 8.35 (m, 2H), 7.81 (d, $J = 5.9$ Hz, 2H), 7.60 (dd, $J = 5.9, 1.3$ Hz, 2H), 4.53 (q, $J = 7.0$ Hz, 4H), 4.37 (q, $J = 7.0$ Hz, 4H), 1.45 (t, $J = 7.1$ Hz, 6H), 1.31 (t, $J = 7.1$ Hz, 6H). ToF MS ES^+ : m/z 819.1027.

The results from the photophysical experiments suggest that a central heavy atom in a molecule can affect the propagation of vibrational energy both during and following electron transfer. This could potentially have implications for our own work, which relies on electron transfer from a semiconductor to the electrocatalyst responsible for CO_2 reduction.

7.3. Work Presented at Symposia

The remainder of the work mentioned in this chapter is from research presented at various symposia attended during the course of this thesis.

Publication (v) relates to work done on platinum(II) complexes and their photophysical properties.

Publication (vi) provided brief details of our research on using electrocatalysts for the purpose of CO_2 reduction, the full details of which are contained in this thesis.

Publication (vii) presented details of our groups work in general on transition metal complexes for the purpose of either H_2 production or CO_2 reduction.

The publication references as presented in the relevant book of abstracts and a summary of my contributions to these studies are given below.

7.3.1. Publication (v)

Photoinduced charge separation in platinum(II) diimine acetylide complexes. S. C. Parker, J. Best, I. V. Sazanovich, R. D. Bennett, O. V. Bouganov, N. M. Shavaleev, A. H. Shelton, S. A. Tikhomirov, M. Towrie, J. A. Weinstein, XXIII IUPAC Symposium on Photochemistry, 11 – 16 July 2010, Ferrara, Italy.

The project had utilised platinum(II) bipyridine complexes that undergo electron transfer as part of a charge separated state upon excitation with visible light.

7.3.2. Publication (vi)

CO₂ reduction utilising photo-electro-catalytic approach based on transition metal complex catalysts anchored to semiconductors. S. C. Parker, J. A. Weinstein, R. N. Perutz, 4th EuCheMS Chemistry Congress, 26 – 30 August 2012, Prague, Czech Republic.

At this congress, we presented some of our work on CO₂ reduction using electrocatalysts. This included the synthesis of [Ru(CO)₂(Me₂bpy){bpy(CH₂PO₃H₂)₂}] [PF₆]₂ and Re(CO)₃Cl{bpy(CH₂PO₃H₂)₂} as well as some of the preliminary results from our photophysical and electrochemical experiments on these complexes. The complete results for the ruthenium and rhenium complexes are shown in chapters 4 and 5 respectively.

7.3.3. Publication (vii)

Transition metal photocatalysts for heterogeneous H₂ production and CO₂ reduction. S. C. Parker, S. Archer, M. Delor, M. Towie, I. V. Sazanovich, J. A. Weinstein, 245th American Chemical Society National Meeting and Exposition, 7 – 11 April 2013, New Orleans, USA.

Some of our groups work on photoinduced electron transfer was presented at this meeting. Our group develops transition metal complexes based on Donor-spacer-Acceptor motifs, which efficiently absorb visible light and are capable of anchoring to semiconductors and acting as photosensitizers for H₂ production. Some of the work on CO₂ reduction was also shown at this meeting in the interest of presenting new ideas to the wider scientific community.

7.4. References

1. C. Metcalfe and J. A. Thomas, *Chem. Soc. Rev.*, 2003, **32**, 215–224.
2. C. Metcalfe, I. Haq and J. A. Thomas, *Inorg. Chem.*, 2004, **43**, 317–323.
3. S. P. Foxon, T. Phillips, M. R. Gill, M. Towrie, A. W. Parker, M. Webb and J. A. Thomas, *Angew. Chem. Int. Ed.*, 2007, **46**, 3686–3688.
4. P. Waywell, V. Gonzalez, M. R. Gill, H. Adams, A. J. H. M. Meijer, M. P. Williamson and J. A. Thomas, *Chem. Eur. J.*, 2010, **16**, 2407–2417.
5. G. M. Davies, S. J. A. Pope, H. Adams, S. Faulkner and M. D. Ward, *Inorg. Chem.*, 2005, **44**, 4656–4665.
6. T. Lazarides, D. Sykes, S. Faulkner, A. Barbieri and M. D. Ward, *Chem. Eur. J.*, 2008, **14**, 9389–9399.
7. N. M. Tart, D. Sykes, I. Sazanovich, I. S. Tidmarsh and M. D. Ward, *Photochem. Photobiol. Sci.*, 2010, **9**, 886–889.
8. D. Sykes and M. D. Ward, *Chem. Commun.*, 2011, **47**, 2279–2281.
9. R. M. Edkins, D. Sykes, A. Beeby and M. D. Ward, *Chem. Commun.*, 2012, **48**, 9977–9979.
10. N. M. Shavaleev, H. Adams, J. Best and J. A. Weinstein, *J. Organomet. Chem.*, 2007, **692**, 921–925.
11. I. V. Sazanovich, M. A. H. Alamiry, J. Best, R. D. Bennett, O. V. Bouganov, E. S. Davies, V. P. Grivin, A. J. H. M. Meijer, V. F. Plyusnin, K. L. Ronayne, A. H. Shelton, S. A. Tikhomirov, M. Towrie and J. A. Weinstein, *Inorg. Chem.*, 2008, **47**, 10432–10445.
12. N. M. Shavaleev, E. S. Davies, H. Adams, J. Best and J. A. Weinstein, *Inorg. Chem.*, 2008, **47**, 1532–1547.
13. S. F. Parker, K. Refson, R. D. Bennett, J. Best, M. Y. Mel'nikov and J. A. Weinstein, *Inorg. Chem.*, 2012, **51**, 9748–9756.
14. M. Delor, T. Keane, P. A. Scattergood, I. V. Sazanovich, G. M. Greetham, M. Towrie, A. J. H. M. Meijer and J. A. Weinstein, *Nat. Chem.*, 2015, **7**, 689–695.

15. T. Lazarides, I. V. Sazanovich, A. J. Simaan, M. C. Kafentzi, M. Delor, Y. Mekmouche, B. Faure, M. Réglie, J. A. Weinstein, A. G. Coutsolelos and T. Tron, *J. Am. Chem. Soc.*, 2013, **135**, 3095–3103.
16. M. Delor, I. V. Sazanovich, M. Towrie, S. J. Spall, T. Keane, A. J. Blake, C. Wilson, A. J. H. M. Meijer and J. A. Weinstein, *J. Phys. Chem. B*, 2014, **118**, 11781–11791.
17. E. Baggaley, M. R. Gill, N. H. Green, D. Turton, I. V. Sazanovich, S. W. Botchway, C. Smythe, J. W. Haycock, J. A. Weinstein and J. A. Thomas, *Angew. Chem. Int. Ed.*, 2014, **53**, 3367–3371.
18. G. Wolfbauer, A. M. Bond and D. R. MacFarlane, *Inorg. Chem.*, 1999, **38**, 3836–3846.

8. Conclusions and Future Work

8.1. Conclusions

8.1.1. Chapter 3

Both the palladium, and copper based phosphine systems were successfully synthesised. In theory these palladium, and copper complexes should have acted as the electrocatalysts we require, however, the electrochemical results obtained were very inconclusive, see chapter 3. In addition, the precursor phosphines that the complexes require are very air sensitive and easily oxidise. Therefore, work on both the palladium, and copper containing complexes was halted and the focus moved onto the ruthenium, and rhenium containing complexes instead.

8.1.2. Chapter 4

A method that allows a stepwise synthesis of ruthenium complexes has been established. This allows for a high degree of customisability when designing and synthesising this type of complex. However, the synthesis of several ruthenium diimine carboxylate derivatives proved near impossible due to a lack of solubility. Modification of the carboxylate ligand to include an alkane chain, (C₇ – C₉), prior to the free ligands complexation could potentially alleviate the insolubility issue. This would then have allowed the successful synthesis of the final desired products.

Synthesis and characterisation of the desired complexes, $\text{Ru}(\text{CO})_2(\text{Me}_2\text{bpy})\{\text{bpy}(\text{CH}_2\text{PO}_3\text{Et}_2)_2\}$ and its hydrolysis product, $\text{Ru}(\text{CO})_2(\text{Me}_2\text{bpy})\{\text{bpy}(\text{CH}_2\text{PO}_3\text{H}_2)_2\}$ was successfully achieved. A full range of photophysical and electrochemical results were obtained and discussed, see chapter 4. The ester complex produced an increase in current when the solution was saturated with CO₂. However, surprisingly, when the complex was hydrolysed this increase in current in the presence of CO₂ disappeared. Gas chromatography experiments were also unable to detect CO₂ reduction products when the acid complex was used.

8.1.3. Chapter 5

Synthesis and characterisation of the desired complexes, $\text{Re}(\text{CO})_3\text{Cl}\{\text{bpy}(\text{CH}_2\text{PO}_3\text{Et}_2)_2\}$ its hydrolysis product, $\text{Re}(\text{CO})_3\text{Cl}\{\text{bpy}(\text{CH}_2\text{PO}_3\text{H}_2)_2\}$ and its analogues was successfully achieved. The results from these experiments demonstrated catalytic activity for the purpose of CO_2 reduction. The electrochemical data from the cyclic voltammetry shows that catalytic current is being produced when CO_2 is present in solution. The GC experiments show that CO_2 is reduced to CO when a potential of -2.3 V is applied, resulting in $6 \pm 0.6\%$ of CO being produced within 1 hour. A series of comparisons with complexes from the literature were then performed. This showed that $\text{Re}(\text{CO})_3\text{Cl}(\text{Me}_2\text{bpy})$ is capable of producing $7 \pm 0.7\%$ CO within 1 hour. This is obviously a larger volume of CO than our complex, however our complex contains a ligand capable of anchoring onto a semiconductor and therefore has the potential to be powered by light rather than electric current. The UV-Vis spectra of $\text{Re}(\text{CO})_3\text{Cl}(\text{Me}_2\text{bpy})$, $\text{Re}(\text{CO})_3\text{Cl}\{\text{bpy}(\text{C}(\text{O})\text{OEt})_2\}$ and $\text{Re}(\text{CO})_3\text{Cl}\{\text{bpy}(\text{CH}_2\text{PO}_3\text{Et}_2)_2\}$ in DCM are very similar. This shows that the anchor group has no effect on the MLCT which is consistent with the very similar cyclic voltammetry results.

8.1.4. Chapter 6

The complex, $\text{Re}(\text{CO})_3\text{Cl}\{\text{bpy}(\text{CH}_2\text{PO}_3\text{H}_2)_2\}$ was successfully anchored onto TiO_2 . This was shown by both the visual observations and UV-Vis spectral data. Work on the N- Ta_2O_5 and Ta_2O_5 semiconductor was also presented and after some initial failure when using DMF as the solvent, attachment does appear to occur when using DMSO instead. This was demonstrated both visually and by XPS, which was able to identify rhenium present on the surface of the semiconductor. Electrochemical and GC experiments were then planned to be carried out using the rhenium complex and the N- Ta_2O_5 semiconductor in conjunction with each other. However, this work was not carried out at this time. Although it could easily be done so in future if a suitable semiconductor electrode can be constructed.

8.2. Thesis Summary

The overarching goal of the work contained in this thesis was to design, synthesise and characterise an electrocatalyst that can be anchored to a light-harvesting semiconductor resulting in a photo-electro-catalytic system capable of CO₂ reduction. In order to fulfil this goal, the work was broken down into several specific aims:

- (i) To evaluate the current literature regarding electrocatalysts for the purpose of CO₂ reduction and identify suitable candidates for modification with anchoring groups.

The first aim, a search of the literature, was essential when starting this work. It allowed us to see what had been done previously, what systems had worked and possibly, what systems would not. It has formed the basis from which the work in this thesis has built upon by providing known electrocatalysts that could then be modified to include anchoring groups enabling attachment to a semiconductor. See chapter 1.

- (ii) To design, synthesise and characterise modified electrocatalysts for the purpose of CO₂ reduction. This modification will take the form of the addition of an anchoring group, either carboxylate or phosphonate, which will enable attachment to a semiconductor at a later stage. The first series of modified electrocatalysts are from known homogeneous catalysts based on either, copper phosphine or palladium phosphine complexes. The second series of modified electrocatalysts are derivatives from known homogeneous catalysts based on either ruthenium(II) diimine or rhenium(I) diimine complexes.

The fulfilment of aim (ii) produced a large amount of synthetic work, often because of syntheses that did not work rather than those that did. In particular, the work on the copper phosphine, and palladium phosphine complexes proved rather difficult due to oxidation of the phosphine ligand, see chapter 3. There were also difficulties concerning the ruthenium diimine complexes, specifically the insolubility of the carboxylate ligand, see chapter 4. Therefore, these classes of catalysts were not investigated any further.

The rhenium diimine phosphonate complexes on the other hand have proven easy to synthesise and have high solubility.

- (iii) To evaluate the capacity of the compounds synthesised during the fulfilment of aim (ii) to act as CO₂ reduction catalysts, whilst the anchoring group is in its protected form of a carboxylate ester or a phosphonate ester. This will be done through photophysical and electrochemical experiments.

Some encouraging results have been obtained; both the ruthenium diimine phosphonate ester and the rhenium diimine phosphonate ester appear to show an increase in current during the electrochemical experiments when in a CO₂ saturated solution. These results demonstrated the applicability of the compounds for CO₂ reduction.

- (iv) To deprotect the ester groups, resulting in either a –C(O)OH or –P(O)(OH)₂ anchoring group on the complex. To evaluate the capacity of the compounds to act as CO₂ reduction catalysts then compare with the anchor-free derivatives, and the carboxylate vs. the phosphonate derivatives. This will be done through photophysical, electrochemical and gas chromatography experiments.

A simple ester hydrolysis resulted in a phosphonic acid containing anchor group on the ruthenium complex. The results from the electrochemical and gas chromatography experiments were controversial and indicated that hydrolysis of the phosphonate ester led to loss of catalytic activity. No current enhancement at the 2nd reduction potential was observed in the cyclic voltammograms, nor were any reduction products detected by GC. It is not clear at present what has caused such a loss of activity. However, the rhenium phosphonic acid complex did produce an increase in current in the presence of CO₂, and reduction of CO₂ to CO was confirmed by GC, see chapter 5.

Anchor-free derivatives of rhenium complexes were also tested for their CO₂ reduction capabilities. It has been shown that introduction of the phosphonic acid anchoring group only slightly reduces the catalytic activity. Thus, the rhenium

phosphonic acid complex demonstrated electrocatalytic activity, which was then taken and used in the fulfilment of aim (vi).

A direct comparison between the carboxylate, and phosphonate derivatives was not performed, as we had been unable to successfully synthesise the former. However, when fulfilling aim (v) a comparison between a rhenium diimine carboxylate ester complex without a $-\text{CH}_2-$ spacer group and a rhenium diimine phosphonate ester with a $-\text{CH}_2-$ spacer group was made.

- (v) To elucidate the effect of the mode of attachment of the anchoring group to the diimine ligand, direct attachment vs. an attachment via a saturated $-\text{CH}_2-$ spacer group; the latter having been designed to alleviate the electron withdrawing effect of the anchors which has been perceived to hinder the catalytic activity.

Aim (v) was achieved by testing the ability of the rhenium diimine carboxylate ester complex without a $-\text{CH}_2-$ spacer group to electrochemically reduce CO_2 and comparing this with the results from the rhenium diimine phosphonate ester with a $-\text{CH}_2-$ spacer group complex. This comparison showed that the former did not produce an increase in current in the presence of CO_2 and that the latter did show an increase. For full details, see chapter 5.

- (vi) Identify the most efficient electrocatalyst from those evaluated. To then establish a method of anchoring the electrocatalyst to a semiconductor, either TiO_2 or Ta_2O_5 , and to determine if anchoring has been successful.

The most efficient anchor group containing electrocatalyst, $\text{Re}(\text{CO})_3\text{Cl}\{\text{bpy}(\text{CH}_2\text{PO}_3\text{H}_2)_2\}$, has been successfully anchored onto TiO_2 , nitrogen doped Ta_2O_5 , and undoped Ta_2O_5 . See chapter 6 for further details.

The overall summary for the work contained in this thesis is that good progress has been made towards the goal of designing, synthesising and characterising an electrocatalyst that can be anchored to a light harvesting semiconductor resulting in a photo-electro-catalytic system capable of CO_2 reduction. This was achieved by

fulfilment of the specific aims of the thesis, the details of which have just been summarised above and are contained in full in the relevant chapters. However, more work is needed, primarily the testing of the catalyst in conjunction with the N-Ta₂O₅ semiconductor. If this were to be done then the goal of the thesis, to utilise an electrocatalyst that can be anchored onto a semiconductor that is capable of absorbing light in order to drive the process of CO₂ reduction, would be completed.

8.3. Future Work

The research of CO₂ reduction can be taken in several other directions. The first area to consider is the modification of the electrocatalyst in which two directions can be followed.

- (i) Changing the ligands used in the complex. One possibility would be to use a phenanthroline ligand containing an anchoring group instead of using bipyridines.
- (ii) Another possibility is to change the metal involved, e.g., systems using manganese have recently started to appear.¹ Manganese is in the same group as rhenium but is a first row rather than a third row transition metal. This means that the chemistry is likely to be similar. There is another advantage to using manganese in that it is significantly more abundant and consequently cheaper than rhenium. This has implications further into the future when trying to consider the costs involved in mass producing a device, should such a device come to pass. These factors have already resulted in a new project directly continuing the work described in this thesis in order to further the research in the field.

A second area of future work to consider is changes to the semiconductor. This could be in the form of changing the nitrogen doping level for the Ta₂O₅. This would allow tuning of the semiconductors light absorption profile. Another idea would be to change the semiconductor altogether, perhaps to a cadmium, gallium or indium based material.

A final area to consider would be something completely different to the work described in this thesis. One idea would be an organic-inorganic hybrid system or bio-inorganic hybrid system. These types of materials have recently been deployed as part of solar cells^{2, 3} and therefore it may be possible to incorporate them into our systems for the purpose of CO₂ reduction.

The purpose of these changes is to try to further improve the catalytic properties e.g. TON, TOF, catalytic selectivity and stability of the system. However, it is often not possible to predict exactly how these changes will affect the properties until the system is synthesised and subsequently tested. If it were then the ideal system would have been designed and produced already. We can of course make a prediction based on previous knowledge and chemical intuition but ultimately we simply have to build a new system and see what happens with the aim of making the desired improvements gradually over time.

8.4. References

1. J. M. Smieja, M. D. Sampson, K. A. Grice, E. E. Benson, J. D. Froehlich and C. P. Kubiak, *Inorg. Chem.*, 2013, **52**, 2484–2491.
2. M. Wright and A. Uddin, *Sol. Energy Mater. Sol. Cells*, 2012, **107**, 87–111.
3. J. H. Noh, S. H. Im, J. H. Heo, T. N. Mandal and S. I. Seok, *Nano Lett.*, 2013, **13**, 1764–1769.